Studies on Melt Processing and Rheology of Poly (lactic acid) and its Efficacy in Recyclable Bionanocomposite, Biodiesel and Biolubricant

Thesis submitted in partial fulfillment of the requirements for the Degree of

DOCTOR of PHILOSOPHY

by

Melakuu Tesfaye Alemea

Roll No: 136107032

Department of Chemical Engineering

Indian Institute of Technology Guwahati

Guwahati – 781039, Assam, India

April 2017

Dedicated to

My beloved parents

&

Finote Brihan

Department of Chemical Engineering
Indian Institute of Technology Guwahati

STATEMENT

I hereby declare that the scientific matter embodied in this thesis entitled, "**Studies on Melt Processing and Rheology of Poly (lactic acid) and its Efficacy in Recyclable Bionanocomposite, Biodiesel and Biolubricant**" is the outcome of the research work carried out by me under the supervision of Dr. Vimal Katiyar at the Department of Chemical Engineering, Indian Institute of Technology Guwahati, Guwahati, Assam, India, for the award of the degree of Doctor of Philosophy. To the best of my knowledge, the work delineated on this thesis is original and has not been submitted elsewhere for any degree of any other Institute or University.

In keeping with the scientific tradition, whatever work done by others has been utilized, due acknowledgement has been made.

Melakuu Tesfaye Alemea

Roll no.: 136107032

Candidate

Department of Chemical Engineering

Indian Institute of Technology Guwahati

Guwahati – 781039, Assam, India.

Department of Chemical Engineering
Indian Institute of Technology Guwahati

CERTIFICATE

This is to Certify that the thesis entitled "**Studies on Melt Processing and Rheology of Poly (lactic acid) and its Efficacy in Recyclable Bionanocomposite, Biodiesel and Biolubricant**" being submitted by Mr. Melakuu Tesfaye Alemea, Department of Chemical Engineering, Indian Institute of Technology Guwahati has been carried out under my guidance and supervision. The work documented in this thesis has not been submitted to any other Universities or institutes for the award of any degree or diploma.

Dr. Vimal Katiyar

Thesis supervisor

Department of Chemical Engineering

Indian Institute of Technology Guwahati

Guwahati – 781039, Assam, India

Acknowledgements

Though only my name appears on the cover of this dissertation, a great many people have contributed to its production. I owe my gratitude to all those people who have made this dissertation possible and because of whom my research experience in IITG has been one that I will remember forever.

First of all, I wish to express my sincere gratitude and heartfelt thanks to my research supervisor, **Dr. Vimal Katiyar**, for giving me an opportunity to pursue this research work, and for his precious advice, continuous care, guidance, encouragement, and supervision. I must acknowledge the unconditional freedom that he gave me to think, plan, execute and express my research work in every step, while keeping faith and confidence on my capabilities. Through him I have learnt how to write a scientific article and enhance its quality, which have extensively contributed to the writing of my Ph.D. thesis. It has been a great privilege to work under him.

Secondly, my gratitude goes to **Dr. Prakash Kotecha** and my doctoral committee members, **Dr. V.V Goud,** and **Dr. Pankaj Tiwari** (Department of Chemical Engineering) as well as **Dr. Mohd. Qureshi (**Department of chemistry) for their periodic assessments on the findings of my research and their constructive suggestions, which helped me to improve my work pertaining to Ph.D. thesis. I must express my sincere thanks to **Prof. Pallab Ghosh, Dr. Mahuya De, Dr. Dipankar Bandyopadhyay, and Dr. Chandan Das** for providing their knowledge and study materials during the course work

I owe special thanks to **Arvind Gupta, Narendren S., Surendra Singh Gaur**, **Randeep Singh, and Atanu kumar Paul,** and to the entire **CoE-SUSPOL** research team for their

unconditional help during the course of my research activities as well as my stay in INDIA in general. **Neha, Tabli and Dr. Purabi,** I would like to say thank you for your unlimited help during the final stage of thesis preparation.

I would like to thank Central Instruments Facility and Department of Chemical Engineering Department of Mechanical Engineering for allowing me to utilize their research facilities. I express my thanks to all the technical staffs of chemical engineering department specially **Ms. Ritumoni Kalita, Mr. Dipak Kumar Barman, Dr. Lukumoni Borah, Mr. Pankaj Sekhar Baruah, Mr. Debajit Borah** and **Mr. Jayanta Kumar Mout** for their assistance during my experimental work. I would also like to thank **Mr. Sailen Das, Mr. Deep Jyoti Sinha** and **Mr. Bhagya Boro** for their support in various forms.

I am grateful to the **Centre of Excellence for Sustainable Polymers (CoE-SUSPOL), IIT Guwahati** for providing me an attractive working environment with all the characterization facilities. I acknowledge **Ethiopian ministry of education**, for the PhD fellowship that had allowed me to undertake this research. I must also thank **IITG** for having me as a student.

I am forever indebted to my parents, **Tesfaye Alemea** and **Zinash Aragaw** for their affections, support, blessings and endless patience. I also acknowledge my brothers, sister, MLAH and all Ethiopian community members in IITG for their constant encouragement and belief throughout my journey. Many other people, not mentioned here but present in my soul, I greatly acknowledge their support to accomplish my doctoral study. Finally and foremost, I thank God for giving me the good times which I enjoyed and the bad times from which I learned many things. I remain thankful for the mental strength given to face adverse situations.

Melakuu Tesfaye Alemea

Abstract

The overall aim of the present study is to focus on the melt processing and rheology of poly (lactic acid) (PLA) and its efficacy towards the fabrication of recyclable bionanocomposite and its end use application as a biolubricant and biodiesel additive. PLA is known to have poor melt strength, which is a major limitation for melt processing and recycling using the conversional technologies. In this thesis, melt stabilization of PLA has been attained through melt extrusion with thermally stable and crystalline silk.

Over the assessment, the impact of silk nanocrystals (SNC) on melt degradation of PLA during thermomechanical process is investigated at melting temperatures (185 ºC and 200 ºC) under shear (40 and 100 rpm). The rate of degradation is studied through the estimation of molecular weight distribution at different residence times (up to 30 min) using gel permeation chromatography (GPC). Simplified two-parameter model which accounts for degradation and recombination is used to predict the kinetic parameters by coupling with Arrhenius equation. The impact of SNC and processing condition on macromolecular change of PLA matrix is also investigated using melt rheology. The incorporation of SNC in PLA matrix is observed to hinder the melt degradation which is confirmed by the increment in degradation activation energy and reduction in degradation rate constant. FTIR results confirm the formation of weak interaction between the SNC and PLA, which can be considered to be the reason for the stabilizing effect of SNC. The morphology of the SNC-PLA composite captured by field emission scanning electron microscope (FESEM) shows network formation, which is absent in neat PLA (NPLA) matrix. Crystallinity is improved and the reduction in number average

molecular weight (M_n) and weight average molecular weight (M_w) with increasing residence time is minimized as compared to pristine PLA.

The recyclability performance of neat PLA (NPLA) and SNC-PLA is also studied through the essential investigations on melt rheology, solution viscosity and thermal degradation behavior under repetitive extrusion at high shear and temperature. The presence of SNCs is observed to facilitate the crystallization process and delay the thermal degradation of PLA matrix. This led to the reduction in cold crystallization peak temperature with lower crystallization half-time and higher growth rate. The substantial improvement in nucleation density observed through Polarized Optical Microscope (POM) proves the nucleating effect of SNC in all processing cycles. Moreover, the rheological investigation (complex viscosity, storage and loss modulus values) revealed the stabilizing effect of SNC and the drastic degradation of pristine PLA in third and fourth cycle is observed to be fortified by the presence of SNC. Cole-Cole plot and cross over frequencies have been correlated with the molar mass distribution of NPLA and SNC-PLA bionanocomposite during processing, which is further supported by the intrinsic viscosity measurement and acid value analysis.

On the other hand, stable onset degradation temperature is obtained for SNC-PLA bionanocomposite ($T_{5\%}$ ~ 334 ºC) as compared to NPLA, which is drastically reduced from 336 ºC (first cycle) to 322 ºC (fifth cycle). The activation energies are estimated using isoconversional methods (Kissinger-Akahira-Sunose (KAS) and Flynn-Wall-Ozawa (FWO)). Stable activation energy values (~130 kJ/mol) are obtained for SNC-PLA bionanocomposite at three consecutive extrusion cycles whereas, in case of NPLA, these values significantly reduce from ~150 kJ/mol (first cycle) to ~110 kJ/mol (second cycle). Nelder-Mead simplex method is used to optimize the kinetic parameters of nucleation and growth model (A2), which

is observed as the best fit of experimental thermogravimetric analysis (TGA) data. Decomposition products are analyzed by thermogravimetric analysis coupled with Fourier transform infrared spectroscopy (TGA-FTIR).

Reactive extrusion is also performed to have branched, crosslinked and SNC grafted chain topology of PLA, with different levels of gel percentage by adding small amount of radical initiator (dicumyl peroxide (DCP)). Grafting of SNCs on PLA macromolecules provide remarkable improvement on rheological and thermal properties, which is confirmed by ^{1}HNMR and FTIR investigation. Significant improvement observed on zero shear viscosities and the crossover point shifts to lower frequencies as compared to branched and crosslinked PLA system. Along with SNC grafting, the crystallization behavior is also enhanced with the formation of stable and uniform crystals during cooling, which leads to a single melting peak. The rate of crystallization of PLA is improved but the percentage crystallinity is decreased with increasing DCP fraction as higher grafting and subsequent crosslinking restricts the macromolecular movements, which is essential for crystallization process. Furthermore, SNC grafting improves the reprocessability performance of PLA and provides improved rheological properties as compared to the branched and crosslinked PLA at all reprocessing cycles.

Subsequently, two other recycling alternatives are introduced in this research for the first time to utilize recycled and waste melt processed PLA and its lower molecular weight oligomers. The first part demonstrates the dissolution of melt processed PLA in lactic acid/water mixture which is blended with soybean oil (SO) to be tested as a biolubricant. Dynamic viscosity and Viscosity-Temperature dependency of the blend is investigated at temperature of 25 ºC, 40 ºC, 60 ºC, 80 ºC and 100 ºC. Promising results are obtained for 30/70 and 50/50 blend of soybean oil and recycled PLA. The second part highlights the recycling of low molecular weight PLA

(oligomer) into biodiesel additives. Four different molecular weight oligomers (500 Da, 1000 Da, 1500 Da and 2000 Da) are synthesized using microwave reactor and dissolved in soybean oil based methyl ester in different concentrations (3, 5, 10 and 25 g/L). The impact of PLA-oligomer on the cold flow properties (cloud point, pour point and dynamic viscosity) are investigated using rheometer and optical polarimetry as per ASTM standards. Furthermore, engine performance and exhaust gas analysis are performed using Kirloskar TV-1 engine. The cloud point and pour point decreases respectively by 6 ºC and 2 ºC with remarkable viscosity reduction at lower temperature, which improves the exhaust gas characteristic.

Table of Contents

List of Figures

List of Tables

List of Schemes

Nomenclature

Abbreviations

ASTM	American Society for Testing and Materials
CNC	Cellulose nanocrystals
DMA	Dynamic mechanical analysis
DSC	Differential Scanning Calorimetry
DCP	Dicumyl Peroxide
DCP-NPLA	Reactively extruded neat PLA
DCP-SNC-PLA	Reactively extruded SNC-PLA
GPC	Gel Permeation Chromatography
FESEM	Field Emission Scanning Electron Microscopy
FTIR	Fourier Transmission Infrared Spectroscopy
FWO	Flynn-Wall-Ozawa
^{1}HNMR	Hydrogen NMR
KAS	Kissinger-Akahira-Sunose
LA	Lactic Acid
LA-D-PLA	Lactic acid degraded PLA
MWD	Molecular Weight Distribution

NMR	Nuclear Magnetic Resonance
NPLA	Neat Poly (lactic acid)
OLLA	Oligomer of L-lactic acid
PLA	Poly (lactic acid)
POM	Polarized Optical Microscope
PDI	Poly Dispersity Index
PET	Polyethylene terephthalate
PP	Polypropylene
PS	Polystyrene
SEM	Scanning Electron Microscopy
SNC	Silk nanocrystals
SNC-PLA	Silk nanocrystals- Poly (lactic acid) bionanocomposite
TGA	Thermogravimetric analysis
TGA-FTIR	Thermogravimetric analysis hyphenated with Fourier transform infrared spectroscopy
XRD	X-Ray Diffraction

Notations

M_n	Number average molecular weight
M_w	Weight average molecular weight
R_i	Recycling cycles
K	Avrami kinetic constant
T_o	Onset degradation constant
T_m	Melting temperature
T_c	Crystallization temperature
α	Fractional Conversion
β	Rate of Heating
k	Rate Constant
θ	Diffraction Angle
T_{max}	Maximum Degradation Temperature
A	Pre-Exponential Factor
E_a	Activation Energy
n	Order of Reaction
R	Gas Constant
λ	Cu-Kα Radiation Wavelength

λ_i	i^{th} moment of molar mass distribution
T_g	Glass Transition Temperature
G'	Storage Modulus
G"	Loss Modulus
tan δ	Loss Factor
ŋ*	Complex Viscosity
ω	Angular Frequency
ŋ	Viscosity
γ	Shear Rate

Chapter 1

Introduction and Literature Review

This chapter presents a brief summary of the basic fundamentals and terminologies about bioplastics, biopolymers and more emphasis have been given to one of the most extensively used synthetic bioplastic, poly (lactic acid) (PLA). Important properties of PLA and its limitation towards the wide application are also highlighted. Melt processing, rheology and thermal degradation behavior of PLA have been covered with extensive literature survey. The advantage of using biofillers such as silk fibroin, as a reinforcement agent for PLA matrix is assessed and the state of the art on different recycling opportunities of PLA are discussed in details. Thereafter, the objectives of the thesis are summarized followed by the organization of the thesis.

Parts of this chapter are in press as book chapter:

Melakuu Tesfaye, Purabi Bhagabati, Naba Kumar Kalita and Vimal Katiyar, Trends on End-of-Life Options: Recycling, Re-using and Composting of Waste Food Packages (Smithers Rapra publishing)

1.1. Introduction

Conventional plastic based environmental pollution has become a major concern of the prevailing modern society due to the large consumption of plastics and their poor disposal techniques [1]. Daily activities of human life are simplified by the products made from plastics including, drinking bottles, food packages, sports equipment, cars, computers electrical wire insulators, pipes, etc. [2]. In 2013, global production of plastics was estimated to be more than 250 million tons, 40% of which holds for packaging. According to the studies, most of the plastics used for food and other simple product packaging are utilized only for 12 min which are then disposed in to the environment and remain there for more than 400 years. About 43% of the total world consumption of plastics are disposed in landfills whereas more than 10 million tons end up in the ocean each year [3].

Waste recovery using different recycling techniques have been developed in order to minimize the waste disposal and convert it into some valuable form [4, 5]. However, comparing the yearly plastic production growth rate with the plastic which has already been deposited on the earth for the last 50 years, it is found that the plastic recycling efficiency has not grown sufficiently enough to tackle the problem due to several limitations. Some of the recycling techniques like energy recovery from the plastic waste by direct incineration create significant air pollution [2]. Moreover, commodity plastics are produced from the petroleum resources, leading to its depletion being a concern for world energy security.

Recently, Biobased polymers have been studied extensively to use their promising performance towards the substitution of petroleum based plastics. Research in the field of Bioplastics can potentially be beneficial in increasing the efficiency of recycling waste management and greenhouse emissions [6]. The natural decomposition process of these

synthetic biopolymers into nontoxic components (CO_2 and CO), make them suitable over petroleum based polymers [7, 8]. However, their higher production cost other than their properties limits bioplastics to be produced in large quantities in such a way which can replace the conventional fossil based polymers [9]. One way of minimizing the cost is to use the technologies which can help to minimize the energy consumption during the synthesis and processing of the materials. Recycling is more energy efficient which may release less carbon dioxide as compared to that of making a new product. By doing so, it is possible to reduce the extensive utilization of feed stock with low cost of the material. Therefore, appropriate recycling mechanisms have to be developed to ensure ultimate utilization of Bioplastics. Based on this fact, before allowing the Bioplastics to degrade naturally into carbon dioxide and water, one can still utilize them as energy harvesting chemicals before end of their life, through efficient processes. Currently, Bioplastics are produced in very small quantities, which hold 2% share of total polymer production in 2013 and are expected to grow up to 4% by 2020 [10]. In addition to this, the infrastructure for recycling of such plastics has not yet fully developed.

1.2. Biobased polymers

Biobased polymers are those class of polymers, which are derived from renewable resources (biomass) including pristine polymer, blend or composite. It can be broadly classified as:

i. Naturally existing biopolymers: These extracted biopolymers can be used directly with some chemical modifications such as, polysaccharides and proteins from plant and animals sources (including cellulose, starch, chitin, cellulose acetate, silk, lignin, gum, pectin, casein, etc.). In addition to this, polymers which are synthesized naturally by microorganisms and plants such as poly (3-hydroxyalkanote), poly (glutamic acid) and bacterial cellulose are also categorized under naturally existing biopolymers.

ii. Synthetic biopolymers: These are mainly synthesized from the biomass originated monomers through biological and chemical transformation with a motivation to produce it at a commercial scale using industrially viable techniques [11]. Monomers originated from the biomass can be utilized to produce biodegradable as well as non-degradable polymers. Poly (lactic acid) (PLA) is the first largely produced synthetic biodegradable polymer whereas, biopolyethylene (PE) and biopolypropylene (PP) are non-degradable polymers which are produced from bioderived monomers.

Degradable synthetic biobased polymers can be considered as sustainable polymers due to their potential to reduce fossil fuel consumption, minimize the waste disposal problem and significantly lower the emission of carbon dioxide during production. Most importantly, in order to meet the sustainability criteria, biodegradable biobased polymers need to be transformed in such a way that it can be processed through industrially viable techniques into different shapes and designs with film forming ability along with the desired mechanical and rheological properties. However, some of the major limitations that restrict the mass production are as follows:

Feed stock: Various food crops such as corn, soy, and sugar cane are currently used as a feed stock for the production of biodegradable plastics and therefore switching to biodegradable plastics may affect the world's food supply. Biodegradable plastics derived from non-food crops like switchgrass would indirectly affect food production by competing for land with food crops [12]. On the other hand, biodegradable plastics derived from agricultural waste or algae would have little or no impact on the food supply. The increasing rate of corn prices as a result of ethanol production is a good example of this effect [13].

Performance limitation: As compared to conventional polymers, biodegradable plastics have limited applicability due to their low thermal stability, inferior mechanical and gas barrier properties. The glass transition temperature (T_g) and heat distortion temperature (HDT) should be improved so as to improve their utilization [14].

Product cost: Currently the cost of bioplastics is higher than that of convectional polymers. For instance, the cost of PLA is 3-5 times more than the cost of polyethylene terephthalate (PET). It is obvious that, other advantages of biodegradable plastics are meaningless, if the material is too expensive.

Generally, biodegradable plastics are superior to petroleum based plastics in terms of energy efficiency, petroleum consumption and carbon emissions, but inferior in cost and applicability span with a negative impact on the food supply. Among all the biodegradable plastics, PLA is the first in terms of production and applicability. In this research work, PLA is selected as a system to study the possible melt processability and recyclability, since it accounts for a large part of the post-consumer biodegradable plastic waste with promising future of expanding its applicability towards the substitution of conventional polymers.

1.3. Poly (lactic acid) (PLA)

PLA is a biodegradable thermoplastic aliphatic polyester derived from renewable resources, such as corn starch, tapioca roots, or sugarcane (life cycle of PLA is described in **fig. 1.1)**. It has been extensively studied for a number of applications such as packaging, orthopedics, drug delivery, sutures, and scaffolds and other biomedical applications. It possesses better mechanical properties and it is relatively easy to process using conventional methods like thermoforming, injection, and blow molding without releasing toxic products [15]. In order to

meet the performance requirements, PLA can be synthesized by various methods such as poly-condensation reaction, ring opening polymerization (ROP) and solid state polymerization using different catalysts [16]. Polycondensation reaction requires continuous removal of water under vacuum and the final molecular weight is highly dependent on the water removal efficiency.

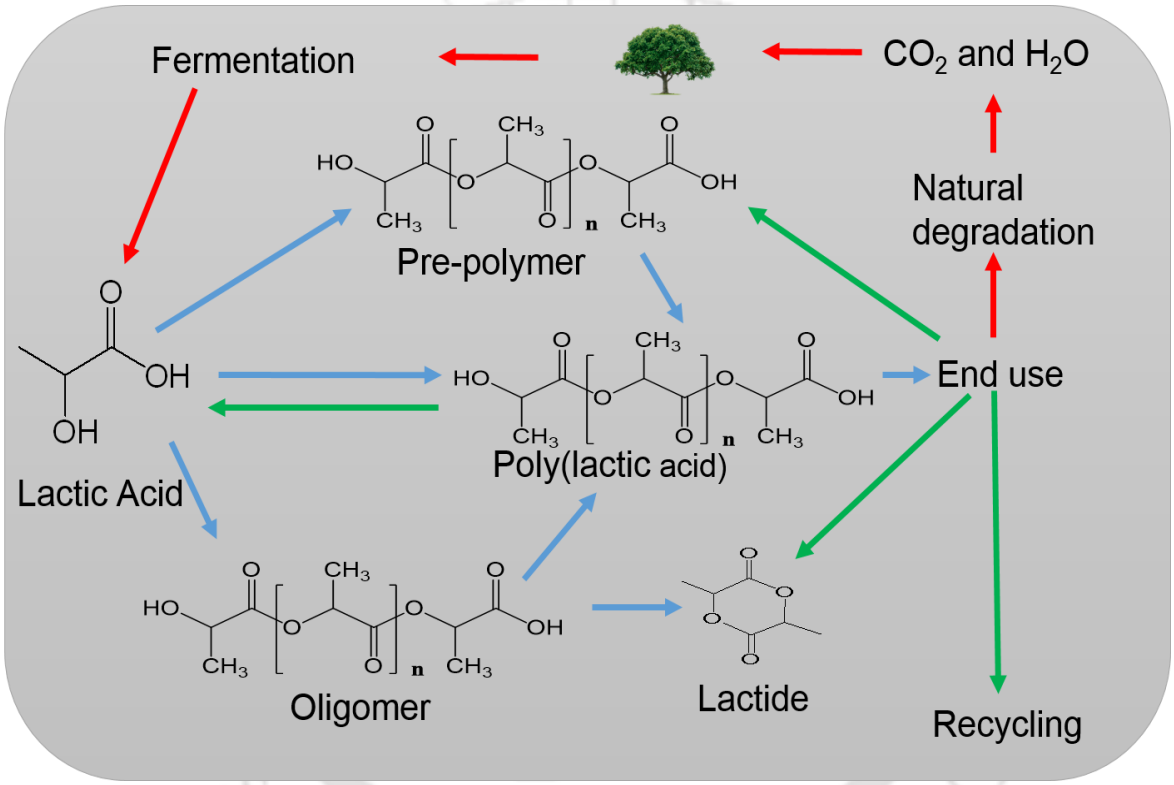

Figure 1.1. Life cycle of poly (lactic acid).

Nowadays, ROP is becoming more popular in which higher molecular weight PLA can be achieved from the cyclic dimer. The monomer, lactic acid is known to be chiral molecule found in L and D (R and S) form. Due to its special characteristic, high molecular weight PLA can be synthesized by ring opening polymerization technique with the following stereoisomers: optically pure poly (L-lactic acid)/ pure poly (D-lactic acid) or racemic mixture of L and D.

Oligomer of lactic acid is produced by polycondensation reaction followed by depolymerization step to produce an intermediate product of cyclic dimer/lactide. Lactides in pure form (L-lactides or D-lactides) or mixture stereoforms (mixture of L and D-lactides, meso-lactids are converted to high molecular weight PLA. Final properties of PLA are extensively dependent on the stereo form. Pure PLA enantiomer exhibits semicrystalline nature with melting point (T_m) ranging from 160-175 ºC, T_g between 55-70 ºC and comparable mechanical properties with PET. Controlled physical blending of PLLA and PDLA have the ability to increase the heat distortion temperature and melting temperature by 40 ºC and 100 ºC respectively [11]. .

In general, PLA is known to have low melt strength and poor thermal stability, which makes it very difficult to be processed at high temperature and shear. Stabilization and/or improvement of the melt strength is highly required to expand the processing window and applicability span. Most importantly, thermally stable PLA with improved melt strength is required in order to enhance the reprocessability performance and in turn, reduce the cost of the material. Additionally, the efficacy of PLA in different forms need to be addressed in order to recover the waste generated during the polymerization stage as well as for randomly degraded polymer after extrusion process. As clearly indicated in **Fig. 1.2**, at the depolymerization stage of oligomer into lactide (before ROP), around 10 % waste (composed of short chain oligomers) is generated due to incomplete conversion. Moreover, PLA is susceptible to drastic degradation after multiple extrusion which leads to the difficulty to process it into a film.

In this particular investigation, more emphasis has been given for the stabilization and improvement of the melt strength of PLA in order to fabricate recyclable biocomposite.

Moreover, the efficacy of randomly degraded PLA and lower molecular weight oligomer for a targeted application in biolubricants and biodiesel have been studied for the first time.

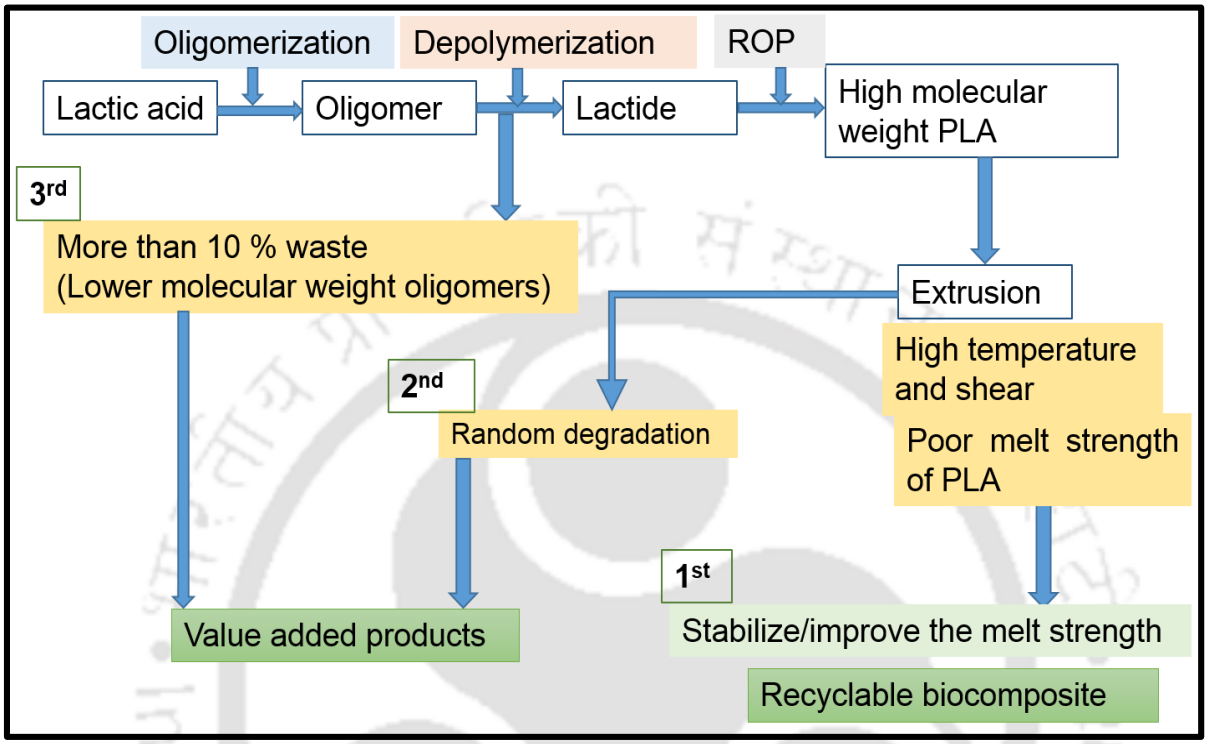

Figure 1.2. Flow chart for high molecular weight PLA preparation and the possible roots of waste generations.

1.4. Melt processing and Rheology of PLA

PLA is an aliphatic polyester having properties similar to that of conventional thermoplastics, which makes it suitable to be used in polymer processing techniques such as extrusion, injection moulding, etc. However, PLA needs to be dried properly before subjecting it into any of the melt processing techniques in order to avoid the drastic degradation, which is the major cause for the deterioration of mechanical properties. Despite the fact that PLA can be processed by extrusion process, its poor melt strength limits its ability to withstand high temperature and shear. Degradation is characterized by an uncontrolled change in molecular

weight or constitution of the polymer; but conventionally, the term degradation is taken to mean a reduction in the molecular weight of the polymer. The degradation phenomenon can be facilitated by trace amount of water during processing [17, 18], acidic end groups, residual catalyst, residual monomers and surface functional fillers [17]. Most importantly, thermal degradation in molten state and its impact on rheology of the melt needs to be addressed properly before loading any fillers or additives during processing.

1.4.1. PLA thermal degradation

PLA degradation can take place through two mechanisms including, chain-end degradation and random degradation. In case of chain end degradation, the degradation starts from the chain ends, resulting in successive release of the monomeric unit whereas, in case of random degradation, the degradation occurs at any random point along the polymeric chain [17]. Several mechanisms have been postulated for PLA in order to describe various complex degradation reactions occurring during processing under high temperature, shear and longer residence time. Random chain scission [19], oxidative degradation [19], intermolecular and intramolecular transesterification [20], pyrolytic elimination and radical reactions [21] are some of the major degradation mechanisms (**Scheme 1.1, Scheme 1.2, Scheme 1.3 and Scheme 1.4.)**.

As already discussed above, degradation of PLA is complex in nature which follows several mechanisms. During thermal processing of PLA, the possibility of chain scissions due to intermolecular transesterification is the dominant factor to decrease the molecular weight of the material. The presence of shorter chain oligomers can significantly facilitate the transesterification reaction and lead to the drastic reduction of molecular weight and

broadening of the molecular weight distribution. In some cases, high shear and temperature may also lead to the formation of colour change on PLA, which is attributed to the presence of conjugated double boned in acrylic end-groups due to pyrolytic elimination. Within the processing window of PLA (170 to 220 ºC), cyclic oligomers and lactides are rare to be produced. Most importantly, PLA is always susceptible to hydrolytic degradation due to the trace amounts of moisture during melt processing, which leads to major reduction in molecular weight. Due to this fact, proper drying of PLA prior to melt processing is strongly recommended.

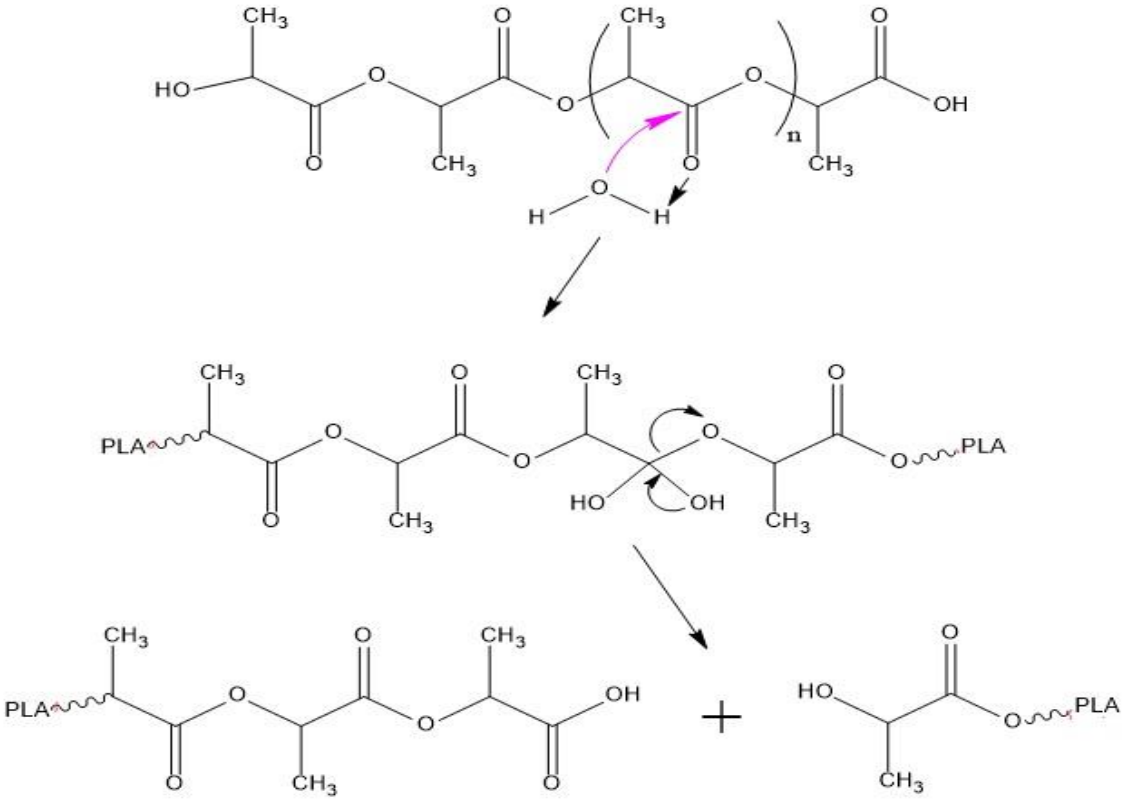

Scheme 1.1. Hydrolytic degradation of PLA.

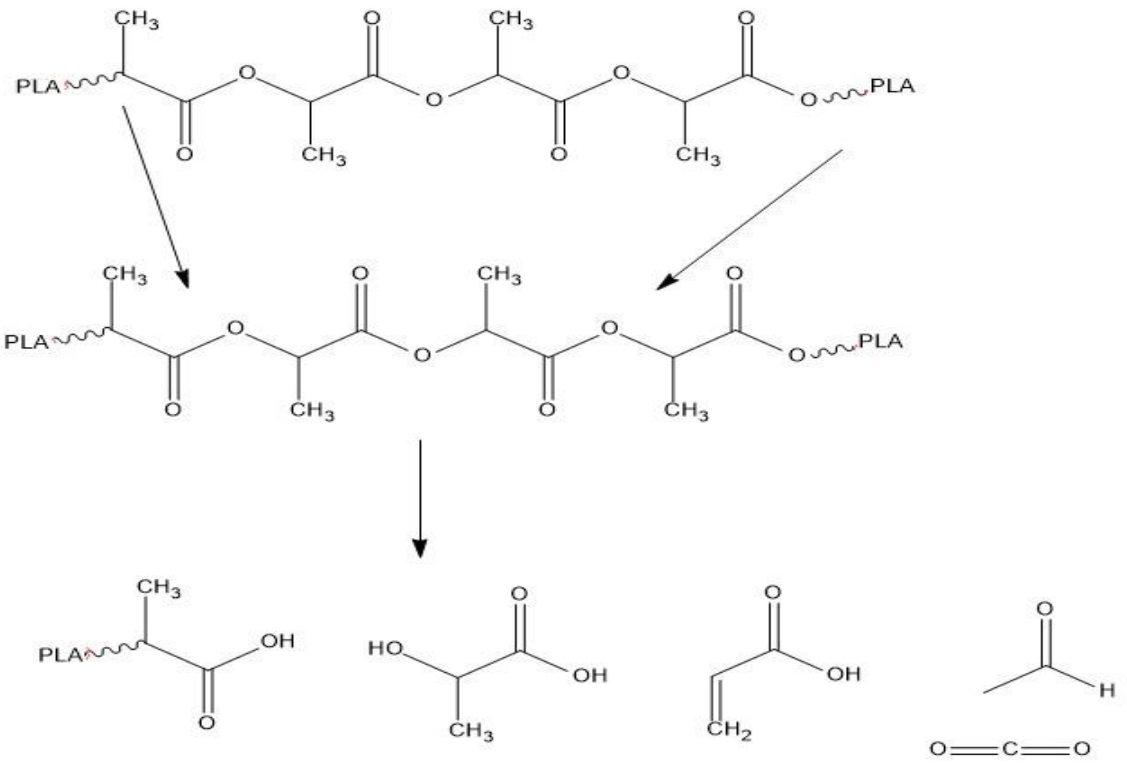

Scheme 1.2. Chain cleavage of PLA by transesterification reaction within the macromolecules.

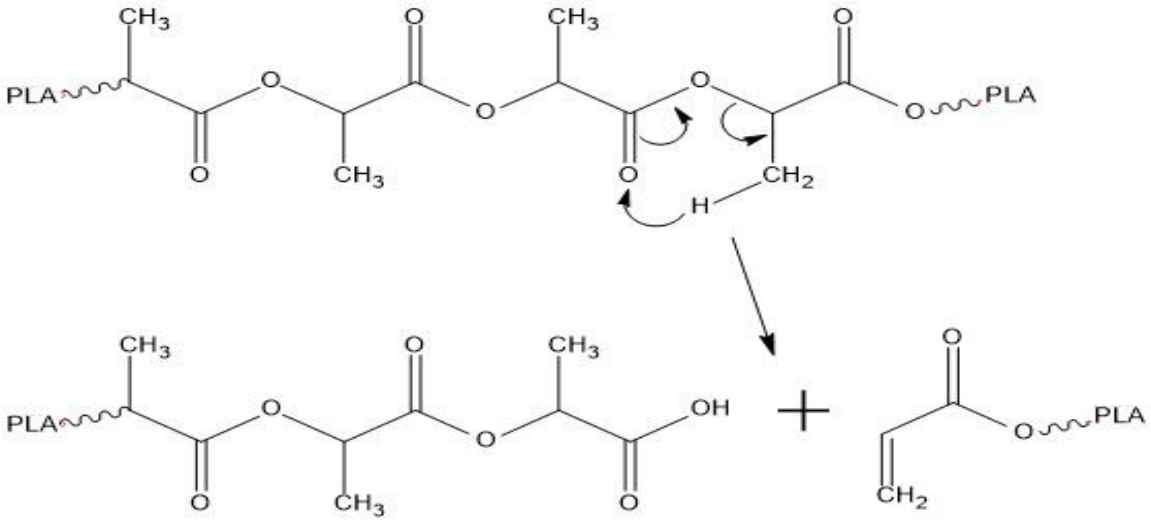

Scheme 1.3. Chain cleavage by pyrolytic elimination.

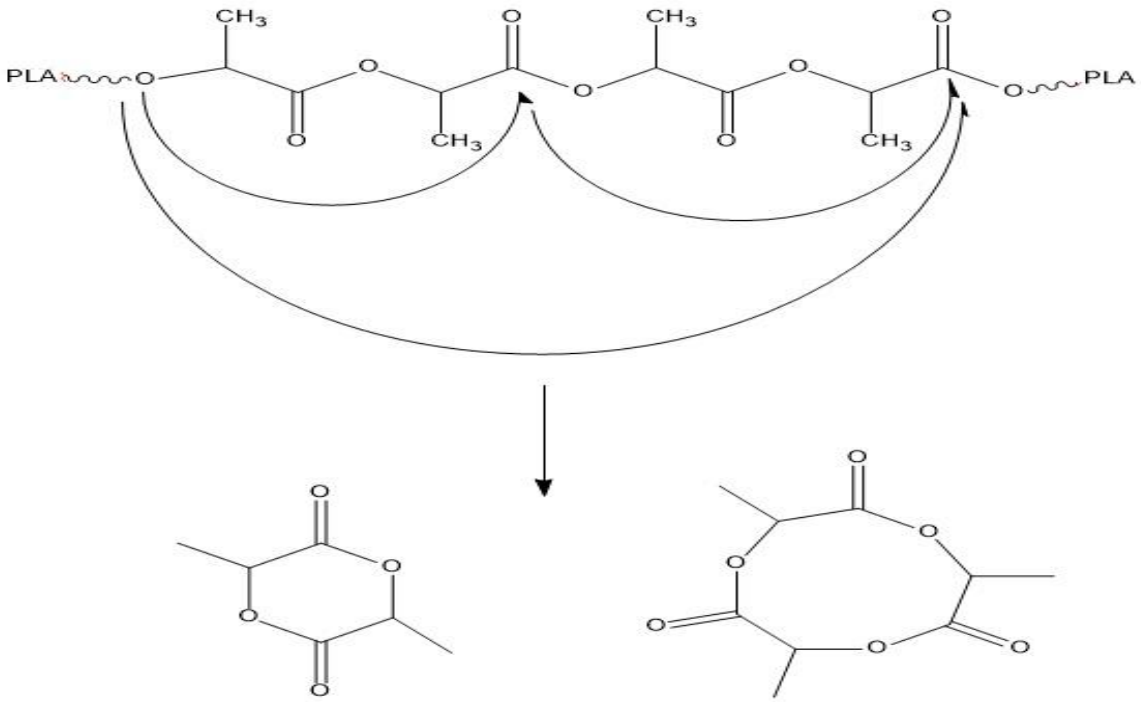

Scheme 1.4. Unzipping polymerization (end chain opening or depolymerization).

1.4.2. Melt strength and rheology of PLA

Rheological study on the viscoelastic characteristics of PLA melt is essential in order to address and solve the instability in the melt strength arising by the change due to chain cleavage during extrusion process at high temperature and shear. Melt strength of a polymer can be expressed as the ability of the polymer melt to withstand maximum force in which thread can be drawn under standard condition before it breaks or deformed by the influence of gravity during stretching in molten state. It is one of important characteristics of any thermoplastic

polymers in order to be processed using various processing techniques such as film blowing and foaming [22]. The melt strength is strongly affected by the molecular weight, molecular weight distribution (MWD) and macromolecular chain topology [23]. It increases with increases molecular weight and broader MWD. Long chain branching and crosslinking chain topology have a tendency to increase the melt strength significantly as compared to linear polymer due to an increase in polymer entanglement. However, short chain branching cannot improve the melt strength, since it is difficult to form entanglement within the polymer matrix. Mostly, the melt strength is related to the elastic modulus and loss angle, in which the improvement can be correlated with the increment in the elastic modulus and reduction in loss angle.

Dynamic small amplitude oscillatory shear study is the crucial technique used to estimate the shear viscosity of viscoelastic materials. For polymers like PLA, dynamic frequency analysis is the best technique to collect sufficient data about the macromolecular change and entanglement nature within sort period before any thermal degradation during analysis. As already mentioned above, PLA is highly sensitive to thermal degradation at high temperature, which makes it difficult to expose to high temperature and shear for longer time during melt rheology investigation. Therefore, dynamic frequency investigation is more preferable than steady shear test. According to Cox-Merz rule, the shear rate and frequency can be considered as equal so that shear rate dependence of steady shear viscosity is equal to the frequency dependence of complex viscosity [24]. Dynamic frequency sweep analysis used to provide reliable result about the viscosity (measured as of complex viscosity) of viscoelastic materials up to frequency of 500 rad/s. In most cases, for polymer matrix composed of linear chains, viscosity is nearly independent of frequency as it approaches to zero and termed as zero shear

viscosity or Newtonian plateau. Zero shear viscosity is an important parameter which depends on the molecular weight of the polymer matrix [25]. For known polymers, zero shear viscosity is used to estimate the molecular weight by applying Mark-Houwink equation [26].

PLA, similar to many of thermoplastic polymers, is found to have a non-Newtonian characteristic with pseudoplastic nature [27]. Maximum information can be extracted about the chain entanglement and macromolecular chain topology using the analysis based on strain and frequencies sweep. There are different methods used to examine the linear viscoelastic (LVE) characteristics of polymers including creep (constant force), stress relaxation (constant strain) and small amplitude oscillatory shear analysis. Small amplitude oscillatory shear test is the most frequently used analysis technique to estimate LVE range (i.e. constant storage modulus is observed at low strain followed by reduction with nonlinear response as the strain increased above the deformation limit of the melt) and has been used as preliminary procedure to fix the strain rate before performing frequency sweep test [22]. The frequency sweep analysis which is performed within the linear viscoelastic region can provide deeper insight about the polymer melt and important information can be obtained from the dynamic properties of change in complex viscosity (η*), storage modulus (G`), loss modulus (G``) and loss angle (tan δ) with respect to frequency (ω). These dynamic properties of a polymer are influenced by the experimental condition (stress, strain and temperature) when the polymer melt is exposed to sinusoidal stress and strain on rotational rheometer. Therefore, the response of the polymer melt to known external sinusoidal stress and strain is measured at constant or transient temperature. In general, perfectly elastic materials develops stresses that are in-phase with strain applied with zero phase angle. On the other hand, when the same stress is applied to a Newtonian viscous liquid, the stress will not be in-phase with the strain and shows phase angle

of 90º. However, viscoelastic martials (polymer melt) exhibit phase angle between zero and 90º (0º < δ < 90º). The viscoelastic characteristic can be expressed by Maxell fluid response as shown in **Eqn. 1.1** in terms of the stored energy (storage modulus (G`)) and viscous dissipation (loss modulus G``) [28].

$$\sigma/\gamma_0 = G' \sin(\omega t) + G'' \cos(\omega t) \quad 1.1$$

Depending on the entanglement nature of the polymer chain, M_W and polydispersity index (PDI), higher values of storage modulus as compared to loss modulus can be obtained which reflects the elastic or solid like nature of the melt. On the contrary, for viscous dominated polymer melt the loss modulus become higher. The point at which the storage modulus become equal to the loss modulus (G`=G``) is termed as cross over point. The characteristic relaxation time of polymer chain at the molten state can be estimated from the inverse of cross over frequency. For a single relaxion time, the storage and loss modules can be expressed by **Eqn. 1.2 and 1.3.**

$$G'(\omega) = G\frac{(\tau\omega)^2}{1+(\tau\omega)^2} \quad 1.2$$

$$G''(\omega) = G\frac{\tau\omega}{1+(\tau\omega)^2} \quad 1.3$$

When the frequency (ω) is equal to the reciprocal of characteristic relaxation time (τ), the two modulus (G` and G``) cross over. At lower frequency the terminal region of the modulus obey the scaling low of $G' \propto \omega^{\beta}$ *and* $G'' \propto \omega^{\alpha}$ in which β and α approaches to 2 and 1 respectively for linear polymers and deviates to lower values depending on the polymer entanglement and percolation effect due to the addition of fillers. Polymer melt with multiple N relaxation time the viscoelastic modulus are expressed as displayed in **Eqn. 1.4 and 1.5.**

$$G'(\omega) = \sum_{i=1}^{N} G_i \frac{(\tau_i \omega)^2}{1+(\tau_i \omega)^2} \quad 1.4$$

$$G''(\omega) = \sum_{i=1}^{N} G_i \frac{\tau_i \omega}{1+(\tau_i \omega)^2} \quad 1.5$$

The overall resistance of deformation (complex viscosity) and the loss factor can be evaluated form the storage and loss modulus as shown in **Eqn. 1.6** [29].

$$G^* = G' + iG'' \quad 1.6$$

The time distribution of the polymer chains relaxation is expressed by weight relation spectra λ.H(λ) which is calculated from linear relaxation spectra H(λ) using the information of complex modulus as expressed in **Eqn. 1.7** [30].

$$G^* = \int_{-\infty}^{\infty} \frac{H(\lambda) i\omega\lambda}{\lambda(1 + i\omega\lambda)} \quad 1.7$$

The chain relaxation and percolation effect have been discussed using different important plots, such as Han plot, Cole-Cole plot and Van Gurp plot (vGP). Han plot is the plot of storage modules versus loss modulus which helps to understand the dependency of solid like behavior on the viscous dissipation. Cole-Cole plot is a plot of imaginary viscosity ($\eta'' = G'/\omega$) versus real viscosity($\eta' = G''/\omega$). Linear polymers with single relaxation time exhibits semicircular curve. Deviation from this arc occurs due to increment in chain entanglement, which leads to additional relaxation and agglomeration arises because of the incorporation of fillers. The widening of the arc can be correlated with the zero shear viscosity of the melt which reflect the molecular weight of the matrix. Another important plot is Van Gurp plot (vGP) (phase angle vs log G*) which can be used as a tool to understand the chain topology. The phase angle can be estimated from the ratio of loss modulus and storage modulus as shown in **Eqn. 1.8.**

$$\tan(\delta) = \frac{G''}{G'} \qquad 1.8$$

Similarly, Complex viscosity is expected to increase as the frequency changes from higher to lower values. Numerous models have been developed to estimate the flow behavior from the complex viscosity data. One of most frequently used model is Carreau-Yasuda model [24]. Which is a five parameter model used to estimate zero shear viscosity, flow behavior and the characteristic relaxation time from complex viscosity vs frequency data with consideration of Cox-Merz rule. High viscosity linear PLA is observed to exhibit zero shear viscosity around 1000 Pa.s at 190 ºC in which it is expected to decrease with reduction in molecular weight. Reactive modification in macromolecular chain topology of PLA (i.e. long chain branching and crosslinking), have a tendency to increase the entanglement which is the main reason for the increment in zero shear viscosity and change in shear thinning behavior of the melt. The effect of macromolecular chain topology of PLA on the rheological characteristic was studied in depth by **Dorgan et al.,** Based on their observation, zero shear viscosity is mostly dependent on the molecular weight and also highly affected by the architecture of the polymer chain. Short chain branching is observed to decrease the zero shear viscosity because of the reduction in radius of gyration and less entanglement of the chain. However, above some critical branching chain length, an increase in zero shear viscosity is observed for the polymer melt due to the increase in the entanglement of the chains [31]. It is well known that, the chain extension and crosslinking of PLA can significantly affect the shear thinning behavior. The Newtonian behavior is observed to shift to lower frequency and zero shear viscosity is used to increase for chain extended PLA as compared to linear PLA. This phenomenon has been explained by the entanglement molecular weight, which is estimated form the cross over

frequency and plateau modulus (G^o_n). The plateau modulus of linear polymers can be estimated from the frequency sweep analysis of storage modulus as shown in **Eqn. 1.9.**

$$G'(\omega) = G_n^o + \left(\frac{c_1}{\omega^{c_2}}\right) \quad 1.9$$

Change in storage modulus with frequencies can be fitted to estimate the plateau modulus where c_1 and c_2 are constants. **Wu et al.,** proposed empirical equation to estimate the plateau modulus for semi-crystalline polymers based on the cross over modulus (G_c) (modulus at the cross over frequency point) and polydispersity index (M_w/M_n) as indicated in **Eqn. 1.10 [32]**.

$$\log\left(\frac{G_n^o}{G_c}\right) = 0.38 + \frac{2.63\log\left(\frac{M_w}{M_n}\right)}{1 + 2.45\log\left(\frac{M_w}{M_n}\right)} \quad 1.10$$

It has been known that, with increasing molecular weight the macromolecular chain relaxation time is intended to increase. This long range relaxation phenomenon is significantly influenced by the entanglement molecular weight which can be estimated from the plateau modulus as described in **Eqn. 1.11.**

$$M_e = \frac{\rho RT}{G_n^o} \quad 1.11$$

So far, the advantages and the limitations of PLA have been discussed. The attractiveness of PLA in the market and research fields is growing due to its cumulative abundance, comparative economical affordability and adequate industrial performance. However, the limitations related to melt processing of PLA in industrially viable techniques need to be addressed properly. Thermal degradation of PLA under high temperature and shear, which leads to molecular weight reduction; relatively low melt viscosity and strength; poor gas-liquid barrier properties, brittleness etc., have to be enhanced in order to improve the processability

performance and application span [33, 34]. Various approaches have been proposed to overcome the limitation, including blending with different polymers, composite preparation, steriocomplextion and reactive extrusion with chain extenders [35-39].

1.5. Reactive extrusion of PLA

Reactive extrusion in the presence of chain extenders have been demonstrated as one of the best mechanism to enhance the limitation of PLA related to melt processing. Chain extenders have a significant tendency to generate radicals at particular processing conditions. It can be used as coupling agents or radical formulators on the backbone of the polymer chain allowing chain modification by crosslinking and branching. The active sites of chain extenders such as epoxide group, hydroxyl, carboxylic, isocyanate and peroxides can react with the carboxyl, hydroxyl and abstraction of H from the main chain for radical formation at the backbone [23, 30]. Reactive extrusion can also enhance the grafting efficiency, when PLA is melt blended with highly surface active fillers. Various properties can be tailored because of enhanced adhesion between PLA matrix and fillers due to grafting. Dicumyl peroxide (DCP) has been proved as an effective radical generator and utilized for macromolecular structural modification of PLA. Grafting of PLA chains on the surface of cellulose nanocrystals is observed to be enhanced by reactive extrusion using DCP [40].

1.6. Biofillers reinforced PLA

The processing and application performance of PLA can be tailored by incorporation of fillers (organic and inorganic). Organic fillers or biofillers can be categorized as polysaccharides and proteins under the class of biopolymers such as cellulose, gum, chitosan and silk. They have a number of attractive properties with abundancy, low cost and sustainability towards the fabrication of fully biodegradable PLA composites for improved barrier, mechanical and

thermal properties. However, high surface functionality of biofillers is considered as a major challenge to have a good dispersion inside the polymer matrix and a tendency to participate as a degradation agent during melt processing. Due to this, fabrication and processing of PLA based biocomposite becomes a challenging task. Surface modification of biofillers can enhance the compatibility with polymer matrix and give better desperation. Some of the biofillers used frequently for the fabrication of PLA based biocomposites are described below:

Cellulose: It is one of the most abundant, strong and stiff fiber to be used as reinforcement in different aspect ratio. Its superior mechanical properties and low cost makes it suitable to prepare fully biodegradable PLA composite. Cellulose can be prepared in the form of fiber, micron and nano size crystalline particles [41]. Hydrophilic nature of cellulose decreases the surface adhesion properties when it is mixed with PLA, which is having hydrophobic characteristics. Due to this, agglomeration occurs and dispersion of the filler is difficult particularly at higher loading.

Chitin/Chitosan: Chitin is the second most abundant biopolymer next to cellulose. It is a polysaccharide with linear polymeric structure of N-Acetyl-D-glucosamine linked by α (1, 4) glycosidic bonds, which is found in various crustacean sources such as shrimp shells, crabs and lobsters. Highly nanocrystal chitin (α –chitin) can be obtained by removing the amorphous part from the chitin micro fibrils. A cationic polysaccharide/chitosan is a derivative of chitin which can be formed by deacetylation of chitin. Both biopolymers show an excellent applicability as a biofiller for PLA with antioxidant, antimicrobial, and antifungal characteristics. However, similar to cellulose, the hydrophilic nature of chitin/chitosan limits the dispersion in the hydrophobic PLA matrix [42, 43].

Gum: Gum is a naturally existing polysaccharide with special properties of binding and adhesive characteristics. It has been used as an emulsifier, stabilizer, thickening and gelling agent. It has the ability to improve the elastic properties of PLA with remarkable reduction in gas barrier properties.

1.7. Silk: High performance biomaterial

Silk is a natural protein, which is produced from a number of animals, mainly silkworms and web-weaving spiders. It has excellent tensile strength which is comparable with Kevlar. Silk fibre structure is constructed with two distinct proteins, fibroins and sericins. Fibroins are composed of smaller diameter bundles (~100 nm) aligned with longer length in fibre axis. Silk fibroin is hydrophobic in nature, which due to the strong linkage of the heterodimeric proteins of large chain fibroin (395 kDa) as well as two small units of 25 kDa (light chain fibroin and P25 proteins). Fibroin is constructed by $(Gly\text{-}Ser\text{-}Gly\text{-}Ala\text{-}Gly\text{-}Ala)_n$ (**Fig. 1.3)** building block which gives remarkable macrostructure of anisotropic β-sheet nanocrystals [44, 45]. Sericin (25-30 % of the fibre) is glue-glycoprotein which plays a major role as cohesive agent for the fibre [45, 46].

The mechanical properties and biocompatibility of silk fibre provides wide applications in various areas such as paper, textile, wound dressing, drug delivery, tissue engineering etc. The extensive hydrogen bonding provides hydrophobic nature and high crystallinity gives superior stability and attractive features to be studied as reinforcing biofiller for different polymers. The crystalline portion can be isolated by simple alkaline or acid hydrolysis and can be used as different size and shapes of fibres, microcrystals or nanocrystals. The hydrophobic nature of silk is a key characteristic to disperse it in the hydrophobic PLA matrix, which is absent in cellulose, chitosan and gum. Highly crystalline and thermally stable silk fibroin is an attractive

material which is not yet fully studied as biofiller for PLA matrix and a lot can be investigated to improve the performance limitations of PLA, which are discussed above.

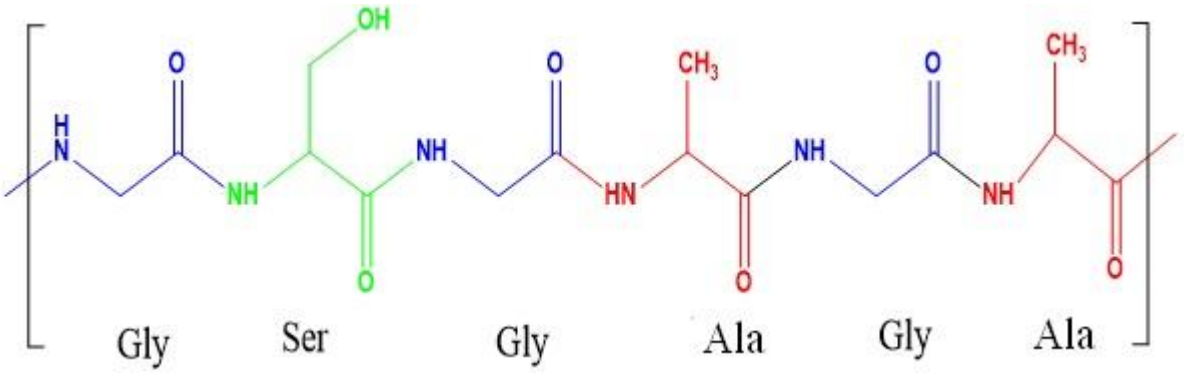

Figure 1.3. Amino acid repeating units of silk fibroin.

1.8. Reinforcement methods

Biofillers can be dispersed in the polymer matrix using different techniques. Most commonly used techniques are: solvent mixing, in-situ polymerization and melt compounding.

Solvent mixing: In this method, biofillers are dispersed in a solvent in which the polymer matrix is solubilized easily. Depending on the mixing mechanism such as mechanical stirring and ultra-sonication, proper dispersion of the biofillers can be achieved in the solvent. After dispersing the biofillers into the polymer matrix, the solvent needs to be evaporated. However, this technique is not industrially viable and difficult to apply in mass production.

In-situ polymerization: In this technique, the active sites of biofillers are modified by initiating the grafting of lactic acid oligomer in order to decrease the hydrophilicity of the biofillers so as to substantially improve their dispersion in the hydrophobic PLA matrix. In-situ polymerization is highly affected by the heating source. Microwave heating facilitates the

reaction giving the required grafting at lower time as compared to conventional heating source. Solution mixing or melt compounding can be used to disperse the modified biofillers inside the PLA matrix.

Melt compounding: Melt compounding involves mixing of biofillers in PLA matrix during a molten state. The dispersion is highly dependent on the processing condition and the filler-to-polymer interaction. Even though melt compounding is easy and industrially viable to produce the required biocomposite in mass production, the dispersion of biofillers within highly thermally sensitive PLA has been identified as a major challenge due to high surface functionality of biofillers and hydrophobic nature of PLA matrix. Furthermore, agglomeration is observed and the biofillers act as degradation agents leading to the reduction in molecular weight.

Generally, melt processing of PLA requires special attention and different reinforcing agents need to be tested in order to get stabilized or improved melt strength without compromising the desired properties.

1.9. Recycling of PLA

Recently, recycling of PLA is becoming an emerging research area with the objective of finding optimum utilization of the material instead of allowing end used PLA to natural degradation. Various recycling strategies of PLA are reported in literature including, reprocessing, chemical recycling, pyrolysis and composting. According to the comparative study done by **Piemonte et al.,** reprocessing of PLA is more preferable than other waste utilization techniques such as, composting and pyrolysis/incineration in terms of feedstock consumption, energy saving and greenhouse gases. Effective recycling of PLA into its

monomer or lower molecular weight re-polymerizable oligomer is also getting much more attention in literature since low cost monomeric unit can be generated as compared to the usual fermentation process [47].

1.9.1. Mechanical recycling of bioplastics

Mechanical recycling is one of the simplest and best energy saving technique to reuse PLA wastes using multiple reprocessing methods under the same system in which the primary product is produced. Reprocessing is mostly done under high temperature and shear, which leads to material degradation when subjected multiple times under these conditions. Therefore, the impact of thermomechanical degradation upon multiple reprocessing on the important physical, mechanical and thermal properties of bioplastics need to be addressed in an appropriate manner. **Pillin et al.,** studied the rheological and mechanical properties of PLA which was subjected to seven reprocessing cycles using moulding machine. Based on their study, only tensile modulus remain constant with the thermo-mechanical cycles while stress and strain at break, rheological properties are found to decrease. This dramatic deterioration can be related to a large decrease in the molecular weight. The possibility of maintaining the properties through molar mass stabilization is also discussed using two chain stabilizers Tropolone and Quinone. Quinone is observed to be an efficient stabilizer to trap free radicals and maintain the molecular weight at the same processing conditions. Due to these, mechanical properties are observed to be improved with reprocessing cycles [48].

In another study, the effect of multiple (up to 10 times) extrusion of PLA on its mechanical properties (determined by a static tension test), Charpy impact strength, melt flow rate, phase transition temperatures, degradation temperature, and permeability of water vapour and

oxygen investigated and reported by **Zenkiewicz et al.,** It is found that with increasing the number of the extrusion cycles, the tensile strength at break slightly diminished and the impact strength clearly decreased, while the melt flow rate and water vapour and oxygen transmission rates steadily increased. Variation of the number of extrusion cycles did not affect the T_g values whereas it led to lowering of the cold crystallisation temperature (T_{cc}) and slight diminishing of the T_m. Based on their investigation, they concluded that PLA is a technological waste which is suitable to be reused as an additive to a pristine polymer [49].

The effects of multiple extrusion on the structure and properties of amorphous poly (lactide) (PLA)**,** and the change on morphology, segmental dynamics, thermal and mechanical performance related to thermomechanical degradation are also addressed by **Badia et al.,** The influence of the thermomechanical degradation induced by means of five successive injection cycles was initially addressed in terms of macroscopic mechanical properties and surface modification. A deeper inspection on the structure and morphology of PLA is associated to the thermal properties and viscoelastic behaviour. Although FT-IR analysis does not show any significant changes in functional groups, and reduction in molar weight is found by viscometer. PLA is continues to remain amorphous throughout the reprocessing cycles, and a cold-crystallization region is observed during DSC and DMTA measurements, whereas increasing enthalpy with each reprocessing step suggested chain scission due to thermomechanical degradation. The effect of chain shortening on the glass rubber relaxation, studied by DMTA showed an increase in free volume affecting the segmental dynamics of PLA particularly after the application of the second reprocessing step [50].

Duigou et al., investigated the recyclability of flax/PLLA (poly (L-lactide)) biocomposite (20% and 30% fibres by weight) for the advantage of biocompatibility of natural fibre-

reinforced biopolymers, also known as biocomposites. Their main objective was providing an attractive alternative to glass fibre-reinforced petrochemical polymers. Mechanical properties are evaluated initially, which are found to be similar to those of glass/ PP composites. Thereafter under repeated injection cycles, tensile properties are found to be conserved until the third cycle. Molecular weight, thermal and rheological measurements are performed to study the effect on mechanical properties, matrix degradation and reduction in fibre aspect ratio. They observed a lower molecular weight, lowering of glass transition temperature, reduction of fibre length, and separation of fibre bundles with injection cycles. Nevertheless, the property retention after three cycles under extreme recycling conditions (100% recycling with no added virgin polymer) indicate the promising recyclability of these materials [51].

1.9.2. Chemical recycling

To study the possibility of producing monomers or re-polymerizable oligomers, the reaction mechanisms need to be addressed. For example, PLA undergoes three reversible reactions during depolymerisation. Firstly, carbonyl carbon in the polymer chain undergoes rapid protonation where the carbonyl oxygen is converted to the second hydroxyl group. Secondly, the hydroxyl oxygen of the added hydroxyl-bearing molecule slowly attacks the protonated carboxyl carbon atom. Thirdly, the carbonyl oxygen (which was converted to hydroxyl group in the first step) and a proton are rapidly removed to form a water or simple alcohol and catalytic proton. The removed by-product type from the third stage depends on the type of the nucleophile. Most of these depolymerisation techniques take place under pressure, heat and catalyst. The combination may give an advantage to the energy economy of lactic acid recovery process. The reaction mechanisms can be broadly classified into backbiting, intra-molecular trans-esterification and inter-molecular trans-esterification. The final product type depends on

temperature and catalyst concentration and the possible outcomes of the reaction are lactic acid, L-lactide, D-lactide, meso-lactide, cyclic oligomers and randomly degraded polymer chains. Chemical recycling of PLA is generally achieved by hydrolysis, alcoholysis, and thermal depolymerization.

Hydrolysis: Highest yield of L-lactic acid (96 %) can be achieved through hydrolysis of PLA at high temperature (270 ºC) within 8 min in batch system [52]. The efficiency of recovering the monomeric unit is highly dependent on the processing conditions. In a study done by **Tsuji et al.,** it was revealed that irrespective of the physical state of PLA (solid or melt state), depolymerisation occurs due to bulk erosion mechanism at a temperature range of 120 ºC-190 ºC. The depolymerization time to recover more than 95% LA in the solid state (at 120 ºC) take 4,000 min whereas under melt state (at 180 ºC) the same can be achieved in 130 min. The use of lower temperature range (120ºC to 190ºC) resulted in a 100-fold increase in depolymerization times as compared to the higher temperature range (250ºC to 350 ºC) [53]. Complete degradation/depolymerization of PLA was observed in aqueous sodium hydroxide solution (NaOH) media. 8 g of NaOH per 10 g of PLLA is required to degrade PLA completely at a temperature of 180 ºC and 160 ºC within 20 min and 60 min respectively [54]. It is important to note that, this is relatively a large quantity of sodium hydroxide, which limits the scale-up process.

In general, hydrolysis of PLA requires high pressure reaction condition which makes it energy intensive. Even though, the presence of basic and acidic medium can facilitate the depolymerisation, the reaction mode (batch process) makes it inefficient as compared to continuous process.

Alcoholysis: Substituting water (weak nucleophile) by alcohols have a tendency to facilitate the reaction and help the depolymeriztion to take place at a lower temperature and pressure relative to hydrolysis. Small carbon chain alcohols and macro molecules of diols can be used as depolymerization agents [55-57]. By using macromolecules having more than one active site, rapid depolymerization can be achieved in a controlled reaction condition. Ionic liquids are used as a catalyst to improve the depolymerisation rate as well as the recovery of the final product [58].

Effect of reaction system needs to be selected on the basis of purity and yield of monomeric unit at minimized temperature and time. Reaction rate is controlled by the diffusion of depolymerization agent (solvent/ catalyst/initiators) into the polymer chain and their activity on macromolecular level. Sufficient mixing environment is required for the reaction to provide maximum homogenization or good stoichiometry in order to complete the reaction within reasonable short time and temperature. Reaction medium such as alcohols, water and ionic liquids coupled with mechanical stirring, ultra-sonication, microwave radiation or supercritical condition increases the rate of depolymerization. Temperature, pressure, initiators and PLA/catalyst ratio influence yield of the final product. Recently microwave reactors are observed to play a vital role in a number of chemical reactions. They provide a concentrated energy to the reactant which helps to minimize the reaction time and energy significantly as compared to the conventional techniques[56].

Thermal depolymerisation: PLA chains open up from the end by back biting reaction and release lactides in a controlled unzip depolymerization above 250 ºC. Compounds (alkoxides, organic acid and enolate salts) of Al, Ti, Zn and Zr have been evaluated to substitute stannous 2-ethylhexanoate ($Sn(oct)_2$) [59, 60]. The purity of lactides are observed to be dependent on

the catalyst concentration and temperature [61, 62]. US Patent filed by **Narayan et al.,** in 2013 describes the mechanism of thermal depolymerisation of PLA with the possibility of batch and continuous production of lactides [63]. The invention provides direct production method of lactide from PLA waste using thermal depolymerisation. Generally, the method has the following stages: pre-heating, depolymerisation and lactide recovery. PLA feedstock is fed into a PLA preheater, where the temperature is maintained at around 190° C (above PLA melting temperature 173-178° C.). After melting, PLA liquid is pumped into PLA depolymerization reactor. The temperature of the reactor is maintained at around 200° C and the reactor headspace is maintained under near vacuum condition (0.1 bar). Catalyst like Ti(ll) ethyl hexanoate (but not limited to it) are used to depolymerize PLA into lactide. Lactide produced in the form of vapour, recovered continuously from this stage and changed into liquid state in the condenser at 100 ^{0}C which is above the melting point of lactide (96 ^{0}C). They proposed the process to be operated with either continuous feeding mode (PLA feed stock is fed to the system continuously via the preheater and then PLA liquid is fed to the reactor and lactide recovered continuously) or fed batch mode (with fed batch mode, the PLA liquid is fed to the reactor till 1/2-1/3 reactor volume and the feed is stopped and the lactide recovered continuously). PLA feedstock was melted in a preheater at 170° C and the liquid PLA intermediate transferred into the reactor. At a temperature range between 195° C - 200° C, depolymerization occurred in the presence of Ti(ll) catalyst (0.05-0.1%, w/w). They have reported that the conversion efficiencies of PLA to lactide are greater than 91- 95% (w/w) and the products are mainly L-lactide, with less than 10% of meso-lactide and cyclic oligomers [63].

1.10. New approach to recycle plastics wastes

Recently, combustion of waste polymers along with biodiesel for their advantage of high calorific value as recycling technique is becoming an emerging area of study. Conventional polymers like polystyrene (PS) shows good miscibility characteristics with biodiesel. Important parameters determining the quality of biodiesel such as the flash point, density, viscosity and cloud point as well as engine performance have been taken into significant consideration. Solubility and dissolution kinetics plays a major role in formation of one phase solution. Because there is no published report on diesel-biopolymers dissolution study, few papers on conventional polymers are reviewed. The dissolution behaviour of polystyrene (PS) and low-density polyethylene (LDPE) in biodiesel was studied by **Zhang et al.,** wherein they observed that PS [17.79–18.61 $(J/cm^3)^{1/2}$] is more soluble than LDPE [16.16–16.56 $(J/cm^3)^{1/2}$] in biodiesel [17.56 $(J/cm^3)^{1/2}$]. The shear viscosity of the polymer solutions is measured to ascertain their suitability as fuel mixtures. Diffusion of polymer chains through a boundary layer adjacent to the polymer/solvent interface control the dissolution of PS [64]. Test results showed that, engine power increased initially with the polystyrene concentration and then decreased for concentrations higher than 5%. The initial increase in engine power was mainly due to the injection timing advancement caused by the increased bulk modulus and viscosity of fuel blends. The declination in engine power at high polystyrene concentrations could be caused by the poor spray atomization and deteriorated combustion efficiency due to the high viscosity of polystyrene mixtures. Emissions of NOx, soot, CO, and HC are found to increase with the polystyrene concentration if the injection timing was free to advance due to the increased bulk modulus and fuel viscosity [65, 66]. This technique can be adapted as one of

the recycling technique for PLA, in which the reprocessing and other techniques become more difficult.

1.11. Research question, hypothesis and choice of systems

Research work presented in this thesis is based on the following hypothesis:

1st Hypothesis: Highly crystalline and thermally stable hydrophobic silk nanocrystals can be dispersed inside hydrophobic PLA in order to significantly enhance the crystallization characteristics and melting behavior, rheological and thermal stability along with processability performance of PLA.

2nd Hypothesis: If sufficient radicals are produced by the help of effective radical initiators at high temperature and shear, the degradation reactions can be dominated by the chain extension reaction, giving more stable chain architecture with longer chain branching and crosslinking. Furthermore, there might be a chance of PLA chains being grafted onto the active sites of silk nanocrystals (SNCs), which may significantly improve the crystallization characteristics and melting behavior along with rheological and thermal stability of PLA.

3rd Hypothesis: If randomly degraded PLA can easily dissolve in vegetable oils, it can be used for improving the viscosity in order to be utilized as a biolubricant. Furthermore, low molecular weight PLA oligomers can be used as an additional oxygen source for biodiesel to facilitate the combustion process and improve the cold flow properties by altering the crystallization phenomenon of biodiesel at low temperature.

Research questions: The present research work aims to answer the following major research questions

1. What is the role of thermally stable and highly crystalline biofiller on the processability performance of PLA and how the rheology and thermal stability can be improved by using chain extender through reactive extrusion?
2. Can we reuse PLA even after several reprocessing cycles and how the PLA waste can be converted into valuable product?

Choice of systems: The present study is framed on the basis of the following systems and characterization techniques.

- SNCs are used as fillers which is fabricated by simple acid hydrolysis technique, as mentioned elsewhere and characterized by FTIR, XRD and polarized optical microscope (POM) techniques.
- Minilab twin screw extruder is selected for melt blending of PLA and SNC, for melt processing studies and reactive extrusion. Possible changes are examined using less amount of materials in a controlled way. Various characterization techniques are selected to analyze the samples after extrusion which include, differential scanning calorimetry (DSC) and polarized optical microscope (POM) are used to study the crystallization and melting behavior; thermal gravimetric analysis (TGA) coupled with FTIR is used to investigate the thermal stability and evolved gasses; viscoelastic behavior is studied by dynamic mechanical analysis (DMA) and rheometer; solution viscosity properties, gel permeation chromatography (GPC), optical polarimetry, FTIR and nuclear magnetic resonance (NMR) studies are performed to understand the chemical structural changes; morphological changes are studied using FESEM and XRD.

- Temperature controlled microwave reactor is selected to randomly degrade reprocessed PLA by using lactic acid/water mixture. Degraded PLA blended with soybean oil in various composition and viscosity at different temperature is measured to study the impact on flow behavior under shear. Dynamic viscosity at different temperatures are analyzed using con and plate rheometer. Furthermore, PLA oligomers are tested as an additive for a biodiesel (prepared from soybean oil using microwave reactor) to enhance the cold flow properties. Cloud point, pour point, flash point and fire point of OLLA blended biodiesel are tested using ASTM standard. Rheometer is used to understand the cold flow properties and flow transitional behavior. Polarized optical microscope (POM) is used to understand the crystal growth and change in morphology at lower temperature ranges. Internal combustion engine test is performed to see the impact of PLA oligomers on the engine performance and emission characteristics.

1.12. Scope and objectives

To answer the above mentioned research questions based on the proposed hypothesis, this research mainly focuses on the improvement of melt processability performance of PLA and its recycling opportunity as a biolubricant and biodiesel additive according to the following objectives.

- Investigate the impact of acid hydrolyzed silk fibrous (silk nanocrystals) on the molar mass distribution of PLA at different processing conditions.
- Investigate the effect of silk nano-crystals on the macromolecular structural change, thermal stability and viscoelastic properties of PLA during multiple extrusion cycle.
- Investigate the effect of silk nanocrystals on the thermal decomposition behavior of melt processed PLA.

- Study the influence of DCP (radical initiator) on the melt strength of PLA in the presence of SNC through reactive extrusion.
- Study the effect of randomly degraded PLA and low molecular weight PLA on the biolubrication properties of vegetable oil and cold flow properties of biodiesel.

1.13. Outline of the thesis

This PhD research work provides fundamental and applied research analysis which is described systematically in the following chapters:

Chapter 1: Introduction and Literature Review

In this chapter, a compressive literature of published articles related to the theoretical aspects of the thesis are reviewed. Research question, hypothesis and objectives of the thesis are formulated.

Chapter 2: Materials and Methods

In this chapter, the materials used, experimental procedure followed, the characterization techniques and equipments used are described.

Chapter 3: The Impact of Silk Nanocrystals on the Molar Mass Distribution of Melt Extruded Poly (lactic acid)

In this chapter, silk fibroin is investigated to be used as a biofiller for PLA. The influence of acid hydrolyzed silk fibroin (silk nanocrystals) on the molar mass distribution of PLA is assessed at different processing conditions (temperature, screw speed and residence time). Additionally, important characteristics including, thermal stability, structural and viscoelastic properties are assessed.

Chapter 4: The Influence of Silk Nanocrystals on Processability Performance of PLA: Studies on Thermal Stability, Crystallization Kinetics, Solution and Melt Rheology

The effect of reprocessing cycles and the influence of silk nanocrystals on the thermal and rheological properties of PLA is addressed. Crystallization and melting behavior is studied and Avrami equation used to describe the phenomenon. The impact of SNC on the viscoelastic properties of multiple times extruded PLA is also discussed with help of dynamic mechanical analysis and melt rheology investigation.

Chapter 5: Decomposition Behaviour of Silk Nanocrystals Stabilized Melt Extruded Poly (Lactic Acid) Nanocomposite Films: Effect of Recycling on Thermal Degradation Kinetics and Optimization Studies

The influence of silk nanocrystals on thermal stability and evolved gas characteristics of PLA is discussed with help of thermal gravimetric analysis coupled with Fourier transformation infrared spectroscopy (TG-FTIR). Different models from isoconversional and model fitting techniques are used to evaluate the degradation kinetics. Moreover, kinetic triplets are optimized by using Nelder-Mead simplex method.

Chapter 6: Silk Nanocrystals Grafted Poly (Lactic Acid): The Influence of Reactive Extrusion on Rheology and Thermal Properties

This chapter describes the possible grafting of SNC on PLA backbone and its impact on the improvement of the melt strength of PLA through reactive extrusion.

The impact of chain topology on rheological, thermal and crystallization properties are presented in depth.

Chapter 7: Recycling of Reprocessed PLA Films for a Targeted Application as Biolubricants and Biodiesel Additives.

This chapter describes the possible recycling alternatives of utilizing randomly degraded PLA films as biolubricant additives. Significant characteristics such as viscosity and viscosity index are estimated using appropriate procedures for all formulations. Moreover, the effect of short chain oligomers on cold flow properties of biodiesel is addressed in this chapter. Optimized preparation of biodiesel using microwave reactor and evaluations of important properties before and after the addition of PLA oligomer is carefully studied and the effect on the car engine performance and exhaust gas characteristic are included.

Chapter 8: Overall Conclusion and Future Work

This chapter conveys the overall summary, major findings and an outlook for future studies.

Chapter 2

Materials and Methods

This chapter aims to present the materials used, sample preparation methods and proper characterization techniques followed for various experiments performed in this research work. For simplicity, the material used, experimental protocols and characterization techniques are categorized into three sections. The first section describes the protocol followed in the melt processing of PLA based biocomposites; the second section describes the protocol followed for complete dissolution of melt processed PLA using lactic acid/water mixture for targeted application as a biolubricant additive; the last section describes the protocol followed for the dissolution of lower molecular weight PLA (oligomer) in a biodiesel for a targeted application in cold flow improvement.

2.1. Melt processing

2.1.1. Materials

Poly (lactic acid) (PLA) was obtained from NatureWorks (grade 2003D) with melt flow index of 6.0 g/10 min at 210 °C was used as the polymer matrix. The number average molecular weight (M_n), weight average molecular weight (M_w) and polydispersity index (PDI) were determined by gel permeation chromatography (GPC) as 135 kDa, 250 kDa and 1.82 respectively. Muga silk fibroin obtained from regional muga research station (Boko), Guwahati Assam India. Silk nanocrystals (SNCs) used in this investigation were prepared in the lab by colleague and the preparation technique is described below. Dicumyl Peroxide (DCP) purchased from Sigma-Aldrich (India) is used for reactive extrusion investigation.

2.1.2. Methods

2.1.2.1. Silk nanocrystals preparation (SNC)

Muga silk (*Antheraea assama*) cocoons were provided by regional muga silk Station, Assam, India. The cocoons were first cleaned to remove eggs and plant debris, then degummed twice using 0.5% (w/w) sodium carbonate (Na_2CO_3) at 98 °C for 30 min and then washed multiple times in de-ionized water to remove salts [67]. The degummed Muga silk fibroin was dried overnight at 60 °C in hot air oven to remove moisture. SNCs were produced via acid hydrolysis of the dried Muga silk fibroin in aqueous sulfuric acid (64 wt.%) for 2 hours at 45 °C [68]. The hydrolysate was washed multiple times with de-ionized water followed by three cycles of centrifugation (each at 10,000 rpm for 15 min) and dialysis under running tap water for 48 hours to ensure removal of free acid and a final pH of 7. Sonication was used to homogenize the dispersion. Insufficiently hydrolyzed fractions were removed by filtration. The SNC

suspension in deionized water was then freeze-dried after quench freezing with liquid nitrogen to obtain dried SNC powder for the current work.

2.1.2.2. Sample preparation for molar mass distribution investigations

After removing the amorphous part of silk fibroin using acid hydrolysis as mentioned in section 2.1.2.1, SNCs were melt blended with PLA at different processing conditions in Haake minilab co-rotating twin screw extruder. The effect of SNC on molar mass distribution of PLA is investigated at two different temperatures (185 °C and 200 °C), two screw speeds (40 rpm and 100 rpm) and at various residence time (0, 5, 10, 15, 20, 25 and 30 min.). Representative sample were taken from the middle of the strip for molecular weight analysis.

2.1.2.3. Reprocessing

The effect of SNC on reprocessing performance of PLA was studied for the nanocomposite prepared by melt mixing of PLA with 1% SNC in a Haake minilab co-rotating twin screw extruder. The nanocomposites are subsequently reprocessed four times. Each processing cycle is achieved by first maintaining the screw speed at 10 rpm (during feeding) followed by recycling of the melt inside the extruder for 1 min at 100 rpm and 200 °C. Pristine PLA is similarly processed as a control. After each reprocessing cycle, the nanocomposite and pristine PLA were collected in the form of strips and designated as Ri-SNC-PLA and Ri-NPLA respectively (where i represents the number of reprocessing cycle ranging from 0 to 4).

2.1.2.4. Reactive extrusion: Processing

Prior to the reactive extrusion process, PLA granules and silk nanocrystals were dried overnight at 60 °C under vacuum. Dicumyl Peroxide (DCP), at three different percentage

weight factions (0.5, 1 and 1.5 wt. %) is dissolved in acetone in order to coat on the surface of PLA granules and dried in oven to remove acetone. The melt blending of NPLA, nanocomposite (SNC-PLA) and the reactive extrusion in the presence of DCP were performed using Haake minilab co-rotating twin screw extruder at a screw speed of 40 rpm, 185 °C and residence time of 5 min. The samples were then collected and kept under vacuum at 40 °C before analysis. Molecular weight analysis was performed for the samples collected at 3 and 5 min. Furthermore, NPLA and SNC-PLA with 1 wt. % DCP are selected and melt reprocessed four times (at a temperature of 200 ºC, screw speed of 100 rpm and 1 min of recycling), rheological investigation is performed and the changes are compared with NPLA and SNC-PLA which was reprocessed at same condition.

2.1.2.5. SNC loading

In this research work, the loading of SNCs into PLA matrix is fixed to 1 wt.% based on the result performed by colleague; preliminary investigation considering the impact of SNC on the molecular weight. PLA/SNC bionanocomposites were prepared using different SNC loading (0.5, 1, 2, and 5 wt. %) and important properties such as barrier, mechanical, thermal properties and molecular weight were estimated. On the basis of these studies, the composite was observed to give a better performance at a lower loading of 1 wt. %. As shown in **Table 2.1,** molecular weight reduction is observed to be lower for SNC loading of 1 wt. % and it was comparable with NPLA. With increasing the loading, significant molecular weight reduction is observed which in turn leads to the deterioration of other properties. Based on this, 1 wt. % SNC loading was selected to study its impact on the melt processing and rheology of PLA and its efficacy towards the fabrication of recyclable bionanocomposite.

Table 2.1 The effect of SNC loading on molecular weight of PLA during melt processing

Samples	M_n (kDa)	M_w (kDa)	PDI (M_w /M_n)
PLA	133	234	1.75
0.5 SNC-PLA	112	208	1.85
1 SNC-PLA	120	214	1.78
2 SNC-PLA	113	201	1.77
5 SNC-PLA	60	150	2.49

2.1.3. Experimental

2.1.3.1. Intrinsic viscosity measurement

A temperature controlled Ubbelhode-type capillary viscometer was used to estimate the intrinsic viscosity of the samples at 25 ºC.

2.1.3.2. Optical polarity

The specific and optical rotation of the samples at different processing conditions (200 mg dissolved in 20 mL chloroform) were measured with AUTOPOL II polarimeter (Rudolph Research Laboratory, USA) at a wavelength of 589 nm using a self-calibrated mechanism. For the case of reactive extrusion, the samples were dissolved in chloroform for three days and filtered by 0.25 μm filters prior to the analysis.

2.1.3.3. Molecular weight analysis

Number average and weight average molecular weights of the samples were estimated using gel permeable chromatography (GPC) system (Shimadzu, communications bus module (CBM-20A), auto sampler (SIL-20A HT), liquid chromatography (LC-20A), degassing unit (DGU-$20A_{3R}$), refractive index detector (RID-10A), agilent two PL gel 5micro MIXED-D column in

series with column oven (CTO-20A)). HPLC grade chloroform was used as a mobile phase, with the eluent flow rate of 1 ml/min and sample injection volume of 40 μL. The samples (30 mg) were dissolved in 1.5 mL HPLC grade chloroform. For the case of reactive extrusion, the samples were dissolved in chloroform for three days and filtered by 0.25 μm filters prior to analysis. The instrument was calibrated with eight narrow molecular weight polystyrene standard (~144 Da-400 kDa).

2.1.3.4. Fourier transform infrared spectroscopy (FTIR)

The chemical structure of samples was monitored using FTIR (Perkin Elmer) attenuated total reflectance (ATR) mode in the range of 4000 to 650 cm^{-1} with 4 cm^{-1} resolution and 64 scan rates.

2.1.3.5. NMR analysis

The chemical structure of samples was investigated by ^{1}H NMR (Bruker Ascend^{TM} 600MHz nuclear magnetic resonance). The samples were dissolved in deuterated chloroform ($CDCl_3$) and filtered with 0.25 μm filter and transferred to 5 mm diameter NMR tube. The analysis were performed by employing 16 scans under 12019 Hz spectra width and 0.3 Hz line broadening for exponential window function with 5 sec relaxation delay at temperature of 299 K. The chemical shift of $CDCl_3$ peak observed at 7.26 ppm was used as an internal reference. For the case of reactive extrusion, the samples were dissolved in chloroform for three days.

2.1.3.6. Differential scanning calorimetry (DSC)

Thermal and crystallization behavior of samples were analyzed using a differential scanning calorimeter (DSC) 204 F1 phoenix, NETZSCH, Germany. Samples weighing ~6 mg were

sealed in a Platinum-Rhodium (Pt-Rh) crucible and scanned for a cycle of heat/cool/heat at a rate of 5 ºC/min for the temperature range of 25 to 200 ºC performed under nitrogen atmosphere. Isothermal conditions were maintained at 200 ºC for 3 min to erase the processing and thermal history after the first heating cycle. Data from the second heating cycle was considered for further analysis. Glass transition temperature (T_g), cold crystallization (T_{cc}), melting temperature (T_m), heat of crystallization (H_{cc}), and heat of fusion (H_m) are estimated [69].

2.1.3.7. Optical microscope study for nucleation and spherulite growth

The effect of adding SNCs and reprocessing on the nucleation and spherulite growth was investigated using polarizing optical microscope (POM) (Nikon H600L, Japan) equipped with charge-coupled device (CCD) camera and T95-linksys32 system with temperature controller and video capturing software. Samples were sandwiched in between two glass slides and heated at a rate of 20 ºC/min to 200 ºC. Isothermal conditions were maintained at 200 ºC for 3 min to erase the processing and thermal history and cooled to the isothermal crystallization temperature of 120 ºC and maintained at 30 min. The growth of spherulites were analyzed at different time intervals and the growth rate was estimated from the slope of spherulite radius versus time plot. Nucleation density was estimated by counting the number of crystals presented on some particular area (mm^2) and ImageJ software was used to count the crystals.

2.1.3.8. XRD

The crystallographic behavior of the samples were investigated by wide angle x-ray diffraction (WAXD) analysis using D8 Advance Diffractometer (Bruker, Germany) which is having X-ray source (40kV, 40 mA) of Cu-Kα radiation (λ=0.1541 nm). Samples were kept in vacuum

oven overnight before the analysis and the test was performed at the scan rate of 0.05º/0.5 s with the 2Θ values ranging from 5-50º. For the case of reactive extrusion, samples were conditioned at 95 ºC for 2 hours prior to analysis.

2.1.3.9. Rheological investigation

Melt rheology of each sample was carried out in the dynamic/oscillatory mode at 190 ºC in the linear viscoelastic region (LVR) at 1% strain in the frequency range of 0.1 to 500 Hz. The material response of the polymer melt is monitored using Anton-Paar rheometer (Model: MCR 301) and is reported as the complex viscosity, storage modulus, loss modulus and the real and the imaginary viscosities; with respect to the frequency. The results from the rheometer were used to make the Cole-Cole plot (imaginary vs. real viscosity), storage and loss modulus vs. frequency, Han plot (storage vs. loss modulus), and power law index values and zero shear viscosity were estimated.

2.1.3.10. Dynamic mechanical analysis

The thermomechanical analysis of the extruded strips were carried out with a DMA 242 (Netzsch, Germany) in the tensile mode under a dynamic force of 2 N, amplitude of 20 μm and at a frequency of 1 Hz. The samples were cut into 5 mm x 5 mm x 0.5 mm strips and measurements were carried out in the temperature range of 25–100 °C at a heating rate of 5 ºC/min.

2.1.3.11. Thermal degradation analysis

Thermal analysis of samples was carried out on Perkin-Elmer TGA4000 equipment. Samples weighing ~8mg were heated from 30°C to 700 °C at the heating rates of 5, 10, 15 and 20

°C/min under nitrogen (N_2) atmosphere. Furthermore, the analysis of evolved gas was performed using Perkin-Elmer TGA-FTIR hyphenated system. An interface line having gas transfer tube and gas cell was used to couple TGA with FTIR spectrophotometry (Frontier 4000) and heated up to 250 ºC to avoid the condensation of evolved gases.

2.1.3.12. Field emission scanning electron microscope

Field Emission Scanning Electron Microscope (FESEM) (sigma, ZEISS) analysis of samples was carried out understand the change on surface morphology at different magnification. The film samples are fixed on carbon tape followed by gold sputtering to have proper conductivity of electrostatic charge during electron irradiation.

2.2. Recycling of reprocessed PLA into lower molecular weight for targeted application as biolubricant

2.2.1. Materials

Melt extruded PLA film was used as a starting material for random degradation. L-lactic acid (LA; PH 90) was purchased from Purac, India. Refined soybean oil was obtained from Adani Wilmar Limited Corporation, India.

2.2.2. Methods

2.2.2.1. Microwave assisted degradation of melt processed PLA

Temperature controlled microwave reactor was used to degrade melt processed PLA using lactic acid. Melt processed PLA film (50 g) and 50 mL LA (10 % water) were added in two necked round bottom flask (RBF) coupled with reflux condenser and magnetic stirrer. The

reaction mixture kept in RBF was placed in microwave at a temperature of 100 ºC. The water escaped from the reaction mixture was reflexed back for 1 hour to facilitate the degradation process. Complete dissolution of PLA in lactic acid was obtained and white viscous liquid without any phase separation was collected and labeled as lactic acid degraded PLA (LA-D-PLA).

2.2.2.2. Biolubricant formulation

Blend of soybean oil (SO) and LA-D-PLA at various proportions of (0/100, 15/85, 30/70, 50/50, 85/15 and 100/0 w/w) were prepared with mild agitation at room temperature and labeled as LA-D-PLA, 15/85 B, 30/70 B, 50/50 B, 85/15 B and SO and respectively.

2.2.3. Characterization

2.2.3.1. Viscosity measurement and activation energy calculation

In the present investigation, dynamic viscosities of LA-D-PLA/SO blend are measured at different temperatures (25 ºC, 40 ºC, 60 ºC, 80 ºC and 100 ºC) using Rheometer (Anton-Paar Model: MCR 301). The shear thinning behavior is investigated for the shear rate range of 1 to 100 s^{-1}. To understand the viscosity dependency on temperature, the dynamic viscosity of each formulation were estimated at their respective temperature under constant shear rate of 500 s^{-1}.

2.2.3.2. Thermal degradation analysis

Thermal stability of LA-D-PLA/SO blends were investigated using Perkin-Elmer TGA4000 equipment. Samples weighing ~8mg are heated from 30°C to 600 °C at the heating rate of 10 °C/min under nitrogen (N_2) atmosphere.

2.2.3.3. Chemical structure modification

The change in chemical structural of LA-D-PLA was monitored using FTIR (Perkin Elmer) attenuated total reflectance (ATR) mode in the range of 4000 to 650 cm^{-1} with 4 cm^{-1} resolution and 64 scan rates. Additionally, ^{1}H NMR analysis is also performed using 600 MHz nuclear magnetic resonance (NMR) for further confirmation. The samples were dissolved in deuterated chloroform (CDCl3).

2.3. Poly (lactic acid)-oligomer dissolution in biodiesel

2.3.1. Materials

Refined soybean oil was obtained from Adani Wilmar Limited Corporation, India. Based on the NMR analysis, the oil was composed of total 78.9% unsaturated fatty acid (i.e. 50.2% linoleic acid (C-18:2), 20.7% oleic acid (C-18:1), 8% linolenic acid) and 21.1% saturated fatty acid (mainly palmitic acid and stearic acid). Methanol with 99.8% purity was purchased from Sisco Research Laboratory Pvt. Ltd. and KOH was obtained from Merck (India) for transesterification of soybean oil into fatty acid methyl ester. L-Lactic acid (80% purity) was obtained from Sigma-Aldrich.

2.3.2. Methods

2.3.2.1. Microwave assisted PLA-oligomer preparation

Preparation of known molecular weight oligomers is essential to investigate the impact of molecular weight on the biodiesel characteristics. A 250 mL three-necked flask was placed in microwave equipped with a mechanical stirrer and a condenser. 150 g of L-lactic acid was charged into a three necked flask and temperature was raised to 120 °C so as to remove water

under nitrogen flow for 10 min. Four different molecular weight oligomers (Mn~500 Da, 1000 Da, 1500 Da and 2000 Da) were prepared using four different temperatures (150, 160, 170 and 180°C) and were used to test their impact on the cold flow characteristics of biodiesel. The prepared oligomers were labeled as OLLA500, OLLA1000, OLLA1500 and OLLA2000.

2.3.2.2. Microwave assisted biodiesel synthesis

All experiments were performed in the temperature controlled microwave system (MILESTONE MicroSYNTH, Microwave Synthesis Labstation, USA) equipped with magnetic stirrer. Firstly, 100 mL of preheated (60°C) soybean oil in microwave reactor was mixed with 25 mL of 1 wt.% KOH solution in methanol, in which methanol-to-soybean oil molar ratio was maintained at~6:1. After complete reaction at above temperature, the reaction mixture was ice cooled in order to stop the esterification reaction. Subsequently, the reaction mixture was allowed to stand overnight in a separating funnel in order to separate the biodiesel and glycerol layer. Thereafter, the residual catalyst present in biodiesel was washed out with warm distilled water. The excess methanol was removed through vacuum distillation. Similar experimental protocol was repeated for different reaction time intervals (1, 3, 5, 15 and 30 min) and optimum condition was maintained at 5 min for subsequent analysis.

2.3.2.3. Fuel preparation and stabilization.

PLA-oligomer with number average molecular weight of 1000 Da was dissolved in soybean oil based biodiesel at a temperature of 60ºC with mild agitation. Oligomer concentration of 3 g/L, 5 g/L, 10 g/L and 25 g/L (denoted as OL3, OL5, OL10, and OL25 respectively) were prepared. Furthermore, the impact of molecular weight (5 g/L) on the biodiesel was also tested. Ethyl lactate (1%, 3%, and 5% v/v) was used to stabilize the oligomer blend solution. The

effect of oligomer concentration, oligomer molecular weight and blend stabilizer on important properties like cloud point, pour point, flash point, fire point, viscosity (dynamic), calorific value, and crystal morphology were investigated.

2.3.3. Oligomer and biodiesel characterization

2.3.3.1. NMR analysis

^{1}H NMR spectra of the soybean oil and fatty acid methyl esters were obtained by using NMR (Bruker Ascend^{TM} 600MHz nuclear magnetic resonance) using a 5 mm diameter NMR tube by employing 16 number of scans under 12019 Hz spectra width and 0.3 Hz line broadening for exponential window function with 5 sec relaxation delay at a temperature of 299 K. Deuterated chloroform ($CDCl_3$) was used as a solvent (0.05 mL of sample dissolved in 0.6 mL of solvent) and the chemical shift of $CDCl_3$ peak observed at 7.26 ppm was used as an internal reference.

2.3.3.2. Gel permeation chromatography (GPC)

The number average molecular weight (Mn), weight average molecular weight (Mw) and the PDI of PLA oligomer (OLLA) were determined using a GPC system (Shimadzu, communications bus module (CBM-20A), auto sampler (SIL-20A HT), liquid chromatography (LC-20A), degassing unit (DGU-20A_{3R}), refractive index detector (RID-10A), agilent two PL gel 5micro MIXED-D column in series with column oven (CTO-20A)). HPLC grade chloroform was used as mobile phase at 1 ml/min eluent flow rate and 40 µL sample injection volume. The samples (30 mg) are dissolved in 1.5 ml HPLC grade chloroform. Before analysis, the solution was filtered with 0.45µm filters. Polystyrene standard were used for calibration.

2.3.4. Testing of important fuel characteristics

2.3.4.1. Cloud point and pour point

ASTM D-2500 and ASTM D-97 procedures were adopted to determine the cloud point and pour point, respectively. The samples are immersed in cooling bath at -33ºC. However, the observations are taken from 9ºC which is well above the expected cloud and pour points of the samples. For cloud point reading, the samples were examined at the intervals of 1ºC, until a cloud is observed at the bottom of the test jar. For the case of pour point, readings were taken for every 3ºC decrease in the temperature until the sample totally ceased to flow (the sample is held in a horizontal position for 5 sec).

2.3.4.2. Viscosity measurement and activation energy calculation

Diesel fuel viscosity not only affects the atomization and density, but also influences the cold flow property. In the present investigation, dynamic viscosities of biodiesel were measured at different temperatures (-5 ºC, -3 ºC, -1 ºC, 0 ºC, 1 ºC, 3 ºC, 5 ºC, 10 ºC and 25 ºC) and 20 s^{-1} shear rate by using Interfacial Rheometer (Anton-Paar Model: MCR 301). The investigation was done for OLLA-biodiesel and EL-OLLA-biodiesel systems. The measurements were repeated two times for each sample and the average results are taken.

2.3.4.3. Crystallization behavior

Crystal morphologies of soybean based biodiesel at low temperatures were investigated using Nikon H600L polarizing optical microscope (Japan), equipped with T95-linksys32 system with temperature controller and video capturing software. Biodiesel samples were gradually cooled using liquid nitrogen from room temperature to 0 ºC and gradually to -10 ºC at the rate

of 2 ºC/min and 1 ºC/min, respectively. Isothermal condition is maintained at 0 ºC, -3 ºC, -5 ºC and -10 ºC for 3min.

2.3.4.4. Calorific value

The calorific values of the samples were obtained using the bomb calorimeter equipped with pressure vessel using 97.7% oxygen at 30 bar.

2.3.4.5. Engine performance and emission characteristics

The impact on brake specific fuel consumption, brake thermal efficiency, and exhaust gases was investigated for blends of OL5-BD as well as OL10-BD with 80% diesel. PLA oligomer with number average molecular weight of ~1000 Da was used in this investigation.

Table 2.2: Engine specifications.

Make	**Kirloskar TV-1**
Type	Vertical single cylinder
Bore	87.5mm
Stroke	110mm
Compression ratio	17.5:1
Related brake power	5.2 kW
Speed	Constant speed (1500rpm)
Cooling system	Water cooled
Fuel	High speed diesel
Lubrication oil	SAE: 40
Static injection timing	20º bTDC (modified)
Nozzle opening pressure	250bar (modified) at full load

Experiments have been performed using single cylinder, 4stroke, constant speed (1500rpm) kirloskar, and TV1 direct injection diesel engine with water cooled eddy current dynamometer. Standard nozzle opening pressure of 240 bar was used at various loading percentage (25%, 50%, 75%, and 100%). The detailed engine specifications were listed in **Table 2.2**. Exhaust

gas emission characteristics for CO, CO_2, NO_x and HC were measured using AVL 444 di-gas analyzer. Steady state condition was maintained for all the experiments.

Chapter 3

The Impact of Silk Nanocrystals on the Molar Mass Distribution of Melt Extruded Poly (Lactic Acid)

This chapter mainly focusses on the impact of silk nanocrystals (SNC) on thermal degradation of PLA during thermomechanical process. The influence of temperature (185 ºC and 200 ºC) and shear (40 and 100 rpm) on the rate of degradation are studied through the estimation of molecular weight distribution at different residence times (up to 30 min.) using gel permeation chromatography (GPC). Simplified two-parameter model coupled with Arrhenius equation is applied to predict the kinetic parameters for degradation and recombination reactions. The impact of SNC and processing conditions on the macromolecular change of PLA matrix is also investigated using melt rheology.

Parts of this chapter are ready for communication as:

Melakuu Tesfaye, Rahul Patwa, Vimal katiyar, Comparative study: The Impact of Acid Hydrolysed Silk Fibrous (silk nanocrystals) on the Molar Mass Distribution and Processability Performance of PLA

3.1. Introduction

The molar mass distribution during melt processing is dependent on the processing conditions such as temperature, shear and residence time. Only a few researchers have addressed this important issue and provided an important model which can predict the degradation characteristic of PLA during processing. The molar mass change of PLA with respect to temperature and time was first proposed by **Wachsen et al.,** using statistical approaches [70]. Later on more generalized and convenient model was proposed by **Yu et al.**, which can provide important information about the molar mass distribution in terms of number average molecular weight (M_n), weight average molecular weight (M_w) and polydispersity index (PDI) of processed PLA at various temperatures [71]. **Le Mareac et al.,** used the proposed models to study the impact of processing conditions on the molar mass distribution of PLA [17].

Mechanical energy plays a major role in the degradation processes in two distinct ways, the first is thermally driven degradation effect, which occurs due to the viscous dissipation increment of temperature; and the second is mechanically driven degradation effect due to breaking of chains by shear stress [17]. Degradation phenomenon of thermally captivated systems have been described by the model which accounts for the kinetics constant of chain scission and recombination using Arrhenius equation. Population-balance equations are used to evaluate the molar mass distribution [70]. The impact of process variables on the molecular weight molecular weight distribution (MDW) of PLA have been discussed in the literature by few researchers. However, the impact of processing variables along with the effect of fillers on the degradation process has not yet been explored. This chapter provides a fundamental understanding on the impact of incorporation of SNCs into PLA matrix and the effect of melt

processing conditions on molecular weight distribution and viscoelastic properties are addressed.

3.2. Theory

Time dependency of molecular weight distribution of polymeric system at various melt processing conditions is described using two-parameter model, which accounts for degradation and recombination at equilibrium condition. This model is used to quantify the reduction in average molecular weight at equilibrium condition [17, 70]. This reversible reaction can be expressed using **Eqn. 3.1 and 3.2.**

$$P_n \rightarrow P_{n-i} + P_i \qquad 3.1$$

$$P_i + P_{n-i} \rightarrow P_n \qquad 3.2$$

The concentration of the polymer chain with n repeating units [P_n] at the time of thermal processing can be described using the decomposition rate constant (k_d) and recombination rate constant (k_c) using **Eqn. 3.3 [70]**

$$\frac{d[P_n]}{dt} = -k_d(n-1)[P_n] + 2k_d \sum_{i=n+1}^{\infty}[P_i] + \frac{1}{2}k_c \sum_{i=1}^{i-1}[P_i][P_{n-i}] - k_c[P_n]\sum_{i=1}^{\infty}[P_i] \qquad 3.3$$

The first term is for n-1 possible decompositions of P_n polymer chain followed by the second term indicating every possible formation of P_n chain by the splitting of P_i polymer chains which is having chain length greater than n. Third and fourth terms describe every possible formation of P_n by recombination of chains (i and n-i) lower than chain length n and every possible disappearance of P_n by recombination with other molecules respectively.

The temperature dependency of degradation (k_d) and recombination (k_c) reaction kinetic constants was described in terms of respective activation energies of degradation (E_{ad}) and recombination (E_{ac}) of the system using Arrhenius equation as follow (**Eqn. 3.4 and 3.5**).

$$k_d = A_d exp\left[-\frac{E_{ad}}{RT}\right] \quad 3.4$$

$$k_c = A_c exp\left[-\frac{E_{ac}}{RT}\right] \quad 3.5$$

where, A_d and A_c are the pre-exponential factors and R is universal gas constant with the value of 8.314 J/molK. **Yu et al.,** have simplified **Eqn. 3.3** using zero (λ_0), 1st momentum (λ_1), and 2nd momentum (λ_2) momentum and 3rd momentum (λ_3) equations as described in **Eqn. 3.6-3.9.**

$$\frac{d\lambda_0}{dt} = k_d(\lambda_1 - \lambda_0) - k_c\frac{{\lambda_0}^2}{2} \quad 3.6$$

$$\frac{d\lambda_1}{dt} = k_d(\lambda_1 - \lambda_0) \quad 3.7$$

$$\frac{d\lambda_2}{dt} = \frac{k_d(\lambda_1 - \lambda_3)}{3} - k_c{\lambda_1}^2 \quad 3.8$$

$$\lambda_3 = \frac{\lambda_2}{\lambda_1\lambda_0}\left[2\lambda_2\lambda_0 - {\lambda_1}^2\right] \quad 3.9$$

Recently **Khanlou et al.,** have considered the total number of moles of monomers (λ_1) to be constant, which helps in simplifying the complicated equation and provide an option to solve it analytically. This important step is made considering no change in number and structure of monomeric unit as the reaction progresses. Their approach provided an important relationship

for λ_0 by solving **Eqn. 3.6** for a constant temperature and constant λ_1 as shown in **Eqn. 3.10 and 3.11** [72]**.**

$$\lambda_0 = -\frac{k_d}{k_c} + \frac{\sqrt{(2k_c k_d \lambda_1 + {k_d}^2)}}{k_c} \tanh\left(\frac{(t+C)\sqrt{(2k_c k_d \lambda_1 + {k_d}^2)}}{2}\right) \quad 3.10$$

C (**Eqn. 3.11)** is an initial condition for λ_0 (total moles of molecules per unit volume) which can be expressed as a function of starting molecular weight ($\lambda_{0,\,initial} = \rho/M_{n,\,initial}$).

$$C = \frac{2}{\sqrt{(2k_c k_d \lambda_1 + {k_d}^2)}} \tanh^{-1}\left((\lambda_{0,intial} + \frac{k_d}{k_c})\frac{k_c}{\sqrt{(2k_c k_d \lambda_1 + {k_d}^2)}}\right) \quad 3.11$$

This simplified equation can be used to estimate the rate of degradation and degradation activation energy of melt extruded PLA reinforced with different fillers coupled with experimental estimation of number average molecular weights as shown in **Eqn. 3.12.**

$$M_{n,ave} = \frac{\sum_{n=1}^{\infty} n[P_n]}{\sum_{n=1}^{\infty}[P_n]} = m_o \frac{\lambda_1}{\lambda_0} \quad 3.12$$

In this chapter the impact of SNC on the degradation characteristic of PLA is discussed and melt degradation model modified by **Khanlou et al.,** expressed in **Eqn. 3.10** is used to estimate the kinetic parameters and activation energies of the systems accounting both chain scission and recombination processes as already discussed above. Nelder-Mead simplex method is used to minimize the error between the experimental and model predicted values as described in simplified flow sheet (**Fig. 3.1).**

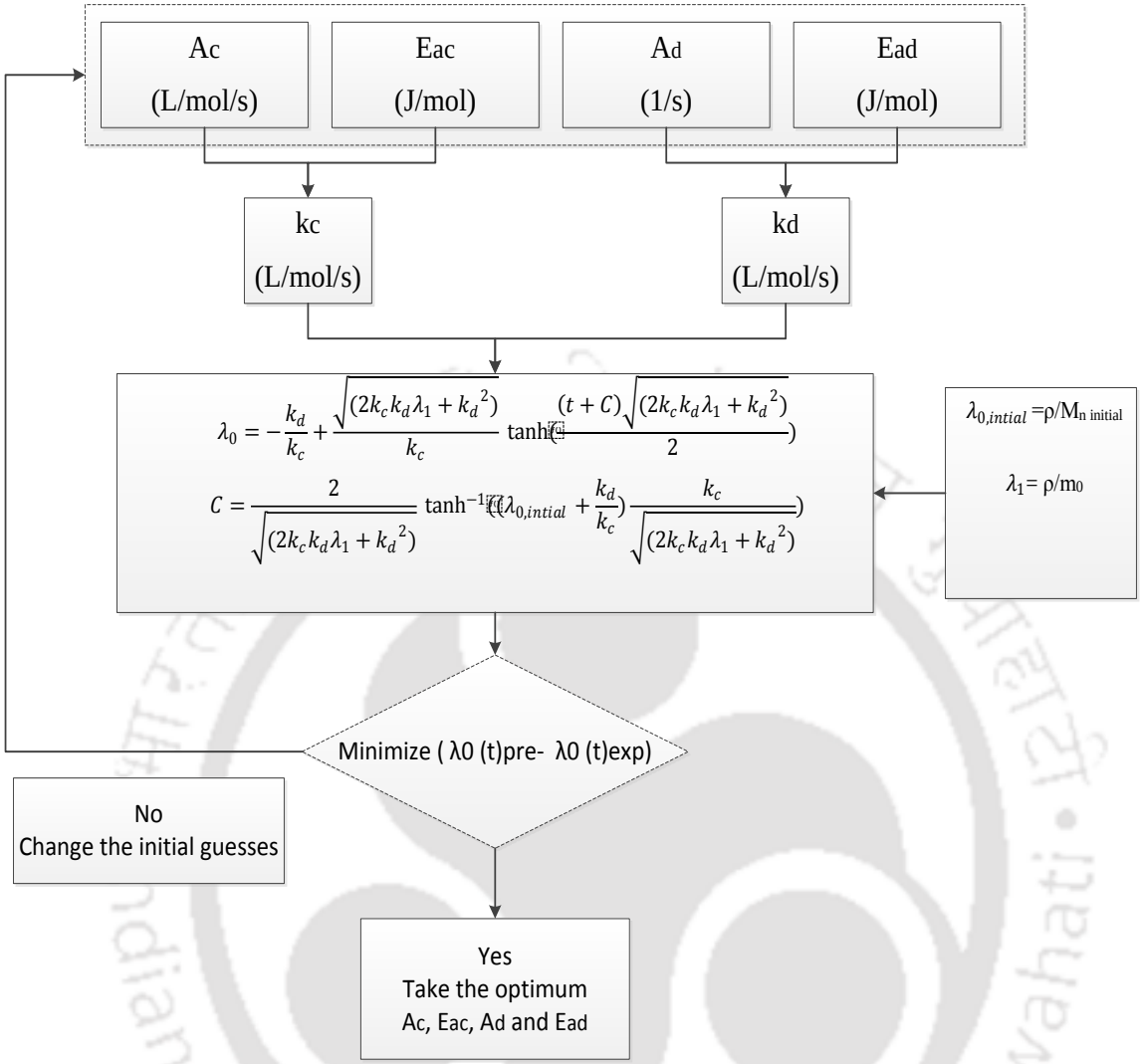

Figure 3.1. Systematic flow chart to optimize the kinetic parameters for degradation and recombination of thermal processing of PLA.

3.3. Results and Discussions

3.3.1. Silk as a biofiller

Silk fibroin (SF) is fibrous protein with unique properties of biocompatibility, biodegradability, high thermal stability and high tensile strength which makes it an attractive

biofiller to reinforce PLA. However, dispersion of silk fibroin inside PLA matrix is a challenging task since delamination and intercalation of fibroin bundle is difficult during melt blending because of the strong binding nature of sericins.

It is already known that, SF is mainly composed of the repeating units of glycine, alanine and serine residues in which highly stable β-sheet structure is formed because of hydrogen bonding between C=O and N-H groups [73]. Acid hydrolysis has been performed to remove sericins and isolate the crystalline region with reduced size from fibrous to powder (nanocrystals). The molecular conformation of degummed silk fibroin (SF) before and after acid hydrolysis is investigated using FTIR (**Fig.3.2)** and supported by X-ray diffraction (XRD) (**Fig.3.3)** and polarized optical micrographs (POM) (**Fig. 3.4 & 3.5**).

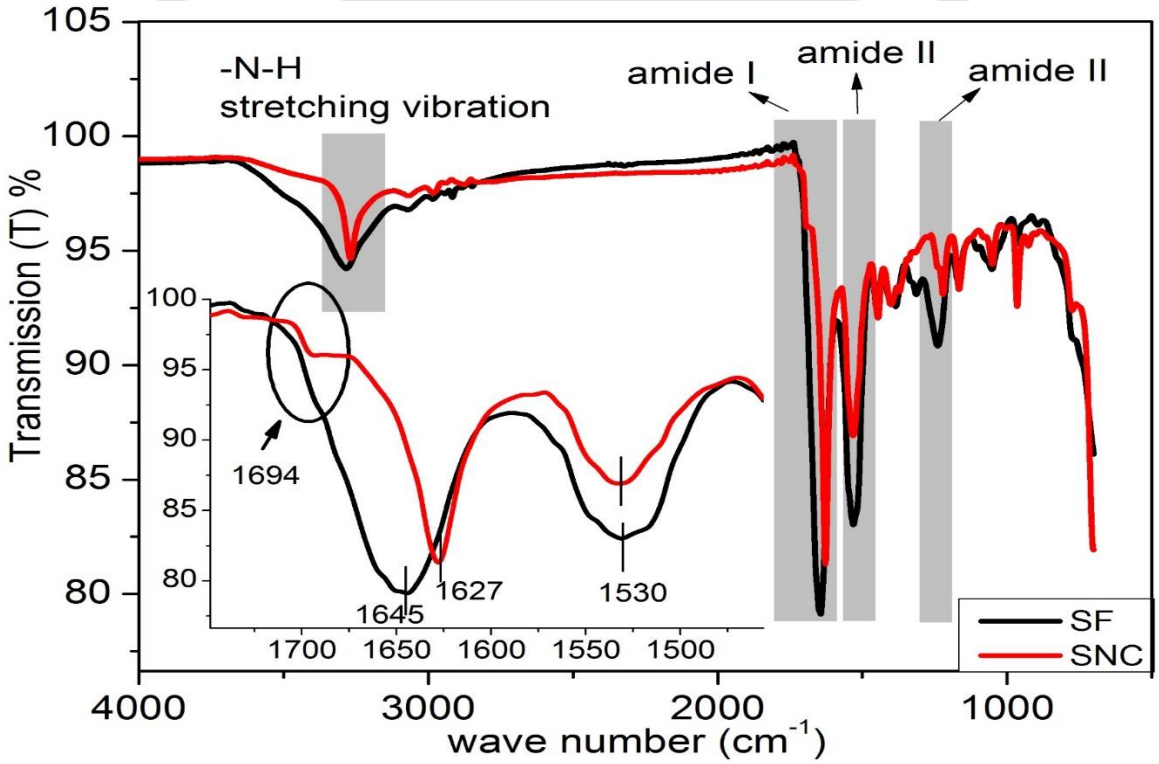

Figure 3.2. FTIR spectra of silk fibroin (SF) and silk nanocrystals (SNC).

Intense transmission bands on the FTIR spectra are observed for amide I and amide II at 1645 cm^{-1} and 1530 cm^{-1} for SF and 1627 cm^{-1} and 1530 cm^{-1} for SNC respectively. The amide I peak shifted form 1645 cm^{-1} (SF) $cm^{-1}$to 1627 cm^{-1} (SNC) which can be accounted for the transformation of random coil molecular conformation (silk I) structure to silk II of well-organized β-sheet structure after the removal of amorphous part from SF through acid hydrolysis [74, 75]. The FTIR peaks at 1627 cm^{-1} and 1530 cm^{-1} are relatively narrow for SNC as compared to the respective peaks of SF at 1645 cm^{-1} and 1530 cm^{-1}. The results are in line with the FTIR spectra presented by **Tao et al., [74].** It is well understood that the crystallinity of SF can increase with prolonged acid hydrolysis due to the removal of the amorphous part and leads to the relatively narrow characteristic absorption peak for the silk II structure. More interestingly, amide I small absorption band identified at 1694 cm^{-1} for SNC (after acid hydrolysis of SF) confirms the presence of highly order β-sheet structure.

Crystallographic investigation (XRD) depicts the intense peaks at 2Θ values of 16.8º, 20.4º and 24.1º, confirms the improvement in crystallinity **(Fig. 3.3)**. Additionally new peaks are observed for SNC at 2Θ values of 30.6º, 34.04º, 40.0º and 43.3º, which may be attributed to the conformational change from silk I to silk II as observed in the FTIR analysis [76].

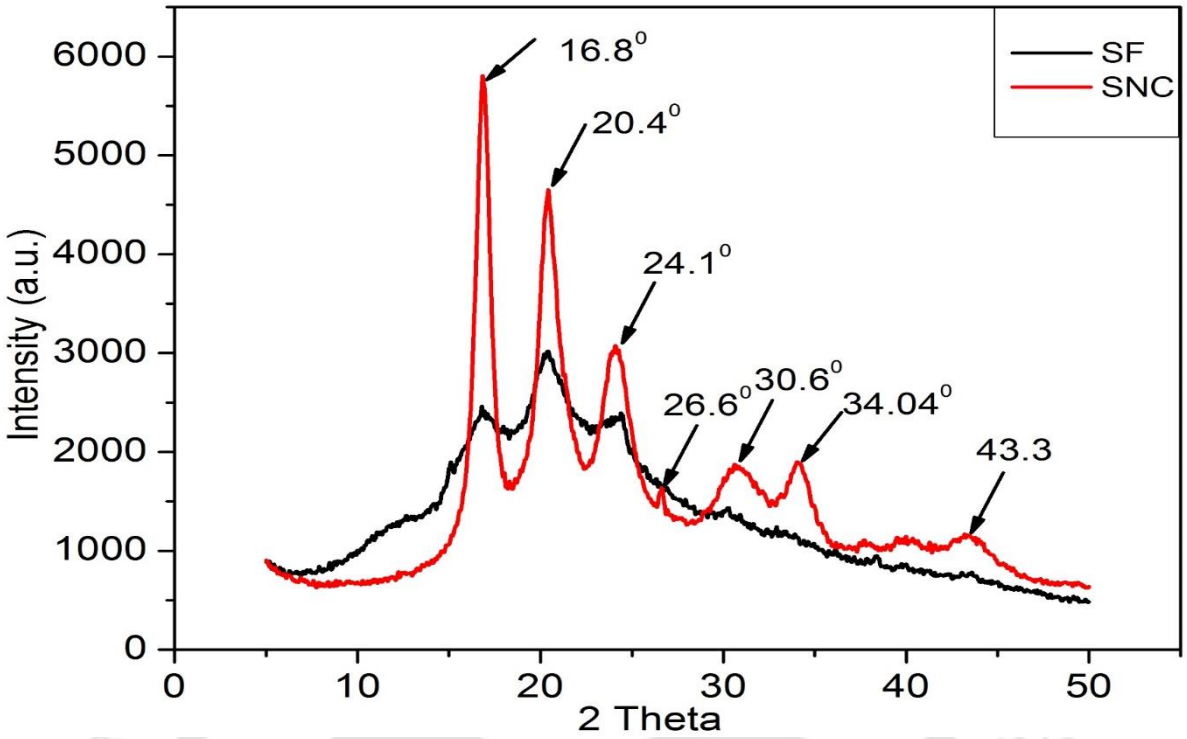

Figure 3.3. X-ray diffraction spectra of silk fibroin (SF) and silk nanocrystals (SNC).

Fibrous structure of degummed silk fibroin (SF) is displayed in **Fig. 3.4,** which shows the bundle of fibroin having a diameter of 3.1 μm. In order to disperse silk fibroin in hydrophobic matrix of PLA, the size needs to be reduced and the amorphous part that binds the fibroin together to form bunch of bundle needs to be removed. In this context, acid hydrolysis is performed with a proper procedure followed by dialysis to remove the acid and maintaining pH>6 after acid treatment. From **Fig. 3.5 (a),** it can be clearly observed that the aggregate of the powders obtained after acid hydrolysis process doesn't have any fibrous structure and it is evident from the **Fig. 3.5 (b)** that the particle size of powder is in nano size ranging of 35 nm to 100 nm. As already discussed above, the sharp peaks obtained on the XRD diffractogram of silk fibroin after hydrolysis confirm the significant improvement in the crystalline fraction.

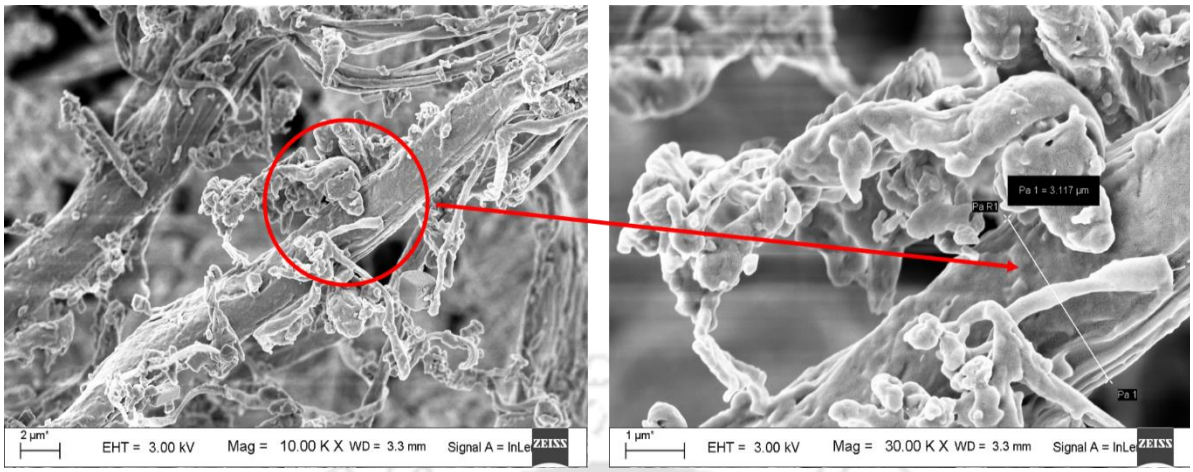

Figure 3.4. FESEM image of silk fibroin.

Furthermore, polarized optical microscope is used to visualize the change in the crystalline part as the silk fibroin is transformed into dense crystalline form after hydrolysis. It is well known that, crystalline part of any material reflects light when it is exposed to a polarized light.

It is clearly observed that long coiled crystalline fibres are trapped within the amorphous region of SF which reflects light when the polarized light strikes the crystalline part **(Fig. 3.6 (a))**. However, as indicated in **Fig. 3.6 (b)** aggregates of crystals are observed after acid hydrolysis which is due to the removal of amorphous part. This observation is in line with the information gathered from XRD and FTIR investigation.

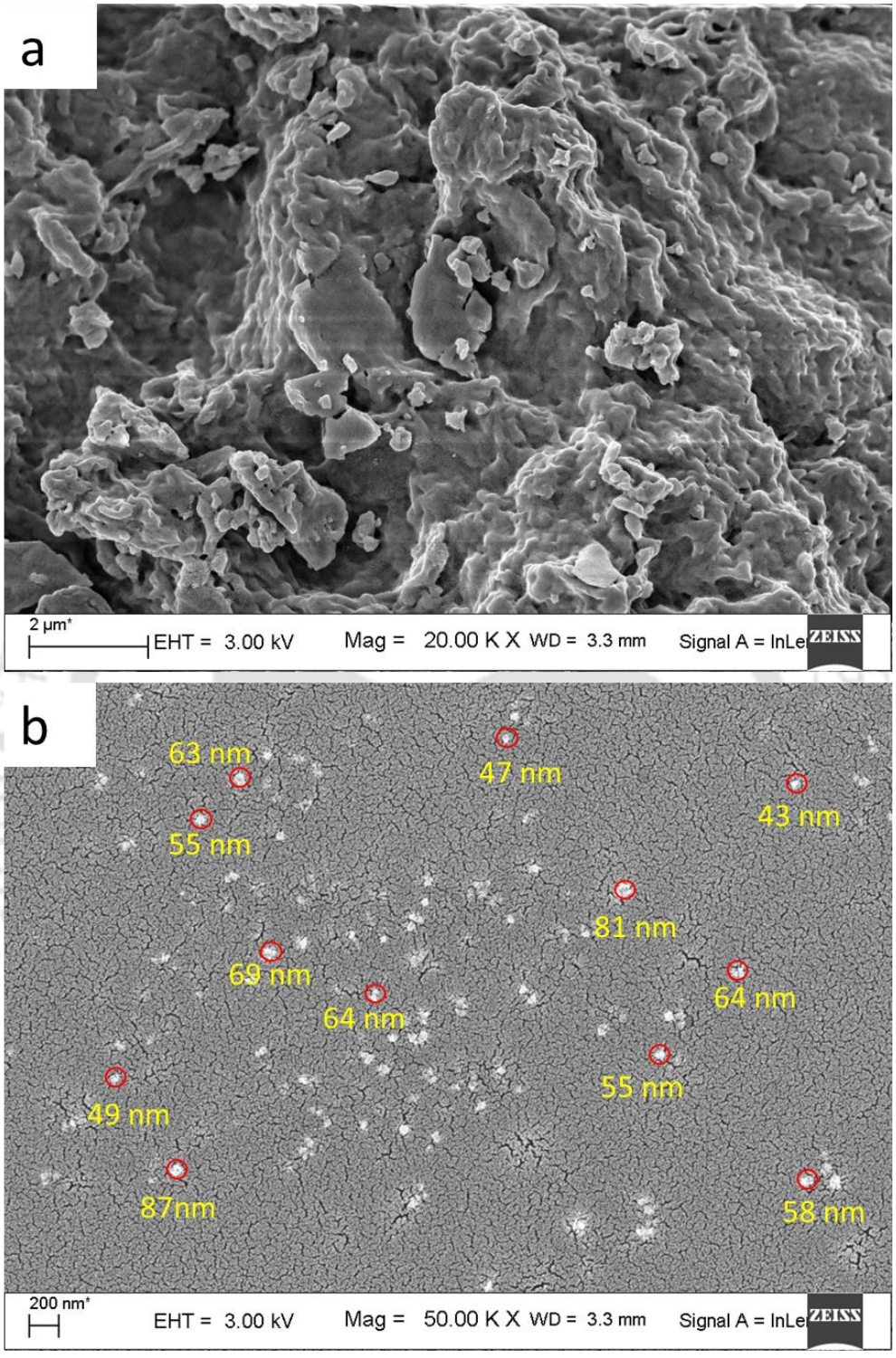

Figure 3.5. FESEM images of (a) aggregates of silk nanocrystals and (b) individual particles of SNC.

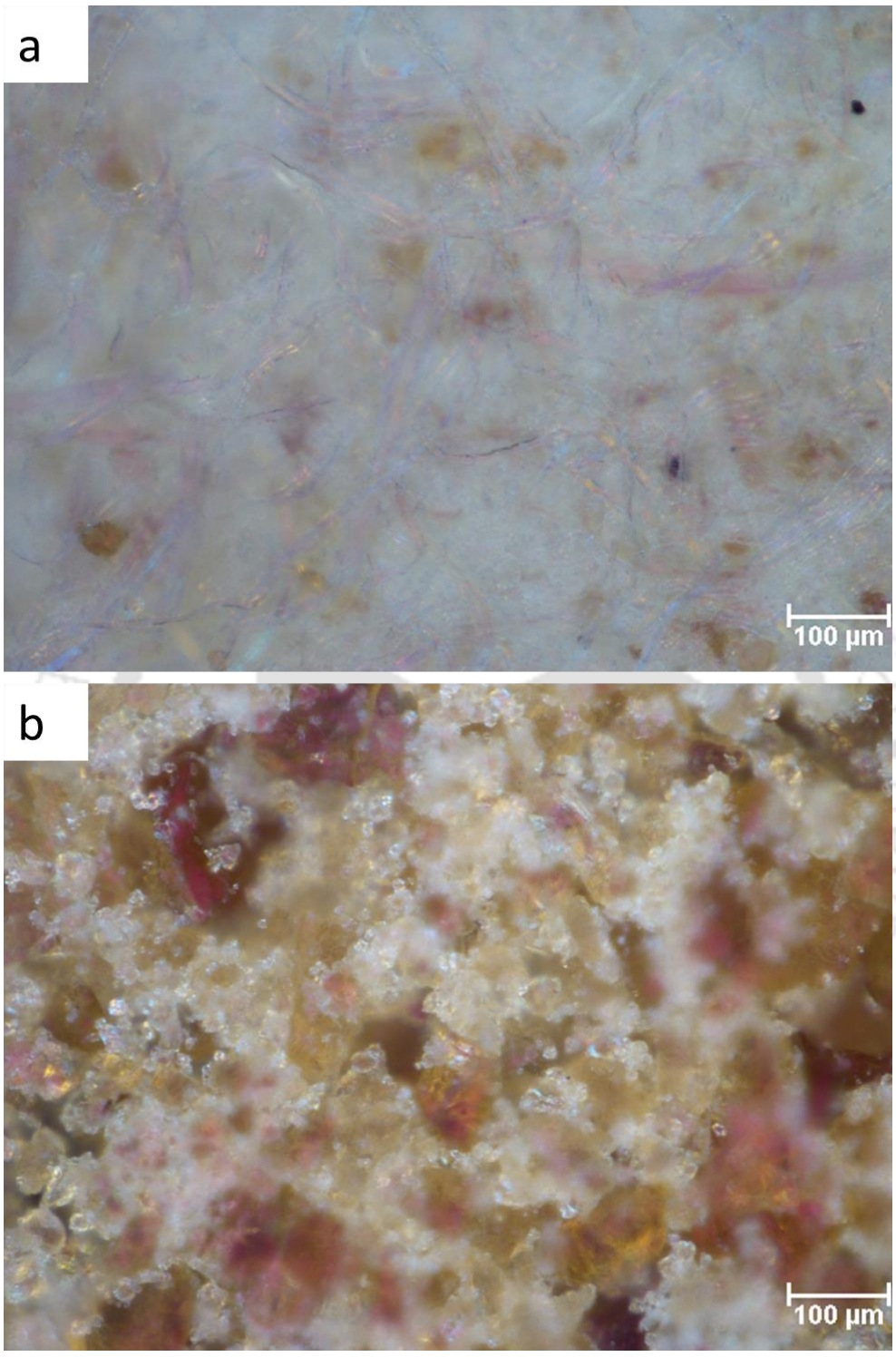

Figure 3.6. Polarized **o**ptical microscopy image of silk fibroin (a) before and (b) after acid hydrolysis.

Before proceeding to the detailed investigation on the impact of SNC towards versatile properties on the melt stability of PLA matrix, it is required to perform preliminary investigations on the thermal stability of SNC as well as PLA, to understand the decomposition behaviour. The thermal decomposition spectra and Gram-Schmidt curve of the evolved gasses for SNC, PLA matrix and SNC-PLA nanocomposite are obtained from TG-FTIR at rate of 5 ºC/min, as indicated in the **Fig. 3.7** respectively.

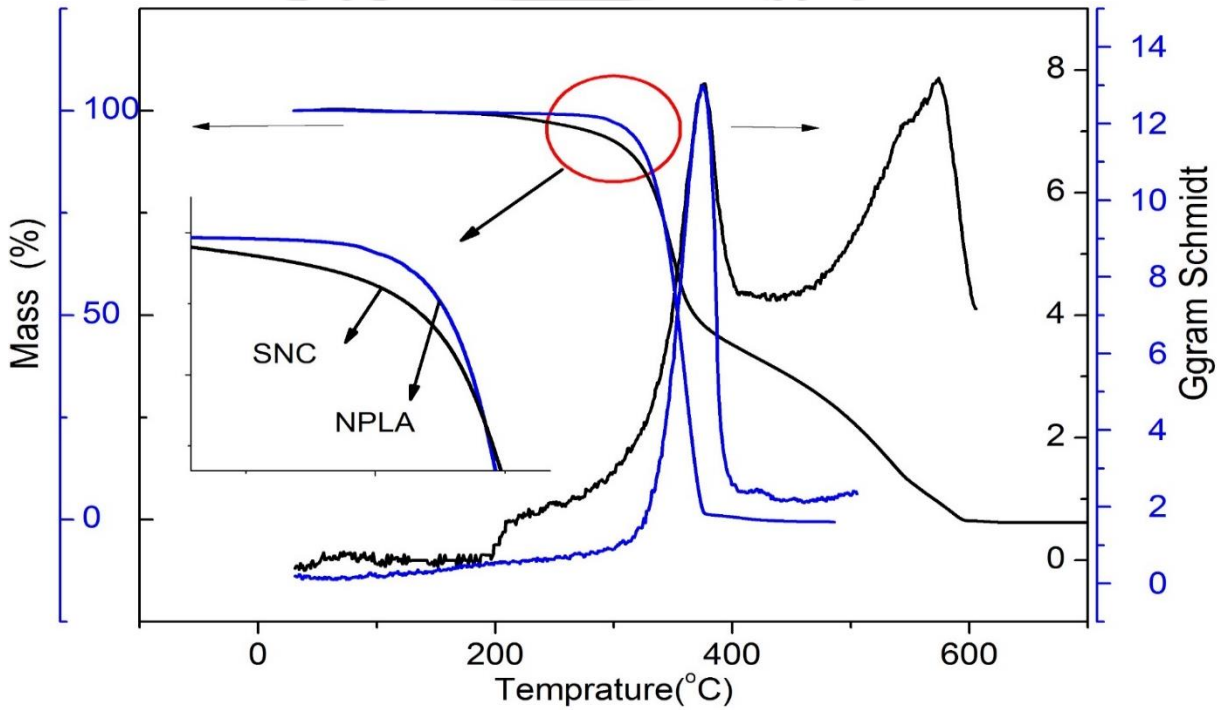

Figure 3.7. Thermal decomposition and Gram-Schmidt curves of the evolved gasses for SNC, NPLA (neat poly (lactic acid**))** and SNC-PLA nanocomposite obtained from TG-FTIR at rate of 5 ºC/min.

The thermal decomposition of SNCs occurs in a wide range of temperature (280-570 ºC) having two major peaks. In the initial stage, 10 wt.% of the sample is degraded having $T_{5\%}$ less by 30 ºC (at 280 ºC) as compared to pristine PLA and its nanocomposite. As observed in Gram-

Schmidt curve, SNC decomposes in two major stages, in 1st stage 30% decomposition occurs over a temperature range of 310 ºC - 404 ºC (the same range for NPLA 100% decomposition). In the 2nd stage, 60% decomposition occurs at higher temperature range (404 ºC - 606 ºC). This high thermal stability of SNCs can be used to enhance the thermal stability of PLA.

3.3.2. The effect of silk nanocrystals and processing conditions on molar mass distribution of PLA

In this section, the effect of processing conditions (temperature and shear) on weight distribution of PLA with/without SNC is investigated. Thermomechanical degradation is mainly occurring due to the influence of processing conditions such as screw speed, temperature and residence time which are already discussed above**.**

Melt extrusion is carried out at temperatures of 185 ºC and 200 ºC and the screw speed of 40 and 100 rpm for different residence times (1, 5 10, 15, 20, 25, and 30 min). The molecular weight of each sample at different processing conditions is estimated using GPC to understand the change in thermomechanical degradation. Reduction in 50 % molecular weight is considered as a reference point to compare the change in NPLA and SNC-PLA.

The reduction in number average molecular weight and weight average molecular weight of NPLA and SNC-PLA at different processing conditions are presented in **Fig. 3.8** and **Fig. 3.9.** The extent of degradation is observed to increase with increasing temperature. Irrespective of the screw speed, both pristine PLA and SNC-PLA are degrading faster at higher temperature (200 ºC). The impact of introducing SNC to PLA matrix during melt processing is clearly observed from 50% reduction of the number average and weight average molecular weight. At

all processing conditions, drastic degradation of PLA matrix is observed and the number average molecular weight is reduced by 50 % within 5 min. However, due to the fortifying effect of SNC, the number average molecular weight of the bionanocomposite is observed to be above the margin of 50 % reduction. Similar remark can also be drawn from the weight average molecular weight of these samples.

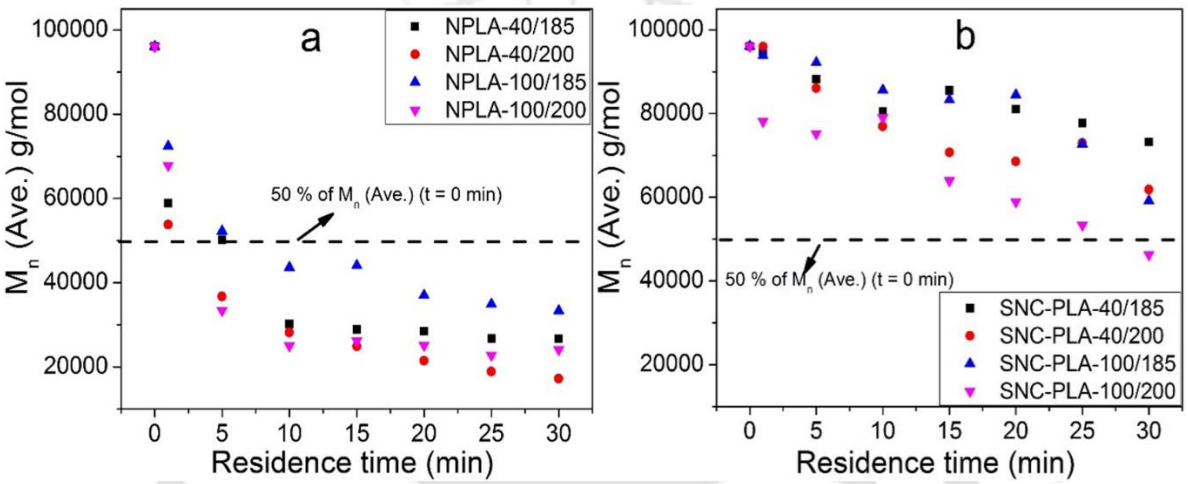

Figure 3.8. Influence of processing conditions (temperature, screw speed and time) on number-average molecular weight of melt processed (a) pristine PLA and (b) SNC-PLA.

The polydispersity index (**Table 3.1)** of melt processed PLA increases from ~2 (0 min) to ~4 (30 min), which confirms that the rate of degradation of lower molecular weight fraction is higher than that of higher molecular weight fraction which leads to drastic reduction in number average molecular weight as compared to weight average molecular weight. However, the polydispersity index remains constant around ~2.2 for chosen SNC-PLA for all processing conditions.

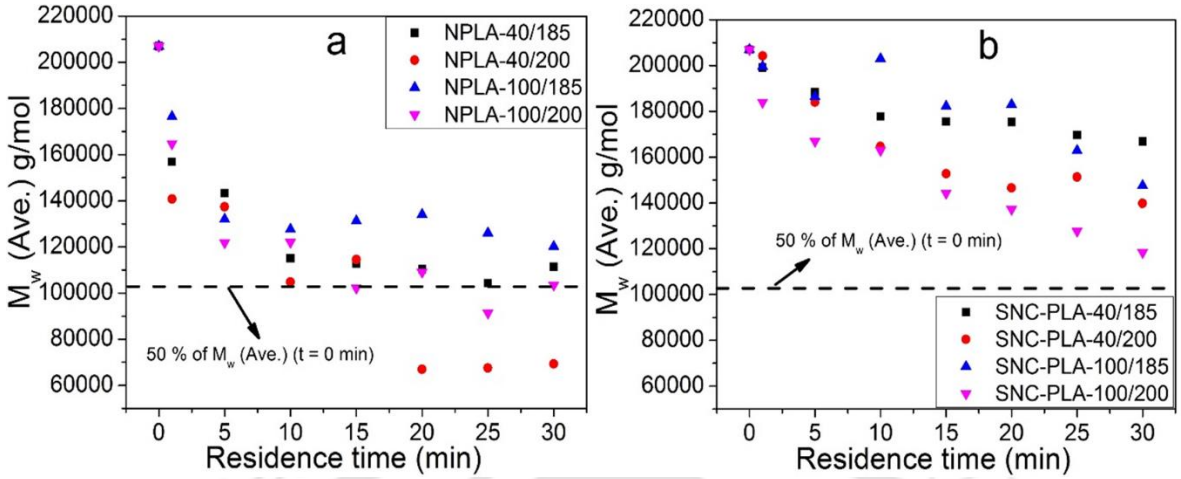

Figure 3.9. Influence of processing conditions (temperature, screw speed and time) on weight-average molecular weight of melt processed (a) NPLA and (b) SNC-PLA.

The degradation process is dependent on the exact temperature of the polymer melt, which is affected by the set temperature and shear. For the fixed screw speed (shear), an increase in set temperature tends to decrease the viscosity of the melt and in turn reduce the self-heating characteristics of the melt. On the other hand, at fixed temperature, the self-heating of the melt increases with increasing screw speed. The increase in temperature of the melt by the viscous dissipation due to shear and increase in set temperature facilitates thermally driven degradation. The other significant cause of degradation which needs to be considered is shear induced mechanically driven degradation due to shear. The incorporation of highly thermally stable nanocrystals (SNC) in the PLA matrix, which helps to stabilize the melt and reduce the rate of degradation.

Table 3.1. The influence of processing conditions on polydispersity index of PLA and SNC-PLA.

Residence time (min)		0	1	5	10	15	20	25	30
NPLA	**40/185**	2.15	2.66	2.85	3.81	3.91	3.88	3.9	4.17
	40/200	2.15	2.62	3.74	3.72	4.6	3.12	3.58	4.03
	100/185	2.15	2.44	2.53	2.93	2.98	3.62	3.61	3.61
	100/200	2.15	2.43	3.65	4.87	3.9	4.34	4.02	4.29
SNC-PLA	**40/185**	2.15	2.10	2.13	2.21	2.05	2.16	2.18	2.28
	40/200	2.15	2.13	2.14	2.14	2.16	2.14	2.07	2.26
	100/185	2.15	2.13	2.02	2.37	2.19	2.17	2.24	2.49
	100/200	2.15	2.35	2.22	2.06	2.25	2.33	2.39	2.56

The incorporation of SNC into PLA matrix during melt processing increases the activation energies of degradation and recombination, which supports the stabilization effect of SNCs. The degradation and recombination rate constants (k_d and k_c) are predicted using **Eqn. 3.10** coupled with Arrhenius equation as described in **Fig. 3.1.** Considering the degradation rate constant (K_d), higher value is obtained for NPLA as compared to SNC-PLA (**Table 3.2)**. However, the K_d values obtained for both the systems at all processing conditions are much lower than that of reported values for hydrolysis K_d (~$6.8*10^{-3}$ s^{-1}) [17, 77]. This is an indication for the insignificant effect of hydrolysis on the degradation pathway. The incorporation of SNCs in PLA matrix significantly suppress the degradation and comparatively higher degradation activation energy is required to degrade SNC-PLA composite.

Table 3.2. Activation energies (E_{ad} and E_{ac}), pre-exponential factors (A_d and A_c) and degradation rate constant (K_d) for NPLA and SNC-PLA at different processing conditions.

	Screw speed (rpm)/temperature(ºC)	A_c L/mol/s	E_a kJ/mol	A_d 1/s	E_d kJ/mol	K_d*10^7 1/s
N PLA	40/185	146	29.6	1896	76.2	39.1
	40/200	137	34.7	1589	78.5	34.4
	100/185	116	29.1	2244	78.9	22.0
	100/200	94	27.6	2506	77.8	66.3
SNC-PLA	40/185	119	30.8	1547	84.4	3.64
	40/200	126.6	31.3	1785	86.0	5.73
	100/185	$9.4*10^{-7}$	47.4	1993	88.1	1.83
	100/200	1.66	98.1	2959	89.2	4.19

3.3.3. The effect of silk nanocrystals and processing conditions on melt rheology of PLA

Frequency sweep analysis is performed for NPLA and SNC–PLA within the linear viscoelastic region (strain rate equals 5 %) for the samples processed at 1, 10, 20 and 30 min to understand the impact of SNC and processing condition on the viscoelastic characteristics of the melt. Melt viscosity is significantly influenced by the molecular weight and it's MWD of PLA matrix. If PLA matrix is reinforced by fillers, additional effect of polymer to filler interaction and filler to filler interaction may influence the viscoelastic properties of the melt.

As already discussed above, the incorporation of silk nanocrystals provides stabilized melt during extrusion process which is also reflected by zero shear viscosity and the cross over frequencies. In this study, complex viscosity at frequency of 0.1 rad/s (η* (ω=0.1 rad/s)) and cross over frequency are taken as reference and 50% reduction is also considered as base line

for comparison. As displayed in **Fig. 3.10,** η* (ω=0.1 rad/s) is decreasing with increasing the processing time; and processing temperature is observed to have more effect than that of screw speed. At lower residence times, comparable η* (ω=0.1 rad/s) values are observed for NPLA and SNC-PLA. With increasing of residence time, higher values of η* (ω=0.1 rad/s) are observed for SNC-PLA, which is due to the reduction in the rate of degradation observed after the addition of thermally stable SNC. Similar information can also be obtained on the crossover frequencies (**Table 3.3)**.

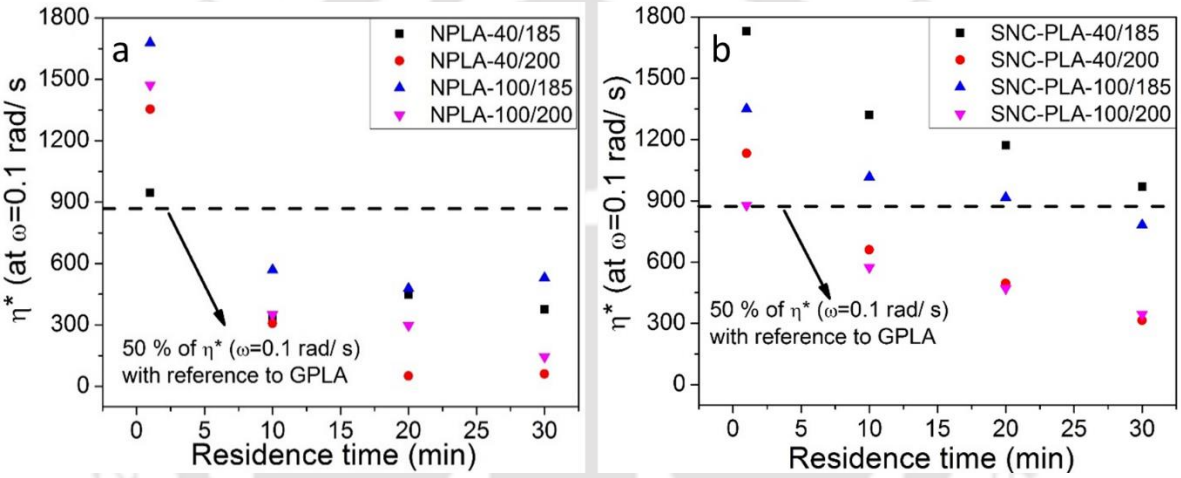

Figure 3.10. Influence of processing conditions (temperature, screw speed and time) on number-average molecular weight of melt processed (a) pristine PLA and (b) SNC-PLA.

Cross over frequency helps to understand the polymer matrix relaxation phenomenon which is dependent on the entanglement nature of the polymer melt. For highly entangled polymer melt, higher relaxation time is required and due to that, the cross over frequency shifts to lower frequencies values. On the other hand, when the polymer matrix entanglement is reduced, the crossover frequency tends to shift to higher vales since low relaxation time is required. Entanglement of the polymer matrix is significantly affected by reduction in molecular weight

and increment in PDI. The molecular weight analysis indicate that SNC stabilized the melt molecular weight and PDI whereas in the case of NPLA a drastic reduction is observed after 5 min. Due to special characteristics of SNC, the melt strength of PLA has improved and lower cross over frequency values are observed as compared to the NPLA particularly at higher processing time. From this, it can be concluded that, SNC can be used as a melt reinforcing additive for PLA to improve the melt processing performance so that it can be recycled multiple times through melt extrusion.

Table 3.3. The effect of processing conditions (screw speed and temperature) on zero shear viscosity (η_0) and cross over point (G_c and w_c).

	Processing time (min)	40				100			
		185		200		185		200	
		η_0	w_c	η_0	w_c	η_0	w_c	η_0	w_c
NPLA	0	1767	79	1767	79	1767	79	1767	19
	1	945	106	1354	130	1679	91	1473	320
	10	333	482	308	388	569	26.3	351	340
	20	448	317	51	>500	479	>500	298	>500
	30	377	>500	61	>500	530	>500	144	>500
SNC-PLA	1	1730	76	1133	144	1351	103	878	94
	10	1322	98	661	352	1017	117	575	166
	20	1172	110	496	304	916	107	471	218
	30	969	120	315	>500	782	>500	345	>500

3.3.4. The effect of silk nanocrystals on the chemical structure of PLA during melt processing

To understand the interaction between PLA macromolecular chains and SNC active sites, FTIR spectroscopy of NPLA and SNC-PLA is performed. The characteristic peaks (**Fig 3.11)** of PLA are identified for CH_3 (symmetric stretching (2854 cm^{-1}), asymmetric stretching (2925 cm^{-1}), symmetric bending (1382 cm^{-1}) asymmetric bending (1455 cm^{-1})), C-H stretching (2996

cm^{-1}) and deformation vibration (1358 cm^{-1}), C-O-C symmetric (1076 cm^{-1}) and asymmetric valance vibration (1180 cm^{-1}) and C=O stretching band (1747 cm^{-1}) are observed for NPLA. However, the additional hump peak observed at 1710 cm^{-1} after the incorporation of SNC may be attributed to weak van der waals forces arising between amide and OH groups of silk and C=O group of PLA. Similarly, CH stretching band of 2996 cm^{-1} also slightly diminished and the peak attributed to C=O stretching band at 1747 cm^{-1} is shifted slightly to lower band.

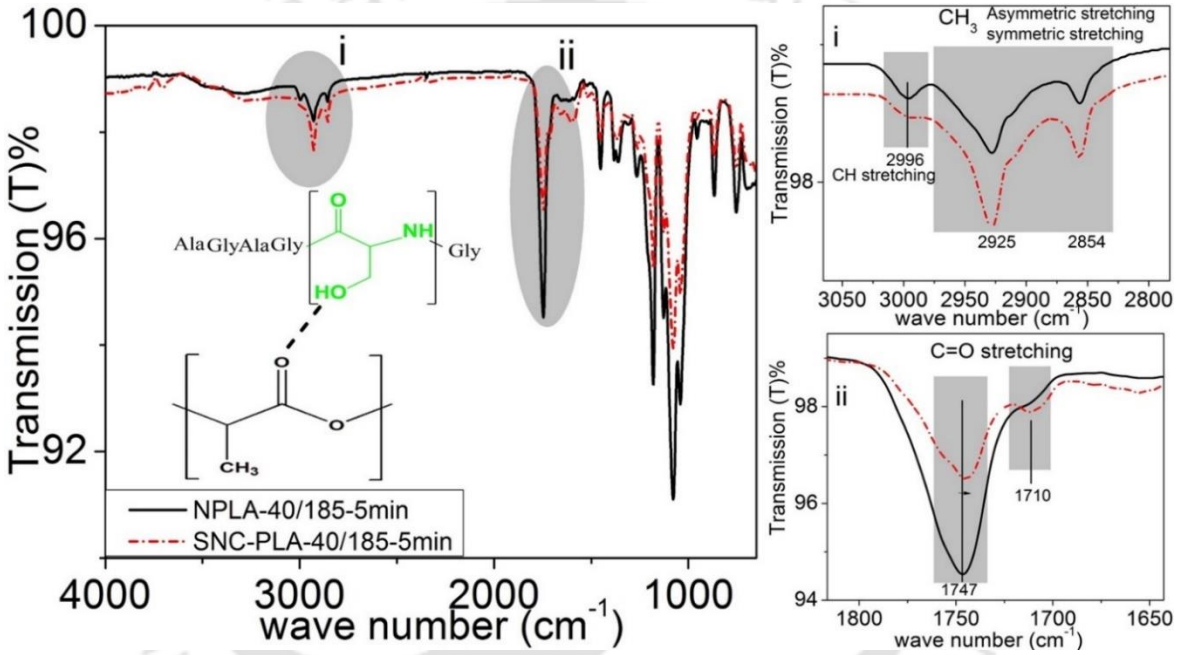

Figure 3.11. The influence of SNCs on FTIR spectra of PLA after melt processing at high temperature (185 ºC) and shear (40 rpm).

The observed interaction between PLA and SNC helps to form network like structure, which could be a reason for the stabilization of the melt during processing. As already discussed above, SNC is highly thermally stable crystalline nanomaterial. Furthermore, with the incorporation of SNCs, crystallinity of the nanocomposite is significantly improved. XRD diffractogram is taken for both the samples (NPLA and SNC-PLA) processed at a temperature

of 185 ºC and screw speed of 40 rpm. Intense sharp peaks are observed for SNC-PLA at 2Θ values of 16.5º and 18.8º,which are the representative peaks for α-form of PLA crystals with crystalline plane of (011) and (110/200) respectively [40]. The 2Θ peak observed at 22.1º confirms the intercalation of SNC in PLA matrix. This result reveals that SNC can be used as a nucleating agent to improve the slow crystallization process, which is one of the limitation of PLA.

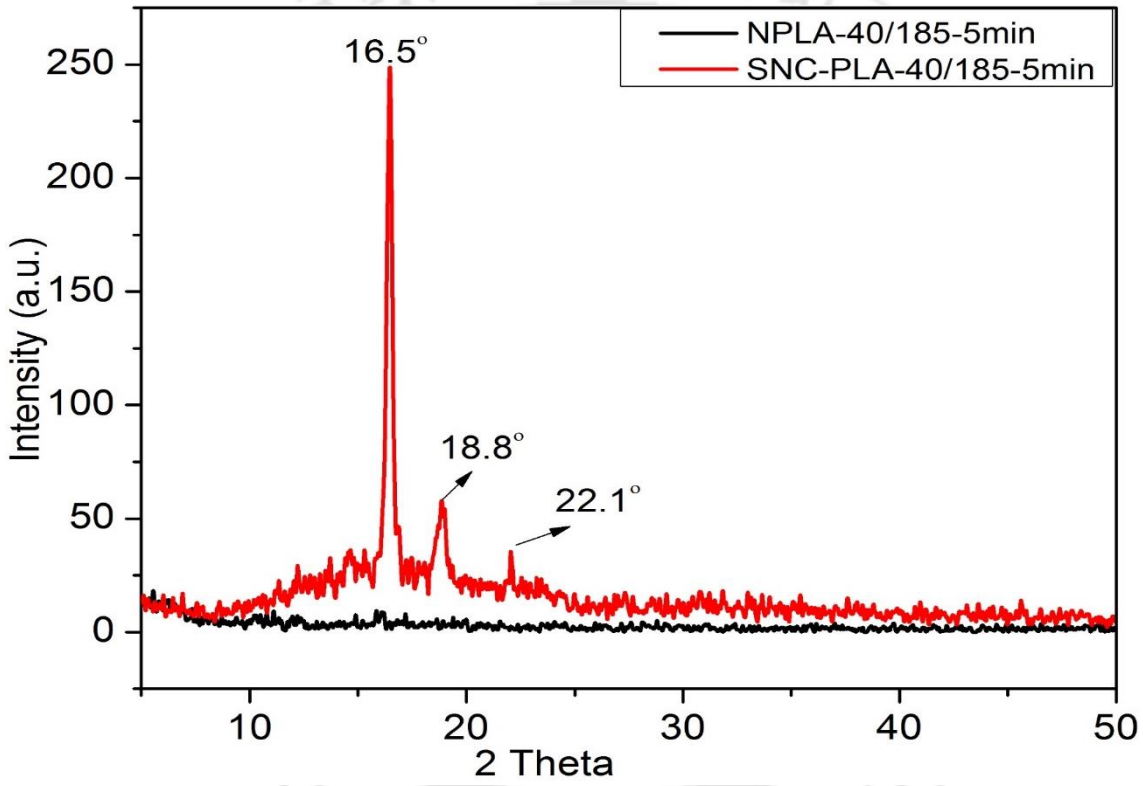

Figure 3.12. X-ray diffractogram of NPLA and SNC-PLA after melt processing (185 ºC and 40 rpm) (Sample is conditioned overnight in hot air hoven at 50 ºC).

Similarly, FESEM image is captured for the samples processed at a temperature of 185 ºC and screw speed of 40 rpm. As clearly observed in the **Fig. 3.13 (a) and (b),** the addition of SNC modified the surface through the formation of network structure which is absent in NPLA

micrograph. It may be related to the observed attraction between SNC active site and PLA chains. The presence of silk nanocrystals is confirmed from the FESEM micrographs as clearly shown at higher magnification of **Fig. 3.13 (c) and (d).** Due to the hydrophobic nature of SNCs, proper dispersion with minimum agglomeration is achieved in the hydrophobic PLA matrix.

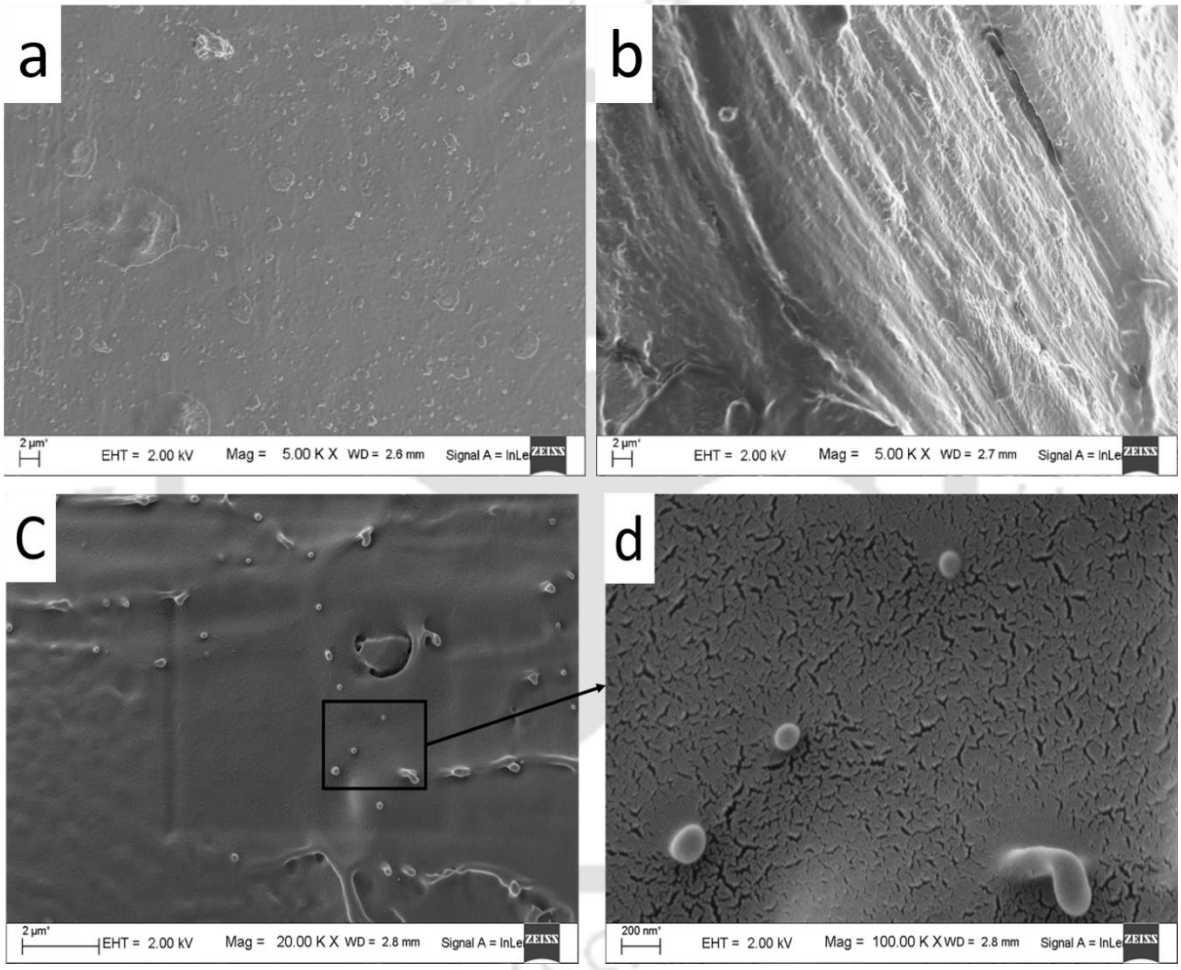

Figure 3.13 FESEM micrographs of (a) NPLA and (b) SNC-PLA.

3.4 Summary

This investigation shows the impact of SNC on the molecular weight distribution of PLA during melt processing. SNCs which are isolated from silk fibroin through acid hydrolysis are observed to have higher crystallinity and thermal stability. Highly ordered β-sheet arrangement is attained after acid hydrolysis because of the removal of the amorphous part. FTIR spectra reveals the conformational change from silk I of SF to silk II of SNC structure as discussed in section 3.3.1. Broad XRD peak of SF is also transformed into intense narrow peak of SNC which proves the increase in crystallinity after acid hydrolysis. SNCs are observed to degrade with two main degradation stages wherein 30% decomposition takes place within the degradation range of PLA (300-404 ºC) and 60 % of SNC is found to decompose above the degradation temperature of PLA (404-606 ºC). High thermal stability, crystallinity and hydrophobicity of SNC are some of the essential characteristics to be used as a filler to reinforce PLA matrix. SNCs are introduced into the PLA matrix during melt processing at different processing conditions (temperature: 185 ºC and 200 ºC, screw speed: 40 and 100 rpm and residence time: 0-30 min). The results obtained from molecular weight analysis revealed the stabilization effect of SNC. The rate of degradation of PLA melt is reduced after the incorporation of SNC and it is proved by the estimation of activation energies required for degradation and recombination reactions. Similar observation is also obtained from the melt rheology study, in which SNC-PLA attained better melt strength than that of NPLA. Weak chemical interaction is identified between SNC and PLA using FTIR, which can be mentioned as one of the reason for the melt stabilization effect of SNC. Furthermore, SNC improves the slow crystallization characteristics of PLA, which is confirmed by the intense sharp peaks of XRD diffractograms of the composite.

Chapter 4

Silk Nanocrystals Stabilized Melt Extruded Poly (Lactic Acid) Nanocomposite Films: Effect of Recycling on Thermal Stability, Crystallization Kinetics, Solution and Melt Rheology

In this study, the effect of silk nanocrystals (SNCs) on the thermal and rheological properties of poly (lactic acid) (PLA) under repetitive extrusion process is investigated. The presence of SNCs facilitates the crystallization process along with delay in thermal degradation of PLA matrix. Incorporation of SNC in PLA matrix leads to the reduction in cold crystallization peak temperature with lower crystallization half-time and higher growth rate. The substantial improvement in nucleation density is observed through Polarized Optical Microscope (POM), which confirms the nucleating effect of SNC in all processing cycles. Moreover, the rheological investigation (complex viscosity, storage and loss modulus values) revealed the stabilizing effect of SNC and the drastic degradation of NPLA in third and fourth cycle are observed to be fortified by the presence of SNC. Cole-Cole plot and cross over frequencies have been correlated with the molar mass distribution of PLA and PLA-silk composite during processing, which is further supported by the intrinsic viscosity measurement and acid value analysis. At last, this investigation suggests that the melt viscosity and thermal properties of PLA can be stabilized by addition of silk nanocrystals.

Parts of this chapter are published as:

Melakuu Tesfaye, Rahul Patwa, Arvind Gupta, Manash Kashyap, Vimal Katiyar, Recycling of Poly (Lactic Acid)/Silk based Bionanocomposites Films and its Influence on Thermal Stability, Crystallization Kinetics, Solution and Melt Rheology. International Journal of Biomacromolecules (2017).

4.1. Introduction

The melt processability performance of PLA needs to be improved in order to recycle it multiple times using simple, cost effective and energy efficient technique such as mechanical recycling. From the previous chapter, it is observed that SNC can be used as a stabilizing agent and maintain the molecular weight of PLA during long exposure to high temperature and shear. Application of PLA is limited by a narrow melt processing window due to its poor thermal stability (when subjected to high temperature and shear) and slow crystallization behavior [78-82]. Versatile applications of PLA are limited due to its low heat distortion temperature (HDT) and poor barrier properties in terms of oxygen and water vapor permeability [78, 83-85].

Incorporation of fillers of biological origin is one of the many approaches implemented to enhance the properties of PLA through formulation of fully biodegradable and environmental friendly nanocomposites [86]. Cellulose [87-90], chitosan [91], chitin [42], starch [92-96] and sucrose palmitate [97] are the most frequently studied biofillers, derived from plant and animal sources in the form of fibers, microcrystals and nanocrystals which are used to reinforce into PLA matrix. However, high surface functionality of these biofillers lead to two major challenges during composite preparation through melt compounding: one is agglomeration, which limits their dispersion in the polymer matrix; and the other is change in polymer macromolecular structure (degradation), which is induced by biofillers active sits [87, 88].

In general, the thermal degradation of PLA during melt processing occurs due to (1) intra-molecular and intermolecular trans-esterification, (2) unzipping depolymerization, (3) hydrolysis and (4) radical degradation [21, 98, 99]. Multiple processing with biofillers containing high surface functionality promotes catalyzed degradation of PLA leading to

reduction in its molecular weight. Grafting of a polymeric chain on the surface of biofiller leads to masking of reactive functionality on the biofiller surface [100]. This results in the inhibited degradation of PLA and at the same time enhancement of biofiller dispersion via prevention of agglomeration.

A study on the melt processing of PLA nanocomposites will be incomplete if the melt rheology is not employed to investigate the flow behavior of polymer melt with respect to the presence of any type of filler [25]. Further, the polymers being complex fluids, the melt rheology (especially in the presence of surface active nano biofillers) is expected to influence the crystallization behavior and hence, the solid properties of the polymer. The crystallization of the polymer is preceded by the role played by the flow of the melt, and the final configuration of polymer chains with/without the nanofillers. Hence, the need arises for the treatment of polymer nanocomposite melt matrix as essentially a two-component system whereby the effect of the polymer/filler rheological properties are studied [101-104]. Generally, Avrami equation can be used to analyze the isothermal crystallization characteristics of polymers. It can also be applied to the non-isothermal conditions by assuming a sequence of infinitesimally small isothermal processes with some model modification [105-107].

Both rheological and thermo-mechanical techniques are useful in understanding the viscoelastic properties of polymers [108]. While rheological properties measured in the shear mode are helpful in predicting the polymer/nano-filler interactions in the molten state, the dynamic mechanical analysis (DMA) provides information on the reinforcement of solid properties of the polymer on addition of nano-fillers across the glass transition temperature. Experiments in the oscillatory mode using the parallel plate geometry provide data on the

complex viscosity, resolved into the real and imaginary components, storage and loss moduli, and damping factor or tan δ values (ratio of the loss to the storage modulus) [109-111].

From the dynamic mechanical analysis (DMA), the elastic modulus, loss modulus and tan δ are plotted with respect to the temperature, providing information on the glass transition temperature and the behavior of solid properties from glassy state up to the rubbery plateau of the polymer. The rheological data on the other hand, can be utilized to analyze different aspects of the polymer-filler interactions [112]. The complex viscosity vs. frequency plots provide information on the shear thinning behavior of the PLA/nano-filler melt matrix in addition to the extent of adherence to power law behavior. Both the Cole-Cole plots (obtained by plotting the imaginary and the real viscosity) and Han plot (which are comparative behavior of the storage to the loss moduli) helps in identifying the miscibility/interaction of nanofiller and the PLA melt matrix. In addition to this, the data from the crossover of loss and storage moduli as a function of the frequency are helpful in predicting alterations of the molecular weight/distribution. Non-linearity of low frequency storage modulus behavior sometimes point towards network formation of the nanofillers within the PLA matrix in the melt state [113-115]. Establishing a correlation between rheological properties and molecular weight distribution results in an interesting proposition to predict micro-structural changes due to high temperature and shear [116-118]. In this chapter, NPLA and SNC-PLA nanocomposite film were prepared as stated in section 2.1.2.3 and the effect of SNC on crystallization and melting characteristics of PLA is investigated using the Avrami equation for multiple extrusion cycles. The viscoelastic properties are assessed by the rheological investigation and dynamic mechanical studies. Furthermore, the macromolecular changes are monitored by the estimation of intrinsic viscosity and acid value measurement.

4.2. Results and Discussion

4.2.1. Crystallinity and melting characteristics

The DSC thermograms described in **Fig. 4.1** and **Table 4.1 (**Calorimetric values of NPLA and SNC-PLA films at various reprocessing cycle) indicate the thermal analysis of NPLA and SNC-PLA at a heating rate of 5 ºC/min for various reprocessing cycles. For both the samples, the glass transition temperature and melting temperature is remained constant at ~57 ºC and ~151 ºC, respectively for all reprocessing cycles.

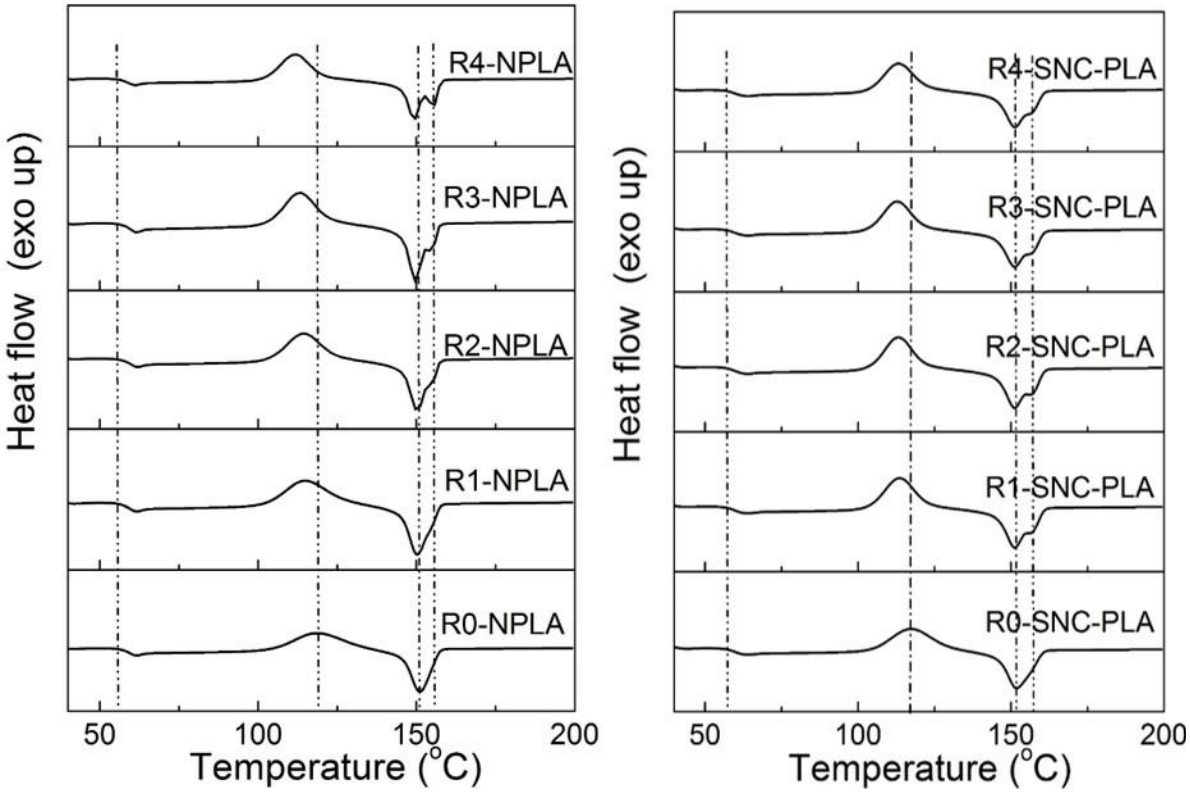

Figure 4.1. Second heating DSC thermograms of (a) NPLA and (b) SNC-PLA at different reprocessing cycles.

The cold crystallization temperature of pristine PLA is observed to decrease from 118.2 (R0-NPLA) to 114.7 ºC (R1-NPLA) and remains constant at ~114 ºC for the subsequent cycles whereas, for the case of SNC-PLA, T_{cc} decreased from 115.8 (R0-SNC-PLA) to 112.2 ºC (R2-SNC-PLA) and remained constant around 111 ºC on the subsequent cycles.

Table 4.1. Calorimetric values of pristine PLA and SNC-PLA at various reprocessing cycles.

Samples	Reprocessing cycle	T_g (ºC)	T_{cc} (ºC)	T_m (ºC)	H_{cc} (ºC)	H_m (ºC)
NPLA	R0	57.7	118	151.2	29.2	-34.4
	R1	57.5	114.7	150.3	27.0	-29.0
	R2	57.2	112.5	149.3	27.0	-31.5
	R3	57.9	114.5	150.1	26.2	-31.4
	R4	57.8	113.4	149.8	28.2	-36.0
SNC-PLA	R0	57.7	115.8	150.5	30.4	-35.2
	R1	57.7	112.2	149.6	34.6	-38.0
	R2	57.4	111.8	149.5	33.0	-37.0
	R3	57.4	111.3	149.3	32.8	-37.4
	R4	57.5	111.8	149.5	33.7	-38.6

The addition of SNC decreases the cold crystallization temperature approximately by 3 ºC, indicating the early stage formation of crystals by nucleating effect of the SNCs. The reduction in T_{cc} with the addition of reinforcing agent is also reported for microfibrillated cellulose-reinforced PLA composites [119]. In the present system, the formation of shorter chains due to thermomechanical degradation can also be mentioned as a reason for the reduction in cold crystallization temperature with reprocessing cycles. The melting endotherm (**Fig. 4.1)** clearly

illustrates that a broader and a shoulder like melting peak in the higher temperature range is an indication of chain scission of polymer chains due to the high shear and temperature, resulting in an increment in the number of shorter chains. It is well known from the literature that; thermomechanical degradation can induce the formation of disordered crystalline phase (α′ phase) at a crystallization temperature lower than 120 ºC [120]. Therefore, chain degradation enhances the probable formation of α′ phase crystals in addition to α crystals. The α′ phase crystals tend to melt recrystallize upon heating exhibited by the double melting peak for both pristine PLA and SNC-PLA systems with increasing reprocessing cycles [120].

The higher cold crystallization enthalpy observed for R0-SNC-PLA (approximately around 33 J/g) as compared to the R0-NPLA (approximately around 27 J/g), which further supported the nucleating effect of SNC and is an indication towards improvement of the slow crystallization process (which is the major drawback of PLA). It has been discussed in various reports that folding of polymer chains can be easily initiated on the filler surface, which increases the interfacial free energy required to overcome the crystallization barrier energy [121].

Avrami equation (**Eqn. 4.1**) can be used to understand in-depth the influence of SNC on the crystallization behavior of PLA during multiple processing [69].

$$1 - X_t = \exp(-Z_t t^n) \quad 4.1$$

Avrami exponent (n) and rate constant (Z_t) are calculated from the slope and intercept of the plot of ln (-ln (1-X_t)) vs. ln (t) (**Eqn. 4.2)** to analyze the crystallization behavior. The crystallization half-time ($t_{1/2}$) and the growth rate (G) are calculated from **Eqn. 4.3** and **Eqn. 4.4**. The values of $t_{1/2}$ and G obtained above are compared with those estimated from experimental data.

$$\ln[-\ln(1 - X_t)] = n\ln(t) + \ln(Z_t) \quad 4.2$$

$$t_{\frac{1}{2}} = \left(ln2/Z_t\right)^{\frac{1}{n}} \quad 4.3$$

$$G = \left(1/t_{\frac{1}{2}}\right) \quad 4.4$$

As shown in **Fig. 4.2(a) and (b),** reprocessing influences the crystallization behavior of both the samples (NPLA and SNC-PLA) with the observation of sigmoid curves, described by the Avrami equation.

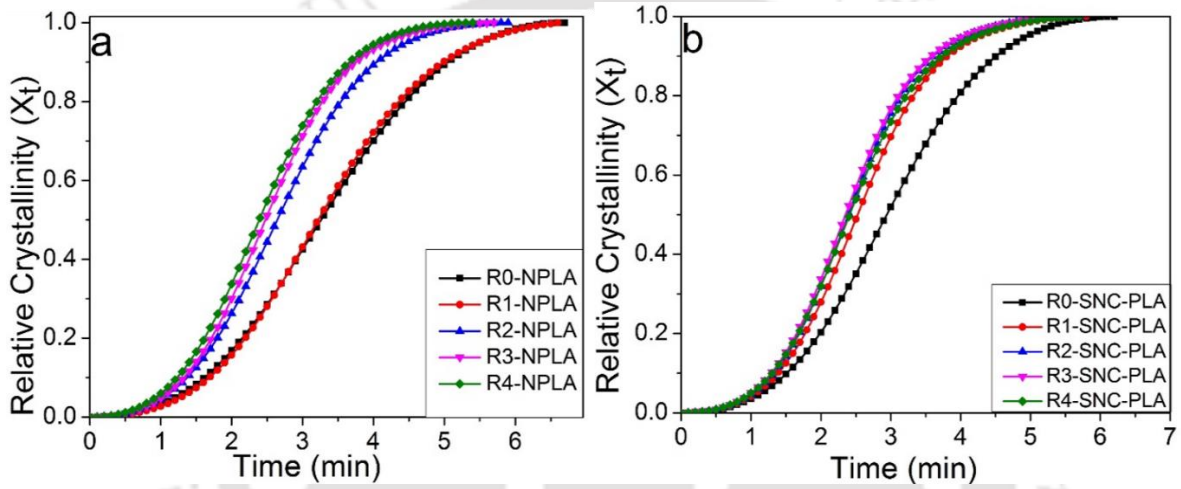

Figure 4.2. Relative crystallinity vs time for (a) NPLA and (b) SNC-PLA at various reprocessing cycles.

Crystallization half-time for SNC-PLA varies from 2.95 to 2.42 min, which are observed to decrease with the subsequent reprocessing cycle. It indicates a faster crystallization process for SNC-PLA compared to NPLA, accompanied by the increment of growth rate from 0.339 to 0.424 min^{-1} along with the progressing reprocessing cycle as indicated in **Table 4.2** whereas the crystallization half-time and growth rate of NPLA fluctuated respectively from 3.26 to 2.39 min (decreasing order) and from 0.316 to 0.419 min^{-1} (increasing order) with the repetitive reprocessing cycles of R0 to R4. Because of the slow crystallization process of

NPLA, higher crystallization half-time and lower growth rate is observed as compared to SNC-PLA. Similar results are also reported for PLA based composites with fillers including, sucrose palmitate and cellulose from organic source and graphene and clays from inorganic sources [119, 122-124]. The consistency of crystallization half-time values determined from the graph (**Fig. 4.2)** and calculated from Avrami equation **(Eqn.4.1)** shows the validity of the Avrami model for both the systems. Furthermore, the crystallization mechanism can be explained through the Avrami exponent (n) and the rate constant (Z_t). These values are estimated from the slope and intercept of the plot of ln (-ln (1-X_t)) vs ln (t) shown in **Fig. 4.3,** considering crystallization data between 10 to 70%. The values of **n** are mostly integers used to explain the dimensions of crystals, which vary from 1 to 4 and are dependent on the behavior of nucleation and the crystal growth.

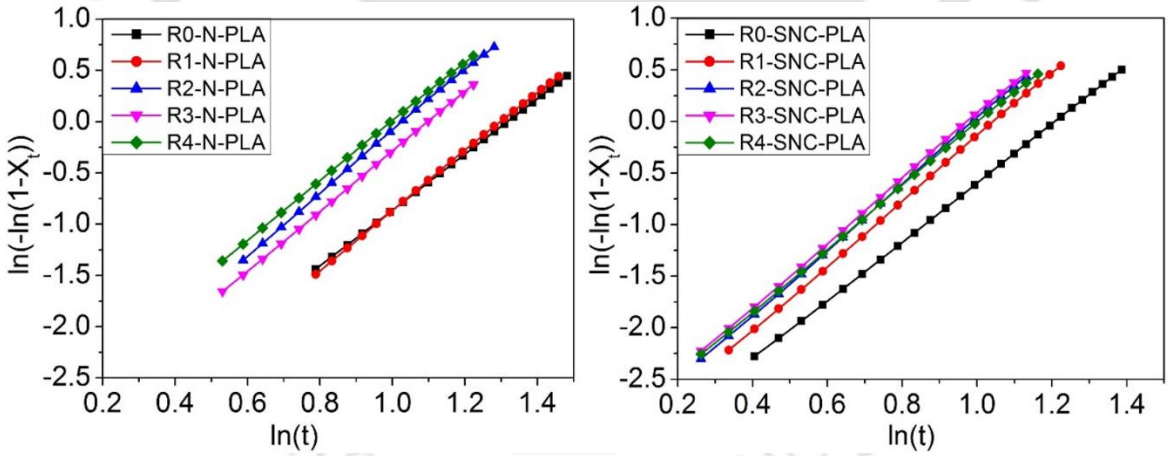

Figure 4.3. Avrami plot of ln (-ln (1-X_t)) vs ln (t) of (a) NPLA and (b) SNC-PLA at various reprocessing cycles.

However, Avrami exponent (n) of PLA is reported between 2 and 4, which depends on the heating rates and nucleation agent. According to **Nofar et al.,** three dimensional (3-D) crystal

growth (i.e. n values are about 3 and 4) is observed for slow heating rate and a two dimensional (2-D) crystal growth at higher heating rates of ~20 and ~30 ºC/min [125].

As described in **Table 4.2,** values of n for NPLA initially increased from 2.58 to 3.03 upto the second reprocessing cycle (R2-NPLA) and decreased to 2.87 (R4). This is an indication of fast crystallization at the initial stage due to the formation of a small extent of shorter chains followed by hindering of the crystallization process due to major thermomechanical degradation. The random values of n implies random distribution of crystals formed ranging from rod and disc like growth to three dimensional spherulite crystal growth.

Table 4.2. Avrami constants (n and Z_t), growth rate (G) and crystallization half-time ($t_{½}$)

		R0	R1	R2	R3	R4
NPLA	n	2.58	2.90	3.03	2.89	2.87
	Z_t	0.033	0.035	0.044	0.044	0.057
	$t_{½}$ (min)[a]	3.27	3.23	2.48	2.59	2.39
	$t_{½}$(min)[b]	3.26	3.22	2.47	2.64	2.39
	G[a]	0.32	0.31	0.40	0.39	0.42
	G[b]	0.31	0.31	0.40	0.38	0.42
SNC-PLA	N	2.85	3.15	3.19	3.14	3.05
	Z_t	0.032	0.037	0.042	0.047	0.046
	$t_{½}$ (min)[a]	2.95	2.53	2.40	2.36	2.42
	$t_{½}$(min)[b]	2.94	2.53	2.39	2.35	2.41
	G[a]	0.34	0.39	0.42	0.42	0.41
	G[b]	0.34	0.40	0.42	0.43	0.42

'a' calculated, 'b' experiment

Similarly for SNC-PLA, values of n initially increased from 2.85 for first cycle to 3.19 for second cycle and remained constant around 3 for the remaining extrusion cycles. This confirmed the three dimensional spherulite crystal growth due to the presence of SNC. Lower crystallization rate (Z_t) is obtained for both the samples at all reprocessing stage. Also, this showed a very slow crystallization process which can be accounted for the disordered entanglement nature of the chain, which is more pronouncing because of reprocessing cycles.

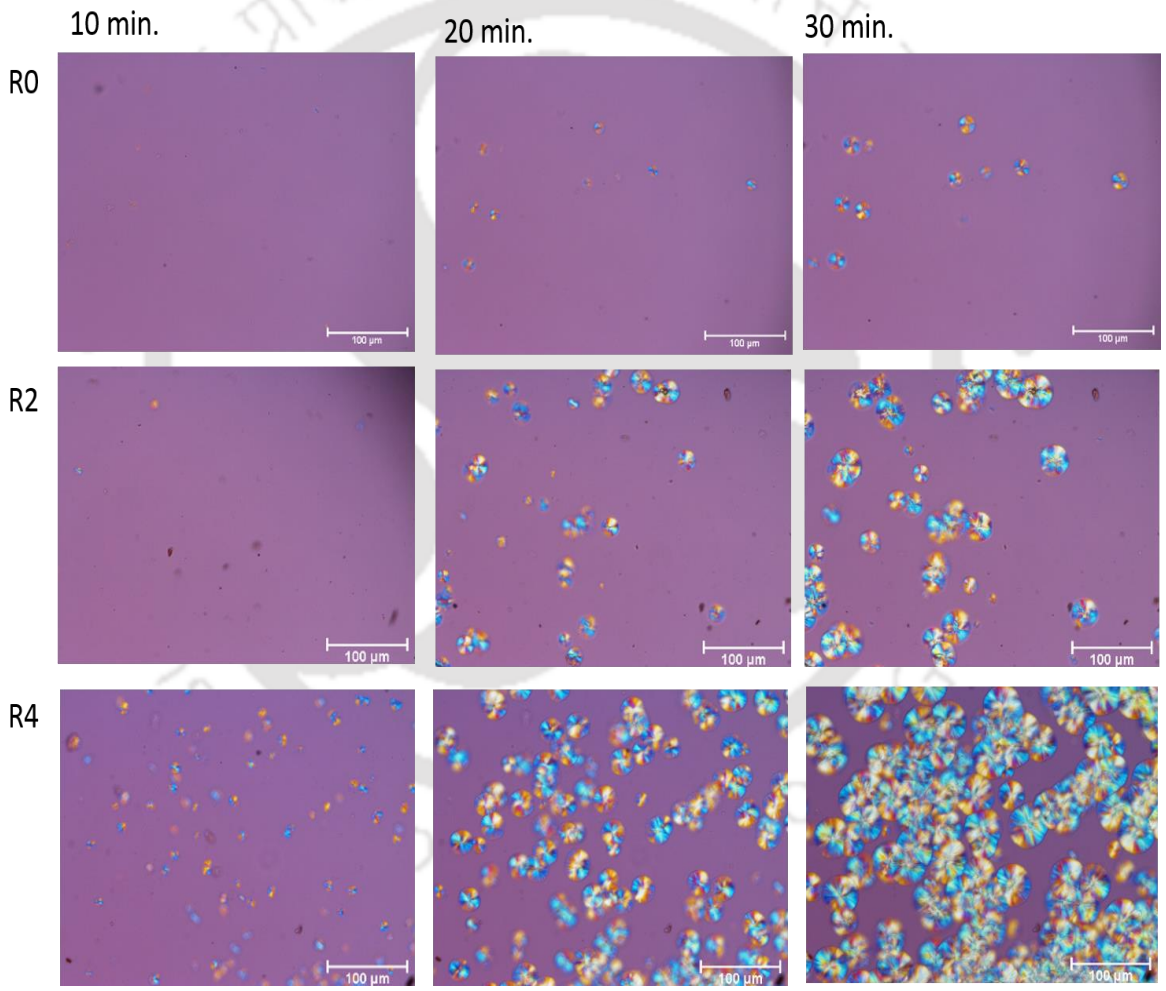

Figure 4.4. Polarized optical micrographs of NPLA at different reproccessing cycles for 10 min, 20 min and 30 min isothermal crystallization at 120 ºC.

POM images of isothermally crystallized (at 120 ºC) NPLA and SNC-PLA at various reprocessing cycles at 10, 20, and 30 min are displayed in **Fig. 4.4 and Fig. 4.5** respectively. It can be clearly observed that reprocessing accelerates the nucleation processes and increase the nucleation density of PLA. An increment in nucleation density with reduction in crystal size is explained by **Tsuji et al.,** which is in agreement with the present study [124].

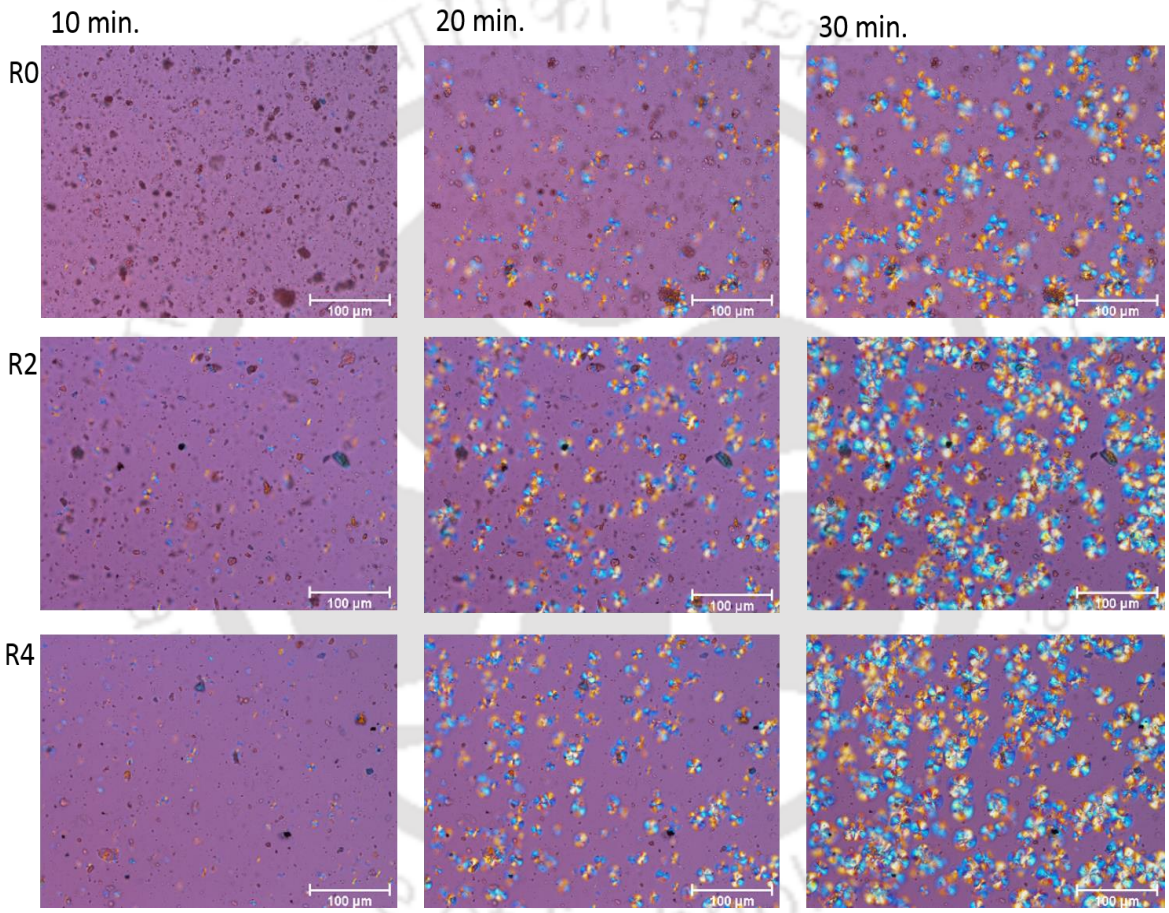

Figure 4.5. Polarized optical micrographs of SNC-PLA at different reproccessing cycles for 10, 20 and 30 min isothermal crystallization 120 ºC.

In the present investigations, thermomechanical degradation favors the formation of shorter chains PLA macromolecules, which might have facilitated the crystallization process, which

leads to increment in the nucleation density and reduction in crystal size as observed in **Fig. 4.4** of optical polarized images for NPLA. Moreover, the addition of SNC into PLA matrix further enhances the nucleation process as it is acting like a nucleating agent.

Nucleating agents are used to initiate the folding process for PLA chains on their surface and tend to increase the crystal growth front. Higher number of crystals (nucleation density) and lower crystal size are observed for SNC-PLA as compared to NPLA in respective processing cycles. It confirms that, in addition to the impact of thermomechanical degradation on nucleation density, the chain folding process is also initiated on the surface of SNC, which further increases the crystal growth. The spherulite radial growth rate is estimated from the slope of spherulite radius vs crystallizing time plot as indicated in **Fig. 4.6 (a & b)** for NPLA and SNC-PLA at three processing cycles (R0, R2 and R4).

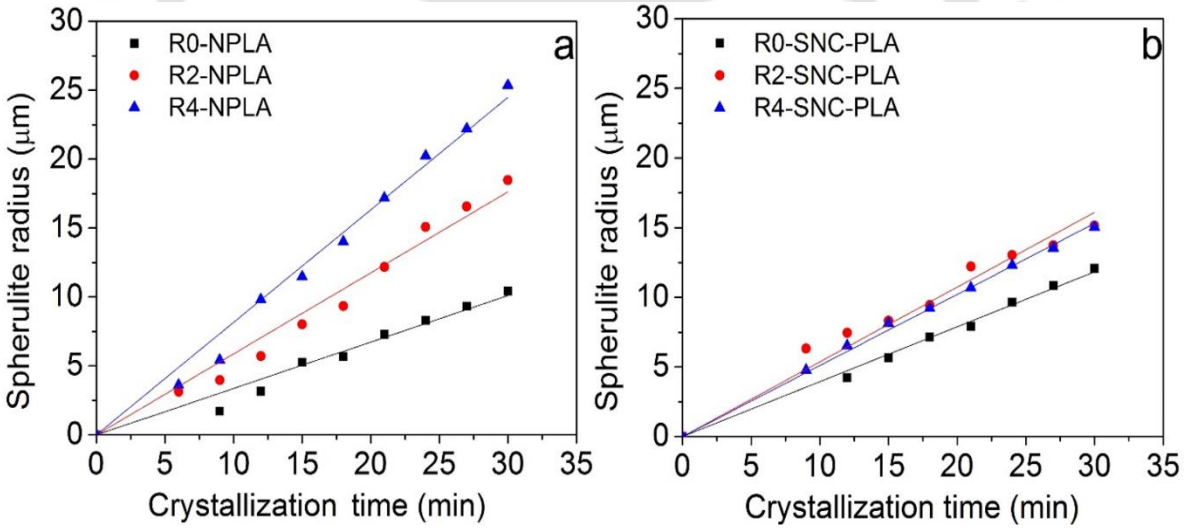

Figure 4.6. Change of spherulite radius with respect to time at 120 ºC for various reprocessing cycles of (a) NPLA and (b) SNC-PLA.

Slightly lower spherulites radial growth is observed for R0-NPLA as compared to R0-SNC-PLA which is subsequently increased while the growth rate remains constant for respective nanocomposites (**Fig 4.7 (a)).** It is an indication for SNCs has a tendency to increase the barrier energy, which is required to transport the polymer chain from the melt region to the crystals growing front [126, 127].

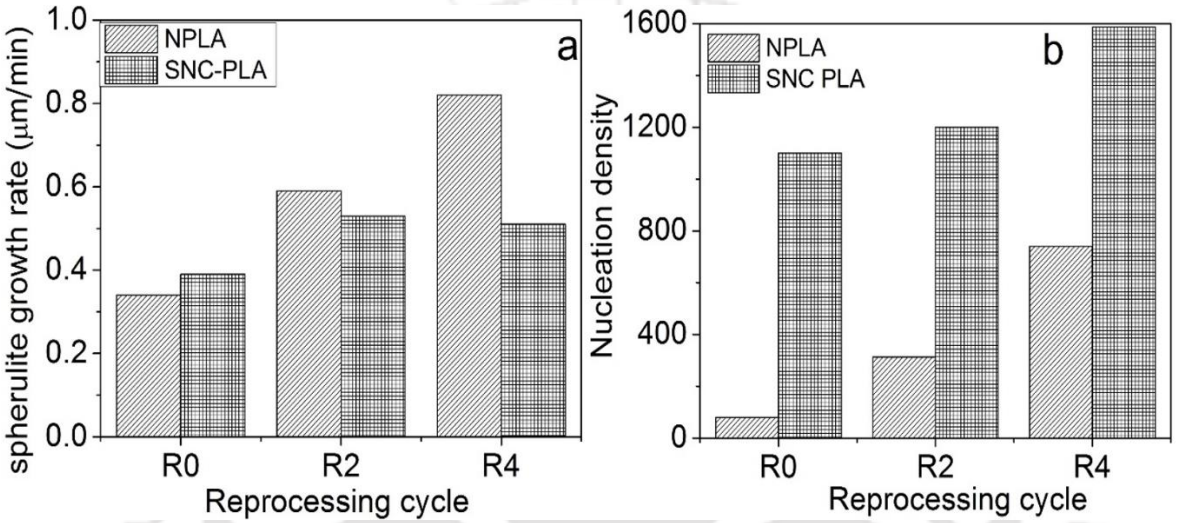

Figure 4.7. (a) Spherulite growth rate and (b) nucleation density (number of spherulites per squre milimetre)

The nucleation density of NPLA and SNC-PLA are estimated by the number of spherulites per square millimeter as indicated in **Fig. 4.7 (b).** The higher values of nucleation density for SNC-PLA proves the nucleating effect of SNCs. Moreover, nucleation density is found to increase with the increasing reprocessing cycles, which is due to degradation of the polymer matrix.

4.2.2. Rheological Measurements

4.2.2.1. Complex viscosity

The complex viscosity results for NPLA and SNC-PLA at various reprocessing cycles have been plotted (**Fig. 4.8**) against the angular frequency. The reprocessing of NPLA and SNC-PLA nanocomposite is expected to degrade the polymer thus leading to lowering of molecular weight. The presence of well dispersed SNCs in the PLA matrix is expected to influence the melt rheology of the polymer.

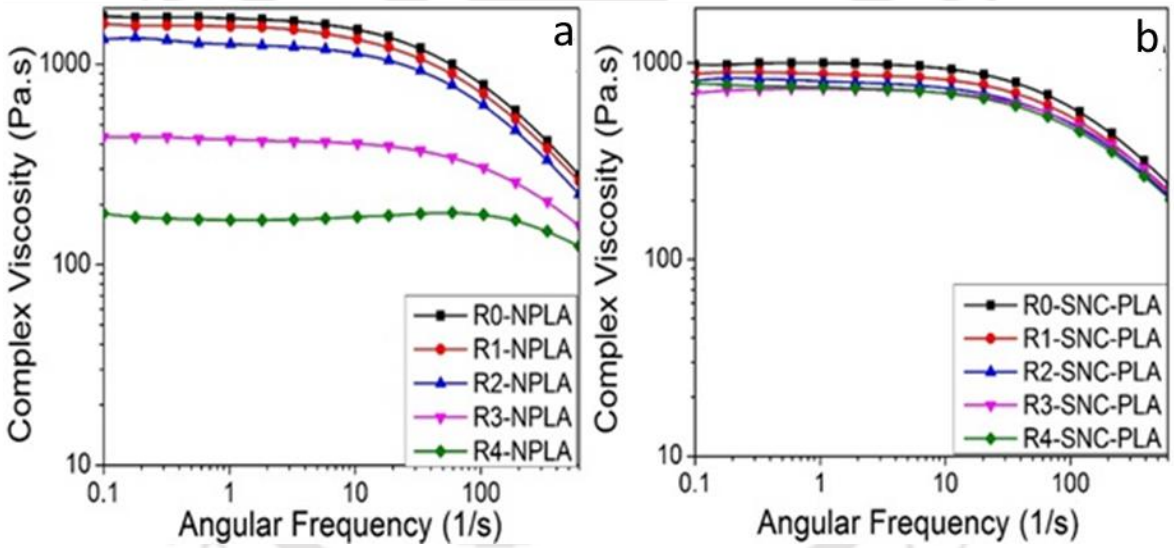

Figure 4.8. Complex viscosity of reprocessed (a) PLA and (b) SNC-PLA nanocomposite samples.

Generally, the complex viscosity has been found to increase with the addition of nano-fillers due to the reinforcing effect of the former. This is usually due to the domination of the particle-particle interaction as compared to the particle-polymer interaction resulting in the formation of a transient network also termed as a rheological percolation structure. At higher frequencies,

this rheological percolation structure is dismantled and the rheology is dominated by polymer-particle interactions [128]. As molecular weight has an inverse relationship with the melt viscosity, the melt viscosity is expected to lower after every consecutive reprocessing cycle due to exposure of high temperature and shear.

Table 4.3. Melt viscosity (Pa.s) at different recycle stages (% decrease in subsequent recycling) of PLA and SNC-PLA nanocomposites at the lowest (0.1 Hz) and highest frequencies (600 Hz).

Sample	R0	R1	R2	R3	R4
NPLA (0.1 Hz)	1730	1590(8%↓)	1330(16%↓)	433(67%↓)	180(58%↓)
SNC-PLA (0.1 Hz)	981	884(10%↓)	811(8%↓)	702(13%↓)	785(12%↑)
NPLA (600 Hz)	281	261(7%↓)	225(14%↓)	157(30%↓)	124(21%↓)
SNC-PLA (600 Hz)	238	216(9%↓)	208(4%↓)	222(6%↑))	202(9%↓)

As the reprocessing of the polymer and the nanocomposites are done in a twin screw extruder, the shear rates are expected to be higher compared to a single screw extruder. From **Fig**. **4.8**, it can be observed that the melt viscosity reduces with every reprocessing cycle. **Table 4.3** shows the viscosity values at high and low frequency range for the reprocessed samples. The decrease in viscosity follows unique patterns for NPLA and SNC-PLA nanocomposites. While the viscosity showed uniform decrease from R0 to R2 for both NPLA and SNC-PLA nanocomposites, NPLA exhibited rapid decrease in melt viscosity for R3 (67%) and R4 (58%) as compared to R2 and R3, respectively. However, the change in melt viscosity of SNC-PLA nanocomposites varies with in the range of 15% along the reprocessing cycles. Further, the

viscosity of SNC-PLA nanocomposites after the first processing (R0) is lower than that of NPLA by 43%, which may be due to the presence of acid functional groups present in SNC resulting from the acid hydrolysis treatment during SNC extraction. These groups are expected to catalyze the degradation of PLA thus lowering the molecular weight and hence the viscosity. However, subsequent rapid degradation of PLA in the SNC-PLA nanocomposites (R1, R2, R3 and R4) are prevented, which is probably due to by the capping effect of the PLA chains on the active reaction sites of SNC.

The zero shear viscosity values and the power law index values have been calculated from the complex viscosity vs. frequency plots. The zero shear viscosity values follow a similar trend to the molecular weight values as measured using the GPC technique (see **Table 4.8**) thus proving that molecular weight estimations from rheological data can be used for comparative analysis.

The power law index (n) values (**Table 4.4**) for SNC-PLA change with narrow range from R0-R4 (0.62-0.68) as compared to NPLA (0.55-0.79) along the reprocessing cycles. Lower values for "n" indicate greater shear thinning behavior as indicated in the greater viscosity drops for NPLA as compared to SNC-PLA (**Table 4.4**). The variation of "n" is significant from the point of view of the processing characteristics of the polymer and hence the decision on the choice of screw design of the extruder. The lower the power law index, higher is the shear thinning and vice-versa. Thus higher the power law index of the polymer melt, lesser is the shear thinning and thus more is the heat energy dissipation. From **Table 4.4**, it is evident that heat dissipation is more for SNC-PLA nanocomposites up to the third processing cycle (R2) due to the effect of SNCs which tend to restrict the flow of the melt. In case of R3 and R4, the shear

thinning of NPLA is high because of the drastic drop in the molecular weight due to the continued exposure to thermal and shear history. From the above viscosity data analysis, it is evident that the addition of SNCs help in fortifying or stabilizing the PLA from excessive reduction in the viscosity on exposure to repeated recycling steps [111, 128].

Table 4.4. Power law index and zero shear viscosity.

Sample		R0	R1	R2	R3	R4
NPLA	Power law index (n)	0.55	0.56	0.56	0.74	0.79
	R^2	0.96	0.96	0.96	0.92	0.94
	Zero shear viscosity (Pa.s)	1721	1566	1264	422	169
	R^2	0.97	0.99	0.99	0.92	0.96
SNC-PLA	Power law index (n)	0.62	0.63	0.65	0.68	0.66
	R^2	0.96	0.96	0.96	0.95	0.96
	Zero shear viscosity (Pa.s)	1005	890	820	737	760
	R^2	0.99	0.94	0.91	0.98	0.97

4.2.2.2. Storage and loss modulus

The storage and loss modulus data from dynamic frequency sweep tests provide an idea on the role of filler (in this case SNCs) on the melt rheology of the polymer. The behavior of storage modulus in the low frequency region is especially sensitive as there is enough time for the polymer to respond to the stress imposed on the melt. The storage modulus and loss modulus have been plotted with respect to the frequency in **Fig. 4.9** The storage modulus vs. frequency curves almost coincide for R0, R1 and R2 with marginal decrease in values with subsequent progress in the reprocessing stages followed by a significant drop in the values for the third and fourth reprocessing stage. This can be attributed to the scission of the NPLA chains due to

thermomechanical degradation, which also results in the drop in the molecular weights and the viscosity values. A similar trend is followed by the loss modulus plots for NPLA showing a decreasing trend with progress in the reprocessing cycle.

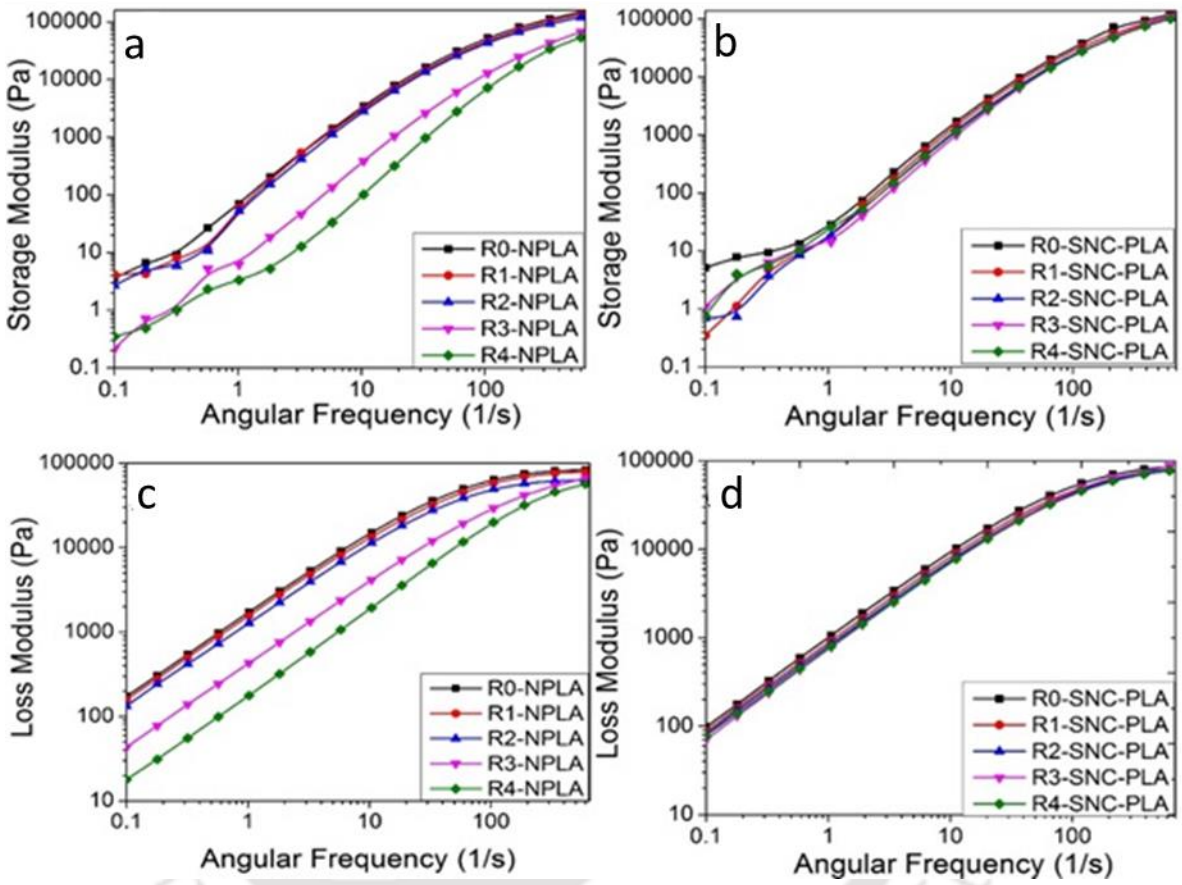

Figure 4.9. Storage modulus vs. frequency for (a) NPLA and (b) SNC-PLA nanocomposites and loss modulus vs. frequency for (c) NPLA and (b) SNC-PLA nanocomposites.

The storage modulus data at low frequencies can be expected to be sensitive in comparison to the data at high frequencies for polymer nanocomposites. This is due to the predominance of nano-filler over the polymer with respect to the exhibition of rheological characteristics. In general, subjected to good dispersion of the nano-filler, the storage modulus is expected to

increase at low frequency on increasing nano-filler loadings compared to the results exhibited by NPLA. [129].

Table 4.5. Storage modulus at lower and higher frequencies.

Samples	G'(0.588 Hz)	G' (119 Hz)
NPLA-R0	26.8	52700
NPLA-R1	11.4	47100
NPLA-R2	10.7	43700
NPLA-R3	5.23	13000
NPLA-R4	2.31	7200
SNC-R0	13.2	37500
SNC-R1	9.2	33500
SNC-R2	8.5	29100
SNC-R3	11.1	28100
SNC-R4	10.3	27700

The storage modulus values at low (0.588 Hz) and high frequency (119 Hz) have been reported in **Table 4.5**. It can be observed that NPLA exhibits a decreasing trend for storage modulus with consecutive reprocessing cycles at both high and low frequencies. Thermal degradation and the resulting decrease in polymer chain lengths of NPLA is manifested in the lower storage modulus responses. A similar trend is not followed for SNC-PLA particularly for the low frequency region, whereas the storage modulus at the low frequency (0.588 Hz) and high frequency (119 Hz) remains almost constant as compared to NPLA from the first to the last processing cycle, probably due to the stabilizing effect of the SNCs [130].

4.2.2.3. Polymer matrix-filler interaction

Cole-Cole plot: A plot of imaginary vs. real viscosity is called the Cole-Cole plot which is made to study the interaction of filler with the polymer matrix in the melt state. Semi-circular plots identical to the base polymer indicate good polymer-filler interactions, while, the width of the semi-circular plots provide relative comparison of the zero shear viscosity [131, 132]. In the absence of higher order structure (such as crosslinking, branching and grafting), perfect semicircular arc can be obtained for a polymer melt with single relaxation time. Polymer to filler interaction and the possible agglomeration of fillers can easily be detected from the arc. The aggregation of $CaCO_3$ in polypropylene (PP) matrix was detected using rheological study trough Cole-Cole plot. Based on **Kiss et al.,** PP/$CaCO_3$ composite deviates strongly from semicircular arc due to possible agglomeration[133]. In the present study, the Cole-Cole plots of NPLA and SNC-PLA nanocomposites are overlaid as shown in **Fig. 4.10**.

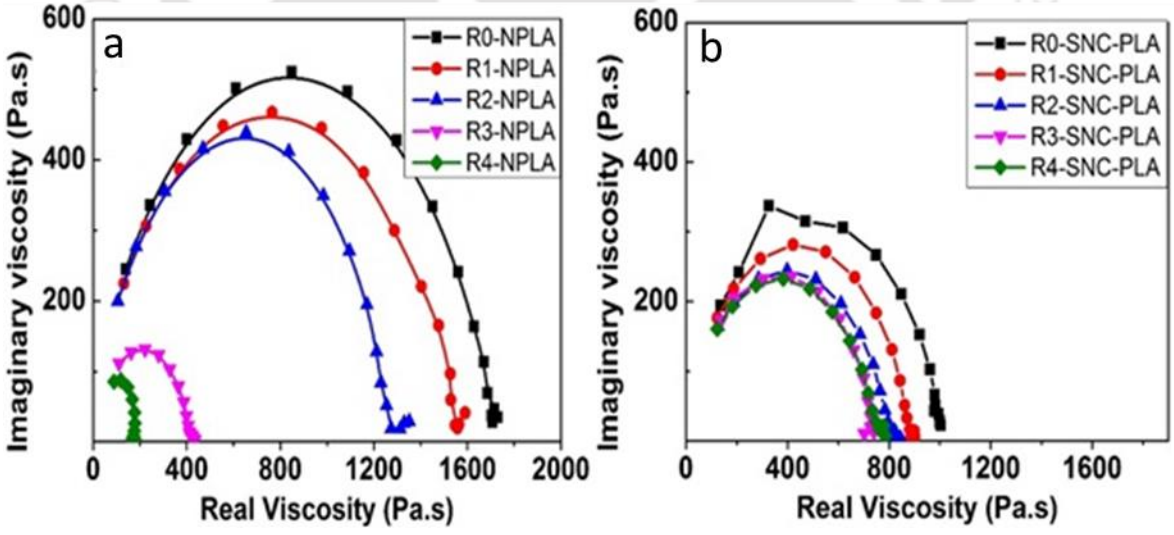

Figure 4.10 Cole-Cole plot of NPLA and SNC-PLA composite for five recycle times.

It can be observed that the top most plot (**Fig. 4.10 (a))** (represented by black square symbol) signifying the composition with highest viscosity is shown by R0-NPLA and the plot with the least width of the semi-circle (light blue rhombus) is shown by R4-NPLA indicating the least zero shear viscosity, which is also confirmed by molecular weight analysis using GPC. **Walha et al.,** observed semicircular Cole-Cole plot for melt processed neat PLA with lower relaxation time [134]. Furthermore, **Nait-Ali et al.,** discussed the relationship between polymer macromolecular structural change with broadening of Cole-Cole arc [135]. The broadening of the arc is highly dependent on zero shear viscosity, in which it decreases with decreasing molecular weight and increasing PDI of polymer melt. The mobility of macromolecular chains increases with number of melt processing cycle due to thermomechanical degradation which leads to the formation of shorter chain fraction [136]. Similar conclusion can also be drawn from the current investigation, in which the zero shear viscosity is significantly affected by the thermomechanical degradation with increasing the processing cycles. Most importantly, all the plots (**Fig. 4.10 (b))** show semi-circular behavior indicating uniform dispersion of the SNC filler in the PLA matrix. Although both the plots for NPLA and SNC-PLA exhibit semi-circular behavior, width of the semi-circles SNC-PLA is more or less preserved for the subsequent reprocessing steps after the initial drop in melt viscosity as compared to NPLA (R0-NPLA) for the first processing cycle (R0-SNC-PLA), indicating a comparatively stable molecular weight distribution from R0-SNC-PLA to R4-SNC-PLA.

Han plot: A plot of the storage modulus vs. the loss modulus, also called the Han plot, is made to evaluate the miscibility in a polymer matrix which is either a composite or a blend of two or more polymers [128, 131]. The Han Plot is made to determine the heterogeneity of the polymer nanocomposite matrix in the melt condition from the concurrence of the plots of the

nanocomposite over the Han plot of the NPLA. The Han Plot for the NPLA and SNC-PLA reprocessed compositions have been shown in. **Fig. 4.11**.

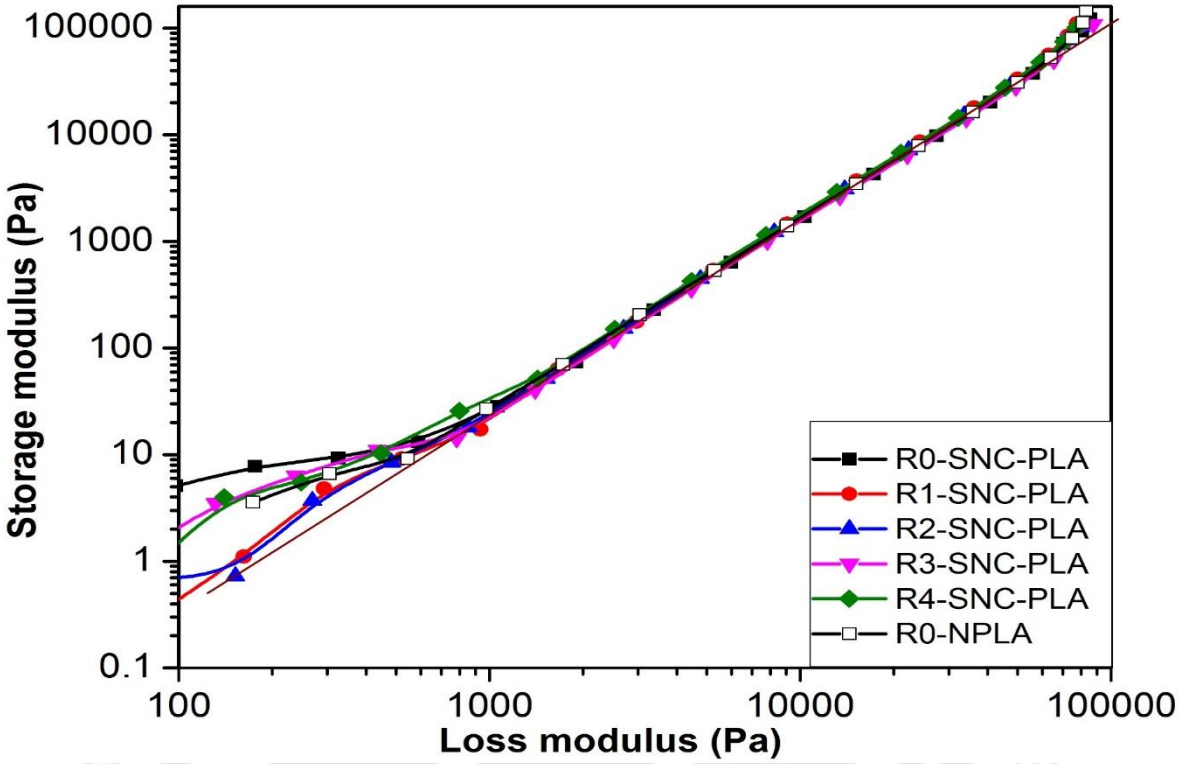

Figure 4.11. Storage vs. loss modulus plots (Han plot) for (a) reprocessed NPLA and (b) reprocessed SNC-PLA nanocomposites.

Table 4.6 shows the slope of storage modulus (G') versus loss modulus (G") plot shown in **Fig. 4.11** in the higher frequency region for the modulus range of 10,000 to 100,000 Pa. For all slope calculations, the R^2 ~0.99 value is obtained. It can be observed that the value of slope is found to be higher for SNC-PLA for the first three processing cycles as compared to R0-NPLA implying a greater rate of increase of storage modulus as compared to the loss modulus which can be attributed to solid-like behavior of the PLA matrix due to uniform

dispersion/miscibility of the SNCs. The values of slope are found to decrease slightly for the third and the fourth reprocessing cycles due to thermal degradation of the PLA.

Table 4.6. Slope and correlation index (R^2) of the curve of the graph G' vs. G" for NPLA and SNC-PLA at all reprocessing cycles.

	NPLA	SNC-PLA				
	R0	**R0**	**R1**	**R2**	**R3**	**R4**
slope	1.75	1.79	1.82	1.77	1.62	1.66
R^2	0.99	0.99	0.99	0.99	0.99	0.99

4.2.2.4. The effect of reprocessing on macromolecular structural change

In a typical storage modulus and loss modulus vs. frequency plot, the polymer matrix is said to exhibit a liquid-like behavior if G'<G" and a solid-like behavior if G'>G". The difference in magnitude between the storage and the loss modulus narrows down on increase in the frequency or the deformation energy till the storage modulus values become greater than the loss modulus, both of which become equal at the cross-over frequency **(Fig. 4.12)** [116, 137]. From **Table 4.7**, it can be observed that from the first to the fifth processing cycle, the cross-over frequency of NPLA shifts from lower values (137-168 Hz) to above 500 Hz while the cross-over modulus reduces in magnitude, which can be inferred as lowering of molecular weight and increase in the polydispersity index with repeated recycling. In case of SNC- PLA nanocomposites, the cross-over modulus appreciates marginally from the first to the third reprocessing cycle (R3-SNC-PLA) while the cross-over frequency increases from R0-SNC-PLA to R2-SNC-PLA, which remains constant for subsequent

reprocessing cycle. The cross-over data of SNC-PLA supports the results obtained from Cole-Cole plots regarding the stabilizing effect of SNC over the molecular weight/ distribution.

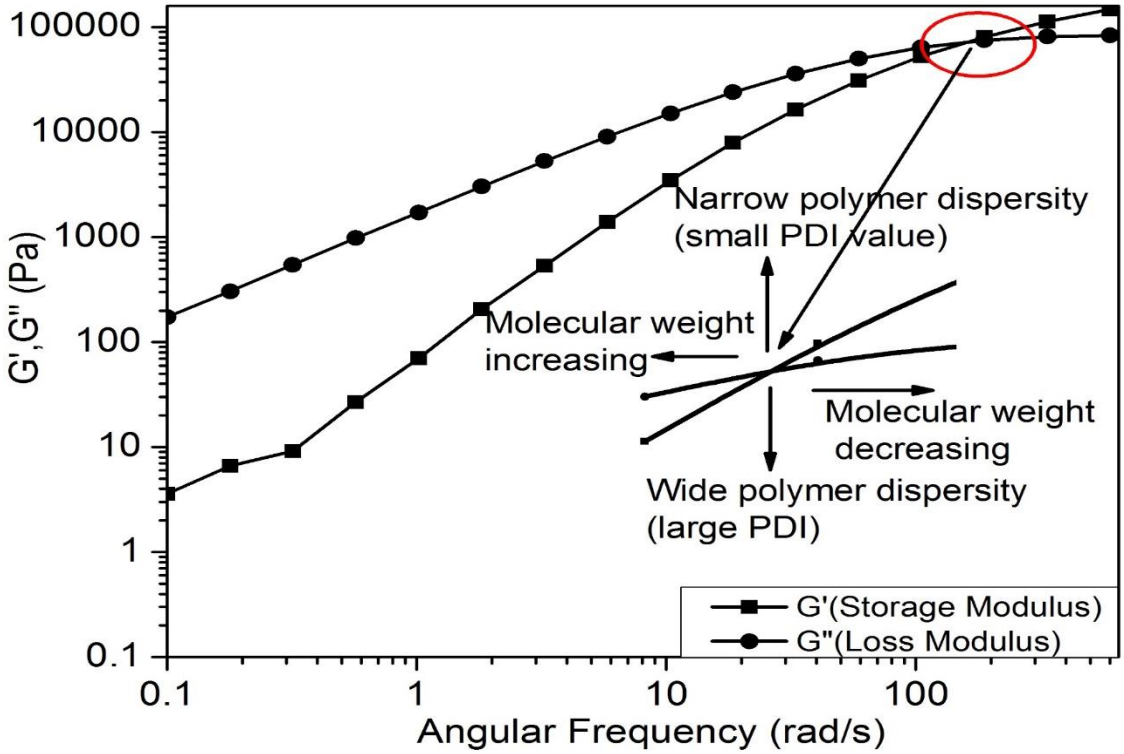

Figure 4.12. Representative plot for cross over frequency of R0-NPLA.

The characteristic relaxation time calculated from the inverse of the cross-over frequency data has been reported in **Table 4.7**. The relaxation time of a polymer is intimately linked to the polymer chain length, presence of branching or the molecular weight.

In the present study, the characteristic relaxation time is calculated from the inverse of the crossover frequency as reported in **Table 4.7**. It can be observed that for NPLA, the characteristic relaxation time reduces with the subsequent reprocessing cycle (from 0.006 s to < 0.001 s)**.** Which is due to the reduced time of relaxation of the polymer chains due to the degradation on exposure to repeated thermal and shear histories. However, the characteristic

relaxation time values for SNC-PLA decrease gradually as compared to that of NPLA in subsequent reprocessing steps with value for the 4th reprocessing being more than that for NPLA, probably due to the stabilizing effect of SNC on the excessive degradation of NPLA. The characteristic relaxation time data is also in good agreement with the molecular weight data as reported in **Table 4.8** [132, 138].

Table 4.7. Cross over data for storage and loss modulus of NPLA and SNC-PLA nanocomposites.

		R0	**R1**	**R2**	**R3**	**R4**
NPLA	G`=G`` (Pa)	7.1 × 10^4	6.7× 10^4	5.2× 10^4	6.5× 10^4	-
	ω_c (Hz)	161	168	137	581	>600
	1/ ω_c (s)	0.006	0.006	0.007	0.002	<0.001
SNC-PLA	G`=G`` (Pa)	6.9× 10^4	6.7× 10^4	7.0× 10^4	7.1× 10^4	6.7× 10^4
	ω_c (Hz)	206	277	338	338	340
	1/ ω_c (s)	0.005	0.004	0.003	0.003	0.003

The Mark-Houwink equation (**Eqn. 4.5**) provides important expression for the estimation of molecular weight from zero shear viscosity (η_o). Zero shear viscosity can be estimated from the small amplitude frequency sweep measurement at low frequency range based on the Cox-Merz rule. According the Cox-Merz rule (**Eqn. 4.6**) steady state viscosity as function of shear rate $\eta(\dot{\gamma})$ can be predicted from the oscillatory measurement at low frequency range.

$$\eta_o = KM^a \quad 4.5$$

$$|\eta(\dot{\gamma})|_{\dot{\gamma}\to 0} = |\eta^*(\omega)|_{\omega\to 0} \quad 4.6$$

For all reprocessed samples, the value of K is assumed to be constant, which is 3.4. **Eqn. 4.5** can be rearranged to the ratio of the molecular weight of reprocessed sample to that of the virgin polymer as function of the respective zero shear viscosity. **Eqn. 4.7** helps to understand the macromolecular structure change arising due to thermomechanical degradation. Where R and V denote the reprocessed and pristine polymer [137].

$$\frac{M_R}{M_V} = \left(\frac{\eta_{0R}}{\eta_{0V}}\right)^{1/3.4} \quad 4.7$$

Zero shear viscosity, molecular weight from GPC and the respective ratio with respect to the unprocessed polymer is described in **Table 4.8**.

Table 4.8. Comparison of molecular data from rheological and GPC measurements.

		η_0(Pa.s)	Mw (GPC) kDa	$M_{wi}/M_{wG\text{-}PLA}$	
				Rheology	GPC
	PLAv	2730	250.0	1	1
NPLA	**R0**	1721	247.3	0.87	0.99
	R1	1566	239.1	0.85	0.95
	R2	1264	196	0.80	0.78
	R3	422	151.1	0.58	0.61
	R4	169	132	0.44	0.53
SNC-PLA	**R0**	1005	247.5	0.75	0.99
	R1	890	218.3	0.72	0.87
	R2	820	222.6	0.70	0.89
	R3	737	189.0	0.68	0.79
	R4	760	184.2	0.69	0.74

The method of evaluation of the GPC (solution of polymer) and rheology (melt state) are different and therefore the molecular weight results obtained from GPC and derived from rheological measurements are not expected to correspond in terms of magnitude[139, 140]. The results in **Table 4.8** have proved quantitatively that the drastic degradation of NPLA chain occur at third and fourth reprocessing cycle. The zero shear viscosity and weight average molecular weight of NPLA decreased from 2730 Pa.s to 169 Pa.s (R4) and from 250 kDa to 132.0 kDa (R4) respectively. In case of SNC-PLA, the stabilizing effect of SNCs is clearly observed from the gradual decrease of the zero shear viscosity and average molecular weight values. Similar remark can be made from the molar mass ratio, which is based on the melt rheology and GPC. This is an indication for the rapid microstructural change occurred to NPLA matrix and which can be stabilized by the addition of SNCs particles. This result also concurs with the findings from the investigations of rheological properties (complex viscosity, storage modulus and loss modulus) and the crystallization and melting characteristics.

4.2.2.5. Intrinsic viscosity and acid value estimation

Intrinsic viscosity measurement and acid value analysis are selected to understand the structural change occurring due to the reprocessing of NPLA and SNC-PLA. A temperature controlled Ubbelhode-type capillary viscometer is used to measure the intrinsic viscosity of solution of reprocessed NPLA and SNC-PLA in chloroform (at concentrations of 2.25 mg/ml, 3.33 mg/ml, 5 mg/ml and 6.67 mg/ml) at 25 ºC. The SNC are filtered from the polymer solutions prepared as mentioned above using 0.2 µm filters.

The relative viscosity [η_r] and specific viscosity [η_{sp}] of the solutions prepared above are calculated from the flow time of the solution (t) with respect to the flow time of the pure solvent

(t_0) as indicated in **Eqn. 4.8 and Eqn. 4.9**. Huggins and Kraemer expressions (**Eqn. 4.10 and Eqn. 4.11**) are used to calculate the intrinsic viscosity [η] in which it is ideally the common intercept of the two equations [30, 141]. The analysis is performed three times and the average values are reported.

$$\eta_r = \frac{t}{t_0} \quad 4.8$$

$$\eta_{sp} = \eta_r - 1 = \frac{t - t_0}{t_0} \quad 4.9$$

$$\frac{\eta_{sp}}{C} = [\eta] + k_H [\eta]^2 C \quad 4.10$$

$$\frac{ln\eta_r}{C} = [\eta] + k_K [\eta]^2 C \quad 4.11$$

Where k_H is Huggins constant, k_K is the Kraemer constant, C is the concentration of polymer solution.

The effect of reprocessing (4 cycles) on the structural changes in NPLA and SNC-PLA is monitored using acid value analysis (AV) **Eqn. 4.12**. The samples are prepared by dissolving 1 g of NPLA or SNC-PLA in 20 ml of chloroform. For this study, Potassium hydroxide (KOH) at 2 mM in methanol is used to titrate the acid end group (carboxylic acid) with 3 drops of phenolphthalein.

$$AV = \frac{V_e \times C \times M}{m} \quad 4.12$$

where, V_e (ml) is the equivalent volume for corresponding equilibrium pH, C (mol. L^{-1}) is the molar concentration of KOH, M (g. mol^{-1}) is the molar mass of KOH and m (g) is the weight of the dissolved polymer.

As observed in **Fig. 4.13**, the linear values (R^2) higher than 0.95 are obtained for both Huggins and Kraemer plots of both the samples at all reprocessing stages. As observed in **Table 4.9** the intrinsic viscosity decreased from 133.5 to 73.8 ml/g and 113.4 to 84.7 ml/g for NPLA and SNC-PLA nanocomposite respectively. The reduction can be related to the reduction in molecular weight due to the thermal degradation. Some of the decomposition mechanisms which are responsible for the reduction in molecular weight are intermolecular and intramolecular transesterification reaction, hydrolysis, and random chain scission. Similar conclusions can be made from the acid value analysis as illustrated **Table 4.9**.

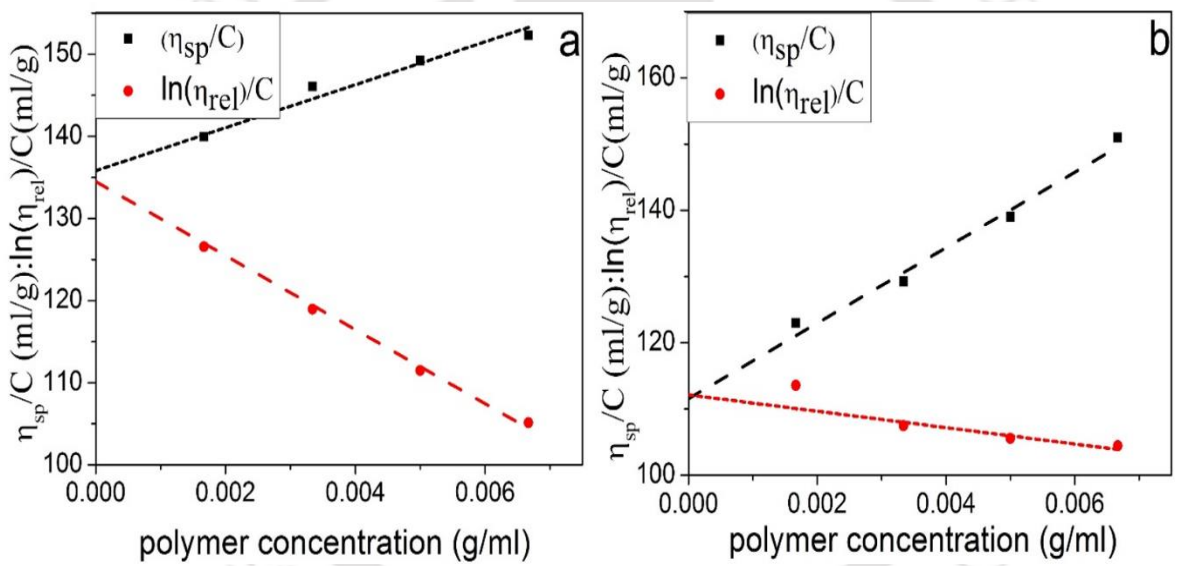

Figure 4.13. Representative plot of reduced viscosity and inherent viscosity as a function of polymer concentration in chloroform for (a) R0-NPLA and (b) R0-SNC-PLA.

Due to successive degradation, reduction in molecular weight and higher number of hydroxyl and carboxyl end groups are obtained. This can be revealed by the increment in acid values with the reprocessing cycle. More interestingly, no significant change on the optical purity is observed for NPLA and SNC-PLA of all reprocessing cycles, which is mostly expected when

the material undergoes successive reprocessing in high shear and temperature. For all the samples (including NPLA) approximately 94% (L form) optical purity is achieved with respect to pure PLA (Angular rotation of -156 ºC).

Table 4.9. Intrinsic viscosity and acid values of NPLA and SNC-PLA for different reprocessing cycles.

	NPLA					SNC-PLA				
	R0	**R1**	**R2**	**R3**	**R4**	**R0**	**R1**	**R2**	**R3**	**R4**
Intrinsic viscosity (ml/g)	133.5	92.0	90.5	84.1	73.8	113.4	99.8	99.7	96.7	84.7
Acid value (mg KOH/g polymer)	1.6	3.4	2.6	4.5	4.9	2.0	2.4	2.5	2.9	3.4

4.2.2.6. Dynamic Mechanical Analysis

The results from DMA help in understanding the retention of the stiffness properties on elevated temperatures in addition to the identification of the glass transition temperature from the peak of the tan δ vs. temperature plots [116, 117, 130].

Table 4.10. Elastic modulus values at 25 ˚C.

	R0	**R1**	**R2**	**R3**	**R4**
NPLA	3715	3253	2752	2353	1528
SNC-PLA	4254	3297	2991	2583	2359

The elastic modulus and tan δ plots have been reported in **Fig. 4.14** and **Fig. 4.15,** respectively. The tan δ value also known as the mechanical loss factor or the damping factor, is found from the ratio of the viscous modulus to the elastic modulus data. The elastic modulus values can be

found to decrease up to 41% with subsequent processing for PLA. The elastic modulus values for SNC-PLA nanocomposites have been found to be higher as compared to those of PLA for all reprocessing cycles as shown in **Table 4.10**. This is due to the reinforcing effect of the silk nanocrystals.

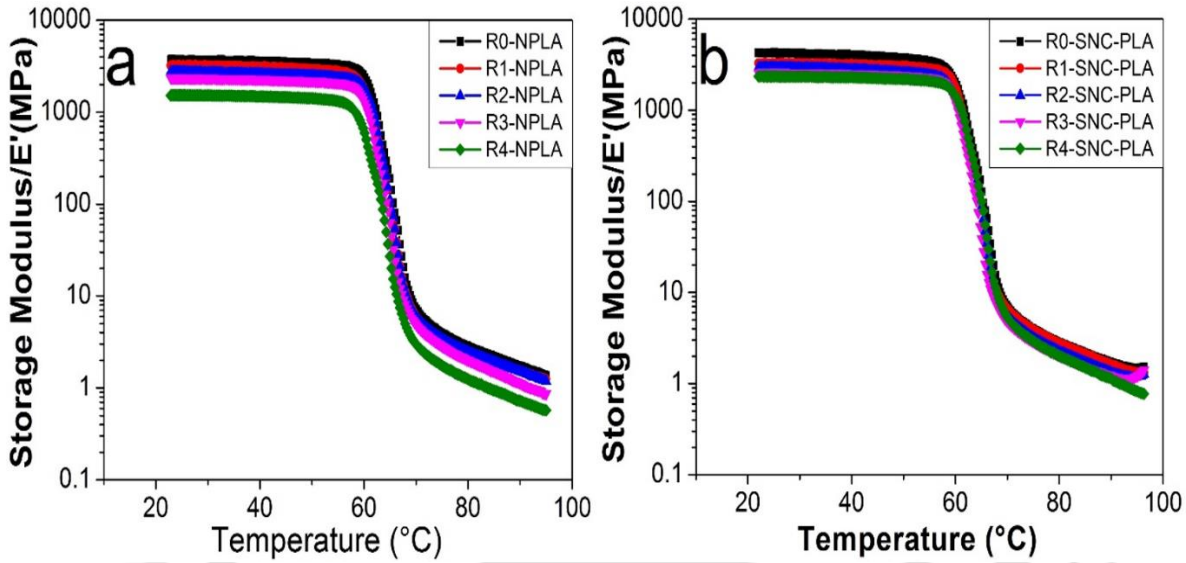

Figure 4.14 Elastic modulus plots for NPLA and SNC-PLA nanocomposites.

The difference in the elastic modulus values however decrease with progressing temperature indicating that the molecular chain mobility of the PLA above the glass transition temperature is not compensated by the reinforcing effect of the SNC nano-filler networks in the PLA matrix. The glass transition temperature is also found to shift/decrease by 2 degrees from 68 to 66◦ C on subsequent reprocessing cycles, earlier increased molecular mobility w.r.t. temperature probably due to decreased polymer chain length resulting from thermal degradation[142].

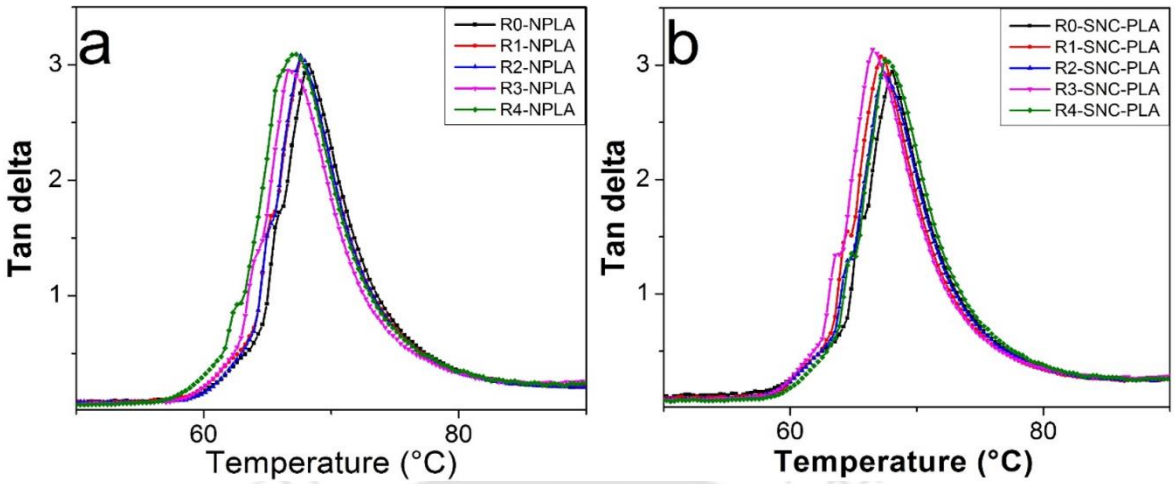

Figure 4.15. Tan δ plots for NPLA and SNC-PLA nanocomposites.

4.3. Summary

This study shows that neat poly (lactic acid) (NPLA) polymer matrix suffers degradation due to the successive shear and temperature during reprocessing. Incorporation of silk nanocrystals in to PLA matrix is observed to stabilize the essential properties; and it can be considered as one way to increase the reprocessability without compromising the required properties. The presence of SNCs act as nucleating agent and leads to enhance the slow crystallization process of PLA. Unlike other biofillers, there is no significant change on glass transition temperature and melting temperature and it signifies the reinforcing effect of SNCs. Linear radial increment of spherulite with respect to the crystallization time is observed by POM study at crystallization temperature of 120 ºC for NPLA and SNC-PLA of various reprocessing cycles. The incorporation of SNCs observed to decrease the spherulite growth rate, which can be attributed to the increment of barrier energy required to diffuse the polymer chain into the crystal front. Furthermore, SNCs are served as nucleating agents, which lead to the increment in nucleation density for SNC-PLA as compared to NPLA.

The PLA viscosity is reduced due to thermal degradation on subsequent processing cycles resulting in subsequent reduction in the molecular weight. Further, the presence of acid functional groups in the SNC resulted in initial lowering of the viscosity of the PLA/SNC nanocomposite for the first processing cycle. The molecular weight results from GPC are comparable to those obtained from rheological measurements with a similar trend followed for reduction in zero shear viscosity corresponding to molecular weight reduction on subsequent processing cycles. The shear thinning behavior of PLA and SNC-PLA melts also suggest the fortification or stabilizing effect of SNC with respect to the thermal degradation of PLA.

The comparably low storage modulus of PLA on repeated processing can be explained from decreased rheological response arising from the lower molecular weight (degraded) PLA chains. The shift of the cross-over frequency of NPLA to high frequency from the fourth to fifth processing cycles indicate a decrease in molecular weight accompanied by an increasing in polydispersity or broadening of the molecular weight distribution. The characteristic relaxation time data computed from the cross-over frequency data also shows shorter relaxation times of both NPLA and SNC-PLA on repeated reprocessing cycles, which also concurs with decrease in the molecular weight as reported in this study. The Cole-Cole plot results further show decrease in the zero shear viscosity and good miscibility of the SNC-PLA matrix which is further verified by the Han Plot which showed concurrence of plots for NPLA and SNC-PLA melts. The reinforcing effect of SNC nano-filler leads to higher elastic modulus values for SNC-PLA nanocomposites for corresponding processing cycles. Further, the negligible shift (~2 ºC) in the glass transition temperature on subsequent processing cycles show marginal increase in the molecular mobility with respect to the temperature due to decreased polymer chain lengths resulting from thermal degradation.

Chapter 5

Silk Nanocrystals Stabilized Melt Extruded Poly (Lactic Acid) Nanocomposite Films: Effect of Recycling on Thermal Degradation Kinetics and Optimization Studies

In this work highly crystalline β sheets of silk nanocrystals (SNCs) have been studied for their effect on the thermal stability of poly (lactic acid) (PLA) during multiple reprocessing cycles. Stable onset degradation temperature is obtained for PLA-SNC nanocomposite ($T_{5\%}$ ~ 334 ºC) as compared to neat poly (lactic acid) (NPLA), which drastically reduces from 336 ºC (first cycle) to 322 ºC (fifth cycle). The activation energies are estimated using isoconversional Kissinger-Akahira-Sunose and Flynn-Wall-Ozawa methods. Stable activation energy values (~130 kJ/mol) are obtained for SNC-PLA at three consecutive extrusion cycles, whereas in case of NPLA, it significantly reduced from ~150 kJ/mol (first cycle) to ~110 kJ/mol (second cycle). Nelder-Mead simplex method is used to optimize the kinetic parameters of nucleation and growth model (A2); which is observed to be the best fit of the experimental thermogravimetric analysis (TGA) data. Decomposition products are analyzed by Thermogravimetry coupled Fourier transform infrared spectroscopy.

Parts of this chapter are published as:

Melakuu Tesfaye, Rahul Patwa, Remya Kommadath, Prakash Kotecha, Vimal Katiyar, Silk nanocrystals stabilized melt extruded poly (lactic acid) nanocomposite films: Effect of recycling on thermal degradation kinetics and optimization studies. Thermochimica Acta, 643, 41-52 (2016)

5.1. Introduction

As already discussed so far, PLA is highly sensitive to processing conditions and thus application of high temperature and shearing force reduces the molecular weight, which is the consequence of thermomechanical degradation [143]. It is already shown that the thermal properties (thermal stability, crystallization and melting behavior) are affected by the reduction in molecular weight and/or increment in molecular weight distribution, which is highly expected when the material is processed multiple times.

Introduction of the fillers into the polymer matrix has the tendency to improve the thermal stability and slow crystallization behavior of PLA [144-146]. Based on the interaction and dispersion of fillers in the polymer matrix, important properties such as thermal stability, mechanical properties (tensile strength, Young's modulus and elongation at break) and oxygen and water barrier properties can be tailored [145, 147-153]. However, in most scenarios processing of PLA/fillers through melt extrusion is a big challenge due to filler induced matrix degradation. This phenomenon is more prominent for the case of multiple reprocessing. In adverse, reprocessing may enhance the dispersion of fillers, which may be the reason for better improvement in material properties. It is therefore important to study the impact of adding different fillers to identify the thermal degradation behavior of PLA matrix when subjected to multiple reprocessing.

Biofillers like cellulose, chitosan, chitin, gum, starch, and sucrose palmitate [154, 155] have been studied as nontoxic reinforcement for PLA matrix. Among all the biofillers, cellulose has been extensively studied as PLA matrix reinforcement in the form of fibers and nanocrystals [41, 156-158]. In recently published research work, agglomeration of cellulose nanocrystals (CNC) due to the presence of strong intermolecular hydrogen bonding has been discussed as

a challenging task in the fabrication of PLA-CNC nanocomposite using melt extrusion process [159]. Beside this, the sulfate functional groups attached to CNCs during the acid hydrolysis increases the degradation rate of PLA matrix when it is subjected to extrusion [159]. Similar phenomena can be observed for biofillers such as chitosan, chitin, gum starch, sucrose palmitate, due to their high surface functionality (presence of –OH functional groups). Therefore, several investigations need to be conducted to determine suitable fillers, which can maintain or enhance the thermal stability of PLA during thermal processing. In view of this, the present chapter is focusing on the effect of silk nanocrystals on the thermal decomposition behavior of PLA during multiple reprocessing.

Isoconversional methods (Kissinger-Akahira-Sunose (K-A-S) and Flynn-Wall-Ozawa (F-W-O)) and Kinetic Invariant Parameters (KIP) methods are used to estimate the activation energy and the "true" kinetic parameters. The kinetic triplets are also studied by coupling the Coats and Redfern method with Nelder-Mead simplex optimization technique for selected models based on the master plot technique. The evolved gases during thermal degradation are also analyzed using the Thermogravimetry coupled Fourier transform infrared spectroscopy (TG-FTIR).

In the present study, the following seven steps are followed to estimate the non-isothermal degradation kinetic parameters of NPLA and SNC-PLA of four reprocessing cycles.

Step 1: Estimation of activation energy using isoconversional methods (Kissinger-Akahira-Sunose (K-A-S) and Flynn-Wall-Ozawa (F-W-O)).

Step 2: Estimation of activation energy and pre-exponential factor using Coats and Redfern method for fourteen different models.

Step 3: Estimation of the 'true' activation energy and pre-exponential factor based on the values obtained from Step 2 using the Kinetic Invariant Parameters (KIP) technique.

Step 4: Selection of best models based on master plot method.

Step 5: Non-linear optimization of the kinetic parameters using Nelder Mead simplex method for models which are selected based on Step 4. In this step, the values of activation energies and pre-exponential estimated from the Coats and Redfern method are used as initial guesses.

Step 6: Comparing the values of the activation energy obtained from the isoconversion model to those obtained using the non-linear optimization to determine a single model along with its activation energy and pre-exponential factor.

Step 7: Analysis of decomposition products.

5.2. Theory

5.2.1. Thermal decomposition behavior of poly (lactic acid)

It is understood that, molecular weight reduction of PLA during melt processing highly affects the thermal stability, which can be observed by the reduction of onset degradation temperature, maximum degradation temperature and end set temperature. Due to high thermal sensitivity of PLA, narrow processing temperature window is observed ranging from 180 to 220 ºC.

The degradation pathway of PLA at decomposition stage is dominated by end chain opening (unzipping depolymeriztion) giving lactides and cyclic oligomers with short chain oligomers formed from random degradation. Similar to other polymers, the rate of degradation of PLA can be assumed to be governed by a single step kinetic equation, in which the rate of change

of mass is dependent on the temperature dependent rate constant k (T) and the reaction model f (α) **Eqn. 5.1**.

$$\frac{d\alpha}{dt} = k(T)f(\alpha) = \beta\frac{d\alpha}{dT} = Ae^{(-E/RT)}f(\alpha) \quad 5.1$$

For constant heating rate β = dT/dt, infinitesimal change of conversion (α) with respect to temperature can be expressed as a function of heating rate (β), activation energy (E), and temperature (T). This fundamental expression coupled with the kinetic model function f(α) can be considered as foundation for kinetic triplet calculation. The conversion values (α) and the reaction rate constant (k) are obtained from thermogravimetric analysis (TGA) by weight loss at different heating rate (β) and from the Arrhenius equation as mentioned in **Eqn. 5.1**. [160, 161].

$$\alpha = \frac{w_0 - w_t}{w_0 - w_\infty} \quad 5.2$$

$$k = Ae^{-E/RT} \quad 5.3$$

In **Eqn. 5.2**, w_0, w_∞ and w_t represents the initial, final and weight at time t respectively. The variables A, E, T corresponds to the pre-exponential factor, activation energy (J/mol), temperature (K) respectively and R is the universal gas constant (8.314 J mol^{-1} K^{-1}).

From the generalized rate equation (**Eqn. 5.1),** it can be clearly observed that the rate of degradation is influenced by the Arrhenius equation parameters (E and A) and kinetic model f (α). Therefore in order to understand the reaction phenomenon, the kinetic triplets (E, A and f (α)) need to be determined carefully [160, 162-164]. Various models have been developed to estimate the kinetic triplets categorized under model free (isoconversional techniques) and model fitting techniques.

Generally, the attractiveness of PLA in market and research fields is due to its cumulative abundance, comparative economical affordability and adequate industrial performance. However, PLA has many limitations such as, thermal degradation under high temperature and shear, which leads to molecular weight reduction; relatively low melt viscosity and strength; poor gas-liquid barrier properties, brittleness etc., [33, 34]. Various approaches has been studied to overcome this limitations, including blending with different polymers, composite preparation, stereocomplexation and reactive extrusion with chain extenders [35-39].

5.2.2. Isoconversional techniques

Kissinger method is one of the widely used isoconversional methods to determine activation energy of solid state decomposition reaction based on the study of rate equation at maximum decomposition temperature. It considers the changes in temperature at which maximum weight loss occurs with respect to the change in heating rate and it depends on the reaction activation energy. As described in **Eqn. 5.4,** activation energy can easily be determined from the slope of the graph $\ln(\beta/T_m^2)$ vs $1/T_m$,where T_m is the temperature at which the rate of weight loss achieved maximum [160, 165].

$$ln\left(\frac{\beta}{T_m^2}\right) = \ln\left(\frac{AR}{E}\right) - \frac{E}{RT_m} \quad 5.4$$

In Kissinger-Akahira-Sunose (K-A-S) method, the maximum temperature is substituted by the temperature at different levels of conversion and activation energy is calculated form the slope of $\ln(\beta/T_\alpha^2)$ vs $1/T_\alpha$ of **Eqn. 5.5** [161, 164, 166]

$$ln\left(\frac{\beta}{T_\alpha^2}\right) = \ln\left(\frac{AR}{Eg(\alpha)}\right) - \frac{E}{RT_\alpha} \quad 5.5$$

In **Eqn. 1.17,** T_α is the temperature at different levels of conversion. Similarly, F-W-O model (**Eqn. 5.6**) is also used to estimate the activation energy along with the conversion value [164].

$$\log(\beta) = \left\{log\frac{AE}{g(\alpha)R} - 2.315\right\} - \frac{0.457E}{RT} \quad 5.6$$

In general without having precise knowledge of reaction mechanism, reliable activation energy can be estimated from the isoconversional methods [167, 168].

5.2.3. Invariant kinetic parameters (KIP) technique

Based on the analysis of compensation effect, KIP method can be applied to estimate the 'true' kinetic parameters. For each heating rate, a linear relationship is observed between ln A and E for each model fitting function listed in **Table 5.1** according to **Eqn. 5.7**

$$ln\ A = \alpha^* + \beta^* E \quad 5.7$$

Lesnikovich and Levchik have defined E_{inv} and A_{inv} as 'true' kinetic parameters that correspond to the intersection point of ln A vs E curve**,** when it is plotted against all heating rates [165, 169]. In order to avoid experimental uncertainties on the determination of the intersection point, super-correlation function is used to estimate E_{inv} and A_{inv} from (**Eqn. 5.8)**.

$$\alpha^* = ln\ A_{inv} - \beta^* E_{inv} \quad 5.8$$

In **Eqn. 5.8,** the compensation parameters (α* and β*) are calculated from **Eqn. 5.7**. This method can provide good estimation of kinetic parameters, if activation energy is not dependent on conversion (α) [170, 171].

Table 5.1. Fourteen different kinetic models and their integral g (α) and conversion functions f (α).

Kinetic model	Sy.	f(α)	g(α)	α
Chemical reaction				
Frist order	**F_1**	$1-\alpha$	$-\ln(1-\alpha)$	$1-\exp(-z)$
Second order	**F_2**	$(1-\alpha)^2$	$(1-\alpha)^{-1}-1$	$1-(1/(z+1))$
Diffusion				
1-D diffusion	**D_1**	$1/(2\alpha)$	α^2	$z^{1/2}$
3-D diffusion	**D_3**	$3/2(1-\alpha)^{2/3}[1-(1-\alpha)^{1/3}]^{-1}$	$[1-(1-\alpha)^{1/3}]^2$	$1-[1-z^{1/2}]^3$
Phase-boundary reactions				
Contracting area	**R_2**	$2(1-\alpha)^{1/2}$	$1-(1-\alpha)^{1/2}$	$1-(1-z)^2$
Contracting volume	**R_3**	$3(1-\alpha)^{1/3}$	$1-(1-\alpha)^{1/3}$	$1-(1-z)^3$
Power law				
	P_4	$4\alpha^{3/4}$	$\alpha^{1/4}$	z^4
	P_3	$3\alpha^{2/3}$	$\alpha^{1/3}$	z^3
	P_2	$2\alpha^{1/2}$	$\alpha^{1/2}$	z^2
	$P_{2/3}$	$(2/3)\ \alpha^{-1/2}$	$\alpha^{3/2}$	$z^{2/3}$
Nucleation and growth				
Avrami-Erofeev	**A_2**	$2(1-\alpha)[-\ln(1-\alpha)]^{1/2}$	$[-\ln(1-\alpha)]^{1/2}$	$1-\exp(-z^2)$
Avrami-Erofeev	**A_3**	$3(1-\alpha)[-\ln(1-\alpha)]^{2/3}$	$[-\ln(1-\alpha)]^{1/3}$	$1-\exp(-z^3)$
Avrami-Erofeev	**A_4**	$4(1-\alpha)[-\ln(1-\alpha)]^{3/4}$	$[-\ln(1-\alpha)]^{1/4}$	$1-\exp(-z^3)$
Avrami-Erofeev	**$A_{3/2}$**	$3/2(1-\alpha)[-\ln(1-\alpha)]^{1/3}$	$[-\ln(1-\alpha)]^{2/3}$	$1-\exp(-z^{3/2})$

Where $\boldsymbol{z} = \frac{ART^2}{\beta E}\left(1-\frac{2RT}{E}\right)e^{-E/RT}$

5.2.4. Degradation mechanism

5.2.4.1. Initial estimation of kinetic degradation mechanisms

Coats-Redfern approach is used as a first step to estimate the degradation mechanism and kinetic parameters. In this approach, the differential form of **Eqn. 5.1** has been transformed into integral form as described in **Eqn. 5.9.**

$$g(\alpha) = \int_0^{\alpha} \frac{d\alpha}{f(\alpha)} = \frac{A}{\beta}\int_{T_i}^{T} \exp(\frac{-E}{RT})dT \qquad 5.9$$

where g(α) is the integral function, which represents conversion dependent reaction models (listed in **Table 5.1)** under the decomposition temperature range of initial temperature (T_i) to final temperature (T). Substituting x for E/RT in **Eqn. 5.9,** provides a general form and the integral part is approximated by p(x) using a Taylor series expansion (**Eqn. 5.11**) as proposed by Coats and Redfern, 1964[172, 173].

$$g(\alpha) = \frac{AE}{\beta R}\frac{e^{-x}}{x^2}dx = \frac{AE}{\beta R}p(x) \qquad 5.10$$

where p(x) represents the integral function.

Taylor series expansion of **Eqn. 4.10.**

$$g(\alpha) = \frac{AE}{\beta R}p(x) = \frac{AE}{\beta R}\left[\frac{e^{-X}}{x^2}\left(1 - \frac{2!}{x} + \frac{3!}{x^2} - \frac{4!}{x^3} + \cdots\right)\right]$$

$$\cong \frac{AE}{\beta R}\left[\frac{e^{-X}}{x^2}\left(1 - \frac{2}{x}\right)\right] = \frac{AE}{\beta R}\left[\frac{e^{-E/RT}}{(E/RT)^2}\left(1 - \frac{2RT}{E}\right)\right]$$

$$= \frac{ART^2}{\beta E}\left(1 - \frac{2RT}{E}\right)e^{-E/RT} \qquad 5.11$$

The kinetic parameters E (activation energy) and A (pre-exponential factor) are estimated from the slope and y-intercept of ln (g (α)/T^2) versus 1/T plot of **Eqn. 5.12** for integral models listed in **Table 5.1.**

$$ln\left[\frac{g(\alpha)}{T^2}\right] = ln\left[\frac{AR}{\beta E}\left(1-\frac{2RT}{E}\right)\right] - \frac{E}{RT} \quad 5.12$$

5.2.4.2. Kinetic mechanism screening

Master plot method is used as a screening technique which is proposed by Criado and Malek [174]. In this method, the concept of generalized time 'Θ' is introduced to the integral function of the kinetic equation in order to describe the degradation phenomenon with respect to a fixed value of conversion (α=0.5) **Eqn. 5.13**.

$$\frac{g(\alpha)}{g(0.5)} = \frac{\theta}{\theta_{0.5}} = \frac{p(x)}{p(x_{0.5})} \quad 5.13$$

In **Eqn 5.13**, the left hand side represents the model equation and the right hand side represents the experimental values. Flynn corrected, Senum and Yang approximation [174, 175] is used (**Eqn. 5.14**) for p(x) to predict the experimental values, with x equals E/RT.

$$p(x) = \frac{e^{-x}}{x}\left(\frac{x^3+18x^2+86x+96}{x^4+20x^3+120x^2+240x+120}\right) \quad 5.14$$

5.2.4.3. Kinetic triplet optimization

The optimum values for the kinetic triplet (E, A and f(α)) are obtained by minimizing error between the experimental conversion values (α_{exp}) and predicted conversion values (α_{pred}) for "i" number of data points with "j" heating rates as stated in **Eqn. 5.15**

$$minimize \sum_{j=1}^{n}\left[\sum_{i=1}^{m}\left[\alpha_{exp,j,i} - \alpha_{pred,j,i}\right]\right]^2 \quad 5.15$$

Conversion values are predicted for those models which are selected based on the above mentioned procedures, using expressions of α (which is function of z) listed in **Table 5.1**. Nelder-Mead simplex method is used to determine improved predictions of E and A values by solving the minimization problem of **Eqn. 5.15**.

5.2.4.4. The Nelder-Mead simplex method

The Nelder-Mead simplex method [176] is an iterative, deterministic algorithm that can be used to solve single objective, unconstrained, non-linear optimization problems. For an n-dimensional problem, it constructs a simplex which has n+1 vertices which are evaluated for their objective function. It primarily consists of four steps, viz., (i) reflection, (ii) expansion (iii) contraction and, (iv) reduction, which helps in the exploration of the search space by utilizing the centroid of the best n points. All the four steps generate a test point which helps in modifying the position of simplex and all the four steps may not be encountered in every iteration. In reflection, the reflected point replaces the worst solution if it is better than the second worst but inferior than the current best solution. However, if the reflected point is better than the current best solution, a new point is computed in the expansion step and compared to the reflected point. The worst point in the simplex is replaced by the best of the expanded and reflected point. The contraction phase is encountered only if the reflected point is inferior to the second worst. An inside contraction is performed if the reflected point is worse than the second worst but better than the worst solution, otherwise an outside contraction is performed. If the contraction step fails to discover a point which is better than the worst point, the reduction step is encountered. Unlike the other steps, the reduction step modifies all the existing points of the simplex except for the best point. For the sake of brevity, a detailed description of the

method has not been provided but the entire method is summarized in **Fig. 5.1**. Additional details on the Nelder-Mead simplex can be obtained from literature [176, 177].

In this work, the activation energy E and the pre-exponential factor A is estimated by fitting a straight line between ln (g (α)/T^2) vs 1/T in accordance to **Eqn. 5.12**. The term g (α) for each of the model is determined using the expressions given in **Table 5.1**. This estimate of E and A is subsequently used to construct the initial simplex in the Nelder-Mead simplex method. The objective function is the minimization of the sum of squares of the observed 'α' and the 'α' that is predicted by a particular model with the activation energy and the pre-exponential factor being the decision variables. The value of 'α' from a particular model is predicted by determining 'z' (using the expressions provided in Table 1) for various models. It should be observed that the strategy used in this chapter does not used any stochastic optimization technique and thus is not only computationally efficient but relieves the user from providing user defined parameters required in such algorithms.

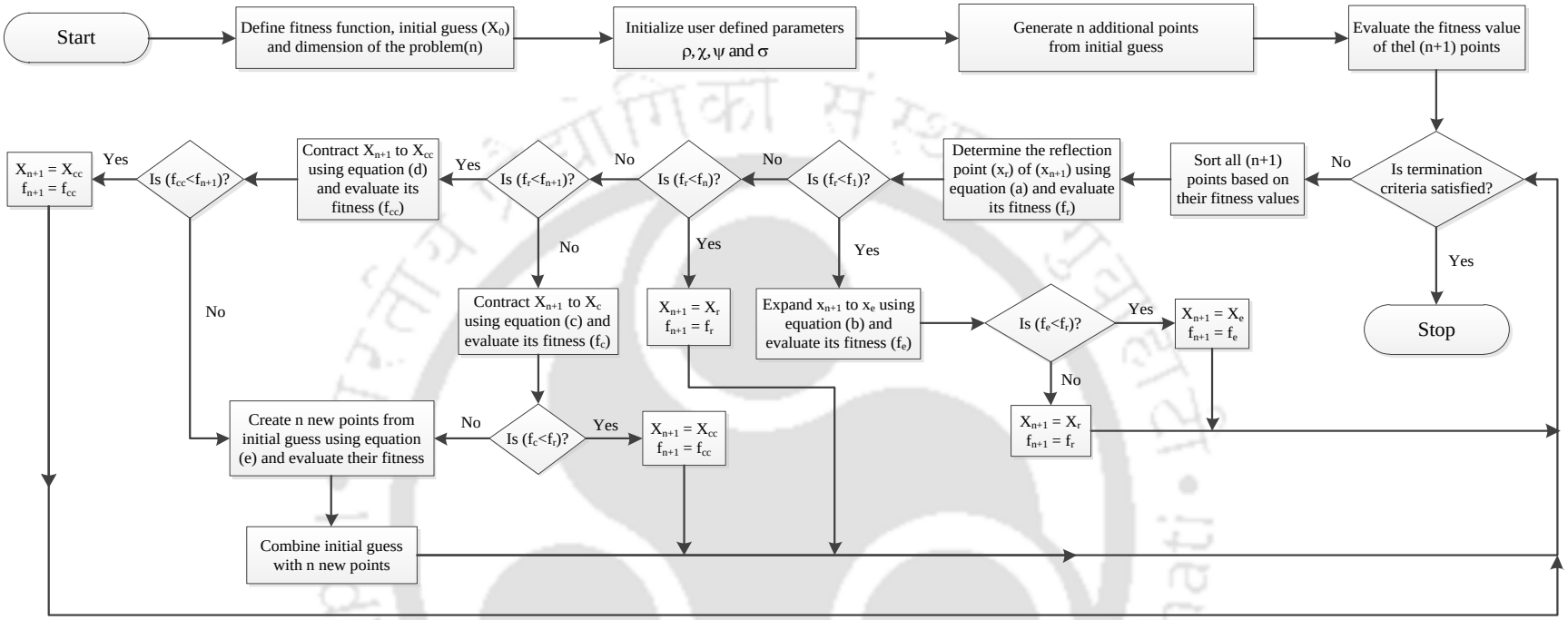

$$X_r = (1+\rho)\bar{X} - \rho X_{n+1} \quad \text{(a)}; \quad X_e = (1+\rho\chi)\bar{X} - \rho\chi X_{n+1} \quad \text{(b)}; \quad X_c = (1+\rho\psi)\bar{X} - \rho\psi X_{n+1} \quad \text{(c)}; \quad X_{cc} = (1-\psi)\bar{X} + \psi X_{n+1} \quad \text{(d)}; \quad X_i = X_1 + \sigma(X_i - X_1) \quad \text{(e)}$$

Figure 5.1. Summarized flowsheet for Nelder-Mead simplex method.

5.3. Results and Discussion

5.3.1. Molecular weight analysis

The molecular weight values of multiple times reprocessed NPLA and SNC-PLA are summarized in **Table 2.** On both the systems, reduction of M_n and M_w are observed due to the cleavage of chains into shorter fractions by various degradations mechanisms as reported in the literature (intramolecular transesterification, intermolecular transesterification, random chain scission, hydrolysis and radical degradation) [178, 179].

To have better insights about the degradation behavior of SNC-PLA and NPLA, a degradation factor K is defined for all the samples at each reprocessing cycle, on the basis of virgin PLA pellet weight average molecular weight (M_w) as described in **Eqn. 5.16.**

$$K = \frac{\overline{M}_{w(pellets)}}{\overline{M}_{w(reprocessed)}} \qquad 5.16$$

The values of K for both the systems increases as the number of reprocessing cycles increase, indicating a reduction in weight average molecular weight. The K values for NPLA varied from 1.004 to 1.88 and drastic degradation is observed from the 2nd reprocessing cycle with approximate percentage reduction of 21, 39 and 47% for R2, R3 and R4, respectively.

More interestingly the K values varied in narrow range from 1.003 to 1.348 for the SNC-PLA samples with number of reprocessing cycles, implying higher stability of molecular weight of SNC-PLA while it is subjected to multiple extrusion, unlike NPLA. The percentage reduction in average M_w for R2, R3 and R4 are approximately 10, 24 and 26%, respectively for the SNC-PLA samples. From the results of molecular weight reduction, it can be concluded that the

effect of thermomechanical degradation is suppressed by the addition of SNC into the PLA matrix. So it is a good approach to have stable thermal properties of PLA under high shear and temperature. Additionally, the recyclability of PLA may also be enhanced by the addition of SNCs. Proper dispersion and/or network formation could be the reason for this significant stability. As indicated in **Fig. 3.13,** the nanoparticles are dispersed in the PLA matrix.

Table 5.2. Characteristic molecular weight obtained from GPC for NPLA and SNC-PLA at different levels of reprocessing cycles

		R0	R1	R2	R3	R4
NPLA	**$M_{n(Ave)}$ (kDa)**	135.8	105.9	91.6	61.1	55.7
	$M_{w(Ave)}$ (kDa)	247.3	238.1	195.9	151.1	132.0
	PDI	1.82	2.25	2.14	2.47	2.37
	K	1.004	1.043	1.27	1.643	1.88
SNC-PLA	**$M_{n(Ave)}$ (kDa)**	131.3	91.6	95.9	82.3	56.3
	$M_{w(Ave)}$ (kDa)	247.5	218.3	222.6	188.9	184.2
	PDI	1.88	2.38	2.32	2.3	3.27
	K	1.003	1.138	1.115	1.314	1.348

5.3.2. Thermal stability

Representative thermal degradation curves of NPLA and SNC-PLA nanocomposite at different reprocessing cycles at a heating rate of 10 ºC/min are presented in **Fig. (5.2).** It is observed that as the number of reprocessing cycles are increased, the thermograms of NPLA shift towards the lower temperatures, whereas in the case of nanocomposite insignificant changes are observed. This is the first indication for stable thermal properties of PLA matrix during

multiple reprocessing by the addition of SNCs. The observed improvement can be further elaborated by using onset temperatures and maximum degradation temperature as presented in **Table 5.3.**

Table 5.3. Thermal gravimetric analysis data obtained from TGA and DTG for NPLA and SNC-PLA nanocomposite at 10 ºC/min heating rate. ($T_{5\%}$ 5 wt.% mass loss, $T_{max.deg}$: maximum degradation and $T_{95\%}$: 95 wt.% mass loss).

		R0	R1	R2	R3	R4
NPLA	$T_{5\%}$	336.3	332.1	329.0	327.6	322.1
	$T_{max.deg}$	379.0	377.7	376.2	372.2	368.3
	$T_{95\%}$	391.8	389.8	387.2	383.5	381.9
SNC-PLA	$T_{5\%}$	333.3	334.1	334.0	336.0	330.9
	$T_{max.deg}$	372.3	372.4	371.8	372.9	372.4
	$T_{95\%}$	383.5	387	383.1	383.6	383.2

The temperature for 5% weight loss **(**$T_{5\%}$), maximum degradation temperature ($T_{max.deg}$) and end set temperature ($T_{95\%}$) of NPLA vary in decreasing order from 336 to 322 °C, 379 to 368 °C and 391 to 381 °C respectively with increasing reprocessing cycles.

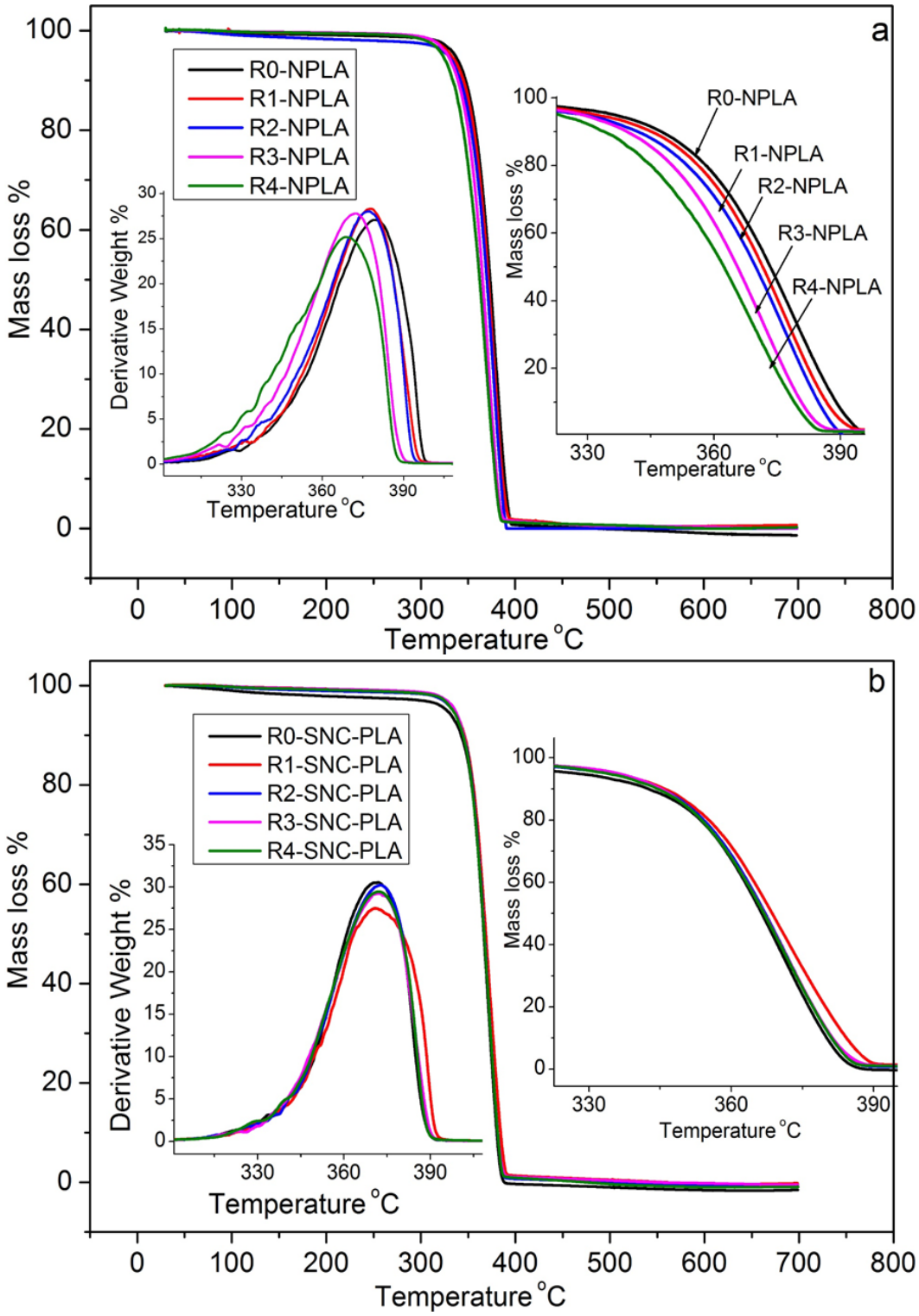

Figure 5.2. Thermal degradation curve of (a) NPLA and (b) SNC-PLA at various levels of reprocessing.

In case of SNC-PLA nanocomposite $T_{5\%}$, $T_{max.deg}$ and $T_{95\%}$ varies randomly with narrow range between 330 to 336 °C, 371 to 373 °C and 383 to 387 °C. With reference to the reprocessed NPLA, more pronouncing improvement on $T_{5\%}$ of SNC-PLA is observed in second, third and fourth cycle, in which $T_{5\%}$ increased by 4, 7 and 8 °C respectively. Therefore, due to the incorporation of SNCs, it is clearly observed that the thermal properties of PLA matrix are stable with the number of reprocessing cycles, by overcoming the effect of thermomechanical degradation. These results further support the conclusion made by molecular weight analysis of reprocessed SNC-PLA samples and the possible reason for it, as discussed in previous section could be the network formation between PLA and SNC during multiple reprocessing.

5.3.3. Degradation kinetics analysis

In the primary stage, the activation energies for NPLA and SNC-PLA nanocomposite at each reprocessing cycle are estimated using the isoconversional methods of Kissinger-Akahira-Sunose (K-A-S) and Flynn-Wall-Ozawa (F-W-O) to have an insight about the impact of SNCs to the PLA matrix. Similar trends of activation energy (E), and its dependency on conversion (α) are observed for both isoconversional methods. According to K-A-S method the activation energy is estimated from **Eqn. 5.5** for the conversion range of 10 to 90%. In every case, the correlation coefficient is above 0.97. As displayed in **Fig. 5.3(a)**, the activation energy (E) of NPLA increases with conversion (α) and similar trends are also reported in literature [154, 179-181]. Therefore, from the kinetic mechanism point of view it could be predicted that, the thermal degradation process of NPLA is governed by complex reaction mechanism including cis-elimination, intra and inter-molecular transesterification, unzipping de-polymerization, random scission, hydrolytic and radical degradation [154, 182-184].

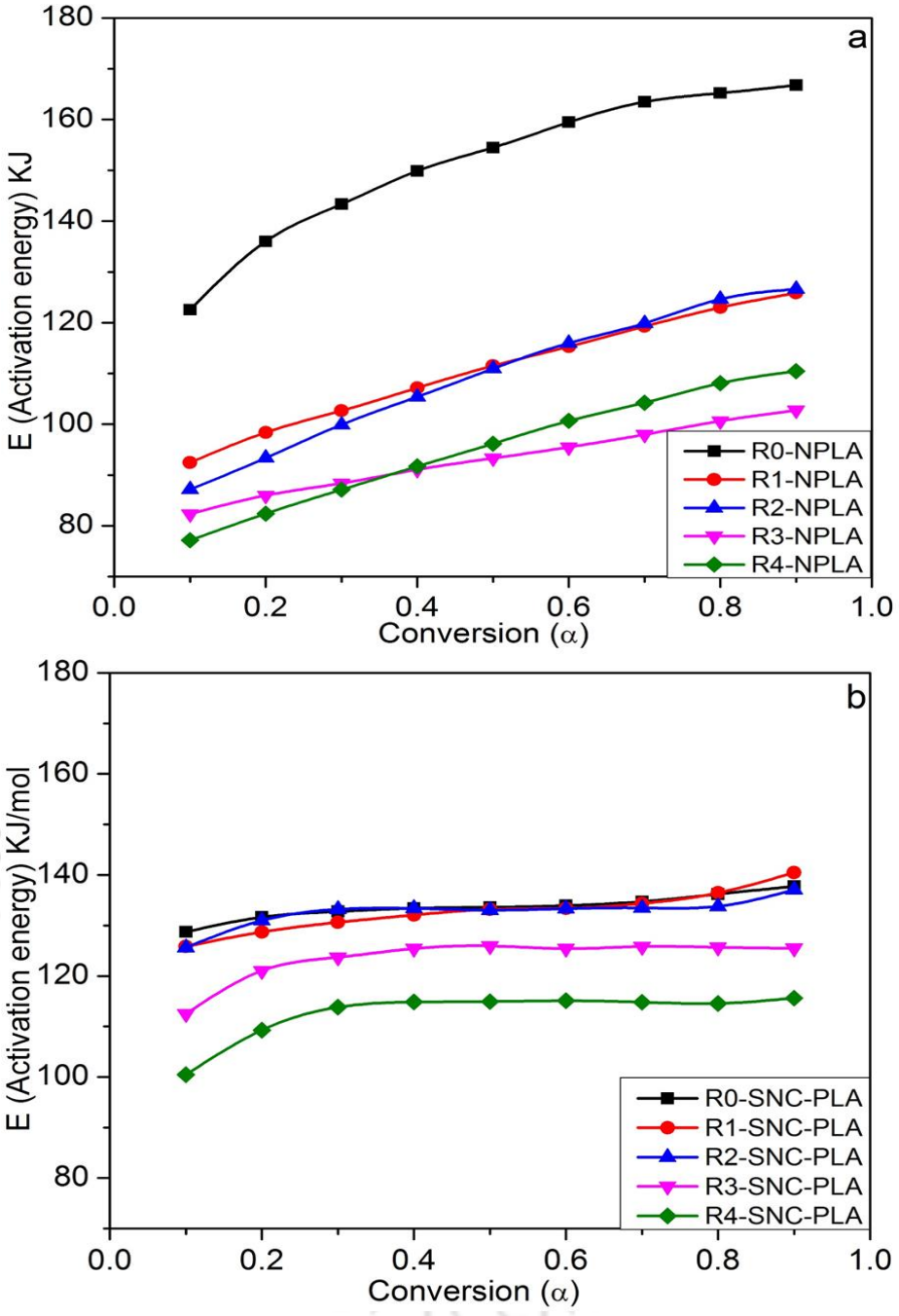

Figure 5.3. Variation of Activation energy (E) with conversion (α) at various levels of recycling for (a) NPLA and (b) SNC-PLA.

The activation energies for R0-NPLA to R4-NPLA varied as 126-168, 97-129, 92-130, 87-107 and 81-115 kJ/mol respectively. The observed significant reduction in activation energies

observed from the first reprocessing cycle and onwards are due to the thermomechanical degradation of PLA matrix. However, from **Fig. 5.3 (b),** it can be easily observed that the addition of SNCs in the PLA matrix has stabilized the activation energy (E) with respect to the change in conversion (α), which shows the simple thermal degradation reaction mechanism.

Table 5.4. Estimated values of activation energy (kJ/mol) using isoconversional methods, kinetic invariant method, Coats and Redfern method and Nelder-Mead simplex method.

Models		**NPLA**					**SNC-PLA**				
		R0	**R1**	**R2**	**R3**	**R4**	**R0**	**R1**	**R2**	**R3**	**R4**
K-A-S		151	111	109	93	95	130	129	129	119	108
F-W-O		152	115	114	98	100	134	133	133	124	113
KIP		147	132	130	106	98	129	129	129	122	109
Nonlinear Optimization	**F1**	260	257	247	241	229	266	269	282	277	253
	A2	125	123	119	116	109	128	130	136	133	122
	A3	80	79	76	74	70	82	83	88	86	78
CR Method	**F1**	275	241	233	229	212	258	253	267	269	266
	F2	353	306	290	298	266	325	321	340	345	342
	D1	457	406	398	381	360	437	427	447	449	444
	D3	521	459	446	435	405	491	482	506	510	504
	R2	246	217	211	205	191	233	228	240	241	238
	R3	255	224	218	212	198	241	236	248	250	247
	P4	48	42	41	39	36	46	44	47	47	47
	P3	68	59	58	55	52	64	63	66	66	65
	P2	107	94	92	88	82	101	99	104	105	103
	P2/3	340	302	296	283	268	325	318	333	335	331
	A_2	132	115	111	109	101	124	121	128	129	128
	A_3	85	73	71	70	64	79	78	82	83	82
	A_4	61	52	50	50	45	57	56	59	60	59
	$A_{3/2}$	180	157	152	150	138	168	165	171	176	174

As shown in **Fig. 5.3(b)** similar trends are observed for R0-SNC-PLA, R1-SNC-PLA and R2-SNC-PLA with average value of E being 130, 129 and 128 kJ/mol respectively. It is very interesting to mention that, an initial increment in activation energy is observed for R3 and R4 of SNC-PLA nanocomposite for $\alpha < 0.3$ and this might be due to the increment in shorter chain

fraction, which is resulted by the successive thermomechanical degradation in the polymer matrix. However, for $0.3 < \alpha < 0.9$, constant values of E are observed with an average value of 119 and 107 kJ/mol for R3 and R4 respectively, as summarized in **Table 5.4**.

Table 5.5. Estimated values of pre-exponential factor using kinetic invariant method, Nonlinear Optimization (Nelder-Mead simplex method).

Models	NPLA					SNC-PLA				
	Pre-exponential factor (ln A)					Pre-exponential factor (ln A)				
	R0	R1	R2	R3	R4	R0	R1	R2	R3	R4
KIP	25.8	23.3	22.9	18.48	17.08	22.7	22.79	22.70	21.3	18.9
F1	46.74	47.33	45.56	44.70	42.21	49.41	49.99	52.38	51.16	46.96
A2	22.35	21.98	21.08	20.65	19.38	23.04	23.33	24.54	23.93	21.79
A3	13.66	13.41	12.811	12.52	11.67	14.13	14.33	15.14	14.72	13.29

Table 5.6. R^2 values for kinetic invariant method and the objective function values (sum of square error) for Nonlinear Optimization (Nelder-Mead simplex method).

Models		NPLA					SNC-PLA				
		R0	R1	R2	R3	R4	R0	R1	R2	R3	R4
R^2	KIP	0.995	0.936	0.990	0.982	0.995	0.998	0.991	0.998	0.998	0.991
Objective	F1	0.045	0.037	0.050	0.060	0.071	0.014	0.012	0.013	0.018	0.027
	A2	0.044	0.036	0.049	0.059	0.070	0.014	0.012	0.013	0.018	0.026
	A3	0.044	0.036	0.049	0.059	0.069	0.014	0.012	0.013	0.017	0.026

The pre-exponential factors estimated using the kinetic invariant method and Nonlinear Optimization (Nelder-Mead simplex method) are provided in **Table 5.5.**

5.3.4. Estimation of kinetic parameters using KIP method

In this work, activation energy and pre-exponential factor (A) are obtained from fourteen different models, for all the samples at each heating rate from Coat Redfern method as stated in **Table 5.4**. Compensation parameters estimated from **Eqn. 5.7** are used to obtain the E_{inv} and ln $A_{inv.}$ Linear relationship is observed for ln A vs E plot for all the samples and it is an indication for the existence of supercorrelation function, which is useful to estimate E_{inv} and ln A_{inv}.

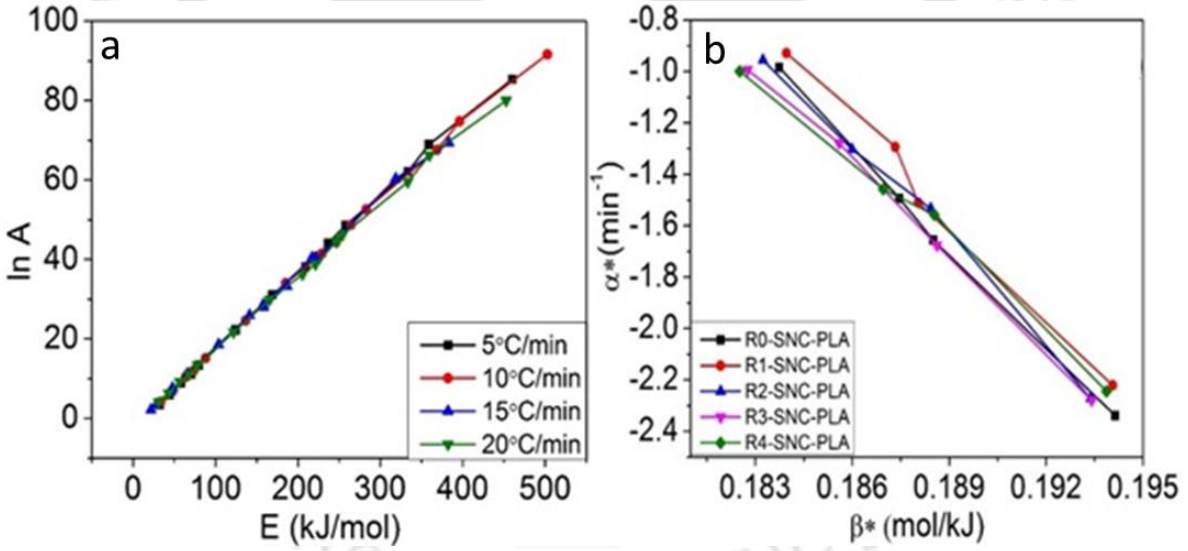

Figure 5.4. Representative (a) compensation plot for R4-SNC-PLA and (b) supercorrection relationship for SNC-PLA (R0 to R4).

Representative plots are displayed in **Fig. 5.4 ('a' and 'b')** which correspond to the compensation graphs of R4-SNC-PLA and supercorrelation graph of R0 to R4-SNC-PLA. It can be clearly observed from **Table 5.4** that the activation energies obtained from KIP method

for PLA-SNC nanocomposite (R0-R4) are matching with values estimated from isoconversional methods. However, in case of NPLA (mainly for R1 and R2) a large deviation in activation energies are observed in between KIP and K-A-S methods, and it may be due to the conversion dependency of E, which is a required criterion to apply KIP method. Therefore, KIP method can be applied to estimate activation energies for SNC-PLA (but not for NPLA) at all reprocessing cycles (mainly for conversion value of 0.3 to 0.8).

5.3.5. Selection of best fitting model for kinetic triplet's estimation

For both the samples, irrespective of their number of reprocessing cycles, the activation energy estimated from nucleation and growth model (A2) resemble with the values obtained from isoconversional methods. Similarly, the generalized master plot curve of both samples in all reprocessing stages clearly illustrates that the simulated curve closely matches the one constructed according to nucleation and growth (A2). In addition to this, chemical reaction model (F1) and nucleation and growth model (A3) are also showing good agreement with the simulated experimental TGA data. Summarized results of activation energy and pre-exponential factor are illustrated in **Table 5.4 and Table 5.5,** and representative master plot (**Fig. 5.5)** is presented for fourth reprocessing cycle of NPLA (R4-NPLA) and nanocomposite (R4-SNC-PLA) at heating rate of 10 ºC/min**.** Therefore, the two nucleation and growth model (A2 and A3) and the chemical reaction model (F1) are selected to determine the optimum kinetic parameters using Nelder-Mead simplex method.

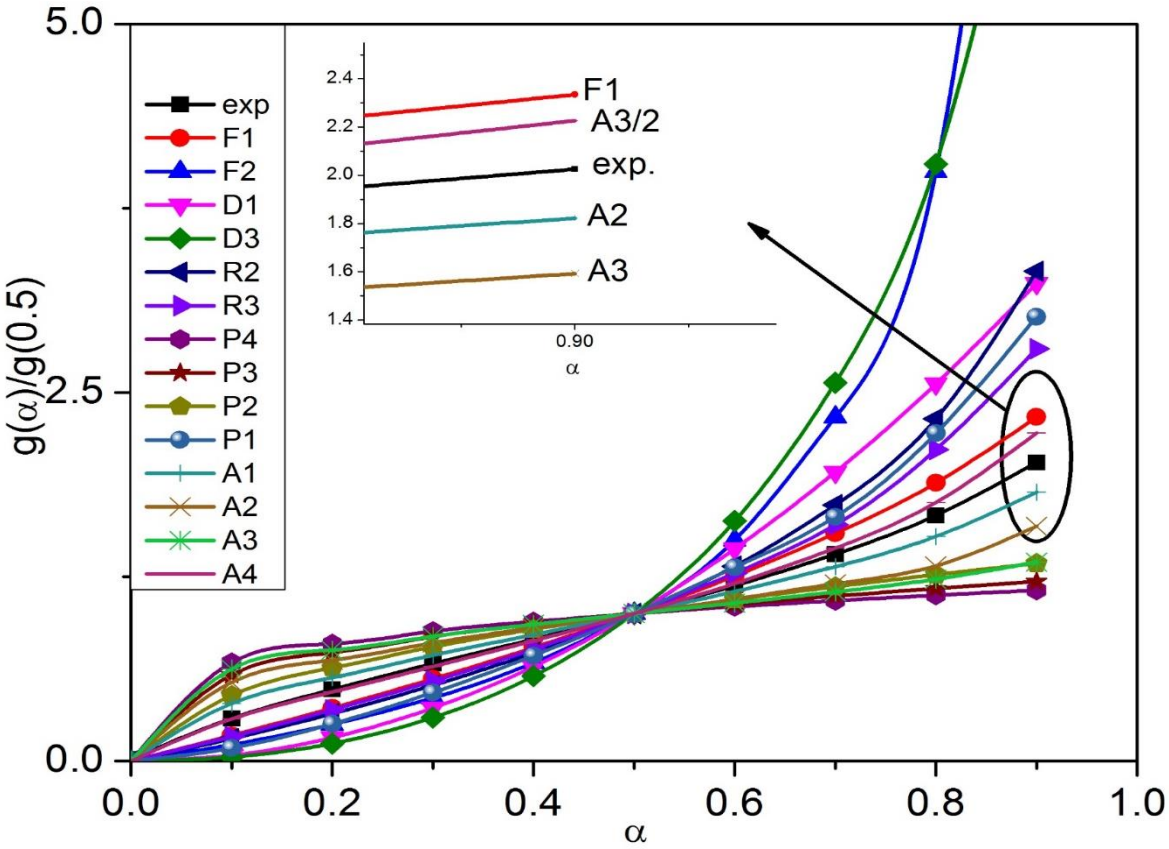

Figure 5.5. Experimental and theoretical master curve plot for R4-NPLA at heating rate of 10 ºC/min.

5.3.6. Best prediction of experimental TGA data

As mentioned in earlier section, Nelder-Mead simplex method is used to determine the optimum kinetic parameters for the three degradation reaction models by minimizing the error between the experimental TGA and the model predicted conversion values. The kinetic parameters (E and A) that are determined from the Coats-Redfern method are used as initial assumptions in the Nelder-Mead simplex method to minimize the objective function in **Eqn. 5.15.**

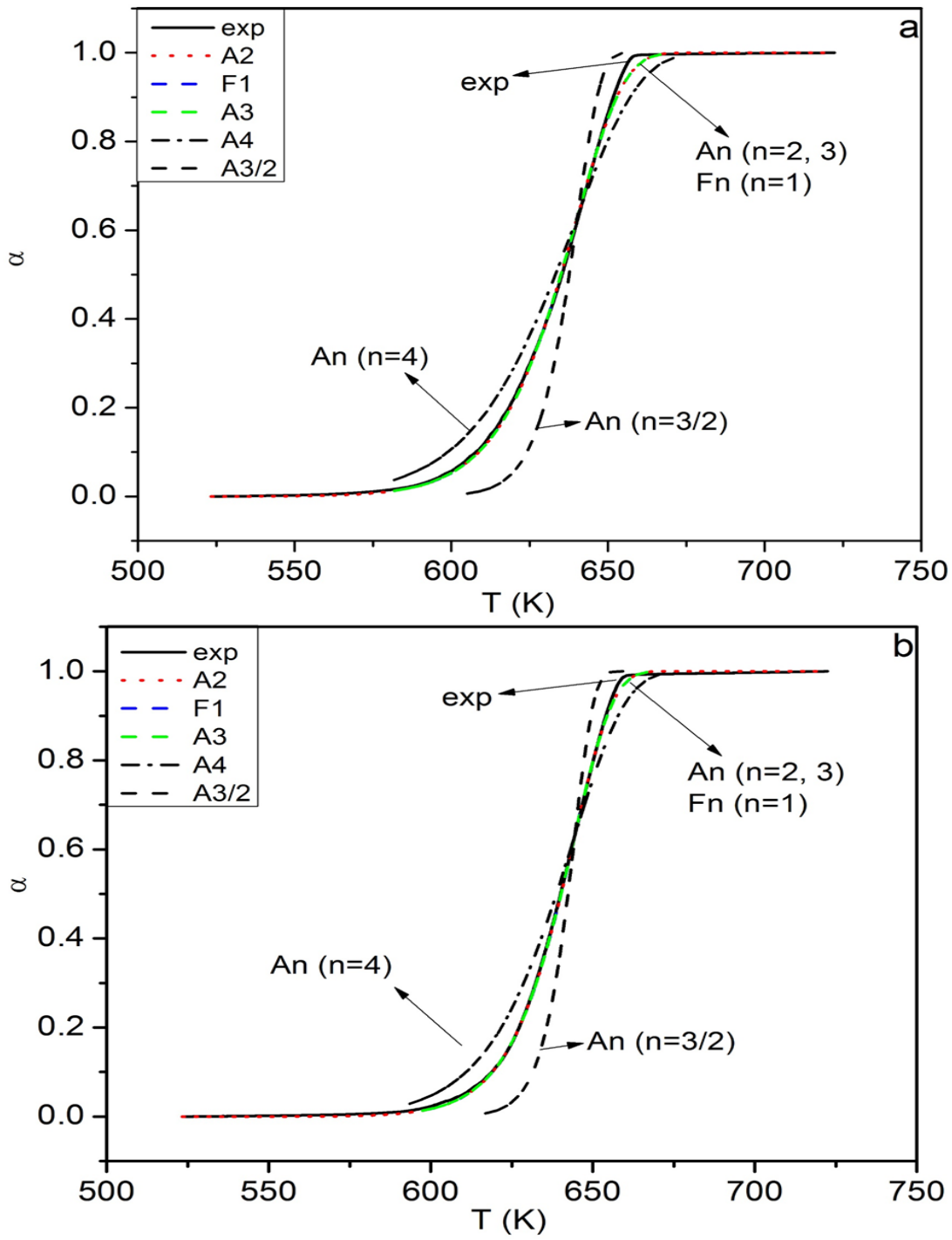

Figure 5.6. Nelder-Mead simplex prediction of experimental degradation conversion values for R4-NPLA and R4-SNC-PLA with nucleation and growth model (for A2, A3, A4, and A3/2) and chemical reaction model (F1) at 10 ºC/min.

Fig.5.6 is a representative figure for R4-NPLA and R4-SNC using the three models (nucleation and growth (A2 and A3) and chemical reaction (F1)) that are likely to be the best fit from all the models for all the samples. From **Table 5.6** it is worth mentioning that for both the samples (NPLA and SNC-PLA) at all reprocessing cycles, the sum of the squares of the error obtained between the experimental and simulated TGA data for nucleation and growth (A2 and A3) and chemical reaction (F1) with different values of thermal decomposition kinetic parameters is very less. This is one of the indication for the possibility of describing similar system with different models having their own distinguished kinetic parameters. Therefore, it is always difficult to generalize the decomposition reaction mechanism based on 'good fit' criterion. For both the samples in all reprocessing cycles, the decomposition reaction seems to be governed by the nucleation and growth and first order reaction model (F1), which can also be considered as a special case of the Avrami-Erofeyev model (nucleation and growth model) (A1) [185]. Polymers are composed of poly-dispersed entangled macromolecules and hence there may be a chance for formation of gases inside polymer matrix in the early stage of polymer melting [186]. Thus, nucleation and growth may be rate controlling factors for the decomposition reaction, followed by diffusion and the gas escapes from the surface as gaseous product. Therefore, for complex system like polymers, it is always important to study the decomposition mechanism supported by techniques which can quantify the mass and molecular structure of the decomposed product through online monitoring with time (TGA coupled with GC-MS).

The activation energy values obtained from nucleation and growth model (A2) are relatively close to the values obtained from the isoconversional methods. Based on this model (shown in **Table 5.4**), the activation energy values are decreasing from 124 to 109 kJ/mol for R0-NPLA to R4-NPLA. However, for the case of SNC-PLA nanocomposite slight increment is observed

(128 to 136 kJ/mol), upto third reprocessing cycle and is subsequently reduced to 121 kJ/mol in fourth cycle. The higher values of activation energy (E) and pre-exponential factor (A) exhibited for SNC-PLA nanocomposite for all the reprocessing cycles as compared to NPLA also confirm the thermal stability of SNC-PLA nanocomposite during multiple extrusion. **Fig.5.7** illustrates the Nelder-Mead simplex prediction of thermal degradation conversion values for representative sample (R0-NPLA) with nucleation and growth model (A2) at each heating rate. From the best fit model, it can be concluded that the method can be applied for increasing the precision for the determination of kinetic triplets.

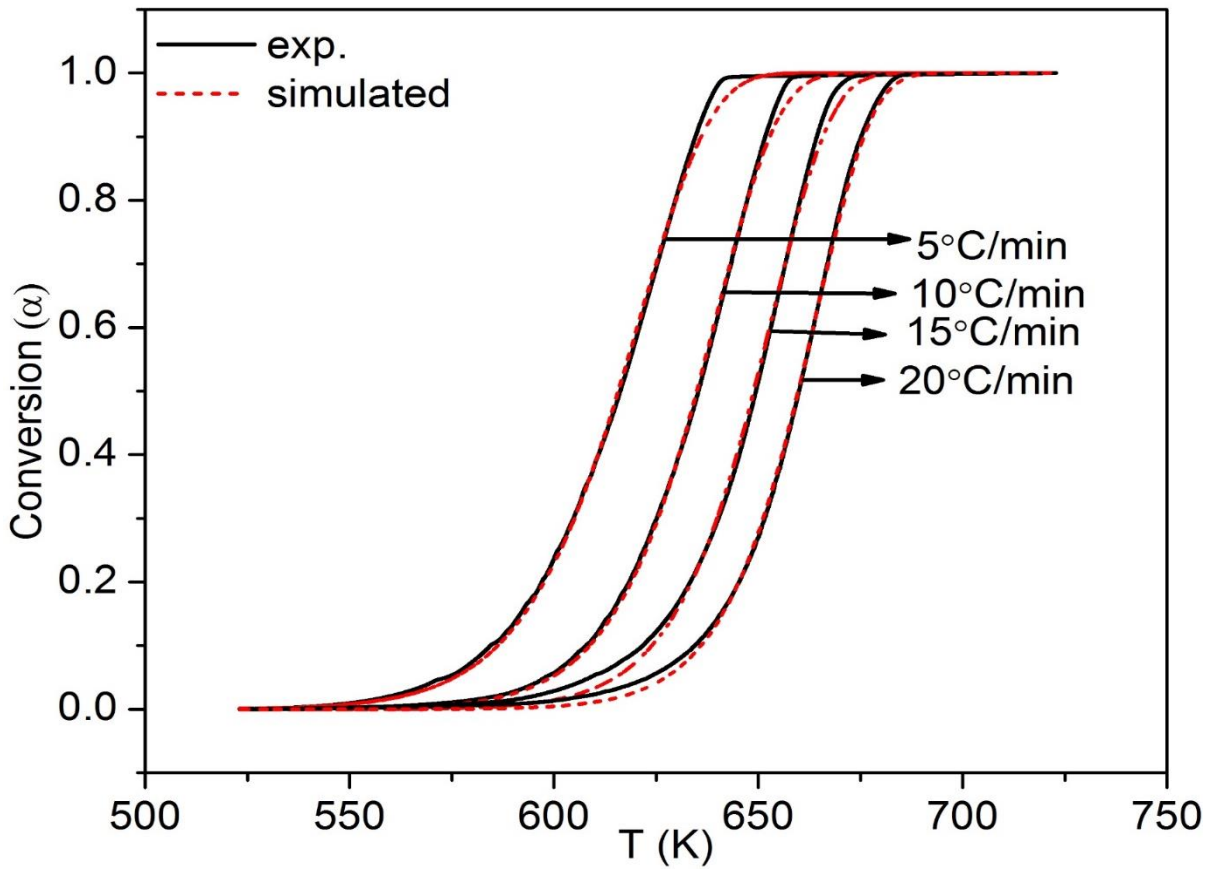

Figure 5.7. Nelder-Mead simplex prediction of exiperimental degradation convertion values for R0-NPLA with nucleation and growth model (for A2).

5.3.7. TG-FTIR: Analysis of the evolved gases

The 3D TG-FTIR are shown in **Fig 5.8 ('a' and 'b')** for R0-NPLA and R0-SNC-PLA. The evolved gasses are observed beyond 290 ºC. The FTIR spectra (**Fig.5.9** representative figure for R0-NPLA**)** obtained for thermal decomposition of NPLA in all reprocessing stages are in agreement with previously reported literatures [178, 187].

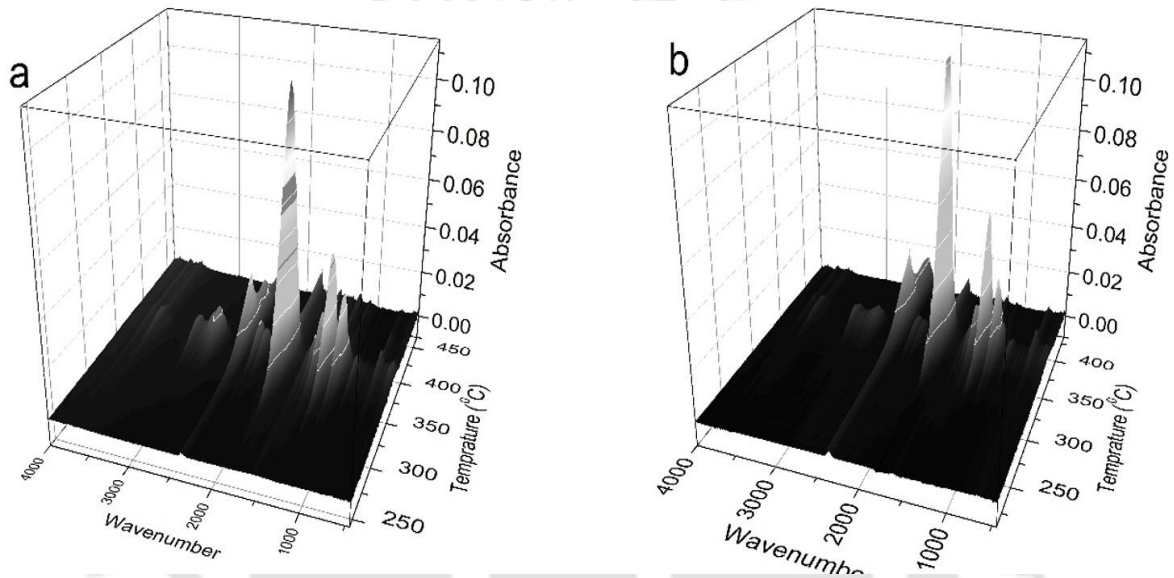

Figure 5.8. 3D-FTIR spectra of (a)R0-NPLA and (b)R0-SNC-PLA evolved gasses at 5 ºC/min

Lactides/cyclic oligomers and aldehyde are the major evolved gaseous products with small amount of carbon dioxide and carbon monoxide. Lactide/cyclic oligomers are detected by valence stretching of C-O at 1260 and 1100 cm^{-1}, C=O stretching at 1792 cm^{-1} of carbonyl group, C-H stretching and bending at 2940 and 1380 cm^{-1} and cyclic skeletal vibration at 930 cm^{-1}. Acetaldehyde is also detected by stretching vibration band at 1764 cm^{-1} for C=O and C-H bending vibration of CH_3 group at 1380 cm^{-1} with vibrational stretching at 3010, 2940 and

2745 cm^{-1}. The peaks identified at 2180 and 2110 cm^{-1} represent bending vibration of C-O for carbon monoxide and CO_2 detected by the band observed at 2360 cm^{-1}. The formation of carbon monoxide and carbon dioxide indicates some extent of hydroxyl end initiated ester decomposition and homolysis of NPLA chains [178]. The effect of SNCs on thermal decomposition behavior of PLA matrix, when subjected to multiple extrusion process are illustrated by using **Fig.5.10** (representative FTIR spectra for R2-NPLA and R2-SNC-PLA).

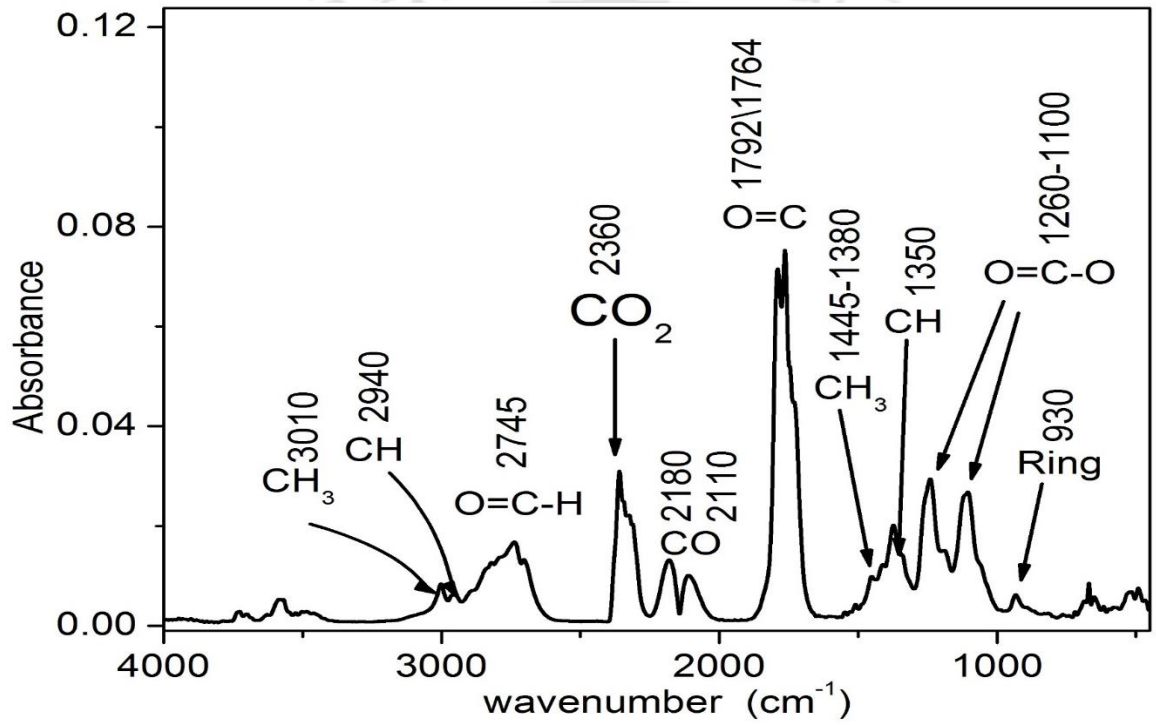

Figure 5.9. NPLA FTIR spectra for evolved gases at maximum degradation temperature (361 ºC) at heating rate of 5 ºC/min.

To have better insights, the spectra is displayed for temperature range between 280 to 370 ºC (with 10 ºC increment). For the comparative analysis of characteristics peaks, the spectra is divided into three zones (3010-2500 cm^{-1}, 2500-2000 cm^{-1} and 2000-1500 cm^{-1}).

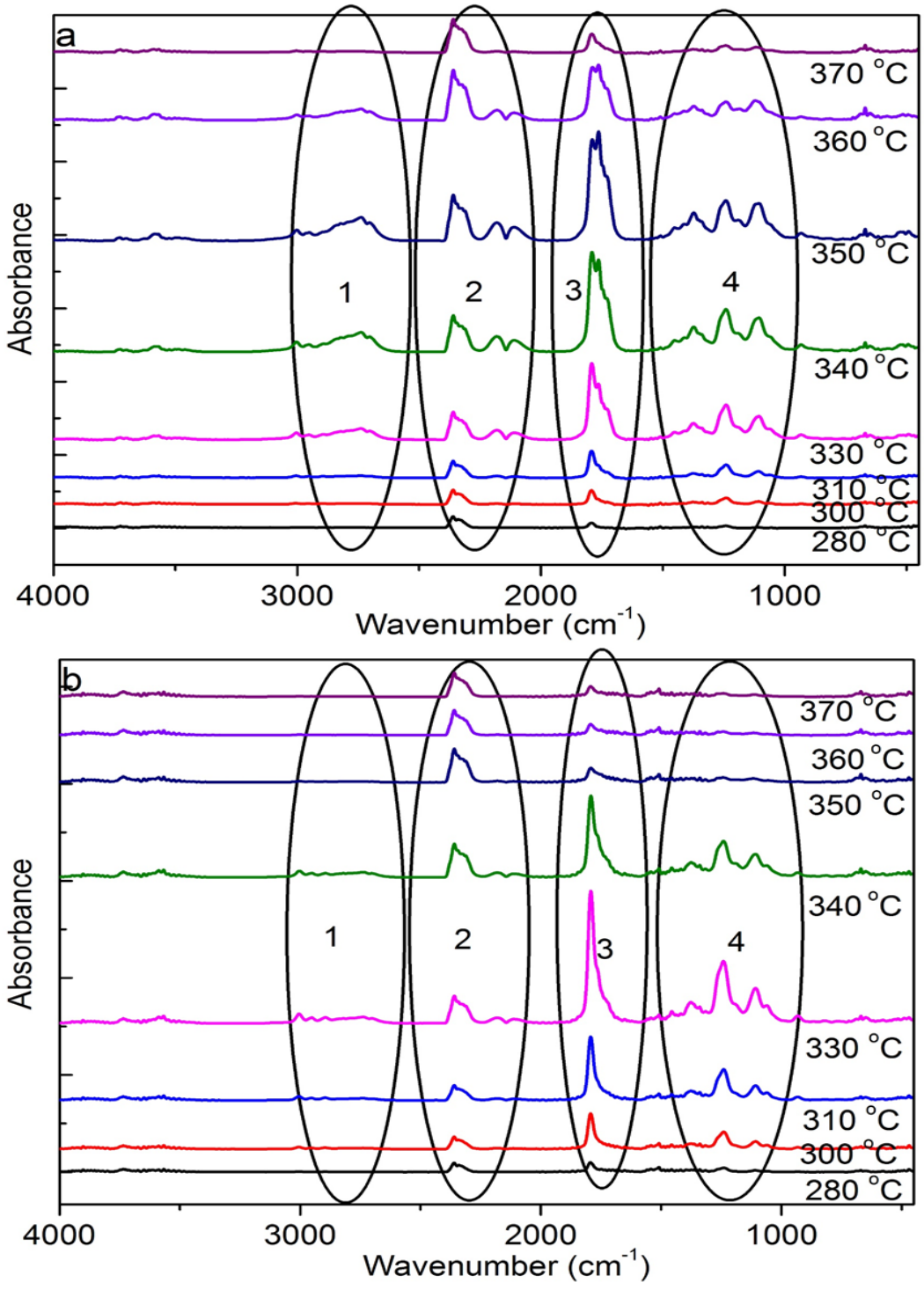

Figure 5.10. Evolved gases FTIR spectra of (a) R2-NPLA and (b) R2-SNC-PLA for temperature ranging from 280 to 370 ºC at heating rate of 5 ºC/min.

It can be clearly observed that the degradation phenomenon happening in the nanocomposite, differs from NPLA. C-H stretching vibration of aldehyde O=C-H group (2745 cm^{-1}), C-H stretching (3010 and 2940 cm^{-1}) and bending vibrations (1445 and 1380 cm^{-1}) of aldehyde CH_3 group are observed significantly from 330 to 370 ºC with maximum intensity at around 361 ºC. However, disappearance of aldehyde characteristic peaks is clearly observed from (**Fig. 5.10(b)**) in zone 1 and zone 3 for R2-SNC-PLA. The reduction of carbon monoxide peak intensity in zone 2 (2180 and 2110 cm^{-1}) for the case of R2-SNC-PLA are the result of insignificant effect of hydroxyl end initiated ester decomposition.

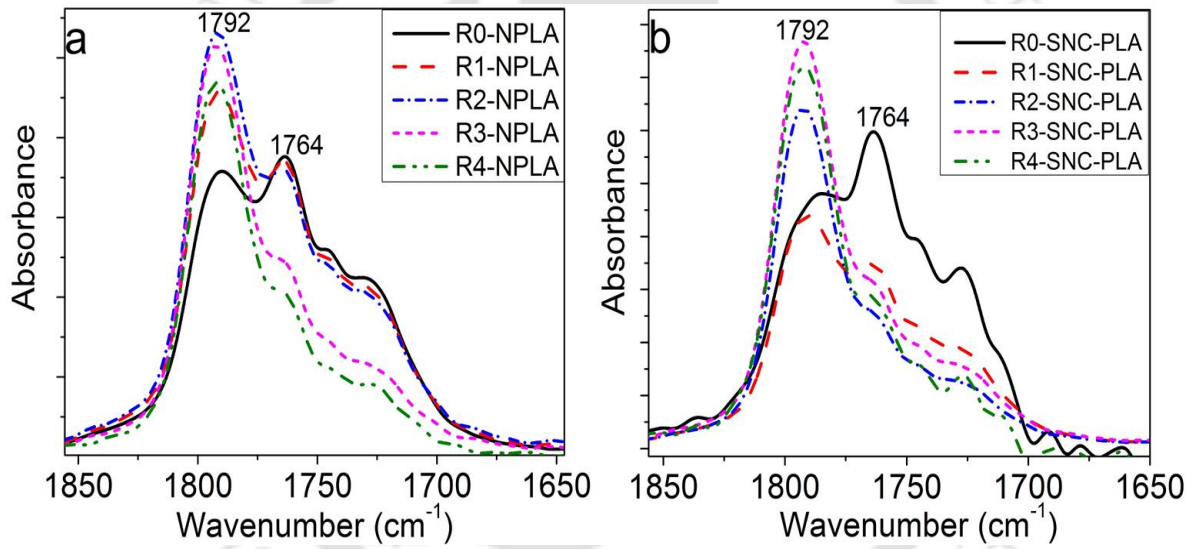

Figure 5.11. The effect of reprocessing on characteristic peaks of (a) NPLA and (b) SNC-PLA C=O stretching at maximum degradation temperature (361 ºC) with heating rate of 5 ºC/min.

The shoulder like peaks observed (**Fig. 5.11)** at 1764 and 1792 cm^{-1} (C=O stretching vibration) for NPLA (R0, R1 and R2) and R0-SNC-PLA are completely shifted into single peak (at 1792 cm^{-1}) for the subsequent reprocessing cycles. Therefore, it is noteworthy that the

decomposition phenomena of the nanocomposite is somehow different than that of NPLA and it is in good agreement with the observation obtained from the isoconversional methods (the trend of the change in activation energy with the conversion).

5.3. Summary

In this work, the thermal degradation of NPLA and SNC-PLA nanocomposites, prepared in the laboratory, is investigated for four reprocessing cycles by using thermogravimetric analysis. Silk nanocrystals are effectively dispersed in the PLA matrix at nano-level. A single step decomposition behavior is assumed from the observed single pattern TGA thermograph for all the heating rates. However, from the dependency of activation energy on conversion for all reprocessing cycles of NPLA, the thermal degradation is found to be complex and a multi stage decomposition process. On the other hand, the activation energy of SNC-PLA composite is observed to be constant with change in conversion and hence it can be concluded that it is following single step decomposition reaction. Unlike NPLA, reduction in the intensity of FTIR spectra (2745, 2180, 2110 cm^{-1}) of the characteristic peaks for aldehyde and carbon monoxide are observed from the evolved gas analysis of SNC-PLA (for all reprocessing cycles). The activation energy of SNC-PLA estimated for all reprocessing cycles using Kinetic Invariant Parameters (KIP) is consistent with the values obtained from isoconversational methods. However, due to the activation energy dependency of NPLA (mainly for R0 and R1), the values obtained from KIP method are not consistent with the isoconversional values. Optimum kinetic triplets are determined successfully by coupling Coats-Redfern method and master plot method with Nelder-Mead simplex method. Results show that the nucleation and growth A2 is the best fit of the experimental TGA data. First order reaction kinetics, nucleation

and growth (A3) can also predict the decomposition reaction perfectly. From this it can be concluded that, two or more reaction mechanisms are taking place at a time for both the systems at all reprocessing stages. In the case of NPLA, decrement in activation energy is observed with increasing number of reprocessing cycles, due to the significant thermomechanical induced molecular weight reduction. However, the incorporation of SNCs in to PLA matrix, improves thermal stability of PLA matrix which is observed by the increment in activation energy. This remarkable thermal stability of the biocomposite may be related to the dispersion of well-ordered, thermally stable silk fibroin structures (β-sheets) in the PLA matrix

Chapter 6

Silk Nanocrystals Grafted Poly (lactic acid):

The influence of crosslinking on Rheology and Thermal Stability

In this chapter, reactive extrusion is performed to obtain branched and crosslinked poly (lactic acid) (PLA) with silk nanocrystals grafted chain topology at different levels of gel percentage by adding small amount of radical initiator (dicumyl peroxide (DCP)). Grafting of SNCs on PLA macromolecules is confirmed through ^{1}HNMR and FTIR, which provides remarkable improvement in rheological and thermal properties. Significant improvement in zero shear viscosities are observed with shift in crossover frequency to lower values as compared to branched and crosslinked PLA system. The grafting of SNC leads to enhance the crystallization behavior and formation of stable crystals during cooling leads to a single melting peak with improved rate of crystallization of PLA. However, the percentage crystallinity decreases with increasing DCP fraction. It is probably due to higher grafting and crosslinking, which restricts the macromolecular motion of polymeric chains, which is essential for crystallization process. Furthermore, the grafting of SNC increases the reprocessability performance of PLA and provides improved rheological properties as compared to branched and crosslinked PLA in all reprocessing cycles.

Parts of this chapter are ready to communicate as:

Melakuu Tesfaye, Rahul Patwa, Prodyut Dhar, Vimal katiyar, Silk nanocrystals Grafted Poly (lactic acid): the influence of Crosslinking on Rheology and Thermal Stability.

6.1. Introduction

PLA is exposed to thermal degradation at high temperature and shear that leads to low melt strength. Investigation of the macromolecular chain modification of PLA is complex due to the existence of simultaneous different reactions. Random chain scission is known to be a major cause of thermal degradation within the processing window of PLA (180 to 220 °C) that leads to the drastic reduction in the molecular weight [188-190]. Furthermore, the reduction in molecular weight may become more severe when trace amount of water molecules, short oligomeric chains, residual catalysts, and monomeric units are present in the polymer matrix.

Reactive extrusion in presence of multifunctional epoxies, highly reactive peroxides such as dicumyl peroxide (DCP) and bezoylperoxide (BPO) have been practiced to enhance the melt strength of polypropylene (PP), poly (ethylene terephthalate) (PET), poly (butylene terephthalate) (PBT), etc. [191-194]. Similar techniques have been adopted to improve the melt strength of PLA which leads to enhancement in the processing performance and other physical properties (mechanical, barrier, and thermal properties) [195]. **Zhou et al.,** have successfully prepared chain extended PLA-epoxy resin copolymers through reactive extrusion using diglycidyl ether of bisphenol A as chain extender [196]. **Cailloux et al.,** have also showed one step reactive calendaring process to improve the thermal sensitivity of PLA with styrene acrylic multifunctional oligomer which leads to improvement in melt rheology due to predominance of long chin branching [197]. Significant macromolecular modification of PLA/PBAT (butylene adipate-co-terephtalate) blend at various proportions is observed due to reactive extrusion in the presence of Joncryl (glycidyl methacrylate), which further enhances the mechanical and rheological properties [30]. Radical initiator dicumyl peroxide (DCP) also proves to be an effective chain extender and helped initiating the grafting of PLA chains on

the surface cellulose nanocrystals (CNC), which results in improved melt strength and mechanical properties (Young's modulus by ~40% and tensile strength by 490%) along with improved recycling performance [40, 198]. The same kind of results are also reported by **Bian et al.,** in which the tensile strength and modulus of poly (lactic acid)/ poly (3-hydroxybutyrate-co-4-hydroxybutyrate) blend significantly increased with the addition of DCP [199].

From our previous investigations, highly thermally stable silk nanocrystals (SNCs) are observed to stabilize the thermal properties of PLA under repetitive extrusion [200]. The hydrophobic nature of SNCs along with its highly structured β-sheet network (arises because of strong hydrogen bonding between C=O and N-H groups) helps to reinforce PLA matrix with good dispersion. The crystalline part of silk fibroin is proved to have amino acids repeating order of glycine-alanine-glycine-alanine-glycine-serine. Similar to cellulose, serine group of SNC is having -CH_2- which is an ideal site to form radicals using radical initiators for grafting of PLA chains which may help to modify the matrix during reactive extrusion. If this approach is successful, then it may increase the remarkable performance of SNCs as a filler and enhance the melt strength which is the major limitation of PLA.

To have a better understanding on the macromolecular level, proper characterization techniques and analysis procedures need to be followed. In the reactive melt extrusion process of PLA, degradation and chain coupling as well as chain modification can take place through long chain branching, short chain branching, crosslinking and grafting on the surface of fillers. Estimation of the gel content and molecular weight analysis of the system can provide a general information about the chain modification and it needs to be supported by rheological investigation which is a powerful tool to have a clear understanding about the macromolecular

level changes [40, 201]. Zero shear viscosity, storage and loss modulus around terminal region, characteristic and cross over frequency can be used to quantify the macromolecular chain modification. Furthermore, the weight relaxation spectrum ($\lambda H(\lambda)$) can be used to verify different microstructural topologies such as chain branching and crosslinking [28, 197]. Along with the melt rheology, changes on the thermal stability (melting and crystallization properties and thermal decomposition behavior) of the sample also need to be investigated.

The present study deals with the reactive modification of PLA/silk nanocrystals nanocomposite with dicumyl peroxide (DCP) and investigates the impact of chain modification on the rheology and thermal properties (crystallization, melting and thermal decomposition behaviors). The structural change and possible reaction mechanisms are also assessed with the help of FT-IR, NMR and GPC. Additionally, the impact of reprocessing on the above mentioned important properties is discussed.

6.2. Results and Discussion

6.2.1. Impact of DCP on the structural modification of PLA/silk bionanocomposite

It is already discussed in literature that DCP decomposes into free radicals at high temperature with a strong ability to abstract hydrogen and initiate radicals on PLA backbone which is the result for propagation of crosslinking reaction between the PLA chains [202]. This reaction takes place inside extruder which is subjected to high shear and temperature which provides sufficient mixing, which leads to modification of chain topology of the chain at any instant by crosslinking or branching (long and/or short chain branching). This phenomenon is totally different when fillers are incorporated into the reactive extrusion system because the radical initiator will get the chance to abstract hydrogen from the weak site of the fillers bond linkage [40]. Gel percentage, which is estimated (samples collected at residence time of 5 min)

using **Eqn. 6.1** (dividing weight of dry gel (W_{gel}) to the sample weight before washing (W_i) it by chloroform to remove unmodified macromolecules) is used as primary analysis parameter to understand the reactive modification of PLA. Due to the weak interaction of cross-linked portion of polymeric system with a solvent, the probability of the formation of gel like structure is high.

$$gel\ \% = \frac{W_{gel}}{W_i} \times 100 \qquad 6.1$$

Two possible modifications are expected during reactive extrusion of current system: PLA-PLA (crosslinking and branching) and PLA-SNC (grafting reaction). Reactive extrusion of neat PLA is used as a controlling system to assess the impact of SNC on PLA chain modification. As indicated in **Table 6.1**, 10 wt.% and 30 wt.% gel percentage is observed for reactive extrusion of NPLA at 1 and 1.5 wt. % DCP which indicates the presence of crosslinking topology. At a lower DCP content, (0.5 wt. %) no gel formation is observed which is confirmed from molar mass distribution and rheological investigation, in which the change can be correlated with branching structures. Similar observation is also reported for poly(3-hydoxybutyrate-co-4-hydroxybutyrate) in which no gel formation is observed at DCP content less than 0.5 wt. % [203]. However, the gel percentage of SNC-PLA increased form 10% (0.5 wt. % DCP) to 60% (1.5 wt. % DCP). This result confirms the existence of a significant interaction between SNC and PLA macromolecules due to crosslinking and long chain branching, apart from polymer to polymer interaction. This result gives a fundamental information to predict the formation of radicals on the SNC macromolecular structure (possible on serine group of $–CH_2OH$ which is going to be explained by ^{1}HNMR analysis) that promotes the grafting on PLA backbone chains. As indicated in **Table 6.1**, the specific rotation and optical rotation of reactively extruded samples are observed to be decreased with increasing

wt. % of DCP. This may be attributed to the hindrance of the specific rotation due to branching of long chains attached on the central chiral carbon of PLA. Incorporation of SNC, decreases the specific rotation of grafted PLA as compared to NPLA system, which may be linked to additional effect of grafting on the chiral carbon [40].

Table 6.1. The effect of reactive extrusion on gel percentage, specific rotation and optical rotation.

Samples	Gel (%)	Specific rotation (°)	Optical rotation (°)
NPLA (extruded)	-	150.56	1.51
0.5DCP-PLA	-	141.91	1.42
1DCP-PLA	13	139.28	1.39
1.5DCP-PLA	31	133.86	1.34
SNC-PLA	-	148.32	1.48
0.5DCP-SNC-PLA	10	137.51	1.38
1DCP-SNC-PLA	43	138.46	1.38
1.5DCP-SCN-PLA	60	130.41	1.31

The macromolecular structural modification after reactive extrusion is also confirmed by FTIR spectroscopy as described in **Fig. 6.1.** Neat poly (lactic acid) (NPLA) has the main characteristic peaks at 2854, 2925, 1382 and 1455 cm^{-1} attributed respectively for symmetric and asymmetric stretching and bending of CH_3, 2996 and 1358 cm^{-1} for C-H stretching and deformation vibration, 1076 and 1180 cm^{-1} is for symmetric and asymmetric valence vibration of C-O-C, transmission band at 867 and 753 cm^{-1} are due to the C-C stretching, C=O stretching band also observed at 1747 cm^{-1}.

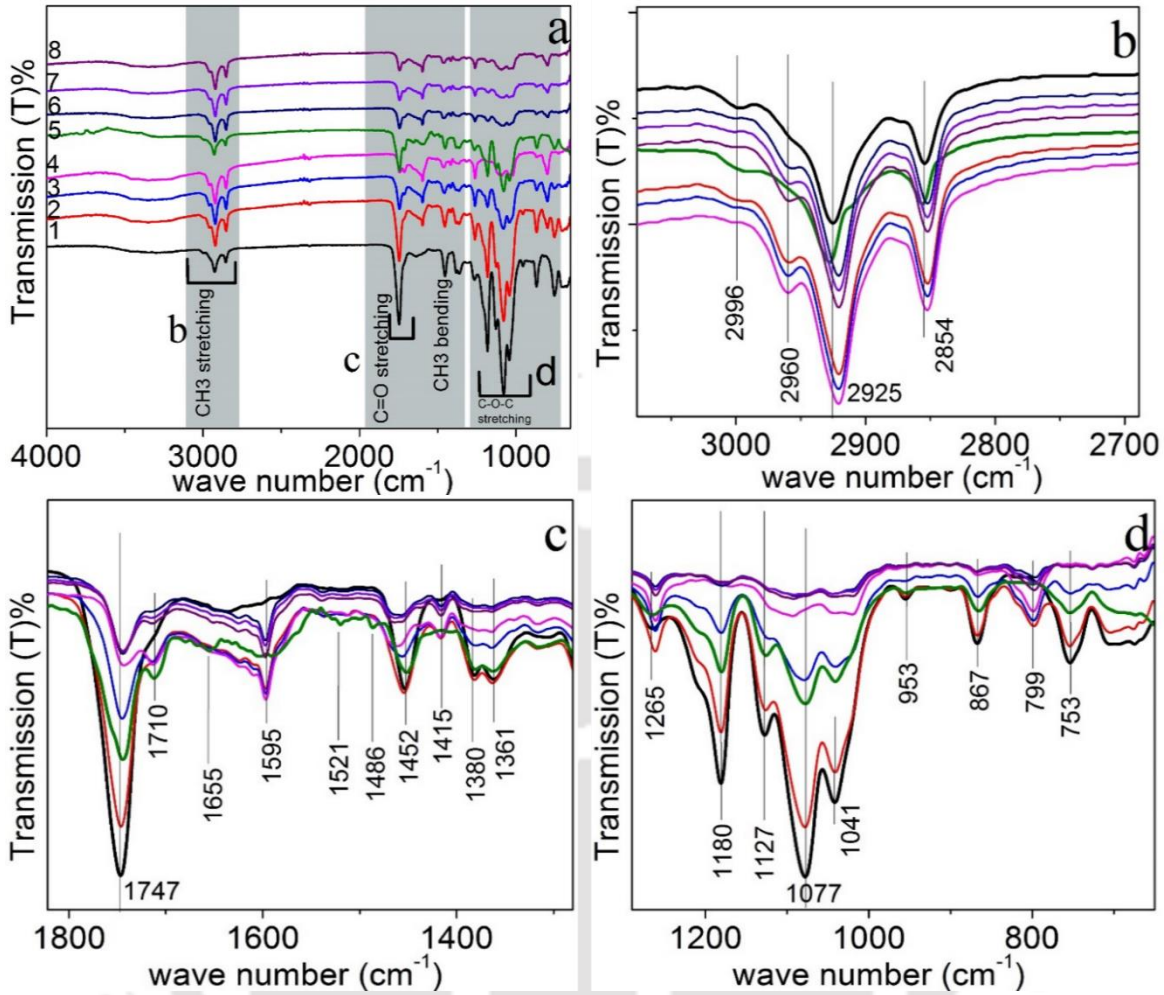

Figure 6.1. Analysis chemical structure for reactively modified NPLA and SNC-PLA samples using FTIR spectra with (a) full range (b) 3010 – 2700 cm^{-1} (c) 1890 cm^{-1} to 1280 cm^{-1} and (d) 1280 to 650 cm^{-1}.

The intensity of the peak between 1230 to 1000 cm^{-1} which is attributed to C-O-C and 1358 cm^{-1} of C-H deformation is observed to decrease with increasing DCP content for NPLA and furthermore diminishes for reactively modified SNC-PLA. It is an indication of chain modification due to branching and cross linking through the formation of new C-C bond at 799 cm^{-1} on the backbone of PLA which will affect the intensity of the ester linkage. The

significant impact of SNC observed on the ester linkage intensity may also be linked with the grafting. The new peak observed at 2960 cm^{-1} for reactively modified samples and peak at 2854 cm^{-1} (symmetric stretching CH_3) and 2925 cm^{-1} (asymmetric stretching CH_3) shifted to 2851 cm^{-1} and 2920 cm^{-1} respectively. Due to the presence of high branching, the backbone of PLA with C-C bond (peak 753 cm^{-1}) stretching band intensity is observed to decrease with increasing DCP wt. %.

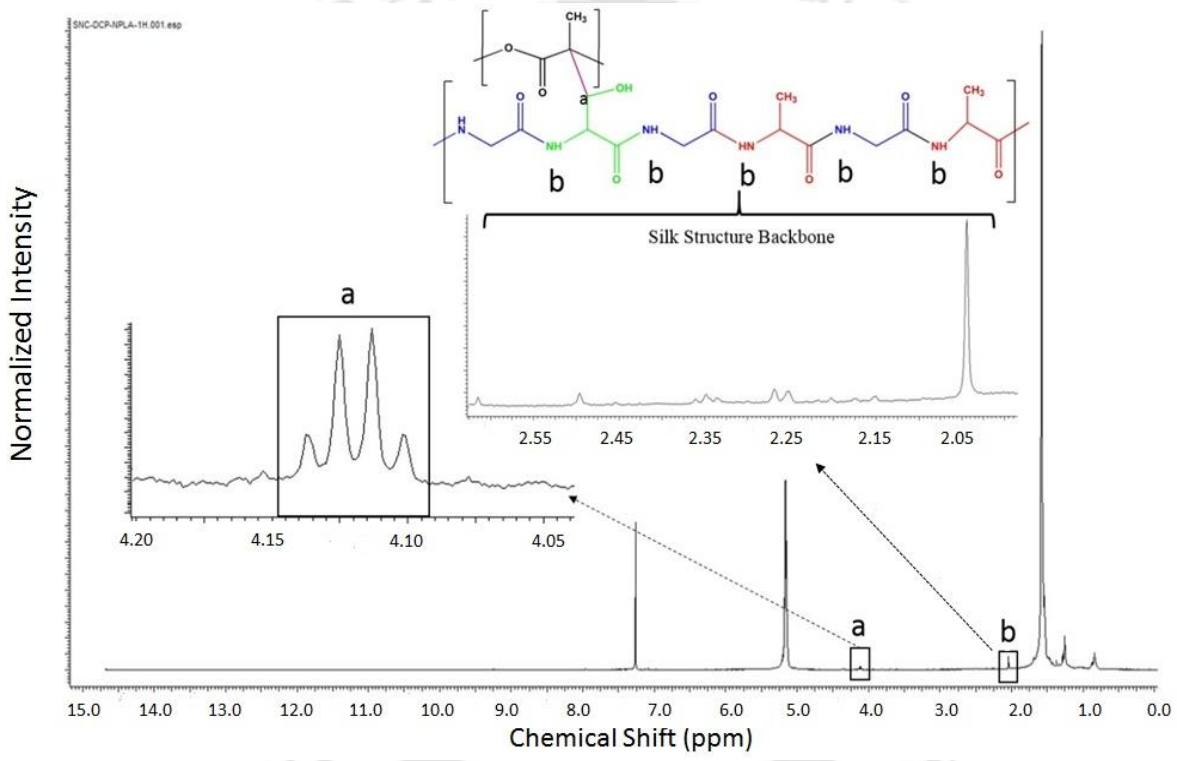

Figure 6.2. ^{1}H-NMR spectra of SNC-PLA grafting sample at 1 wt. % DCP

Due to high branching and crosslinking van der waals interaction arise between the C=O and CH_3 of H groups of the branched chains and it is identified as shoulder like peak at 1710 cm^{-1}. The disappearance of transition peak at 2996 cm^{-1} which corresponds to C-H stretching and diminishing of C-H vibration deformation peak at 1361 cm^{-1} supports the formation of radicals

imitated with abstraction of hydrogen leads to the chain modification possibly by crosslinking, branching and grafting. NMR investigation of reactively modified SNC-PLA system can provide insights about the grafting of SNC on PLA chain.

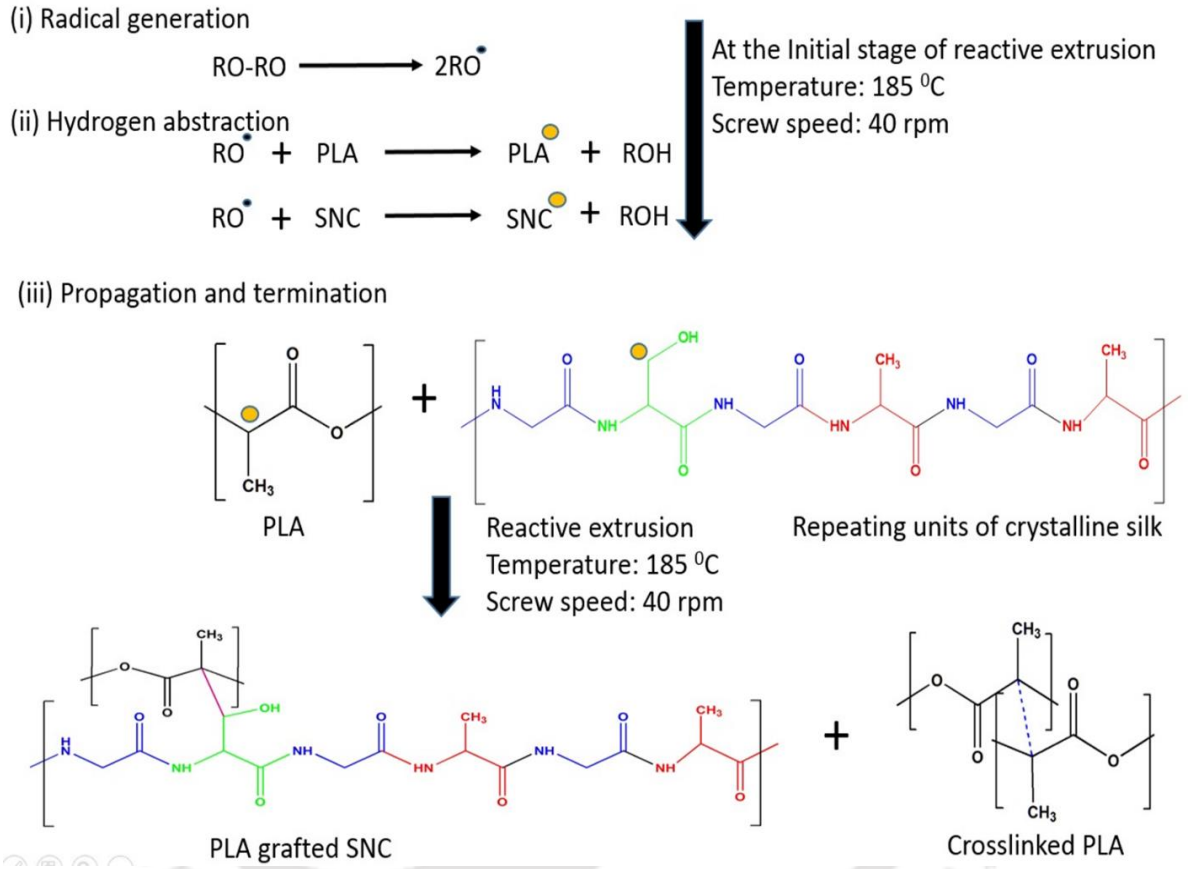

Scheme 6.1. Summarized reaction pathway for the modification of SNC-PLA chain topology by crosslinking and grafting through reactive extrusion process.

^{1}H-NMR analysis is performed for NPLA and SNC-PLA at 1 wt % DCP to study the possibility of grafting. As indicated on **Fig. 6.2** a new characteristic peak is observed for SNC-PLA system at the range of 4.10-4.15 ppm (marked as 'a') and 2.0-2.5 ppm (marked as 'b') which is missing in reactively modified NPLA samples (^{1}H-NMR attached with the supporting information). This may be attributed to the methane proton formed due to the grafting of PLA chains on

serine –CH_2OH group of SNC backbone. DCP forms radicals at high temperature and shear which have a strong tendency to abstract hydrogen and generate radicals on PLA backbone and serine (-CH_2OH) group of silk fibroin, which is the reason for the initiation of grafting of PLA chains on the silk macromolecular structure. Based on the results obtained from gel percentage, FTIR and NMR analysis, the reaction mechanism for the reactive modification can be summarized as shown in reaction **scheme 6.1.**

The significant change observed on the chemical structure due to grafting is further addressed by the molecular weight analysis using GPC. Furthermore, the molar mass distribution (M_n, M_w and PDI) is used to monitor the reaction progress and chain modifications of reactively extruded SNC-PLA at various compositions of DCP (0.5 wt. %, 1 wt. % and 1.5 wt. %). As compared to PLA granules (GPLA), molecular weight of extruded PLA (NPLA) is reduced (22% in M_w and 36% in M_n) due to thermo-mechanical degradation at the processing time of 5 min with poly-dispersity index (PDI) of 2.6. The addition of SNC leads to the formation of lower molecular weight fraction (14% area) and 86% area is showing higher molar mass fraction with 8% increment in M_n and 10 % increment in M_w as compared to NPLA. In this study, reactively extruded samples are collected at residence times of 3 min and 5 min for molecular weight analysis**. Fig. 6.3** shows the molecular weight distribution curve of SNC-PLA (at all DCP wt. %) for residence time of 3 min and 5 min. Interestingly, the percentage area for larger macromolecules of reactively extruded SNC-PLA samples are observed to increase from 48% (0.5DCP-SNC-PLA) to 90% (1DCP-SNC-PLA) and 100% (1.5DCP-SNC-PLA) with 108 kDa, 96 kDa and 133 kDa in Mn and 295 kDa, 317 kDa and 267 kDa of M_w respectively, at residence time of 3 min (**Fig. 6.3 (a))**. It indicates that sufficient amount of radicals are generated (at 1.5 wt. % of DCP) to give higher molecular weight with shorter

residentce time and it is in agreement with the life time of DCP radicals (190 sec) reported by **Takamura et al., [202]**.

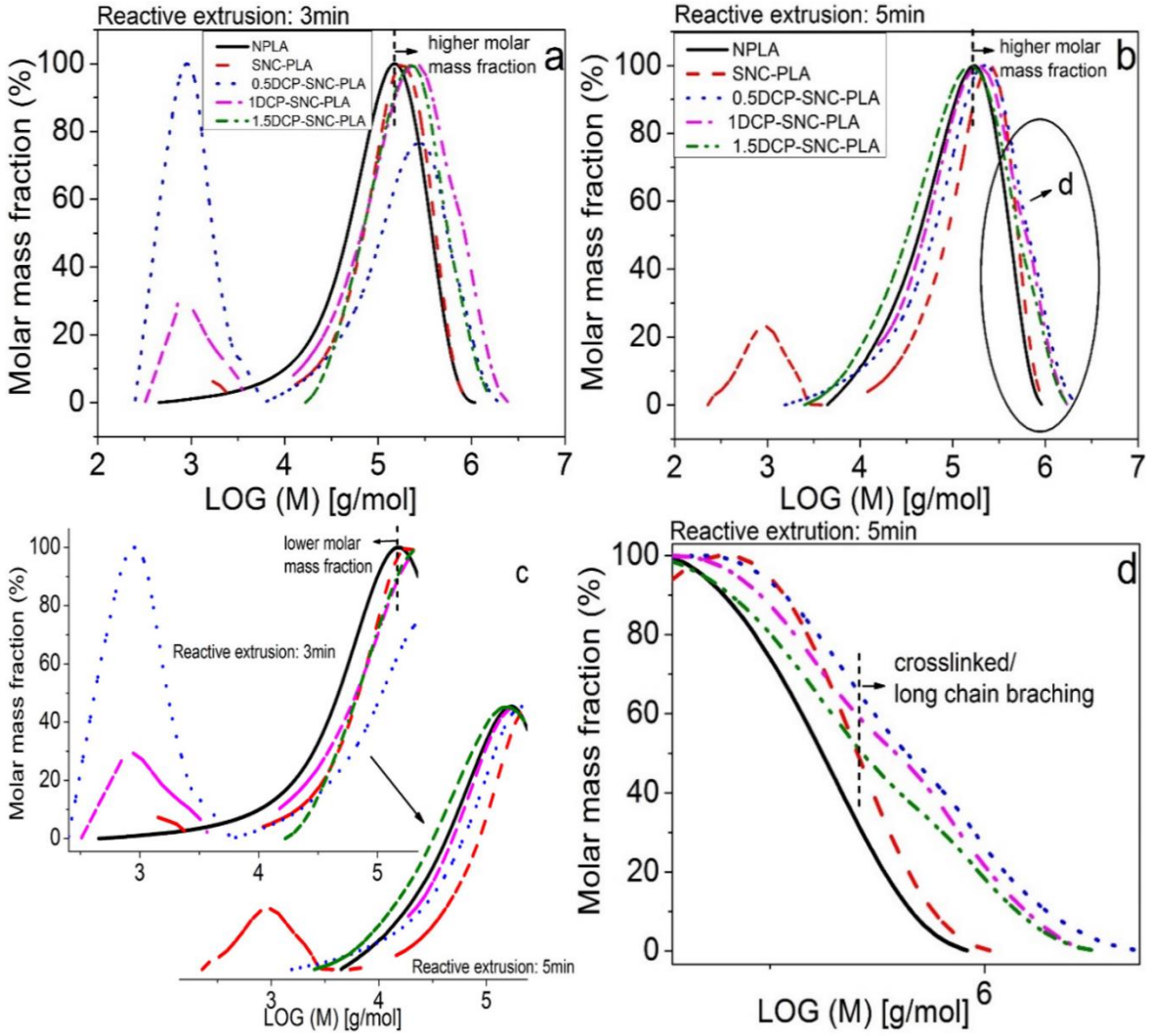

Figure 6.3. Molecular weight distribution of reactively extruded SNC-PLA at residence time of 5 min.

As the residence time increases to 5 min, the molecular weight is reduced with increase in DCP concentration. However, the lower molecular weight fraction observed at residence time 3 min is merged with the higher molecular weight fraction as indicated in **Fig. 6.3 (c).** From **Fig. 6.3**

(b & d) it can be clearly observed that the new broad peak is appearing in higher molecular weight population side because of crosslinking and grafting. Due to the fact that the hydrodynamic volume is highly affected by the molecular chain topology, estimation of molecular weight distribution using GPC alone may not be satisfactory technique. Additionally, it is difficult to conclude about the changes in chain topology with the results obtained from GPC alone. Rheological investigation can provide deep insights about changes related to long chain branching, cross-linking and grafting, which are confirmed by FTIR, NMR and GPC.

6.2.2. Rheological characteristics of reactively modified neat and PLA/SNC nanocomposite

Melt rheological investigation is an ideal tool to examine the macromolecular chain modification of polymeric system. The melt response of the polymer matrix is dependent on the molar mass distribution, chain length, branching, and crosslinking and grafting. As already confirmed by gel percentage, FTIR, ^{1}HNMR and molecular weight analysis, reactively extruded SNC-PLA attains additional chain topology due to grafting. The influence of grafting on the viscoelastic shear dependency and the relaxation spectra are assessed using dynamic rheological measurement performed at 190 ^{o}C for the frequency range of 0.1 to 500 rad/sec within the viscoelastic region (5 % strain is taken based on the small amplitude strain sweep analysis). The frequency (ω) dependency of complex viscosity (η^*) is displayed in **Fig. 6.4** for all reactively modified samples in comparison with NPLA and SNC-PLA extruded at same condition without DCP.

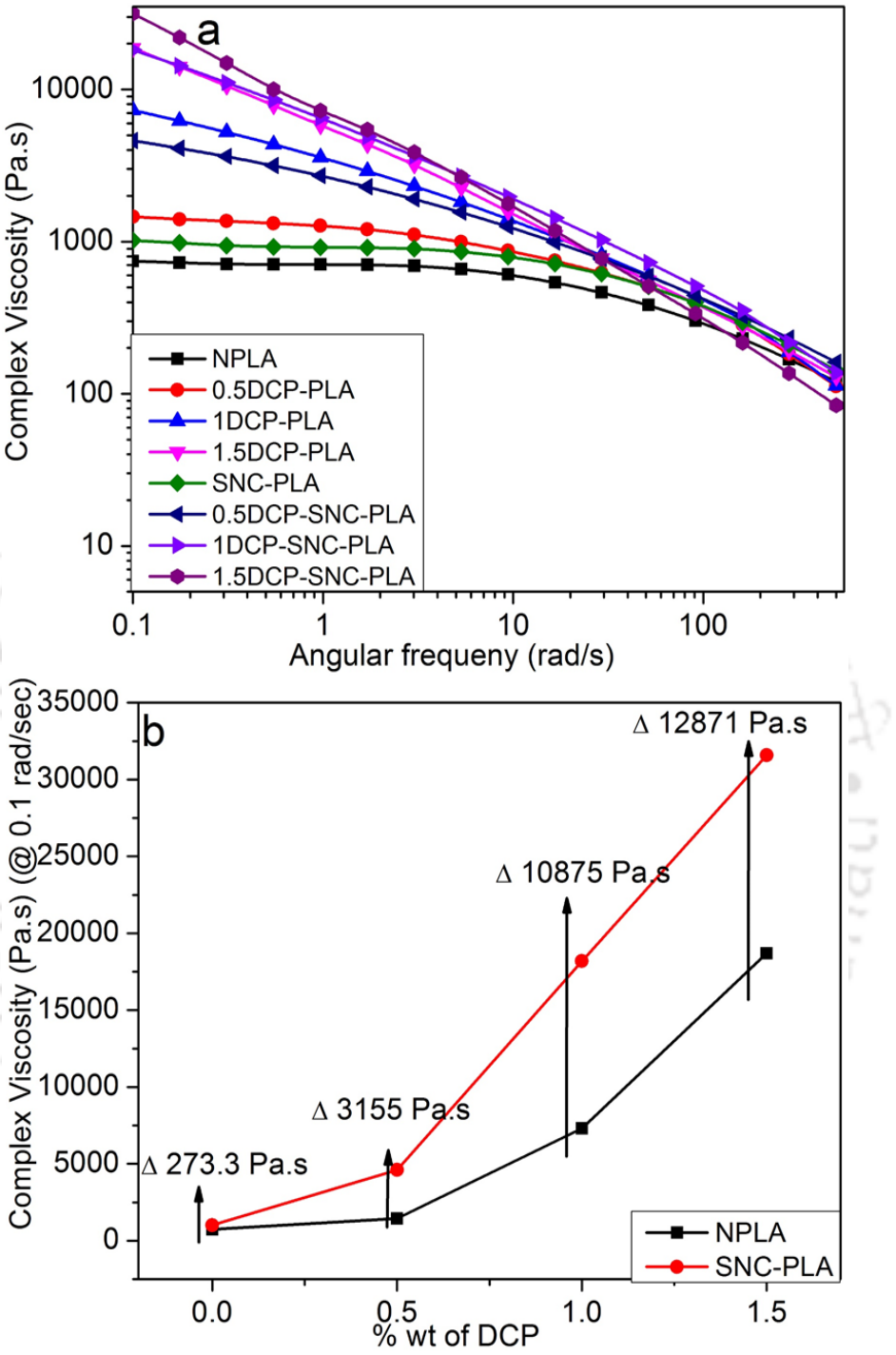

Figure 6.4. The effect of macromolecular chain modification on the change of complex viscosity with respect to frequency and the impact of SNC grafting on PLA backbone on the change in viscosity at 0.1 rad/ sec frequency.

It is clearly noticed that the NPLA, SNC-PLA and 0.5DCP-NPLA exhibit the same trend with the Newtonian behavior up to 10 rad/sec. 0.5DCP-NPLA shows higher viscosity due to the observed increment in molecular weight. With increasing the DCP amount, the Newtonian behavior shifted to lower frequency region and significant increment in viscosity and shear thinning behavior is observed for both reactively extruded NPLA and SNC-PLA. This pronounced improvement on rheological characteristic can be related with the long chain branching and crosslinking. As shown in the gel percentage, and ^{1}HNMR, the incorporation of SNC into PLA matrix gives additional reinforcement which leads to increase in the melt strength. More interestingly, complex viscosity of SNC-PLA at a frequency of 0.1 rad/sec is observed to be higher than that of NPLA by 273, 3155, 10875 and 12871 Pa.s at respective DCP amount (0, 0.5, 1 and 1.5 wt. % respectively). This result gives a strong evidence of SNC grafting on PLA backbone long chain branching and cross linking, which hinders the mobility of macromolecules by forming more entangled networks. In **Fig. 6.5**, frequency dependency of storage modulus (G') of all analyzed samples and the increment observed at lower frequency (0.1 rad/sec) due to grafting of SNC are displayed. The results related to the loss modulus are attached with the supporting information. It clearly shows that the storage modulus exhibit more plateau at lower frequency with increasing wt. % of DCP. Similar to the complex viscosity, the storage modulus values of SNC-PLA are increased by 3.8, 109, 789 and 126 Pa as compared to NPLA system at the respective DCP amount of 0, 0.5, 1 and 1.5 wt. % respectively, which support the grafting phenomenon due to the improvement in elastic behaviour of the matrix. The percolation effect of SNC is also enhanced because of grafting which provides thermally stable entangled network that increases the dominancy of storage modulus over the loss modulus.

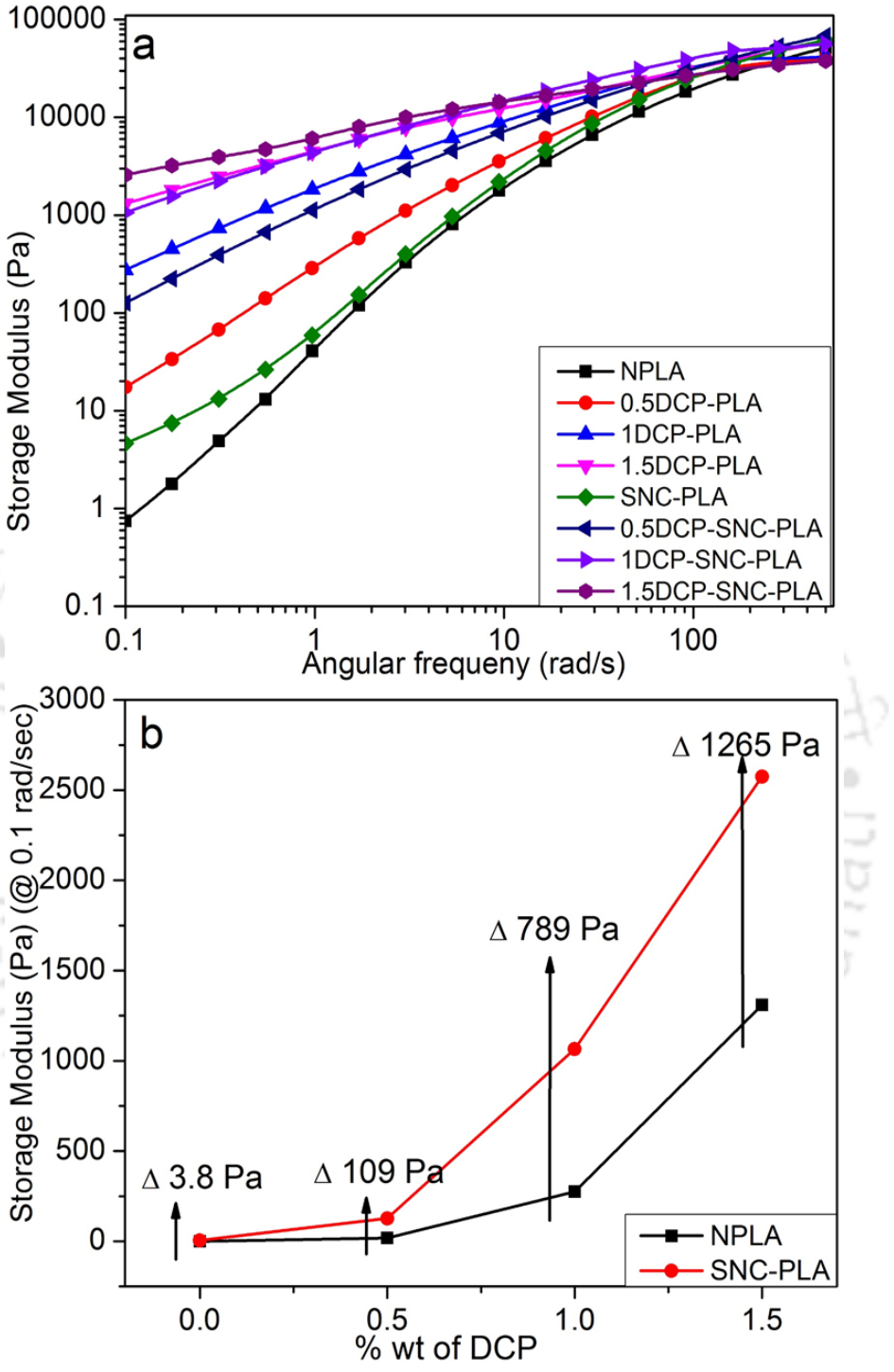

Figure 6.5. The effect of angular frequency and DCP content on the storage and loss modulus of NPLA and SNC-PLA.

Reactive extrusion induced macromolecular chain modification can be further explained by using the cross over frequencies of storage and loss modulus, terminal region properties (the slope storage and loss modulus) and the slope of storage vs loss modulus graph (Han plot). As already discussed in literature, this transition point is strongly affected by the macromolecular topology of polymer melt. The presence of long chain branching, linear chain extension and crosslinking or any kind of network formation (network formation due to grafting) provides the ability to absorb energy and relax slowly, which leads to higher relaxation time.

Table 6.2. The effect of DCP amount on various rheological properties of NPLA and SNC-PLA.

Samples	Crossover values			Terminal region		Han plot	
	ω c (rad/s)	G'=G" (Pa)	η* (Pa.s)	G'~ω^x	G"~ω^y	slope	R^2
NPLA	123	22695	262	1.76	0.95	1.83	0.999
0.5DCP-PLA	119	28602	340	1.19	0.76	1.40	0.999
1DCP-PLA	21	14216	955	0.76	0.59	1.28	0.999
1.5DCP-PLA	0.1	1413	17509	0.50	0.41	1.20	0.998
SNC-PLA	116	28619	296	1.40	0.95	1.65	0.998
0.5DCP-SNC-PLA	58	22842	561	0.88	0.68	1.35	0.998
1DCP-SNC-PLA	1.4	5324	5462	0.57	0.46	1.24	0.998
1.5DCP-SNC-PLA	<0.1	-	-	0.39	0.36	1.10	0.996

As illustrated in **Table 6.2**, it can be noted that the cross over frequency decreases with increasing DCP wt. % for both NPLA and SNC-PLA. The reactive extrusion in the presence of SNC decrease the cross over frequency values from 123 to 116, 119 to 58, 21 to 1.4 and 0.11 to < 0.1 rad/sec of NPLA to SNC PLA at the DCP amount of 0, 0.5, 1 and 1.5 wt. %

respectively. The impact of SNC grafting can be easily observed from the significant reduction of cross over points that define the transition of solid like behavior of the melt into the liquid like behavior. This improvement is more prominent as DCP wt. % increases which is due to the increment in grafting efficiency with DCP content.

Interestingly, no significant change is observed at higher frequency of storage and loss modulus values, which indicate that the short range dynamics of the polymeric melt are not get affected by the chain modification. However, at low frequencies both properties decrease monotonically and the terminal characteristics are observed to deviate from the regular linear polymer power law relationship of ($G'(\omega) \alpha \omega^2$) and ($G''(\omega) \alpha \omega$) for both reactively modified NPLA and SNC-PLA. It has been found that for polymeric melt in which the solid like behavior is becoming more and more prominent, the respective G' and G" modulus dependency on the power of lower frequencies will significantly diminish from 1 and 2 to lower values respectively. Reactive modification of PLA in presence of DCP which can form active radicals leads to the formation of more networked melt having solid like behavior. This phenomenon is related with polymer to polymer interaction due to long chain branching and crosslinking. Note that in **Table 6.2**, the terminal region G' and G" dependency on frequencies are further diminished in the presence of SNCs as compared to NPLA at all DCP contents similar to the above observation which is indicative of intense grafting characteristic. Similar observation can also be drawn from the Han plot shown in **Fig. 6.6** (the slope of log G' vs log G") which provides information about the dependency of the elasticity on loss properties. As illustrated in **Table 6.2,** the slope of the reactively extruded NPLA samples is observed to decrease from 1.83 of NPLA (without DCP) to 1.40, 1.28 and 1.20 of 0.5, 1 and 1.5 wt. % DCP respectively. As expected, the introduction of SNC further decreases the slope at the respective DCP

amount. This result strongly supports the SNC grafting on PLA which is the reason for the melt to have more solid like behaviour at higher temperature.

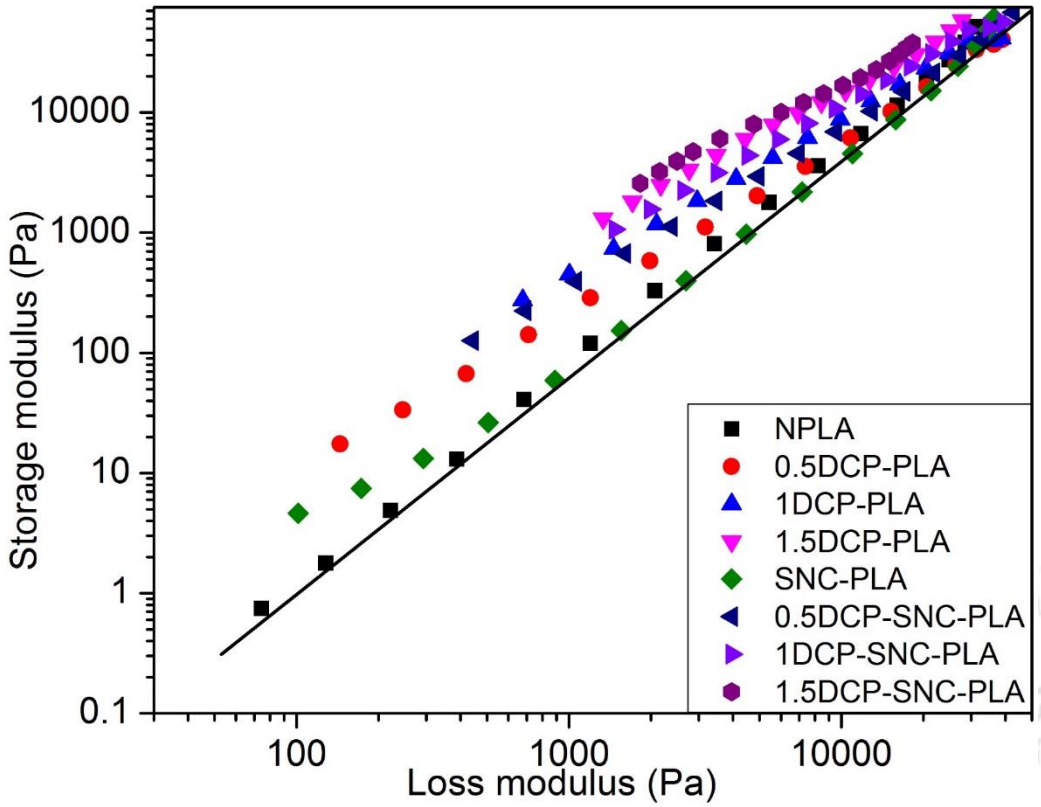

Figure 6.6. Han plots of NPLA and SNC-PLA at different concentrations of DCP.

Similar observation can also be generated using Cole-Cole plot, which relates with the molecular weight and its distribution. As shown in **Fig. 6.7,** the semicircle curve is becoming larger and wider with increasing DCP wt. % fraction and with the addition of SNC. This clearly indicates the long chain branching, crosslinking and grafting which is already observed through molecular weight analysis using GPC. All these important observations are an indication for the improvement of the melt strength of PLA due to reactive modification where SNC plays a major role to give remarkable rheological properties.

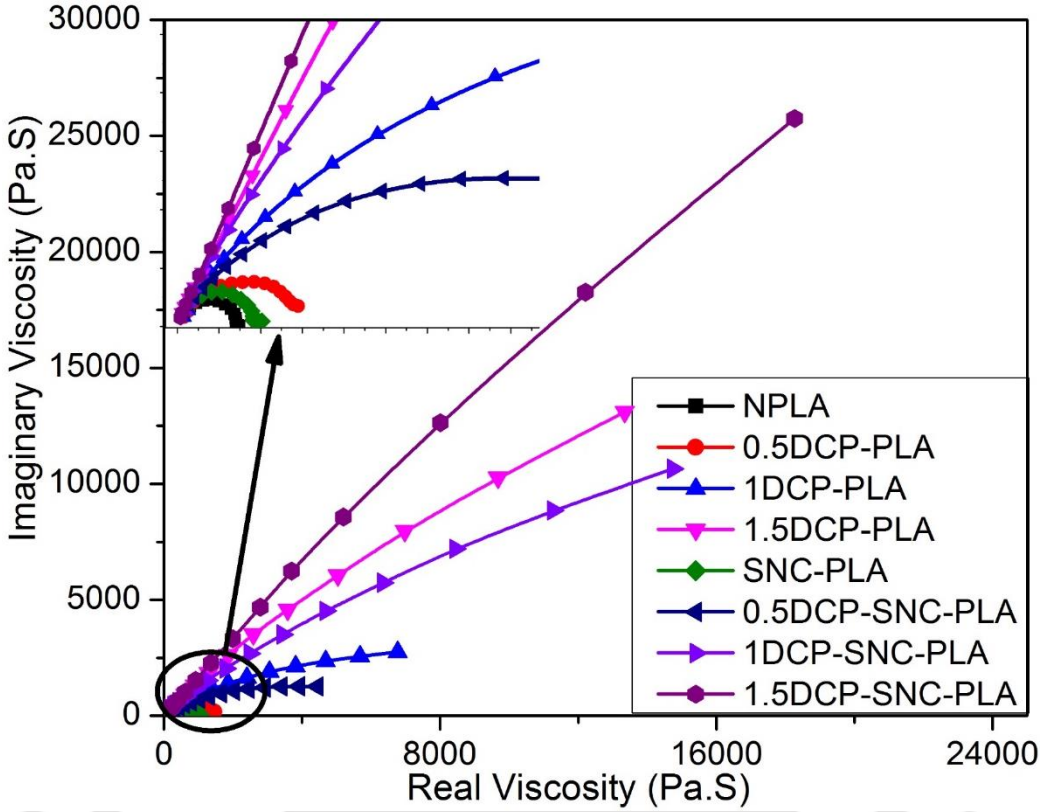

Figure 6.7. Cole-Cole plots of NPLA and SNC-PLA at different concentrations of DCP.

Van Gurp plot (vGP) (phase angle vs log G*) has been used as a tool to understand the impact of long chain branching on the mobility of polymers in melt condition. **Fig. 6.8** shows shifting of phase angle into lower values for modified sample with increasing DCP wt. %. The grafting phenomenon observed in reactively modified SNC-PLA reduces the phase angle as compared to reactively modified NPLA. Since more solid like property is introduced into the PLA matrix because of the grafting of thermally stable and highly crystalline SNC, it limits the macromolecular movement in PLA melt, which in turn leads to the reduction of phase angle (δ).

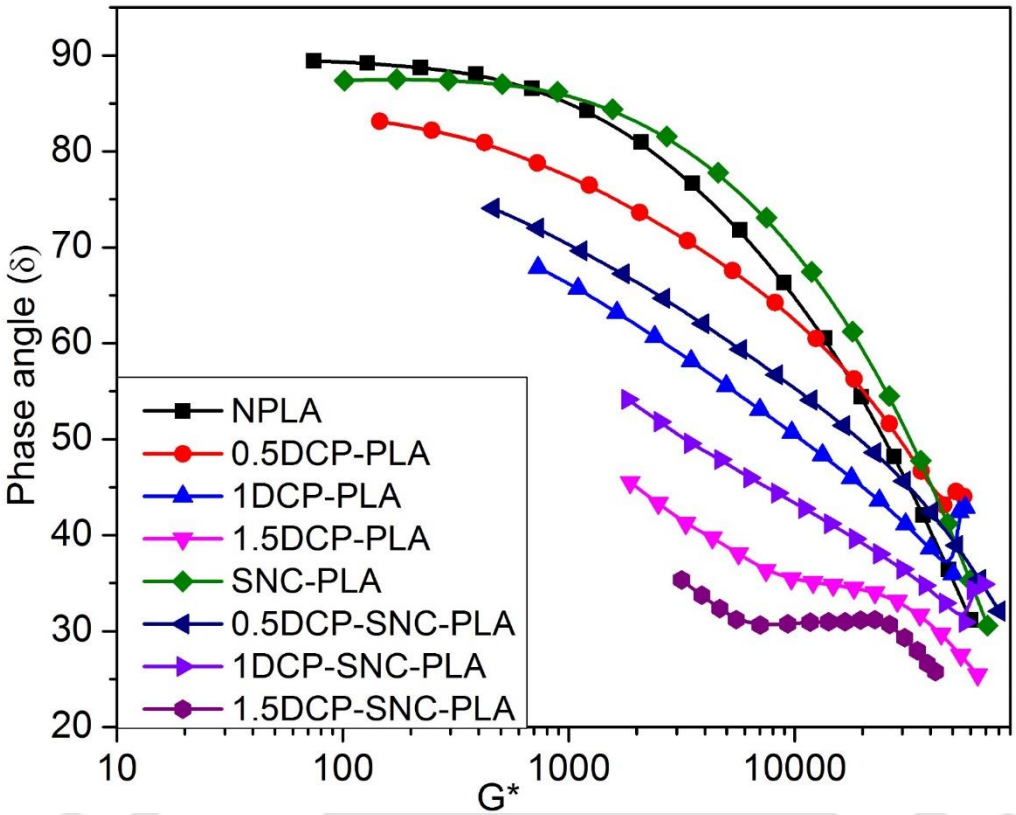

Figure 6.8. The VGP plots of NPLA and SNC-PLA at various DCP content.

Investigation of the rheological properties of modified samples is very complicated and it needs to be correlated with other characterization techniques. Predicting the macromolecular structural change is a challenging task since many simultaneous reactions take place which give different macromolecular melt topology. Due to this fact, limitation arises to fit the rheological data to numerous rheological models in order obtain insights about the relaxation process. Considering this, Carreau-Yasuda model **(eqn. 6.2)** is used to fit the melt rheology data and provide macromolecular chain relaxation phenomena through estimation of characteristic relaxation time (λ), zero shear viscosity (η_0), the Newtonian transition factor (a) and power low index (n).

$$\eta(\omega) = \eta_0[1 + (\lambda.\omega)^a]^{\frac{n-1}{a}} \quad 6.2$$

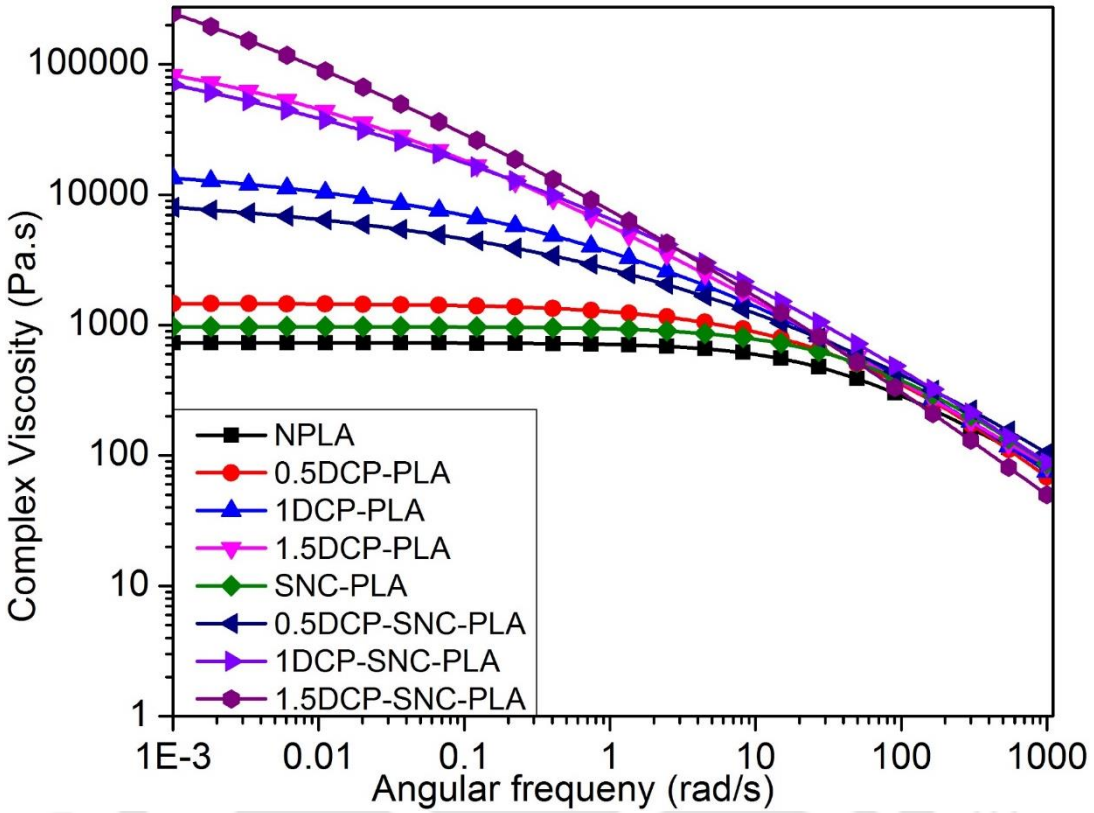

Figure 6.9. Carreau Yasuda model fitting for the complex viscosity data of NPLA and SNC-PLA at various wt.% of DCP.

As illustrated in **Fig. 6.9** with the values listed in **Table 6.3**, the zero shear viscosity (η_0) significantly increases from 730 Pa.s (NPLA) by a factor of 2, 25 and 225 for DCP wt. % fraction of 0.5, 1 and 1.5 respectively. As compared to NPLA, the change further increased by the factor of 1.6, 15, 40 and 1012 at DCP wt. % of 0, 0.5, 1 and 1.5 for reactively SNC-PLA system. As already discussed above, enhancement in the molecular weight through chain extension, long chain branching, crosslinking with significant grafting can be mentioned as a reason for the observed significant increase in zero shear viscosity. Due to the same reason the

modified samples take relatively longer relaxation time and characteristic relaxation time (λ) of NPLA increases from 0.032 s to 94 s for modified NPLA (1.5% DCP) and 35 s for modified SNC-PLA (1.5% DCP)and.

Table 6.3. Carreau-Yasuda model fitting parameters for NPLA and SNC-PLA at various % wt. fraction of DCP.

Samples	η_0	λ	a	n
NPLA	730.66	0.032013	0.9445	0.3689
0.5DCP-PLA	1468.1	0.015565	0.5826	0.0001
1DCP-PLA	18530	0.086437	0.2608	0.0001
1.5DCP-SCN-PLA	164320	94.908	0.3500	0.0001
SNC-PLA	1232.4	0.03952	1.3711	0.3767
0.5DCP-SNC-PLA	11009	0.018595	0.2350	0.0001
1DCP-SNC-PLA	29636	0.64697	0.1721	0.0001
1.5DCP-SNC-PLA	739440	35.671	0.1424	0.0001

The weighted relaxation spectrum (λH(λ)) which is estimated from linear relaxation spectrum as proposed by Honerkamp and Weese can be used to understand the time distribution of the chain relaxation mechanism. The relaxation process of unmodified, modified NPLA and SNC-PLA samples are displayed in **Fig. 6.10 (a-d)** and the chain relaxation process is further presented at various range of relaxation time (0.001 to 1 and 0.001 to 100), for better insight.

As indicated in **Fig. 6.10 (a),** NPLA is observed to have one relaxation peak at λ~0.05 s, which indicates the linear polymer chain relaxation. Due to the possible long chain grafting of PLA chains on the active surface of SNCs, second melt relaxation is observed at λ~230 s other than the linear polymer chain relaxation peak at λ~0.05 s.

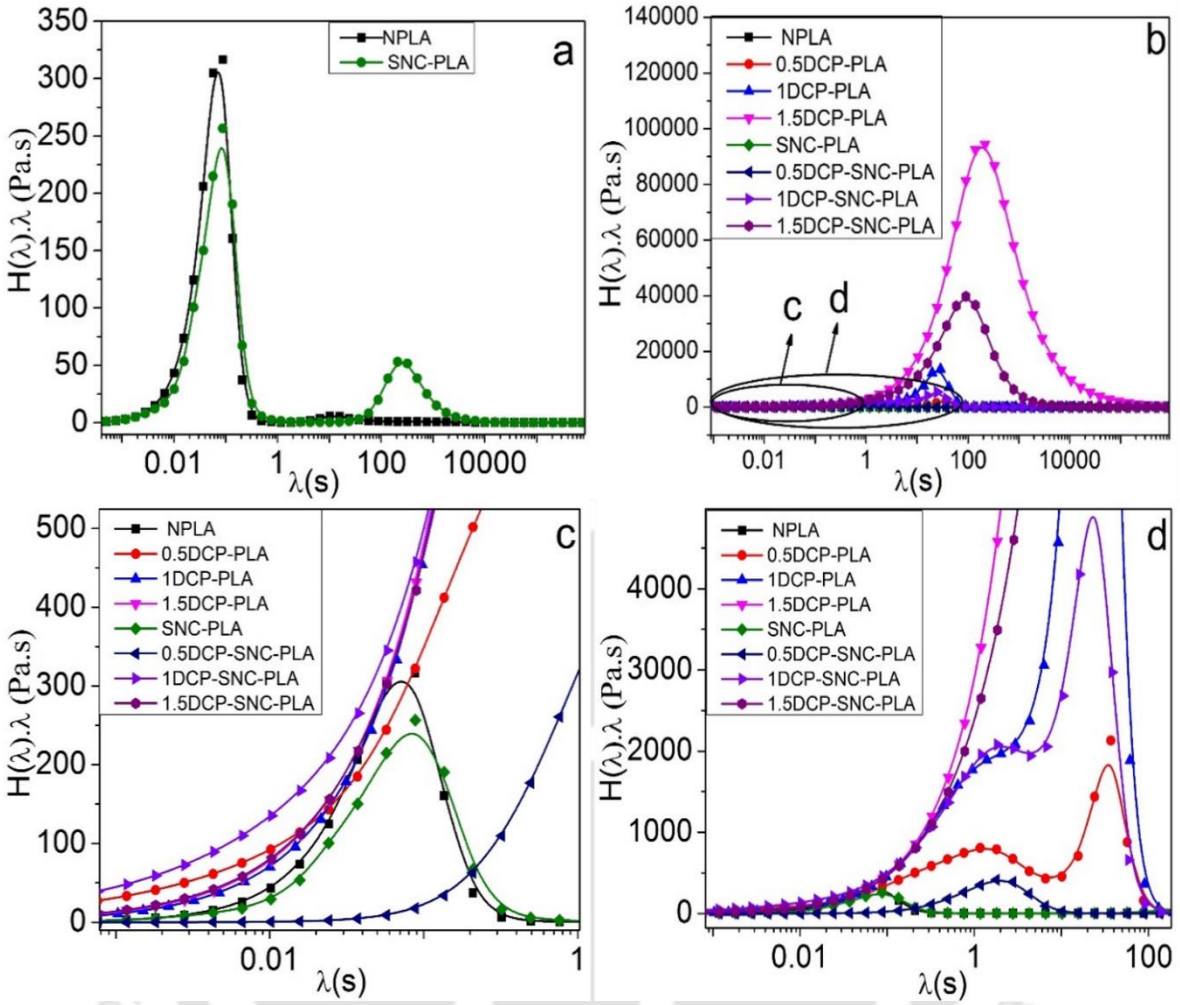

Figure 6.10. Relaxation spectrum of NPLA and SNC-PLA at different wt.%. fraction of DCP.

In a **Fig. 6.10 (b, c and d),** the polymer macromolecular chain structure in molten state is completely modified after loading of DCP. Long chain branching and crosslinking can be confirmed from the longer time relaxation peak, which is noticed to increase with increasing DCP wt. %. The increase in the entanglement of the chains due to reactive modification of

polymer melt can also be mentioned as one of the reason for the observed significant change in the relaxation process.

6.2.3. Crystallization, melting behavior and thermal stability

PLA is known to have slow crystallization behavior due to which it is difficult to crystallize even at low cooling rate. The melting and crystallization characteristics of polymer matrix are strongly influenced by the chain topology. Because of this, it is required to summarize and categorize the chain topology induced by the reactive extrusion before explaining the thermal characteristics of reactively modified sample. Based on the above obtained results, the macromolecular chain modification is grouped into three scenarios to simplify the explanation. **Scenario 1** short and long chain branching (0.5DCP-PLA). **Scenario 2** crosslinking and branching (1DCP-PLA and 1.5DCP-PLA). **Scenario 3** grafting (in all DCP-SNC-PLA). The effect of reactive chain topology modification on the DSC thermographs of cooling and 2nd heating is displayed in **Fig. 6.11** and the values of glass temperature (T_g), onset crystallization temperature ($T_{c,\,onset}$) and maximum cold crystallization temperature ($T_{c,}$), onset and maximum melting temperature ($T_{m,\,onset,}$ $T_{m,\,max}$) and enthalpies of crystallization and melting are listed in **Table 6.4.** In all scenarios, no significant change is observed on T_g values. Melt extruded PLA at high temperature and shear is known for melt recrystallization process and produces defect or imperfect crystals which melt in two stages. If lower molecular weight fraction is increased, the melt recrystallization phenomenon can occur relatively at lower temperature because of the short chains that are easily rearranged to recrystallize at a lower temperature. On the other hand, the melt crystallization process can occur at lower temperature due to the effect of nucleating agent present in the polymer matrix. However, the reduction observed in cold crystallization temperature (T_{cc}) by 3 ºC (**scenario 1**) as compared to NPLA (T_{cc} ~ 115

ºC) can be related to the increment in the free volume by the short chain branching which leads to the formation of unstable crystals thereby increasing the chain mobility that gives double melting peak that shifts at a lower temperature as compared to NPLA. This phenomenon is briefly explained by **Bian et al.,** for reactively extruded short chain branched poly (3-hydoxybutyrate-co-4-hydroxybutyrate) [203].

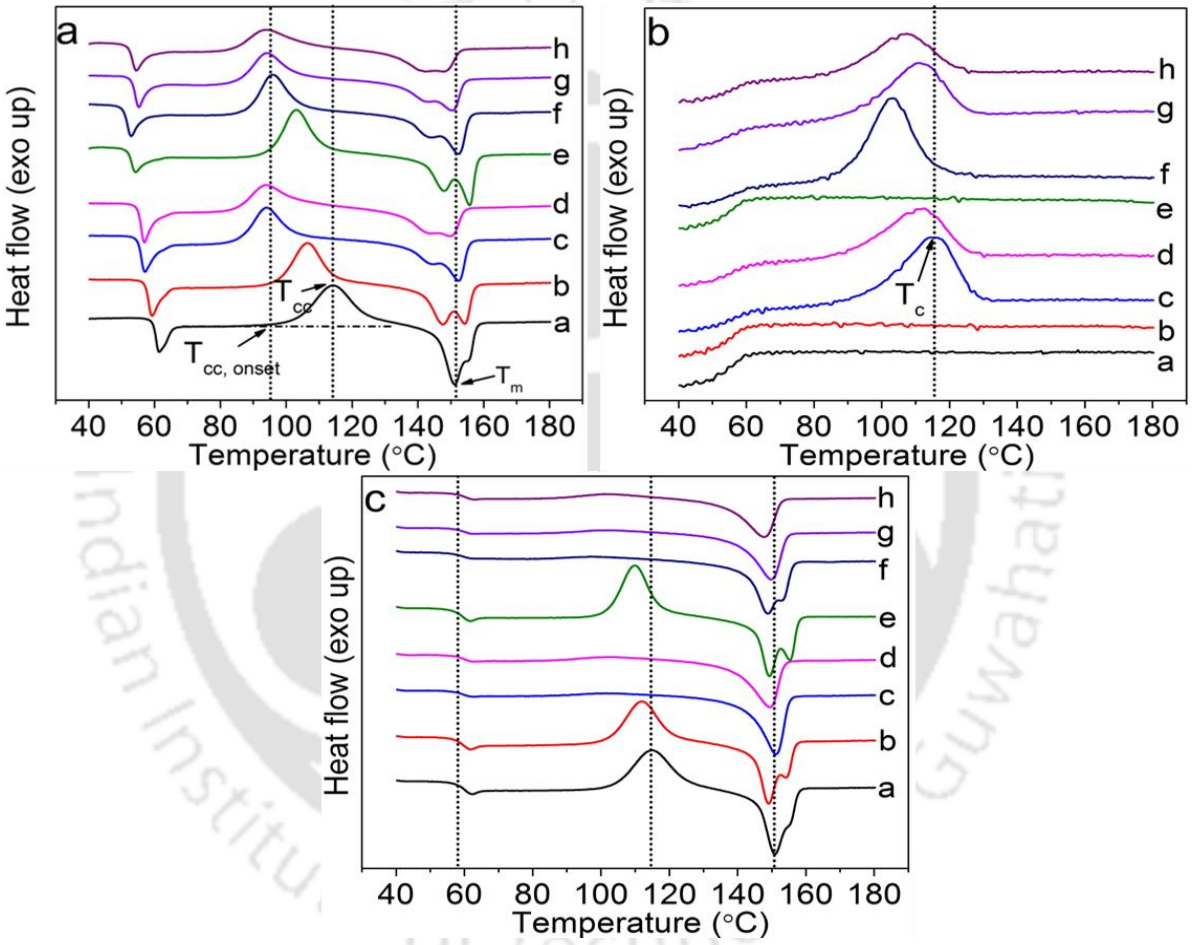

Figure 6.11. DSC thermograms of (a) cooling and (b) 2nd heating of NPLA and SNC-PLA at various wt.% fraction of DCP. a: NPLA, b: 0.5DCP-PLA c: 1DCP-PLA d: 1.5DCP-PLA, e: SNC-PLA, f: 0.5DCP-SNC-PLA, g: 1DCP-SNC-PLA and 1.5DCP-SNC-PLA.

The melt crystallization phenomenon of NPLA did not get affected by the reactive modification at lower DCP content (0.5 wt. %) and no crystallization peak is observed during cooling, that indicates the slow crystallization process in which the cooling rate (5 ºC/min) is too fast for the nucleation and growth of crystals as shown in **Fig.6.11**. On the other hand, the slow melt crystallization process of NPLA is significantly enhanced for **scenario 2** (1DCP-PLA and 1.5DCP-PLA) with small fraction of melt recrystallization which can be strongly related to the crosslinking and branching as shown by gel percentage and other rheological results. Interestingly, the percentage crystallization is increased from 1 % (0.5DCP-PLA) to 22 % (1DCP-PLA) and decreased to 17 % (1.5DCP-PLA). This crystallization behavior can be explained as: the rate of crystallization increased significantly as the macromolecular chain topology is changed from short chain branching into crosslinking with lower gel percentage (low crosslinking fraction). Further, the increase in crosslinking fraction hinders the chain rearrangement due to intense entanglement which results reduction in crystallization rate. As clearly shown in **Fig. 6.11 (b)** the double melting peaks observed for NPLA and 0.5DCP-PLA merged into one for crosslinked and branched samples (1DCP-PLA and 1.5DCP-PLA) which is due to the formation of more stable crystals. As reported in **Table 6.4,** lower T_{cc} (by 5 ºC) and distinguished double melting peaks are observed for SNC-PLA as compared to NPLA which is processed at the same condition. However, in **scenario 3,** unlike 0.5DCP-PLA, the reactive extrusion at lower DCP content (0.5 wt. %) and 1 % SNC changes the melting and crystallization process. The rate of crystallization is enhanced and melt crystallization is observed at the given cooling rate, which is missing in 0.5DCP-PLA. This interesting characteristic can be correlated with the grafting of SNC on PLA chain that provides nucleation site for the melt to arrange in order. The crystallization percentage decreases from 23%

(0.5DCP-SNC-PLA) to 19 % (1DCP-SNC-PLA) and 15% (1.5DCP-SNC-PLA) due to the increase in grafting and crosslinking fractions that leads to the restriction of macromolecular movement in melt (increase in entanglement).

Table 6.4. Calorimetric values of NPLA and SNC-PLA at various wt.%. fraction of DCP (1st heating, cooling and 2nd heating).

Samples	Cooling/ heating	T_g (°C)	$T_{c,onset}$ (°C)	$T_{c,max}$ (°C)	H_c (J/g)	$T_{m,onset}$ (°C)	$T_{m,min}$ (°C)	H_m (J/g)	X_c (%)
NPLA	Cooling	-	-	-	-	-	-	-	
	2nd heating	58	104	115	23	146	151	24	1
0.5DCP-PLA	Cooling	-	-	-	-	-	-	-	
	2nd heating	57	103	112	22	145	149	23	1
1DCP-PLA	Cooling	-	95	115	19	-	-	-	
	2nd heating	58	88	103	3	144	151	23	22
1.5DCP-PLA	Cooling	-	95	112	16	-	-	-	
	2nd heating	57	86	103	4	140	151	20	17
SNC-PLA	Cooling	-	-	-	-	-	-	-	
	2nd heating	58	102	110	23	146	149	24	1
0.5DCP-SNC-PLA	Cooling	-	92	103	20	-	-	-	
	2nd heating	58	85	98	3	144	150	24	23
1DCP-SNC-PLA	Cooling	-	92	116	17	-	-	-	
	2nd heating	58	86	100	3	143	150	21	19
1.5DCP-SNC-PLA	Cooling	-	91	107	13	-	-	-	
	2nd heating	58	88	101	4	140	148	18	15

The double melting peak observed at 0.5DCP-SNC-PLA is merged into one at 1 wt. % and 1.5 wt. % DCP. As already discussed above, the double melting peak occurred because of the melt recrystallization due to the short chain branching which further improves and forms stable crystals with increasing grafting efficiency and crosslinking.

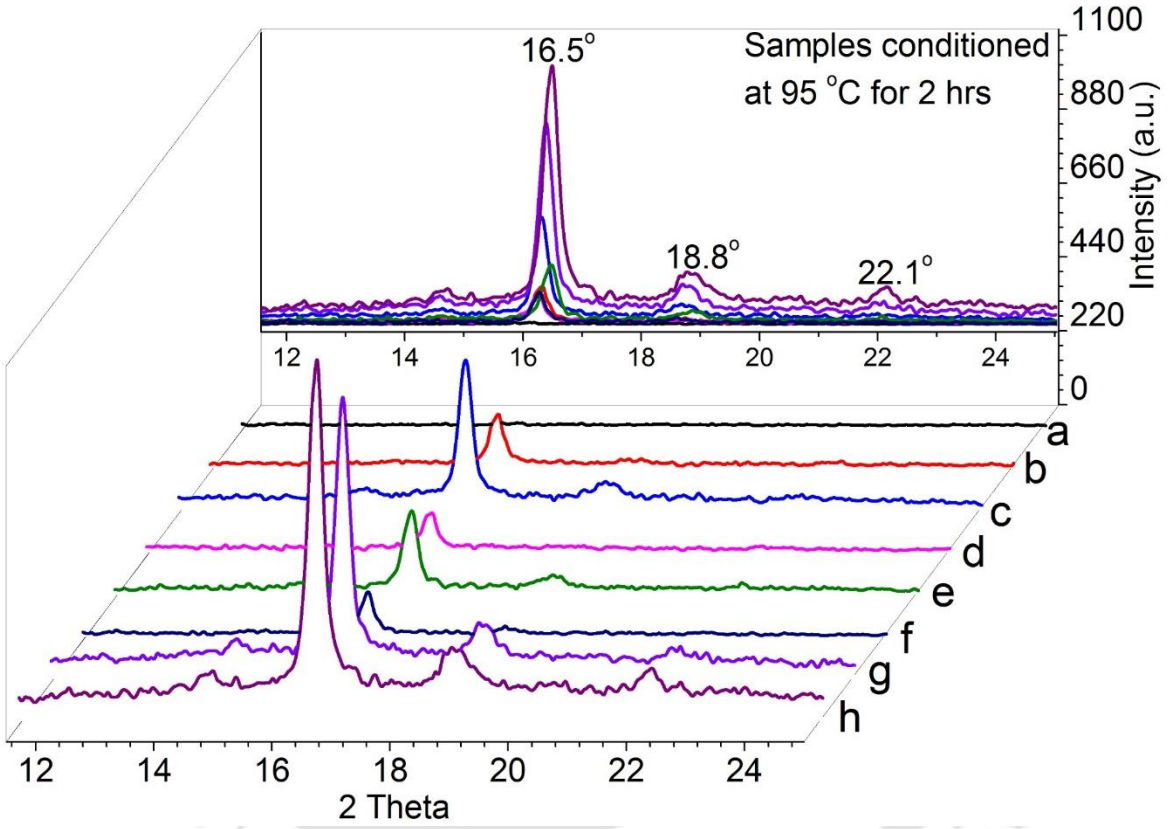

Figure 6.12. Crystallographic orientation of reactively modified samples conditioned at 95 ºC.

Prior to XRD analysis, reactively extruded samples are kept in vacuum oven at 95 ºC for 2 hours. The onset temperature for cold crystallization (95 ºC) process of PLA obtained from the first heating cycle is taken as reference point. The representative peak observed at 16.5º and 18.8º on the XRD diffractogram is representing the α-form of PLA crystals having crystalline

plane of 011 and 110/200 respectively [40]. As clearly indicated in **Fig. 12,** the crystallinity of NPLA is improved by the addition of SNC and further by the reactive extrusion. No intense peak is observed for neat PLA whereas addition of DCP improves the crystallization process which can be confirmed by the intense peak at 16.5º. Maximum intensity is revealed at 1 wt. % DCP for the case of NPLA and decreases with increasing the DCP contents to 1.5 wt. %, indicating the fraction of crosslinking site up to some extent can be used as a nucleation site to rearrange the macromolecules, in which further crosslinking may lead to restriction of the macromolecular chain rearrangement and in turn tend to hide the crystallization process. However, the intensity at 16.5º is observed to increase with increasing DCP content for the case of SNC-PLA system. This shows, the crystallization process is highly influenced by grafting of SNCs, in which the macromolecular arrangement of PLA chains is directed by highly ordered SNC β-sheets.

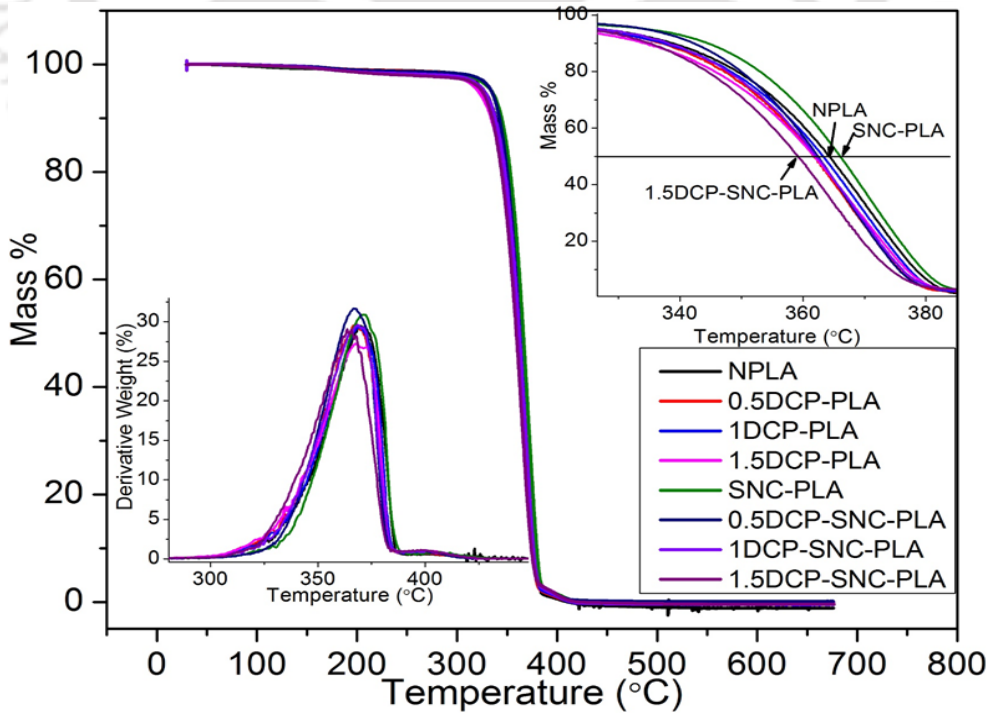

Figure 6.13. Thermogravimetric analysis (TGA) of NPLA and SNC-PLA at various wt.% of DCP.

Fig. 6.13 illustrates the effect of reactive modification on the thermal stability of NPLA and SNC-PLA nanocomposite with their values listed in **Table 6.5**. SNC-PLA (without the addition of DCP) exhibits the highest thermal stability, in which $T_{5\%}$ ~334 ºC is observed to be 10 ºC, which is superior to NPLA. It confirms that, the incorporation of SNC alone can enhance the thermal stability of PLA. Stabilizing effect of SNC has already been studied in our previous investigations for PLA system under multiple extrusion [200].

Table 6.5. The impact of reactive modification on the thermal stability NPLA and SNC-PLA.

Samples	$T_{5\%}$ ºC	$T_{95\%}$ ºC	T_{max} ºC
NPLA	326	381	371
0.5DCP-PLA	325	379	368
1DCP-PLA	325	380	369
1.5DCP-PLA	322	380	363
SNC-PLA	335	382	371
0.5DCP-SNC-PLA	328	379	368
1DCP-SNC-PLA	327	380	369
1.5DCP-SNC-PLA	325	378	363

A slight reduction in $T_{5\%}$ is observed with addition of DCP and reaches ~322 ºC for 1.5DCP-PLA. Relatively higher values of $T_{5\%}$ are obtained for SNC-PLA as compared to NPLA at all DCP wt.%fractions. No significant change is observed for $T_{95\%}$. However, T_{max} is found to reduce from ~371 ºC (NPLA and SNC-PLA) to ~363 ºC (1.5DCP-PLA and 1.5DCP-SNC-

PLA). Decomposition process of the polymeric system is facilitated when the number of shorter chains are increasing. The broadening in MWD (increasing in PDI) with increasing DCP wt.% cloud be the reason for the lowering of thermal stability at the decomposing temperature.

The physical appearance of neat PLA, SNC-PLA and the SNC grafted PLA samples at different DCP content are displayed in **Fig. 6.14 (a),** the transparency of the film is decreased with increasing of DCP % wt.

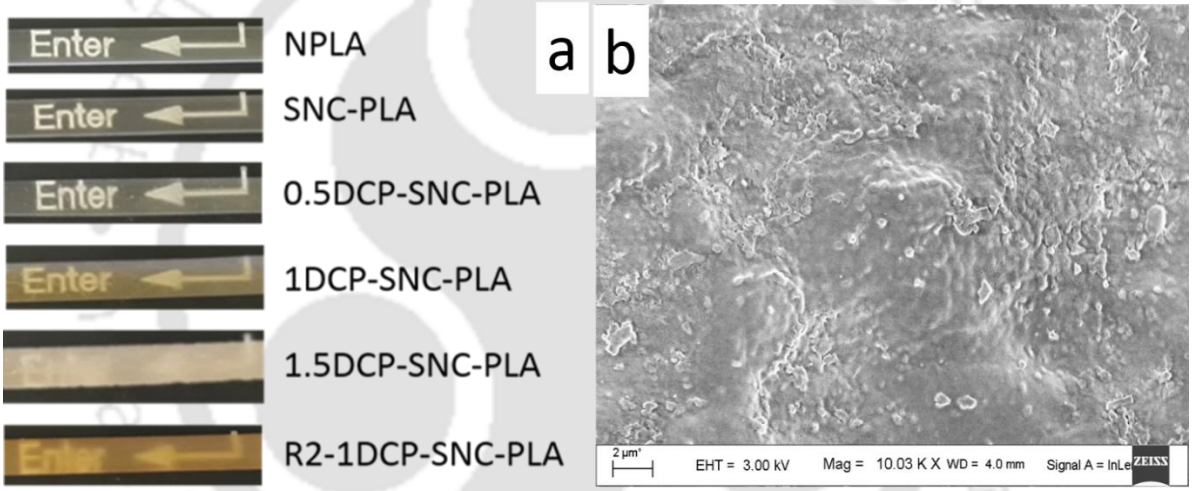

Figure 6.14. Melt extruded (a) PLA strips, and (b) reactively modified SNC PLA at 1 wt. % DCP.

As discussed above, the reactive extrusion in presence of SNC provides significant grafting opportunity for the PLA macromolecules on the surface of SNC, which is an instantaneous process that improves the crystallinity. Transparency of the polymer film tends to decrease with increasing crystallinity and crosslinking. Furthermore, SNC is encapsulated inside PLA matrix due to grafting and micro-gel structure is observed on the morphology of the reactively extruded SNC-PLA (**Fig. 6.14 (b)).** From this, it can be concluded that, the interfacial

compatibility between PLA and SNC is improved and the grafting structure increases the dispersion and forms more crosslinking networks.

6.2.4. The effect of reactive modification on recyclability performance of PLA

The influence of reactive extrusion on the reprocessability performance (up to 3 cycles) of NPLA, 1DCP-PLA, SNC-PLA and 1DCP-SNC-PLA are studied. Zero shear viscosity, crossover points and ratio of zero shear viscosity R_i ('i' represent reprocessing cyles) ($\eta_0 R$) to NPLA ($\eta_0 V$) of R_0 and R_3 are used to evaluate the macromolecular change induced by reprocessing cycles.

Table 6.6. The effect of processing cycles on the rheological properties.

	Zero shear viscosity		**Crossover frequency**		**$\eta_0 R/ \eta_0 V$**	
	R0	R3	R0	R3	R0	R3
GPLA	1767	-	79	-	1	-
NPLA (ext)	744	433	262	>500	0.78	0.61
SNC-PLA	1232	702	116	338	0.9	0.76
1DCP-PLA	7310	2397	21.1	67	1.52	1.09
1DCP-SNC-PLA	18186	4698	1.4	15.2	1.98	1.33

As observed in **Table 6.6** the zero shear viscosity of reactively modified samples drastically reduced after recycling. However, compared to zero shear viscosity of R3-NPLA (433 Pa.s) it is clearly observed that the reprocessed reactive extrusion samples have higher melt strength. Furthermore, the grafting of SNC increases the zero shear viscosity and lower crossover frequency values.

6.3. Summary

Reactively extruded NPLA and SNC-PLA with possible branching/crosslinking and branching chain topologies are prepared successfully and the chemical structure, molar mass distribution rheological characteristics and thermal stability are investigated in detail. Three different scenarios are distinguished: branching (0.5DCP-PLA), crosslinking and branching (1DCP-PLA and 1.5DCP-SNC-PLA) and grafting (DCP-SNC-PLA at 0.5, 1 and 1.5 wt. % of DCP). These three scenarios give different level of impact on the important characterized properties. Bond formation between SNC (serine $–CH_2OH$) and PLA main backbone carbon identified by ^{1}HNMR confirm the grafting of SNC. The increasing in higher molecular weight fraction observed on the molecular weight analysis provides vital information about the impact of SNC grafting. Furthermore, all the rheological properties (i.e zero shear viscosity, storage modulus, crossover frequency) are found to significantly improve with the grafting and it increased the reprocessability performance of PLA. The melting and crystallization phenomenon of PLA also completely changed with crosslinking and SNC grafting. Crystallinity percentage improved and PLA is observed to crystalize during cooling with crosslinking and SNC grafting. From this study it can be concluded that the reactive extrusion of PLA in presence of SNC leads to the grafting topology with improved melt strength and other essential properties.

Chapter 7

Recycling of Melt Extruded PLA Film and Low Molecular weight Oligomer for Targeted Application in Biolubricants and biodiesel

In this chapter, two recycling alternatives are introduced for the first time to recycle melt processed PLA and lower molecular weight oligomers. The first part covers the dissolution of melt processed PLA in lactic acid/water mixture followed by blending with well-known biolubricant (soybean oil) to be tested as a biolubricant. Dynamic viscosity and viscosity-temperature dependency of the blend are investigated at temperature of 25 ºC, 40 ºC, 60 ºC, 80 ºC and 100 ºC. The second part covers the recycling of lower molecular weight PLA (oligomer) into biodiesel additives. Four different molecular weight oligomers (500, 1000, 1500 and 2000 Da) are synthesized using microwave reactor and dissolved in soybean oil based methyl ester in different composition (3, 5, 10 and 25 g/L). The impact of PLA-oligomer on the cold flow properties (cloud point, pour point and dynamic viscosity) are investigated by ASTM standard method, rheometer and optical polarimetry. Furthermore, the engine performance and exhaust gas analysis are tested using Kirloskar TV-1 engine.

Parts of this chapter are published/ready to communicate as:

Melakuu Tesfaye and Vimal Katiyar, "Microwave assisted synthesis of biodiesel from soybean oil: Effect of poly (lactic acid)-oligomer on cold flow properties, IC engine performance and emission characteristics." Fuel, 170,107–114 (2016)

Melakuu Tesfaye, Vimal Katiyar, Alternative Recycling of Poly (lactic Acid) as Biolubricant Additive (ready to communicate)

7.1. Introduction

The growing interest towards substituting conventional polymers with biodegradable polymers is leading to the increase in the production capacity of biodegradable plastics worldwide [204]. In this category, PLA [45] is one of the synthetic biodegradable polymers which has been extensively studied to replace petroleum based polymers [42]. Because of the growing demand, the global PLA market is increasing each year [205]. This compostable and ecofriendly polymer is extensively used in food packaging and other commodity products [206]. Although PLA is biodegradable, it is essential to explore its recycling ability so as to achieve a lower carbon footprint and reduce the price. Recycling can ensure the utilization of the polymer by creating the shortest processing loop to generate the raw material with minimized energy [207]. Depolymerization of PLA is one of the best technique used to recover monomer which can be re-polymerized having short chain PLA oligomers as a byproduct, which may not be recycled back [53, 208, 209].

Recently, the use of plant based oils and their methyl ester (biodiesel) as a solvent to dissolve waste polymers for the special benefits to improve the lubrication properties of the base oil and increase calorific value of methyl esters, has become a common approach [210].

Viscosity is the most essential property of lubricants and need to be maintained within the required range for a particular application in order to achieve proper boundary regime film thickness. Maintaining the proper boundary regime film thickness is essential to avoid failure due to friction and wear at low viscosity and to minimize the energy required to start any

movement at high viscosity. Viscosity index is an important parameter used to classify lubricants which is defined as the temperature dependency of the viscosity of lubricants. Vegetable oils are promising candidates to formulate biodegradable nontoxic and environment friendly biolubricants that can substitute petroleum based lubricants and mineral oils. However, the viscosity, viscosity index and oxidative stability of vegetable oils need to be improved. Different polymers such as polypropylene (PP), poly (methyl methacrylate) (PMMA), ultra-high molecular weight polyethylene (UHMWPE), polytetrafluoroethylene (PTFE), polyacrylate copolymers, recycled low density polyethylene (LDPE) and ethyl vinyl acetate (EVA), have been studied to enhance the rheological properties.

Polymers are also used as an additive to solve the performance limitations related to biodiesel. The main challenge in using biodiesel as a fuel in diesel engine is its poor cold flow properties[211] and high viscosity [212]. The presence of higher amount of saturated fatty acids cause thickening of biodiesel at low temperature and leads to fuel starvation followed by clogging of fuel lines and filters [213-215]. Additionally, the degree of conversion (presence of unconverted oil) plays a major role on flow properties of biodiesel. The rate of growth and agglomeration of wax crystals increase when the temperature falls down to its cloud point (CP)[215]. Higher viscosity of biodiesel affects spray atomization process during the time of injection which influences the combustion process [216]. Further, it has been indicated that biodiesel blend with diesel (B20) can provide an improvement in thermal brake efficiency and specific fuel consumption [217].

Different studies have been reported towards improvement in the cold flow properties of biodiesel by blending it with solvents [218], petrol diesel [219, 220], surfactants [221] and using polymeric additives [222]. Polymeric additives as cold flow enhancers are widely used

and a number of polymeric additives are already commercialized [223]. Olefin-ester copolymer (OECP), ethylene vinyl acetate copolymer (EACP) and polymethyl acrylate (PMA) [224-226] are some of polymeric additives which are commercially available. **Wang et al.,** have reported the reduction in pour point ~8^{o}C by addition of only 0.04 wt. % PMA in waste cooking oil based biodiesel [222].

The current investigation has successfully demonstrated for first time, the use of melt processed PLA and low molecular weight oligomer [OLLA] to formulate biolubricate and effective additive for cold flow improvement in biodiesel.

Theory: The estimation of flow activation energy is an essential parameter in analyzing the viscosity dependency of the formulated biolubricant which indirectly predicts the viscosity index. Furthermore, it can also estimate the lower temperature at which transition point for the flow characteristics takes place. The activation energy for flow is calculated from Arrhenius equation.

$$\eta = Ae^{\Delta E\eta/RT} \quad 7.1$$

The natural logarithm of the **Eqn. 7.1** gives

$$ln\eta = \frac{\Delta E\eta}{R}\left(\frac{1}{T}\right) + lnA2 \quad 7.2$$

Where η is dynamic viscosity (mPa.s) which is obtained from viscosity analysis, A is pre-exponential factor (mPa.s), T is absolute temperature in K, R is universal gas constant which is 8.3145 J/mol·K and ΔE_η is flow activation energy (J/mol). Flow activation energy are calculated from slope of ln (η) vs 1/T graph.

7.2. Results and Discussion

7.2.1. Dissolution of melt processed PLA using lactic acid/water mixture

Melt extruded PLA is degraded using lactic acid/water mixture (90/10) under a temperature controlled microwave reactor. The degradation reaction is performed at a temperature of 100 ºC with water refluxing. After 1-hour, melt processed PLA is found to be completely dissolved by the reaction mixture and white, one phase viscous liquid is obtained. As indicated on the NMR analysis, the degraded sample is composed of lower molecular weight PLA. The most intense signal observed at 5.24 ppm, 4.36 ppm, 1.49 ppm and 1.25 of ^{1}HNMR spectra of lactic acid degraded PLA (LA-D-PLA) (**Fig. 7.1)** corresponds respectively to the CH (main chain), CH (hydroxyl terminated end chain), CH_3 (main chain) and CH_3 (hydroxyl terminated end chain) [227]. The peak identified at 6.32 ppm and 1.58 ppm confirms the presence of acryl ended, low molecular weight oligomers. From the area of the ratio corresponding to all CH peaks of main chain to total area of hydroxyl terminated CH, the molecular weight of the degraded PLA can be estimated within the range of 500 to 5000 Da.

The spectra shows the mixture of oligomers with different chain length starting from dimer and trimer to higher molecular weight. During the degradation reaction, lactic acid is observed to polymerize and it is confirmed from the disappearance of monomer peak at 4.03 ppm. The degradation is observed to take place through hydrolysis of the main chain by water molecules. In addition to this, OH group of lactic acid acts as an active site for degradation and facilitate hemolysis of the main chain. Simultaneously, polymerization of lactic acid takes place by polycondensation reaction. Therefore, degradation of PLA as well as polymerization of lactic acid takes place at the same time to give one phase viscous liquid. This viscous one phase

liquid is blended with soybean oil in different blending ratios and rheological investigations are performed to understand the lubrication characteristics of the blend.

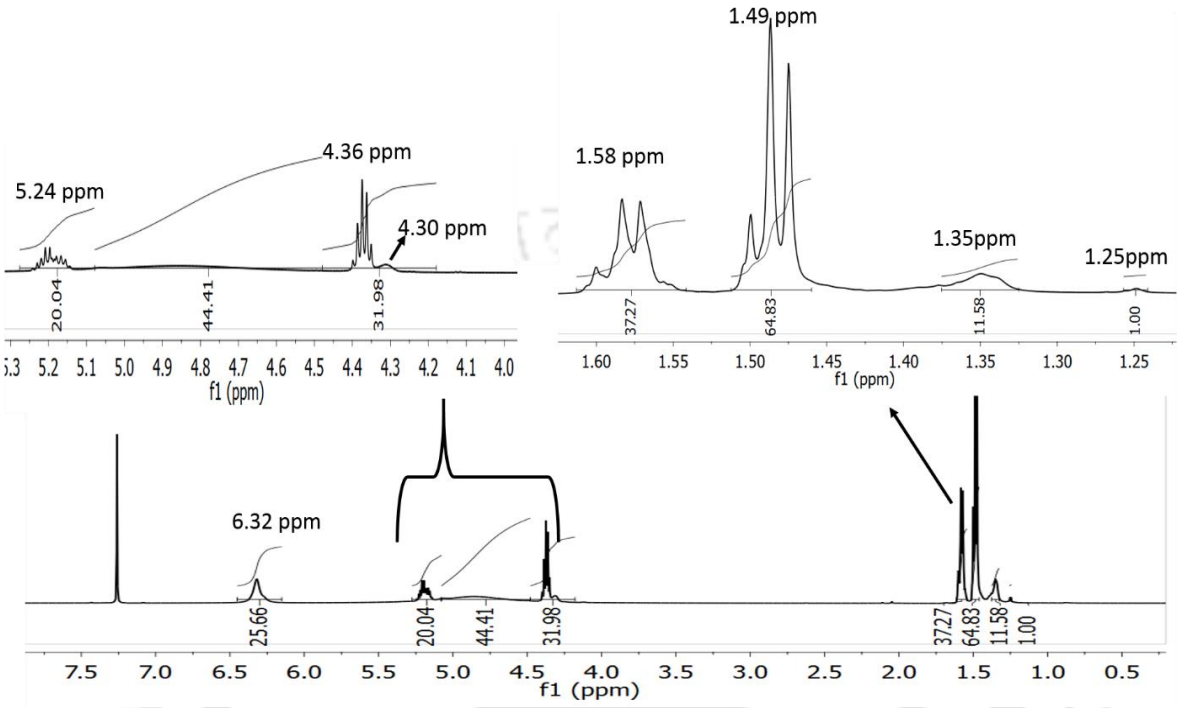

Figure 7.1. NMR spectra of degraded PLA using lactic acid/water mixture.

7.2.1.1. Viscosity: Shear thinning behavior

Shear thinning behavior of lactic acid degraded PLA (LA-D-PLA), soybean oil (SO) and their blends at different proportions is investigated by steady-shear test which is performed at three different temperatures (25, 40, 100 ºC) for shear rate ranging from 0.1 to 100 s^{-1}.

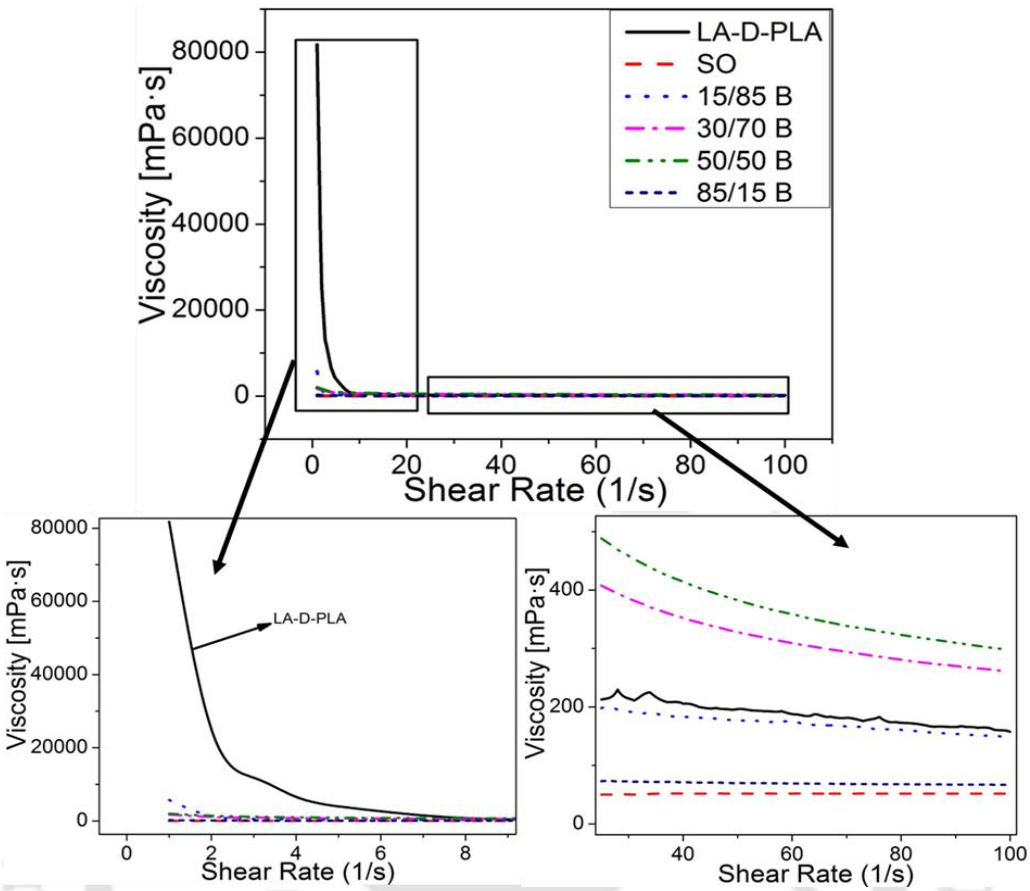

Figure 7.2. Flow behavior of base fluids and their blend at 25 ºC.

Shear thinning behavior is observed for the LA-D-PLA, 15/85 B, 30/70 B and 50/50 B within the range of the applied shear rate. However, the flow characteristics of soybean oil and 85/15 B shows Newtonian behavior. Large viscosity observed for the LA-D-PLA at the starting of the experiment can be mentioned as main drawback to be used as lubricant since it requires higher energy to start the motion.

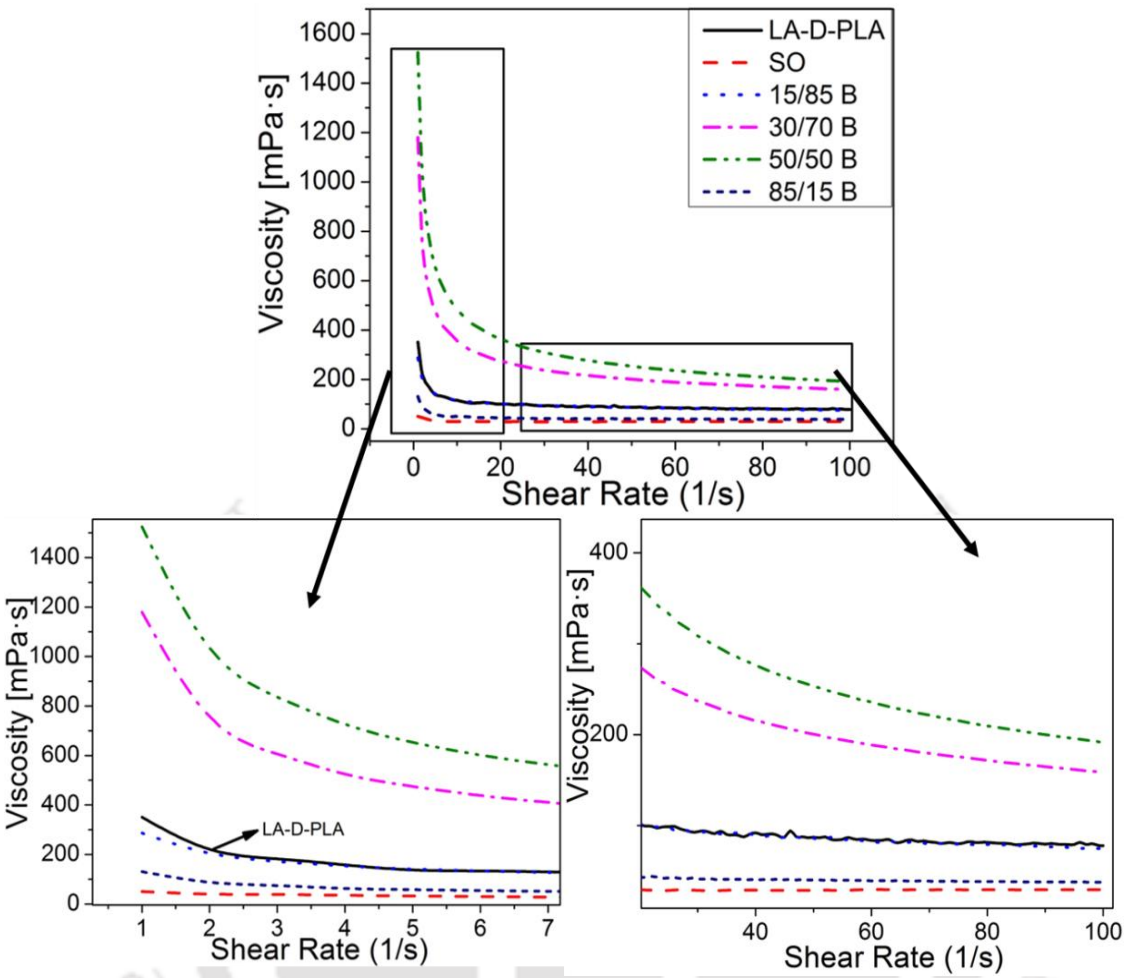

Figure 7.3. Flow behavior of base fluids and their blend at 40 ºC.

The viscosity at lower shear rate is observed to decrease with increasing temperature. Newtonian characteristics observed with increasing the temperature for LA-D-PLA, SO, 85/15B and 15/85B (**Fig. 7.3 and 7.4).**

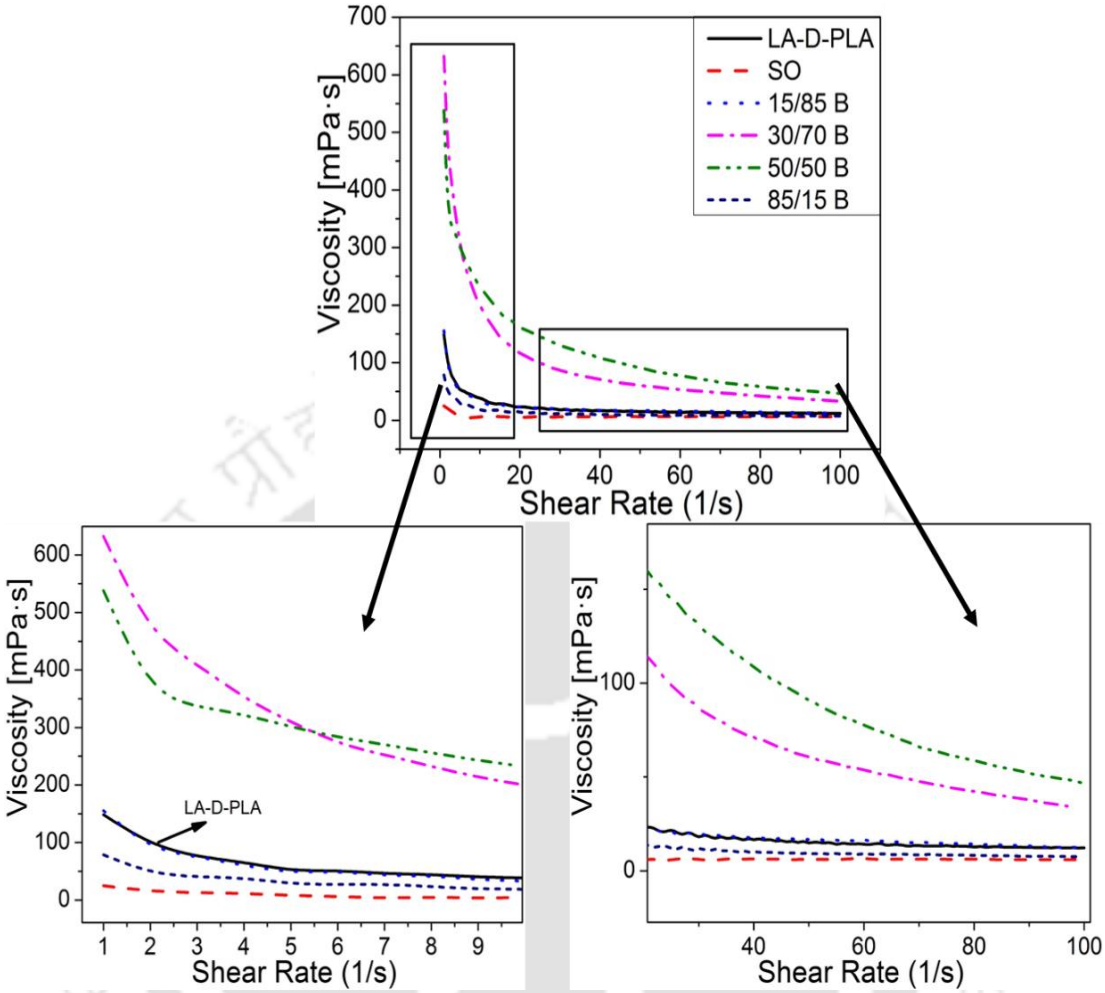

Figure 7.4. Flow behavior of base fluids and their blend at 100 ºC.

The shear dependency of the base fluid and formulated blends are well described by the power law model equation (**Eqn. 7.3),** where the shear rate dependent viscosity η (γ) is expressed as a function of shear rate and constant value K indicates the consistency index (i.e. viscosity at lower shear rate) and the flow characteristic is defined by the power low index (n).

$$\eta(\gamma) = K(\gamma)^{n-1} \qquad 7.3$$

Predominant shear thinning behavior of any fluid attains n values converging to zero and Newtonian behavior occurs when n value converges to 1. The shear thinning flow behavior obtained in **Fig. 7.2, 7.3 and 7.4** at different temperature are fitted to **Eqn. 7.3** with R^2 value higher than 0.98 and the values for n and K are listed in **Table 7.1.**

Table 7.1. Shear thinning flow characteristics: power law index.

Temperature	LA-D-PLA	SO	15/85 B	30/70 B	50/50 B	85/15 B
25	0.02	1	0.6	0.6	0.6	0.8
40	0.8	0.96	0.8	0.6	0.6	0.8
100	0.5	0.9	0.5	0.3	0.4	0.5

Soybean oil (SO) shows Newtonian behavior with all the tested temperatures having power law index of 1, 0.96 and 0.9 with respect to the temperature 25 ºC 40 ºC and 100 ºC. On the other hand, LA-D-PLA exhibits completely different flow characteristics, in which the power law index significantly changes from predominant shear thinning characteristics (n=0.02) at 25 ºC to Newtonian flow behavior at 40 ºC (n =0.8) followed by moderate shear thinning behavior at 100 ºC (n =0.5). The observed Newtonian flow characteristic at 40 ºC may be attributed to the relaxation of polymeric chains at their glass transition temperature (T_g), which is the main reason for the decrease in viscosity at lower shear rate. With increasing in temperature, the kinetic motion of macromolecular chains tends to increase and in turn the shear thinning behavior is slightly increased. The flow characteristics of LA-D-PLA is changed with increasing the blend proportion of SO. At 25 ºC the power law index is changed from 0.02 to 0.6 for 15/85B, 30/70B and 50/50B. At higher content of SO (85/150B) the flow characteristics resemble Newtonian behavior at a temperature 25 ºC and 40 ºC with power law index of 0.8. For the blend having low content of LA-D-PLA (85/15B), Newtonian

characteristics is obtained at 25 ºC and 40 ºC having a power law index of 0.8. However, as the temperature is increased to 100 ºC, power law index decreased to 0.5.

The viscosity of the blends are observed to be higher than that of the base fluid LA-D-PLA and SO. This unexpected behavior may be attributed to the increment in compatibility between the two base fluids, which arises due to the formation of chemical interaction. As clearly indicated in **Table 7.2,** the viscosity at shear rate of 100 s^{-1} (taken from shear thinning investigation) increases with increasing the SO content upto some limits. Based on the obtained results, 30/70B and 50/50B exhibits higher viscosity. This result is analyzed in depth through the estimation of viscosity at constant shear rate (500 s^{-1}).

Table 7.2. Shear thinning viscosity values taken at 100 s^{-1} [mPa.s].

Temperature	LA-D-PLA	SO	15/85 B	30/70 B	50/50 B	85/15 B
25	157.5	48.5	150.3	260.3	297.6	66.9
40	77.9	27.8	74.8	158.7	191.7	37.8
100	12.3	5.8	12.4	33.1	46.7	7.7

7.2.1.2. Viscosity: Temperature dependency

The temperature dependent viscosity of LA-D-PLA, SO and their blends are determined at higher shear rates (500 s^{-1}). From the above investigation, it is observed that the LA-D-PLA and the formulated blends depict non-Newtonian behavior particularly at lower temperature. Due to this behavior, the viscosity needs to be studied at a higher shear rate at which the flow characteristics of the sample resembles Newtonian behavior. **Fig. 7.5** shows the influence of temperature on the viscosity of the base fluids and formulated blends, at a temperature dependent viscosity graph for the temperature range of 25, 40, 60, 80 and 100 ºC. Higher

viscosity is obtained for 50/50B at all the temperatures as compared to the other formulations and base fluids. Wide range of viscosity is required for lubricants to be suitable for specific applications. The intermolecular attraction force between the LA-D-PLA and SO may be more predominant having a tendency to increase the compatibility and in turn increase the viscosity [228]. As already known, viscosity increases with increasing the intermolecular attraction force and decreases with increasing temperature.

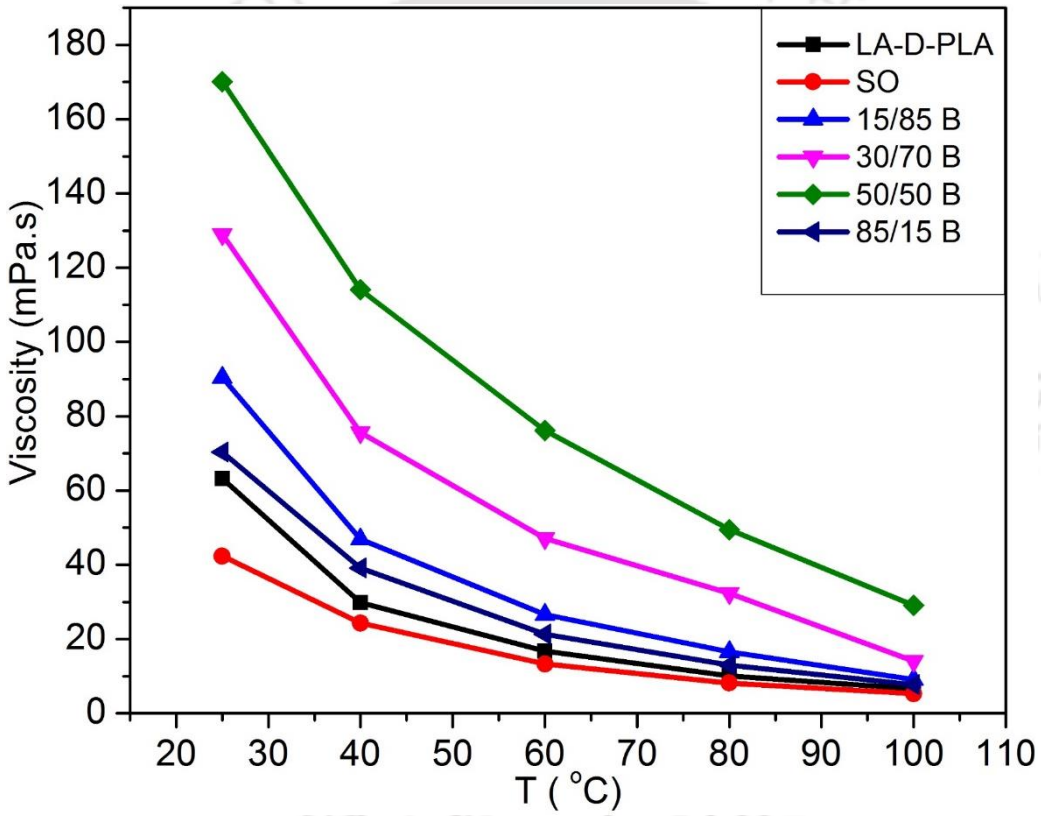

Figure 7.5. Temperature dependent viscosity of LA-D-PLA, SO and their blends.

The viscosity of the blend at 40 ºC varies from 39.2 mPa.s (85/15B) to 114.1 mPa.s (50/50) is within the application range of lubricants required for automation industry (30 mm^2/s) to lubricants required for bearings (120 mm^2/s) **(Table 7.3)**.

Table 7.3. Viscosity of the base fluids and the formulated blends at 500 s^{-1} [mPa.s].

Cycle	LA-D-PLA	SO	15/85 B	30/70 B	50/50 B	85/15 B
25	63.2	36.3	90.4	128.9	170.1	70.4
40	29.8	24.3	46.9	75.6	114.1	39.2
60	16.8	13.3	26.6	47.1	76.2	21.3
80	10.1	8.2	16.5	32.3	49.5	12.9
100	6.6	5.3	9.1	14.1	29.1	7.7
Ea (KJ/mol)	27.3	24.1	27.3	25.5	21.2	26.8
A*1000 (Pa.s)	1.36	0.94	1.41	4.47	34.3	1.36
R^2	0.99	0.99	0.99	0.97	0.99	0.99

However, in order to use any fluid as a lubricant, small change in the viscosity with respect to a wide temperature range is required to maintain proper film thickness between the solid bodies to avoid friction. This property is usually measured by the viscosity index. However, by estimating the flow activation energy of the lubricants, the temperature dependency of the viscosity can be analyzed. **Eqn. 7.2** is used to estimate the flow activation energy, which helps to predict the thermal susceptibility of the base fluids and formulated blends more accurately than the viscosity index estimation. Most commonly, viscosity index is calculated using the viscosities measured at two different temperatures (40 ºC and 100 ºC). However, the flow activation energy, which is estimated from the slope of **Eqn. 7.2** accounts for more viscosity values at different temperatures [229]. For this particular investigation viscosity is measured at five different temperatures, ranging from 25 ºC to 100 ºC to fit the Arrhenius equation as shown in **Fig. 7.6** and the values are listed **in Table 7.3.**

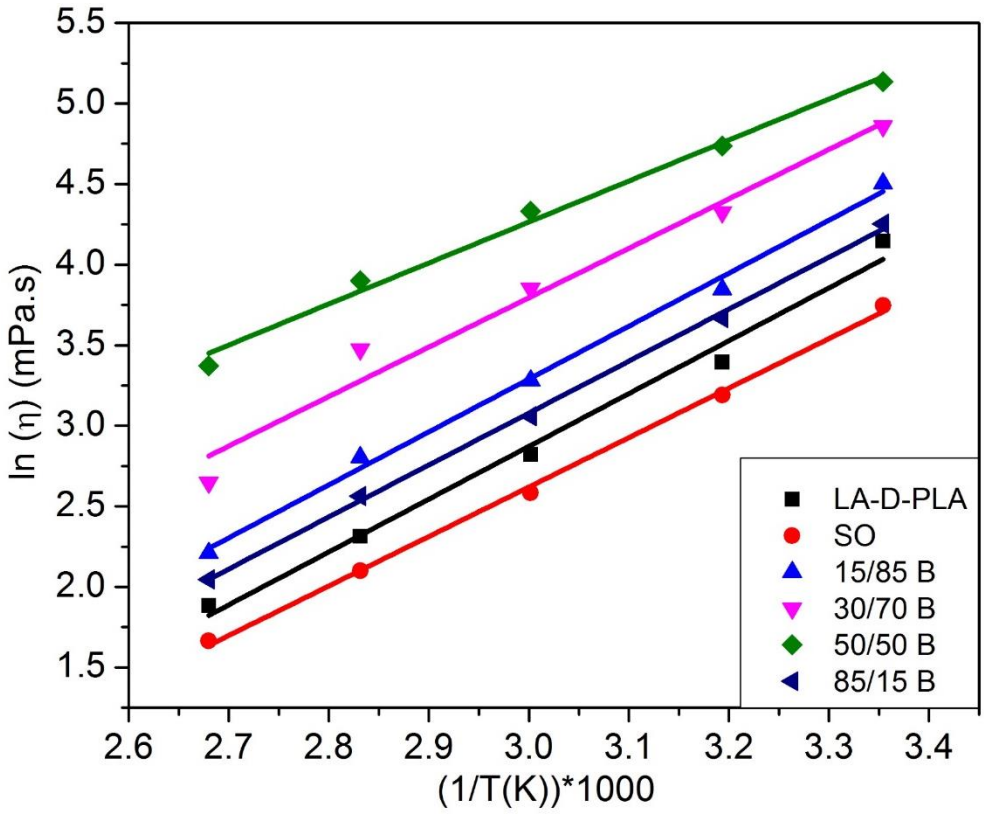

Figure 7.6. Plot of viscosity with respect to temperature: Estimation of activation energy using Arrhenius' equation.

Higher thermal susceptibility is observed for LA-D-PLA, 15/85B and 85/15B, which is confirmed from the estimated higher values of activation energy, 27.3 kJ/mol., 27.3 kJ/mol. and 26.8 kJ/mol. respectively. The flow activation energy is reduced to 25.5 kJ/mol. and 21.2 kJ/mol. respectively for 30/70 B and 50/50 B. The observed lower activation energy for the case of 50/50 B confirms less thermal susceptibility (i.e. lower change of viscosity with increasing temperature). This result reveals the promising opportunity to recycle PLA and use it as a biodegradable lubricant as a blend with soybean oil. Various viscosity ranges with their respective specific viscosity index are obtained by changing the blending ratios between 30/70 to 70/30.

7.2.1.3. Viscosity: Stability

Another important characteristic essential for the lubricants is the stability of the viscosity within the operating time and the temperature that it can withstand without undergoing degradation. Lubricants are required to maintain their lubrication film thickness throughout the operating time in order to avoid the failure due to friction.

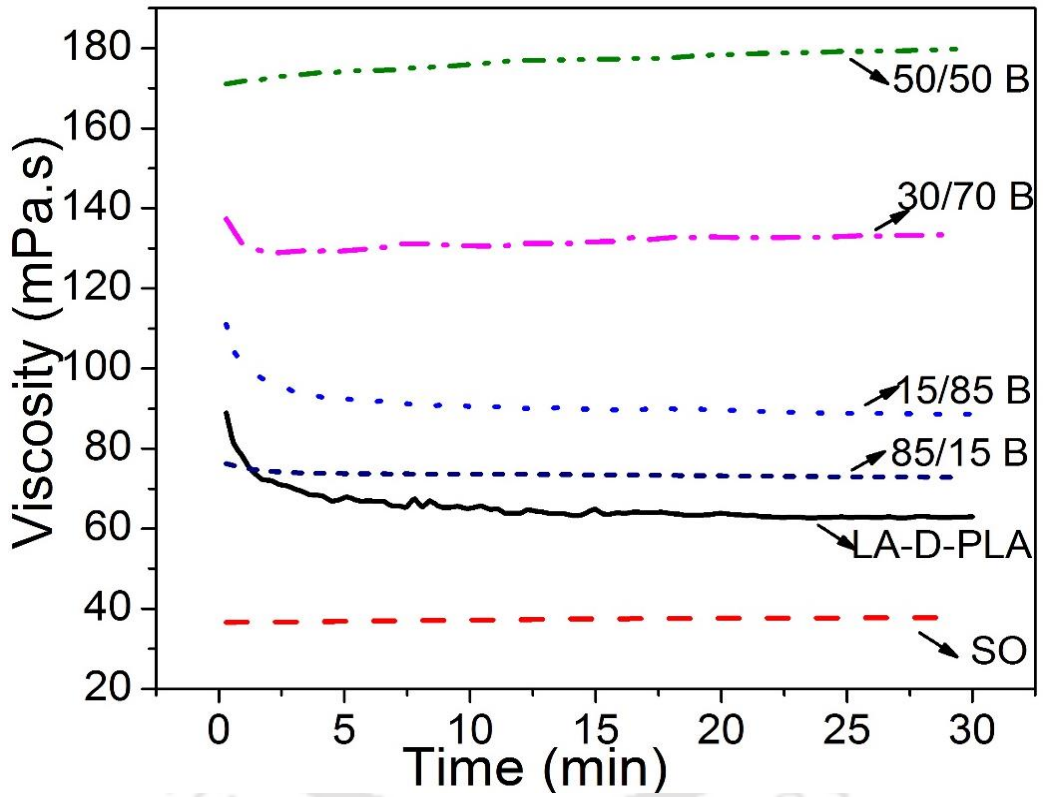

Figure 7.7. Stability of the viscosity with increasing time.

Fig. 7.7 shows the impact of time (up to 30 min) on the viscosity of the base fluids and the formulated blends tested at higher shear rate (500 s^{-1}). Within the first 3 minutes, sudden reduction in viscosity is observed for LA-D-PLA and 15/85B followed by insignificant of viscosity at ~65 mPa.s and ~90 mPa.s respectively for the given analysis time. The stability of

the formulated blends is enhanced with increasing the blending content of SO. Investigating the thermal stability is very essential to determine the service life of the lubricating fluids in the friction assembly, which is highly susceptible to chemical degradation due to heat frictional dissipation. As clearly observed in **Fig. 7.8,** LA-D-PLA starts degrading at a lower temperature, which is because of the presence of water and monomer. The main degradation takes place within the temperature range of ~100 to 250 ˚C. However, SO is known to be stable up to ~350 ˚C. Increasing the content of SO, the thermal stability of the formulated blend is significantly enhanced and the onset degradation temperature is increased.

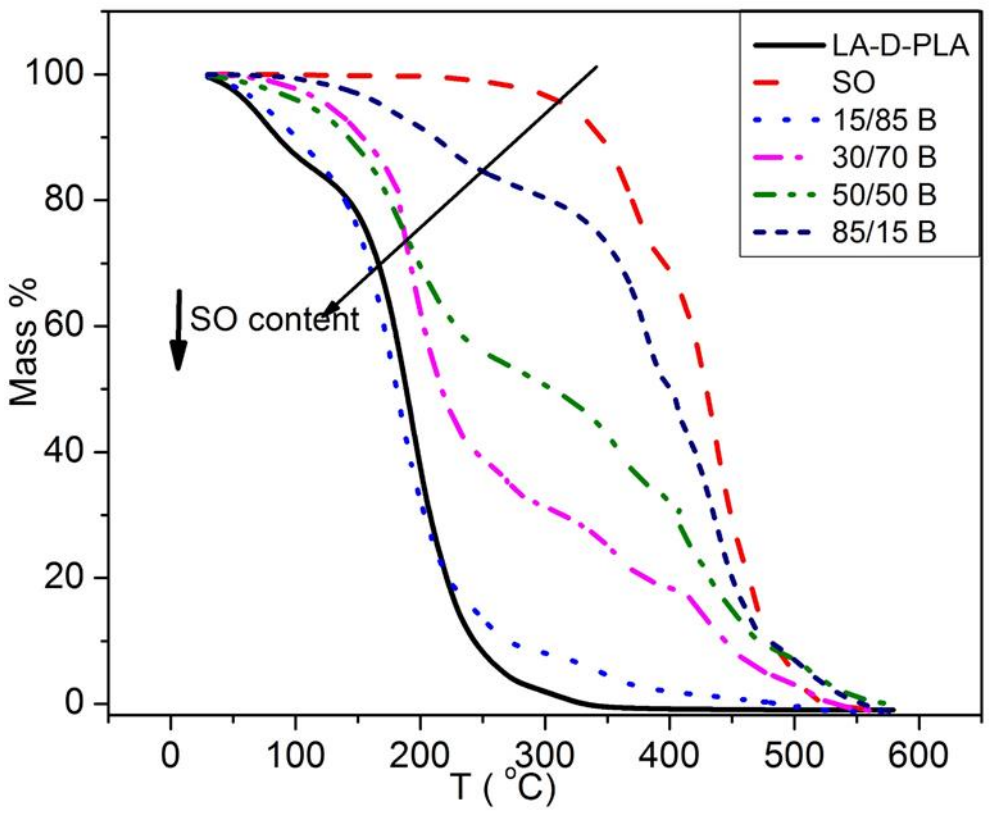

Figure 7.8. Thermal stability of LA-D-PLA, SO and the formulated blends.

7.2.2. The impact of lower molecular weight PLA (PLA-oligomers) on biodiesel characteristics

7.2.2.1. Characterization of biodiesel and oligomer

Microwave assisted trans-esterification reaction of soybean oil leads to maximum biodiesel conversion (99%) within 5 min. Due to the reversible nature of the reaction, the conversion decreased with the reaction time higher than 5 min.

Table 7.4. Effect of conversion on biodiesel properties.

Rxn. time (min.)	Conv. NMR (%)	Cloud point (ºC)	Pour point (ºC)	Flash point (ºC)	Fire point (ºC)
1	81	5	-5	169	174
3	86	5	-2	151	164
5	99	4	-2	146	155
15	93	5	-2	148	159
30	91	5	-2	148	161
Soybean oil	-	7	-9	295	>300

Effect of conversion of soybean oil into fatty acid can be seen in **Table 7.4**. The observed values of flash point and fire point are higher for lower reaction time due to low conversion during trans-esterification reaction. At higher reaction time, the conversion again decreased due to reversible nature of transesterification reaction. Similar observation can be made for cloud point and pour point also, where the increase in conversion had positive effect on cloud point but little increase in pour point is observed. From the **Table 7.4**, it can be clearly seen that 5 min is the optimum reaction time where maximum conversion is achieved. On the basis of these observations, further investigations are done on biodiesel produced by using 5 min

reaction time. Based on GPC analysis, synthesized OLLA is found to have number average molecular weight ~1000 Da with PDI ~ 1.2 and density of 1.205g/cm^3. The short chain oligomers of PLA [OLLA] used in this study contains ~44 wt.% oxygen, as along with the terminal carboxylic acid and hydroxyl group, it contains ester group in the backbone. Availability of more number of interaction sites and oxygen content may affect the fuel properties and can work as effective sites for miscibility [230].

7.2.2.2. The effect of OLLA and Ethyl Lactate on cloud point and pour point

Changes in the cold flow properties of biodiesel by the addition of OLLA have been described in **Table 7.5.** For BD-OL3, BD-OL5, and BD-OL10, it is observed that cloud point and pour point temperature are reduced by 4ºC and 2ºC as compared to the biodiesel obtained at optimum reaction time.

Table 7.5. Properties of biodiesel after addition of OLLA oligomer.

Properties	BD-OL0	BD-OL3	BD-OL5	BD-OL10	BD-OL25	ASTM limit
Density (g/cm^3) @ 25ºC	0.891	0.888	0.887	0.889	0.890	--
Kinematic viscosity @ 25 ºC mm^2/s	4.17	4.25	4.19	4.19	4.22	1.9-6
Cloud point	4	0	0	0	1	--
Pour point	-2	-4	-4	-4	-3	--
Flash point(ºC)	146	173	168	178	164	>130
Fire point (ºC)	155	181	177	185	171	--
Higher heating values MJ/kg	41.69	41.30	41.32	41.34	40.85	--

Most importantly the addition of the oligomer did not significantly affect the kinematic viscosity (at 25ºC) and higher heating value of the fuel. The effect of the ethyl lactate as solvent

on cold flow properties of biodiesel with or without oligomer is investigated and described in **Table 7.6**. The addition of 1% and 2% (v/v) ethyl lactate improved the cloud point and pour point by 4ºC and 3ºC respectively, while addition of 3%, 5%, and 10% (v/v) resulted in reduction of cloud point by 6ºC and in pour point by 3ºC, compared to the produced soybean based biodiesel.

Table 7.6. Effect of ethyl lactate and OLLA content on produced soybean based biodiesel properties.

EL% (v/v)		Cloud point (ºC)	Pour point (ºC)	Flash point (ºC)	Fire point (ºC)
0		4	-2	146	155
1		0	-5	131	141
2		-1	-5	125	138
3		-2	-5	118	135
5		-2	-5	115	132
10		-2	-5	97	110
5% Ethyl Lactate	**OL3**	-2	-4	115	135
	OL5	-2	-4	115	135
	OL10	-2	-4	115	139
	OL25	-1	-3	115	138

On the other hand, flash point and fire point of the EL-biodiesel blend decreased drastically with the increasing percentage of ethyl lactate. Furthermore, it can be clearly observed from **Table 7.6** that the addition of 5% (v/v) EL in OL3-BD, OL5-BD and OL10-BD reduced the cloud point and pour point by 6ºC and 2ºC, respectively.

7.2.2.3. Viscosity analysis

The dynamic viscosity at different temperatures of biodiesel and its blends with OLLA and EL is presented in **Fig. 7.9**.

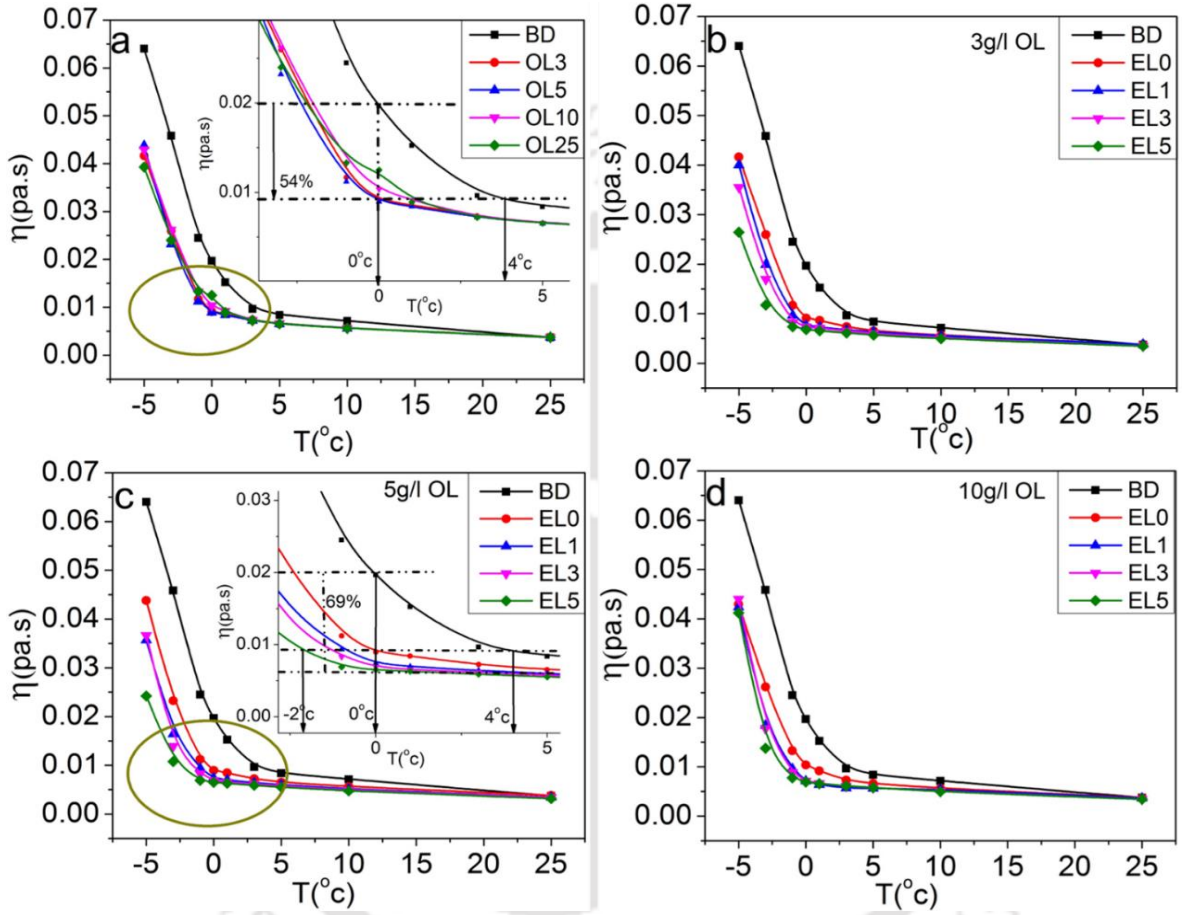

Figure 7.9. The effect of temperature on dynamic viscosity of (a) different wt.% of OLLA in biodiesel without EL (b) with 3wt.% OLLA and different EL vol.% (c) with 5wt.% OLLA and different EL vol.% (d) with 10wt.% OLLA and different EL vol.%.

The dynamic viscosity of biodiesel increases with decreasing temperature which follows two different patterns with a transition region, from Newtonian to non-Newtonian behavior. This phenomenon occurs above the temperature of biodiesel at which the blend ceases to flow and below the temperature of formation of wax like structure and it falls in between pour point and cloud point. OLLA and EL plays a major role to decrease the viscosity and cut-off point for the transition of Newtonian and non-Newtonian behavior of biodiesel (**Fig. 7.9)**, which indicates the enhancement in cold flow properties [231]. For neat biodiesel, the transition of fluid behavior started around 3 ºC whereas for OL-BD, it is observed around 0 ºC (**Fig. 7.9 (a)**). Furthermore, the viscosity of OL-BD system decreases with increasing volume fraction of EL and the cut-off point shifts to lower temperature around -2 ºC (**Fig. 7.9 (b), (c) & (d)**). By comparing the data from **Fig. 7.9 (b), (c) & (d)**, it can be seen that 5wt.% OLLA and 5 vol.% EL in biodiesel is the best combination to have lower viscosity and cut off point for the transition of fluid from Newtonian to non-Newtonian. This improvement is further verified by comparing the activation energy of each system which is calculated by using Arrhenius equation (**Table 7.7**).

Table 7.7. The effect of PLA-oligomer and ethyl lactate on activation energy of biodiesel.

		OL0	OL3	OL5	OL10
Activation energy	**Slop**	4.1044	2.6338	2.6227	2.774
	R^2	0.9398	0.9755	0.9837	0.9636
	Eη(0% EL) KJ/mol	34.1	21.9	21.8	23.1
	5% EL		2.159	2.2056	2.3299
	R^2		0.9976	0.9996	0.9987
	Eη(5% EL) KJ/mol		17.9	18.3	19.4

Activation energy gives the insights about the amount of energy required to overcome the viscosity and allow macromolecular motion to occur [225] The observation can be made from **Fig. 7.10** that the slope becomes less steep for the OLLA-biodiesel and OLLA-EL-biodiesel

blends as compared to the neat biodiesel, which indicates less energy requirement for the movement in macromolecular level and decrease in viscosity.

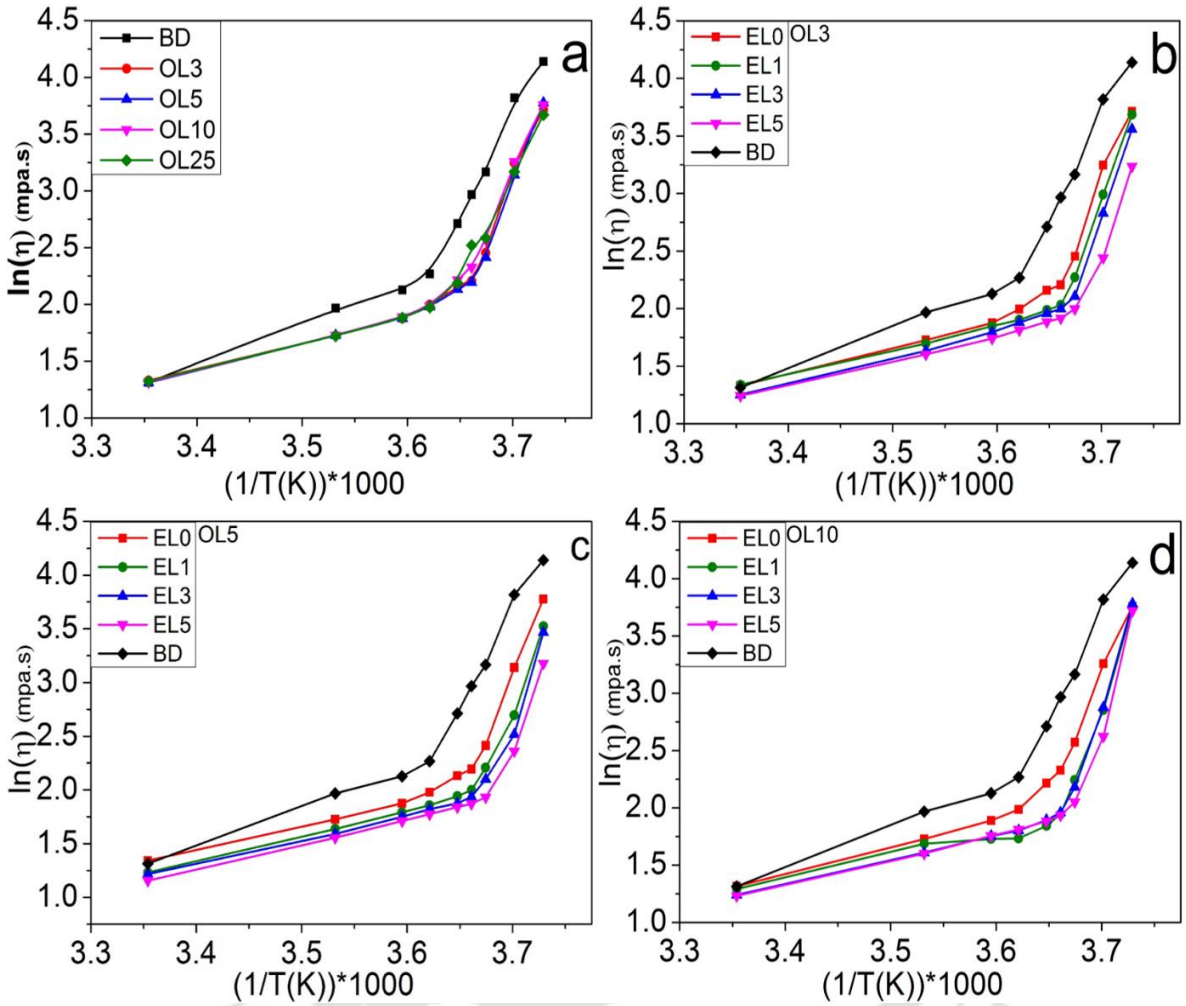

Figure 7.10. ln(η) vs (1/T) for OL-BD system, with and without ethyl lactate (a) and with 5% EL at different percentage of OL3 (b), OL5 (C) and OL10 (d).

7.2.2.4. The effect of PLA oligomer molecular weight on the flow behavior of biodiesel

Different molecular weight OLLA (500 Da, 1000 Da, 1500 Da and 2000 Da) is prepared by using a method described in section 2.3.2.1 to understand the impact of molecular weight on the flow characteristic of biodiesel at lower temperature. **Fig. 7.11** shows the impact of changing oligomer molecular weight on the cold flow characteristics of biodiesel.

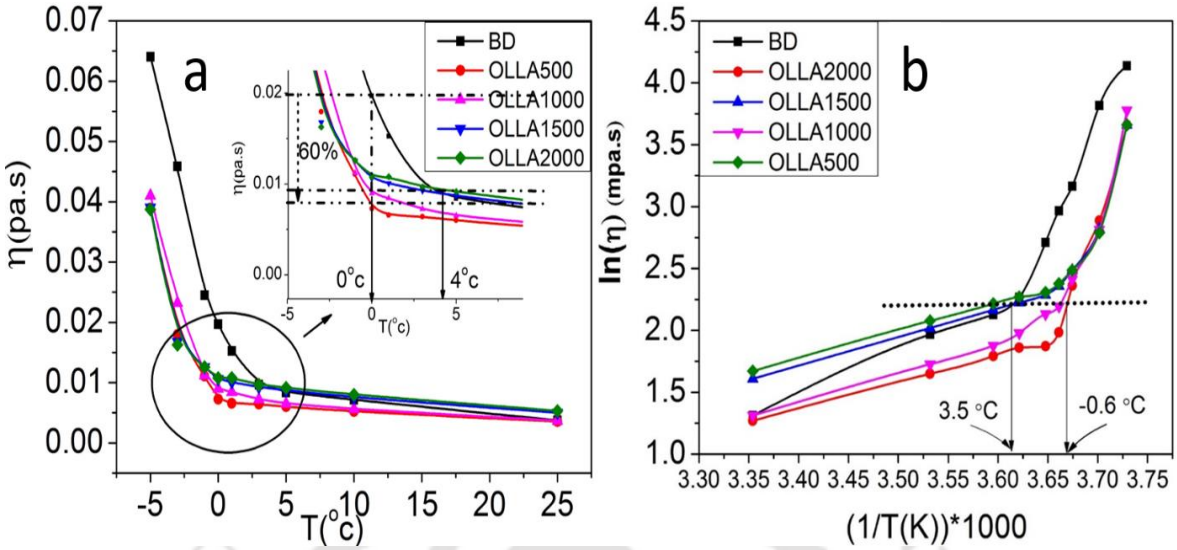

Figure 7.11. The effect of molecular weight of OLLA on (a) dynamic viscosity and (b) ln(η) vs (1/T)

As clearly observed from the figure, the viscosity decreases with decreasing the molecular weight. However, no significant change is observed on the flow behavior at transition point. The dynamic viscosity at transition temperature (0 ºC) is reduced by 60% when 5 g/L of OLLA500 is introduced to biodiesel. **Table 7.8** displays the flow activation energy which is estimated using **Eqn. 7.2.** Insignificant change is observed on the flow activation energy when the molecular weight is decreased from 2000 Da to 500 Da.

Table 7.8. The effect of molecular weight of PLA-oligomer on flow activation energy.

	BD	OL500	OL1000	OL1500	OL2000
Slope	4.1	2.32	2.63	2.41	2.56
R^2	0.94	0.99	0.98	0.99	0.99
E (0% EL) KJ/mol	34.1	19.28	21.8	20.03	21.28

7.2.2.5. Crystal growth

The crystal growth of neat biodiesel and OL5-BD at 0 ºC, -3 ºC and -5 ºC can be visualized through the reflection of polarized light as shown in Fig. **7.12.**

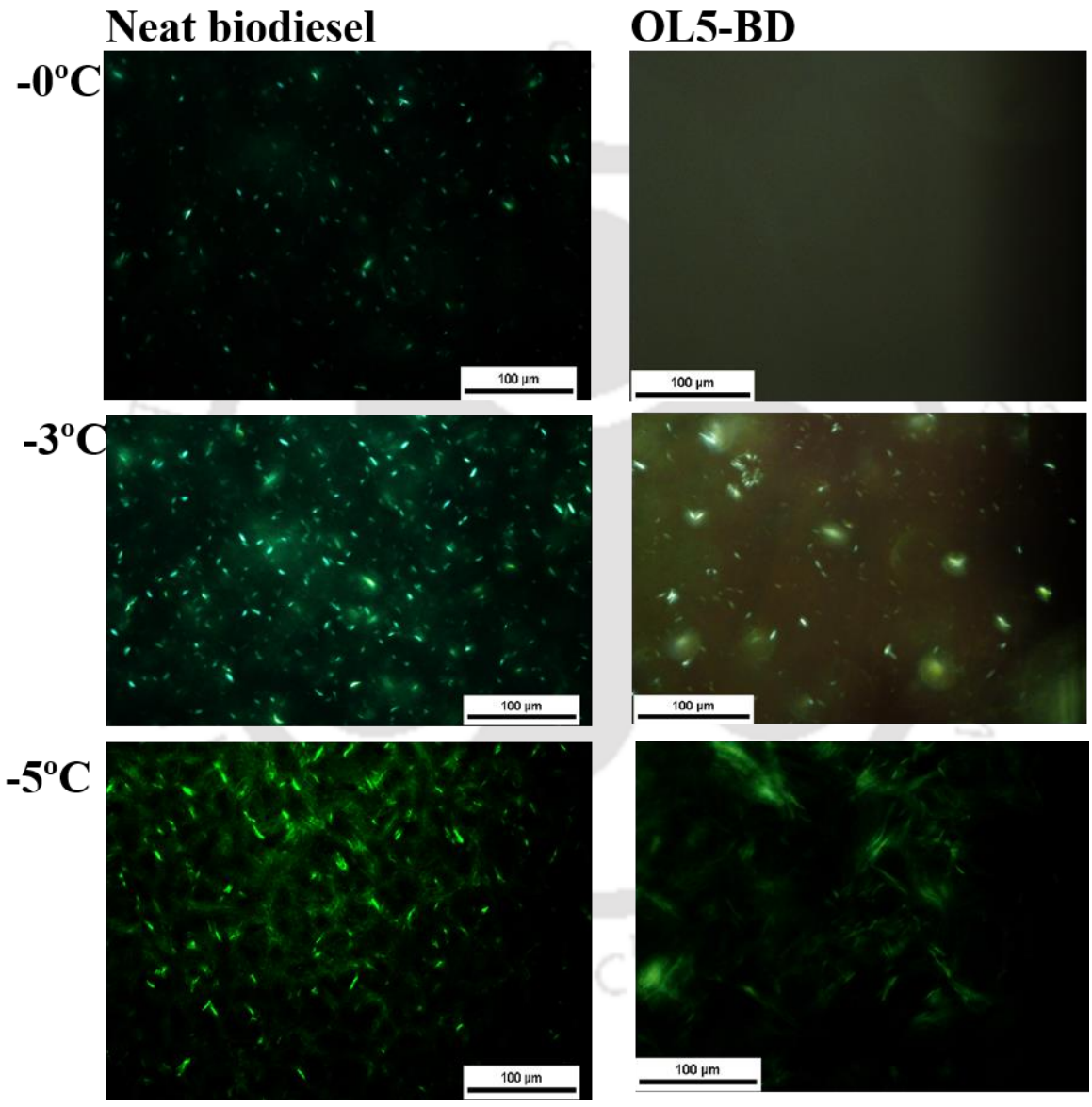

Figure 7.12. Polarizing optical microscope images of crystals of neat biodiesel ((A), (B) and (C)) and BD-OL5 ((D), (E) and (F)) at 0 ºC, -3 ºC and -5 ºC.

From **Fig. 7.12 (A), (B)** and **(C),** it can be observed that the number of crystals and crystal size grows with decrease in temperature. **Fig. 7.12 (D)** clearly implies that addition of OLLA has lowered down the crystal growth initiation temperature to below 0ºC. Another observation can be made from **Fig. 7.12 (E)** and **(F)** that addition of OLLA has slowed down the crystal growth rate, which further supports the viscosity results that OLLA improved the cold flow properties of biodiesel.

7.2.2.6. Engine performance and emission characterization

Brake power (BP) which is obtained by varying the engine load at constant speed of 1500rpm, increases linearly with respect to engine load as described in **Fig. 7.13.**

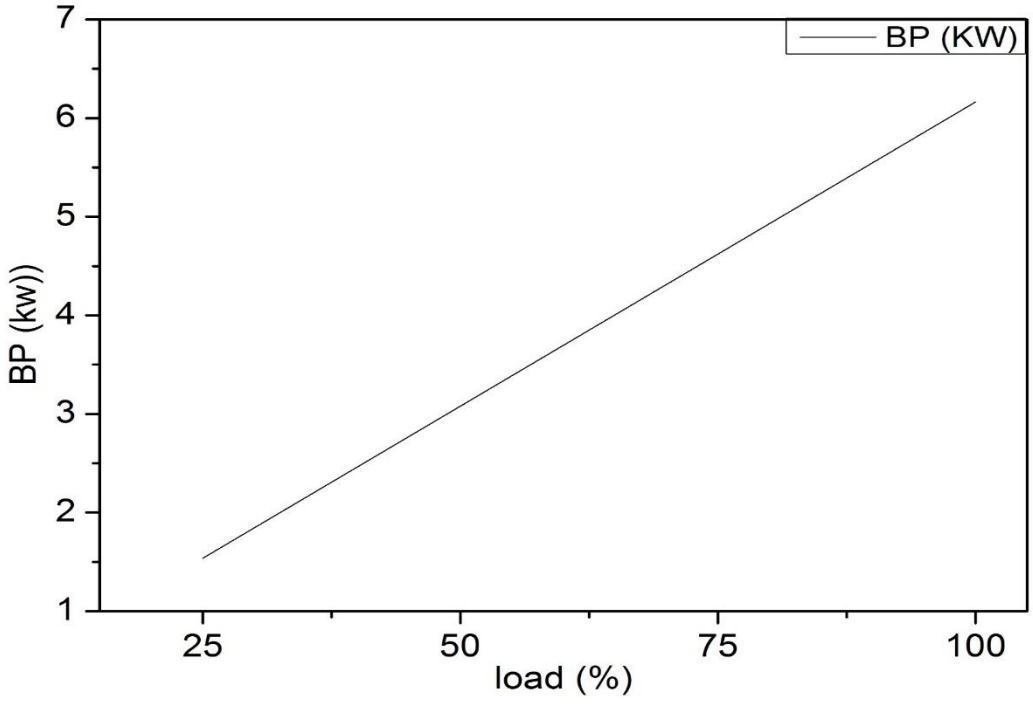

Figure 7.13. Brake power of engine with respect to engine load at fixed speed (1500rpm).

The brake specific fuel consumption (BSFC) and brake thermal efficiency (BTE) of the engine are analyzed for diesel (D100), B20, OL5-B20 and OL10-B20 systems at different engine load and by calculating BP. It can be observed from **Fig. 7.14** that for all engine load, lower BSFC and higher BTE values are obtained for diesel fuel as compared to B20 and OL-B20, due to higher heating value of diesel. The major observation which can be made from the **Fig. 7.14** is that the addition of OLLA does not significantly affect BSFC and BTE of B20.

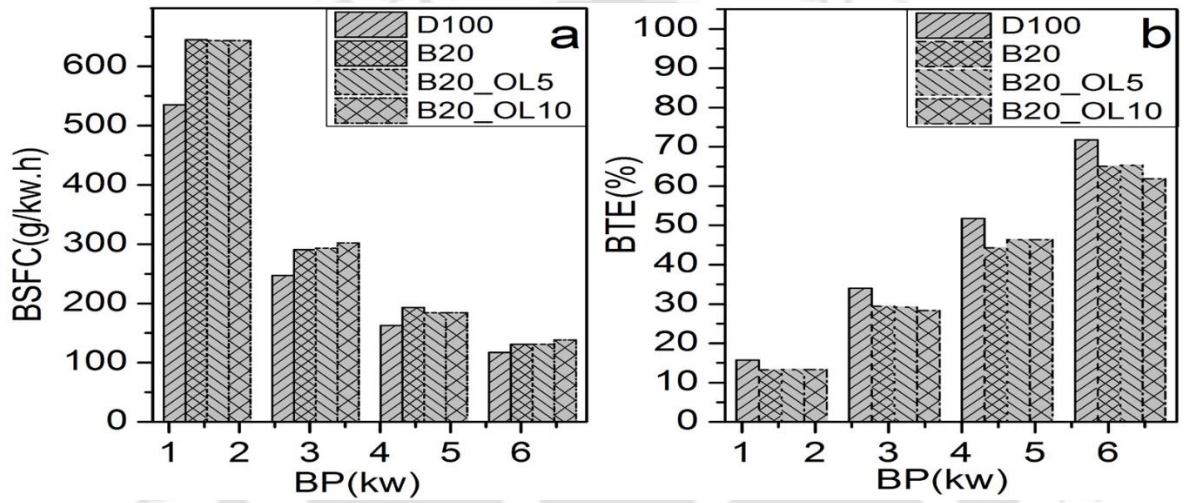

Figure 7.14. Variation in (a) BSFC and (b) BTE with increase in BP for D100, B20, B20-OL5 and B20-OL10 as fuel.

As discussed in previous sections, viscosity reduction of soybean based biodiesel by the addition of oligomer would influence the spray atomization and combustion properties. **Fig. 7.15** shows the effect of addition of OLLA in biodiesel on exhaust gases. From **Fig. 7.15 (b)** and **(c)** it can be seen that CO and HC emission concentration decreased for B20-OL as compared to B20 due to the reduction in viscosity and additionally available oxygen provided by OLLA which helps to facilitate the combustion process. At lower load with lower temperature inside the cylinder, providing rich fuel mixture to the engine leads to releasing of

smaller amount of CO as compared to higher load which requires more power that leads to incomplete combustion. On the other hand, NO_x concentration is not affected by the presence of OLLA in biodiesel. However, the CO_2 concentration is increased, especially at lower engine loads as the concentration of OLLA increased.

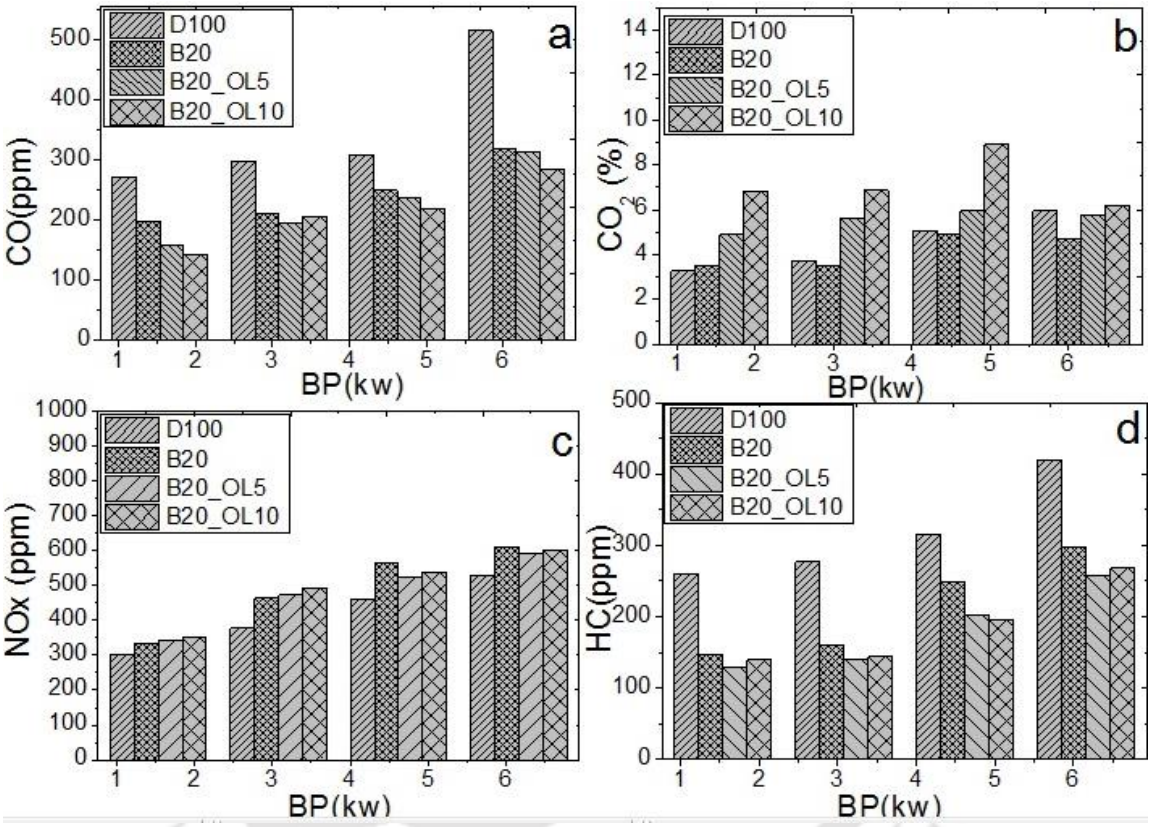

Figure 7.15. The effect of addition of OLLA in biodiesel on exhaust gas emission characteristics (a) NOx, (b) CO, (c) HC and (d) CO_2.

7.3. Summary

Melt processed PLA is randomly degraded using lactic acid/water mixture in microwave to give one phase viscous solution. A blend of lactic acid degraded PLA and soybean oil (SO) is formulated with different fractions to be tested as lubricant. Dynamic viscosity and viscosity-

temperature dependency of the blend is investigated at different temperatures: 25 ºC, 40 ºC, 60 ºC, 80 and 100 ºC. Promising results are obtained for 30/70 and 50/50 blend of soybean oil and recycled PLA with improved viscosity and viscosity index.

On the other hand, PLA oligomer (OLLA) has been studied as an additive to improve cold flow and rheological properties of soybean based biodiesel. Cloud point, pour point, flash point and fire point of synthesized biodiesel are found as 4°C, -2°C, 146°C and 155°C, respectively. Subsequently, by blending ethyl lactate stabilized OLLA with biodiesel, it further reduces the cloud point, pour point, flash point and fire point by 6°C, 2°C, 31°C and 20°C, respectively. Captured polarizing optical microscopic (POM) images during temperature scan relate the effect of OLLA on cloud point confirms the delay in crystal growth followed by reduction in crystal nucleation density. Rheological analyses suggest the shifting of Newtonian flow regime at lower temperature and decrease in dynamic viscosity and flow activation energy of biodiesel by addition of OLLA, which improves the spray atomization during injection process. The engine performance test shows that the presence of OLLA in biodiesel did not significantly affect the brake specific fuel consumption and brake thermal efficiency whereas, in presence of OLLA during combustion process, significant reduction in both carbon monoxide and hydrocarbon emission are found in the exhaust gases.

Chapter 8

Conclusions and Future Scope

In this doctoral thesis, melt processing and rheology of poly (lactic acid) (PLA) and its efficacy in recyclable biocomposite film and it's novel end use as a biolubricant and biodiesel additive are investigated. This chapter conveys the overall summary, major finding and an outlook for future studies.

8.1. Conclusions

The major conclusions drawn on the overall studies and the main findings of this research work can be broadly classified and present into four subsections:

The first part focused on the incorporation of acid hydrolyzed silk fibroin into the PLA matrix in order to study its melt reinforcement effect under different melt processing.

- The major drawback of PLA, melt degradation caused at high shear and temperature is observed to be hindered, the degradation rate constant decreased and higher degradation activation energy is obtained for PLA matrix after the addition of silk.
- Weak chemical interaction between SNC and PLA is confirmed by the additional hump peak at 1710 cm^{-1} of FTIR spectra, which is missing in PLA spectra. The amide and OH groups of silk have a tendency to form weak van der waals interaction with C=O group of PLA, which helps to stabilize the macromolecular structure of PLA during melt processing.
- The morphology of the SNC-PLA capture by FESEM, shows network formation which is missing in neat PLA matrix.
- Furthermore, the crystallinity is improved and the reduction in number average molecular weight (M_n) and weight average molecular (M_w), with increasing residence time is minimized as compared to neat PLA.

The second part conveys, the impact of SNC on the crystallization, melting, rheology and thermal decomposition behavior of PLA during multiple extrusion.

- The presence of SNCs observed to facilitate the crystallization process and delay the thermal degradation of PLA matrix. This leads to the reduction in cold crystallization peak temperature with lower crystallization half-time and higher growth rate.
- The substantial improvement in nucleation density observed through Polarized Optical Microscope (POM) proves the nucleating effect of SNC in all processing cycles.
- The rheological investigation revealed the stabilizing effect of SNC and the drastic degradation of neat PLA in third and fourth cycle is observed to be fortified by the presence of SNC.
- The molecular weight results from GPC are comparable to those obtained from rheological measurements. The comparably low storage modulus of PLA on repeated processing cycles can be explained from decreased rheological response arising from the lower molecular weight (degraded) PLA chains. The shift of the cross-over frequency of NPLA to high frequency from the fourth to fifth processing cycles indicates a decrease in molecular weight accompanied by an increase in polydispersity or broadening of the molecular weight distribution.
- The reinforcing effect of SNC nano-filler leads to higher elastic modulus values for SNC-PLA nanocomposites for the corresponding processing cycles.
- Similarly, stable onset degradation temperature is obtained for SNC-PLA nanocomposite ($T_{5\%}$ ~ 334 ºC) as compared to neat poly (lactic acid) (NPLA), which is drastically reduced from 336 ºC (first cycle) to 322 ºC (fifth cycle).
- The activation energies are estimated using isoconversional methods (Kissinger-Akahira-Sunose and Flynn-Wall-Ozawa). Stable activation energy values (~130 kJ/mol) are obtained for SNC-PLA at three consecutive extrusion cycle whereas in

case of NPLA, it significantly reduces from ~150 kJ/mol (first cycle) to ~110 kJ/mol (second cycle).

- Nelder-Mead simplex method is used to optimize the kinetic parameters of nucleation and growth model (A2); which is observed to be the best fit of the experimental thermogravimetric analysis (TGA) data.
- Unlike NPLA, reduction in the intensity of FTIR spectra (2745, 2180, 2110 cm^{-1}) of the characteristic peaks for aldehyde and carbon monoxide are observed from the evolved gasses analysis of SNC-PLA (for all reprocessing cycle).

In the third part, the reactive extrusion is performed to have branched, crosslinked and silk nanocrystal (SNC) grafted chain topology of PLA.

- Small amount of dicumyl peroxide (DCP) is used as radical initiator and the level of chain modification is controlled by the estimation of gel percentage. Grafting of SNCs on PLA macromolecules provides remarkable improvement on rheological and thermal properties and the grafting is confirmed by ^{1}HNMR and FTIR investigation.
- Significantly higher zero shear viscosity is obtained for SNC grafted PLA system and the crossover frequency point is shifted to lower frequencies as compared to branched and crosslinked PLA system.
- With SNC grafting, the crystallization behavior is enhanced and stable crystals are formed during cooling, which leads to a single melting peak. The rate of crystallization is significantly improved. The percentage crystallinity is decreased at higher DCP fraction, shows the hindrance of macromolecular movements which is essential for crystallization process by higher grafting and crosslinking.

- ❖ Furthermore, SNC grafting increases the reprocessability performance of PLA and provides higher rheological properties as compared to branched and crosslinked PLA at all reprocessing cycles.

In the last part, two recycling alternatives are introduced for the first time to recycle melt processed PLA and lower molecular weight oligomers.

- ❖ The first part covers the dissolution of melt processed PLA in lactic acid/water mixture and blending it with soybean oil (SO) to be tested as a lubricant.
    - o Dynamic viscosity and Viscosity-Temperature dependency of the blend is investigated at temperature of 25 ºC, 40 ºC, 60 ºC, 80 and 100 ºC. Promising results are obtained for 30/70 and 50/50 blend of soybean oil and recycled PLA.
- ❖ The second part covers the recycling of lower molecular weight PLA (oligomer) into biodiesel additives. Four different molecular weight oligomers (500, 1000, 1500 and 2000 Da) are synthesized using microwave reactor and dissolved in soybean oil based methyl eater in different compositions (3, 5, 10 and 25 g/L).
    - o Rheological analysis confirm the shifting of Newtonian flow regime at lower temperature and decrease in dynamic viscosity and flow activation energy of biodiesel by addition of OLLA. The reduction in viscosity can improve the spray atomization during injection process.
    - o The cloud point and pour point are observed to be decreased respectively by 6 ºC and 2 ºC.
    - o The flash point and the fire point of biodiesel are increased by more than 30 ºC.
    - o The viscosity is observed to be decreased with decreasing the molecular weight. However, no significant change is observed on the flow behavior transition

point. The dynamic viscosity at transition temperature (0 ˚C) is reduced by 60% when 5 g/L of OLLA500 is introduced to biodiesel.

- The engine performance test shows that the presence of OLLA in biodiesel did not significantly affect the brake specific fuel consumption and brake thermal efficiency.

8.2. Scope for future work

Based on the outcome of this work, some recommendations for future research work are presented as follows:

- ❖ Impact of extrusion cycle on other properties of PLA/SNC nanocomposite such as gas barrier and mechanical properties can be examined.
- ❖ Surface modified silk can be investigated in order to increase the melt stabilizing effect of PLA without compromising other important characteristics.
- ❖ The effect of plasticizers can be explored in order to improve the elongation at break of SNC-PLA composite and can be processed in to blown film for packaging application.
- ❖ Modelling and optimization of melt processing of SNC-PLA for large scale melt degradation needs to be investigated.
- ❖ This research work opens up possibilities of exploring other cross-linkers, chain extenders and stabilizers in order to improve the melt strength of SNC-PLA nanocomposite.
- ❖ Macromolecular chain modification of randomly degraded PLA can be investigated in order to expand its applicability in biolubricates, biodiesel as well as other different areas.

References

1. P.M. Subramanian, *Plastics recycling and waste management in the US.* Resources, Conservation and Recycling, 2000. **28**(3–4): p. 253-263.
2. S.M. Al-Salem, P. Lettieri, and J. Baeyens, *Recycling and recovery routes of plastic solid waste (PSW): A review.* Waste Management, 2009. **29**(10): p. 2625-2643.
3. G. Gourmelon. *Global Plastic Production Rises, Recycling Lags*. 2015; Available from: http://www.worldwatch.org/global-plastic-production-rises-recycling-lags-0.
4. I. Fortelný, D. Michálková, and Z. Kruliš, *An efficient method of material recycling of municipal plastic waste.* Polymer Degradation and Stability, 2004. **85**(3): p. 975-979.
5. A.K. Panda, R.K. Singh, and D.K. Mishra, *Thermolysis of waste plastics to liquid fuel: A suitable method for plastic waste management and manufacture of value added products—A world prospective.* Renewable and Sustainable Energy Reviews, 2010. **14**(1): p. 233-248.
6. S.-H. Lee and S. Wang, *Biodegradable polymers/bamboo fiber biocomposite with bio-based coupling agent.* Composites Part A: Applied Science and Manufacturing, 2006. **37**(1): p. 80-91.
7. A.K. Mohanty, M. Misra, and G. Hinrichsen, *Biofibres, biodegradable polymers and biocomposites: An overview.* Macromolecular Materials and Engineering, 2000. **276-277**: p. 1-24.
8. E. Zini, M. Baiardo, L. Armelao, and M. Scandola, *Biodegradable polyesters reinforced with surface-modified vegetable fibers.* Macromolecular Bioscience, 2004. **4**(3): p. 286-295.

9. B. Imre and B. Pukánszky, *Compatibilization in bio-based and biodegradable polymer blends.* European Polymer Journal, 2013. **49**(6): p. 1215-1233.

10. F. Aeschelmann and M. Carus. *Bio-based Building Blocks and Polymers in the World – Capacities, Production and Applications: Status Quo and Trends Towards 2020*. 2015; Available from: http://news.bio-based.eu/fast-growth-of-based-polymers-production/.

11. K. Madhavan Nampoothiri, N.R. Nair, and R.P. John, *An overview of the recent developments in polylactide (PLA) research.* Bioresource Technology, 2010. **101**(22): p. 8493-8501.

12. P. Morone, V.E. Tartiu, and P. Falcone, *Assessing the potential of biowaste for bioplastics production through social network analysis.* Journal of Cleaner Production, 2015. **90**: p. 43-54.

13. S.-Y. Liu and C.-Y. Lin, *Development and perspective of promising energy plants for bioethanol production in Taiwan.* Renewable Energy, 2009. **34**(8): p. 1902-1907.

14. A.N. Nakagaito, A. Fujimura, T. Sakai, Y. Hama, and H. Yano, *Production of microfibrillated cellulose (MFC)-reinforced polylactic acid (PLA) nanocomposites from sheets obtained by a papermaking-like process.* Composites Science and Technology, 2009. **69**(7–8): p. 1293-1297.

15. E.T.H. Vink, K.R. Rábago, D.A. Glassner, and P.R. Gruber, *Applications of life cycle assessment to NatureWorks™ polylactide (PLA) production.* Polymer Degradation and Stability, 2003. **80**(3): p. 403-419.

16. B. Bax and J. Müssig, *Impact and tensile properties of PLA/Cordenka and PLA/flax composites.* Composites Science and Technology, 2008. **68**(7–8): p. 1601-1607.

17. P.E. Le Marec, L. Ferry, J.-C. Quantin, J.-C. Bénézet, F. Bonfils, S. Guilbert, and A. Bergeret, *Influence of melt processing conditions on poly(lactic acid) degradation: Molar mass distribution and crystallization.* Polymer Degradation and Stability, 2014. **110**: p. 353-363.

18. V. Taubner and R. Shishoo, *Influence of processing parameters on the degradation of poly(L-lactide) during extrusion.* Journal of Applied Polymer Science, 2001. **79**(12): p. 2128-2135.

19. M.C. Gupta and V.G. Deshmukh, *Thermal oxidative degradation of poly-lactic acid - Part II: Molecular weight and electronic spectra during isothermal heating.* Colloid & Polymer Science, 1982. **260**(5): p. 514-517.

20. F.D. Kopinke, M. Remmler, K. Mackenzie, M. Möder, and O. Wachsen, *Thermal decomposition of biodegradable polyesters—II. Poly(lactic acid).* Polymer Degradation and Stability, 1996. **53**(3): p. 329-342.

21. Y. Wang, B. Steinhoff, C. Brinkmann, and I. Alig, *In-line monitoring of the thermal degradation of poly(l-lactic acid) during melt extrusion by UV–vis spectroscopy.* Polymer, 2008. **49**(5): p. 1257-1265.

22. P. Sarazin and B.D. Favis, *Morphology control in co-continuous poly(L-lactide)/polystyrene blends: A route towards highly structured and interconnected porosity in poly(L-lactide) materials.* Biomacromolecules, 2003. **4**(6): p. 1669-1679.

23. Y.M. Corre, J. Duchet, J. Reignier, and A. Maazouz, *Melt strengthening of poly (lactic acid) through reactive extrusion with epoxy-functionalized chains.* Rheologica Acta, 2011. **50**(7-8): p. 613-629.

24. H.J. Lehermeier and J.R. Dorgan, *Melt rheology of poly(lactic acid): Consequences of blending chain architectures.* Polymer Engineering and Science, 2001. **41**(12): p. 2172-2184.

25. L.T. Lim, R. Auras, and M. Rubino, *Processing technologies for poly(lactic acid).* Progress in Polymer Science, 2008. **33**(8): p. 820-852.

26. N. Najafi, M.C. Heuzey, P.J. Carreau, and P.M. Wood-Adams, *Control of thermal degradation of polylactide (PLA)-clay nanocomposites using chain extenders.* Polymer Degradation and Stability, 2012. **97**(4): p. 554-565.

27. J.J. Cooper-White and M.E. Mackay, *Rheological properties of poly(lactides). Effect of molecular weight and temperature on the viscoelasticity of poly(l-lactic acid).* Journal of Polymer Science, Part B: Polymer Physics, 1999. **37**(15): p. 1803-1814.

28. S.-Y. Gu, K. Zhang, J. Ren, and H. Zhan, *Melt rheology of polylactide/poly(butylene adipate-co-terephthalate) blends.* Carbohydrate Polymers, 2008. **74**(1): p. 79-85.

29. X. Leng, Z. Wei, Y. Bian, Y. Ren, Y. Wang, Q. Wang, and Y. Li, *Rheological properties and crystallization behavior of comb-like graft poly(l-lactide): influences of graft length and graft density.* RSC Advances, 2016. **6**(36): p. 30320-30329.

30. R. Al-Itry, K. Lamnawar, and A. Maazouz, *Improvement of thermal stability, rheological and mechanical properties of PLA, PBAT and their blends by reactive extrusion with functionalized epoxy.* Polymer Degradation and Stability, 2012. **97**(10): p. 1898-1914.

31. J.R. Dorgan, J.S. Williams, and D.N. Lewis, *Melt rheology of poly(lactic acid): Entanglement and chain architecture effects.* Journal of Rheology, 1999. **43**(5): p. 1141-1155.

32. S. Wu, *Chain structure and entanglement.* Journal of Polymer Science Part B: Polymer Physics, 1989. **27**(4): p. 723-741.

33. S. Solarski, M. Ferreira, and E. Devaux, *Characterization of the thermal properties of PLA fibers by modulated differential scanning calorimetry.* Polymer, 2005. **46**(25): p. 11187-11192.

34. J.R. Dorgan, H. Lehermeier, and M. Mang, *Thermal and rheological properties of commercial-grade poly(lactic acids)s.* Journal of Polymers and the Environment, 2000. **8**(1): p. 1-9.

35. S.-l. Yang, Z.-H. Wu, W. Yang, and M.-B. Yang, *Thermal and mechanical properties of chemical crosslinked polylactide (PLA).* Polymer Testing, 2008. **27**(8): p. 957-963.

36. H. Xu, C. Teng, and M. Yu, *Improvements of thermal property and crystallization behavior of PLLA based multiblock copolymer by forming stereocomplex with PDLA oligomer.* Polymer, 2006. **47**(11): p. 3922-3928.

37. M. Shibata, N. Teramoto, and Y. Inoue, *Mechanical properties, morphologies, and crystallization behavior of plasticized poly(l-lactide)/poly(butylene succinate-co-l-lactate) blends.* Polymer, 2007. **48**(9): p. 2768-2777.

38. H. Urayama, C. Ma, and Y. Kimura, *Mechanical and thermal properties of poly(L-lactide) incorporating various inorganic fillers with particle and whisker shapes.* Macromolecular Materials and Engineering, 2003. **288**(7): p. 562-568.

39. Y. Di, S. Iannace, E. Di Maio, and L. Nicolais, *Reactively modified poly (lactic acid): Properties and foam processing.* Macromolecular Materials and Engineering, 2005. **290**(11): p. 1083-1090.

40. P. Dhar, D. Tarafder, A. Kumar, and V. Katiyar, *Thermally recyclable polylactic acid/cellulose nanocrystal films through reactive extrusion process.* Polymer, 2016. **87**: p. 268-282.

41. A. Iwatake, M. Nogi, and H. Yano, *Cellulose nanofiber-reinforced polylactic acid.* Composites Science and Technology, 2008. **68**(9): p. 2103-2106.

42. N. Herrera, H. Roch, A.M. Salaberria, M.A. Pino-Orellana, J. Labidi, S.C.M. Fernandes, D. Radic, A. Leiva, and K. Oksman, *Functionalized blown films of plasticized polylactic acid/chitin nanocomposite: Preparation and characterization.* Materials & Design, 2016. **92**: p. 846-852.

43. A.K. Pal and V. Katiyar, *Nanoamphiphilic Chitosan Dispersed Poly(lactic acid) Bionanocomposite Films with Improved Thermal, Mechanical, and Gas Barrier Properties.* Biomacromolecules, 2016. **17**(8): p. 2603-18.

44. J.G. Hardy and T.R. Scheibel, *Composite materials based on silk proteins.* Progress in Polymer Science, 2010. **35**(9): p. 1093-1115.

45. S.C. Kundu, B.C. Dash, R. Dash, and D.L. Kaplan, *Natural protective glue protein, sericin bioengineered by silkworms: Potential for biomedical and biotechnological applications.* Progress in Polymer Science, 2008. **33**(10): p. 998-1012.

46. X. Nirmala, K. Mita, V. Vanisree, M. Žurovec, and F. Sehnal, *Identification of four small molecular mass proteins in the silk of Bombyx mori.* Insect Molecular Biology, 2001. **10**(5): p. 437-445.

47. V. Piemonte, *Bioplastic Wastes: The Best Final Disposition for Energy Saving.* Journal of Polymers and the Environment, 2011. **19**(4): p. 988-994.

48. I. Pillin, N. Montrelay, A. Bourmaud, and Y. Grohens, *Effect of thermo-mechanical cycles on the physico-chemical properties of poly(lactic acid).* Polymer Degradation and Stability, 2008. **93**(2): p. 321-328.

49. M. Żenkiewicz, J. Richert, P. Rytlewski, K. Moraczewski, M. Stepczyńska, and T. Karasiewicz, *Characterisation of multi-extruded poly(lactic acid).* Polymer Testing, 2009. **28**(4): p. 412-418.

50. J.D. Badia, E. Strömberg, S. Karlsson, and A. Ribes-Greus, *Material valorisation of amorphous polylactide. Influence of thermo-mechanical degradation on the morphology, segmental dynamics, thermal and mechanical performance.* Polymer Degradation and Stability, 2012. **97**(4): p. 670-678.

51. A. Le Duigou, I. Pillin, A. Bourmaud, P. Davies, and C. Baley, *Effect of recycling on mechanical behaviour of biocompostable flax/poly(l-lactide) composites.* Composites Part A: Applied Science and Manufacturing, 2008. **39**(9): p. 1471-1478.

52. T. Saeki, T. Tsukegi, H. Tsuji, H. Daimon, and K. Fujie, *Depolymerization of poly (L-lactic acid) under hydrothermal conditions.* Kobunshi Ronbunshu, 2004. **61**(11): p. 561-566.

53. H. Tsuji, T. Saeki, T. Tsukegi, H. Daimon, and K. Fujie, *Comparative study on hydrolytic degradation and monomer recovery of poly(l-lactic acid) in the solid and in the melt.* Polymer Degradation and Stability, 2008. **93**(10): p. 1956-1963.

54. M. Yagihashi and T. Funazukuri, *Recovery of L-lactic acid from poly(L-lactic acid) under hydrothermal conditions of dilute aqueous sodium hydroxide solution.* Industrial and Engineering Chemistry Research, 2010. **49**(3): p. 1247-1251.

55. A. Plichta, P. Lisowska, A. Kundys, A. Zychewicz, M. Dębowski, and Z. Florjańczyk, *Chemical recycling of poly(lactic acid) via controlled degradation with protic (macro)molecules.* Polymer Degradation and Stability, 2014. **108**: p. 288-296.

56. K. Hirao, Y. Nakatsuchi, and H. Ohara, *Alcoholysis of Poly(l-lactic acid) under microwave irradiation.* Polymer Degradation and Stability, 2010. **95**(6): p. 925-928.

57. A. Grala, J. Ejfler, L.B. Jerzykiewicz, and P. Sobota, *Chemoselective alcoholysis of lactide mediated by a magnesium catalyst: An efficient route to alkyl lactyllactate.* Dalton Transactions, 2011. **40**(16): p. 4042-4044.

58. X. Song, H. Wang, X. Yang, F. Liu, S. Yu, and S. Liu, *Hydrolysis of poly(lactic acid) into calcium lactate using ionic liquid [Bmim][OAc] for chemical recycling.* Polymer Degradation and Stability, 2014. **110**: p. 65-70.

59. M. Noda and H. Okuyama, *Thermal catalytic depolymerization of poly(L-lactic acid) oligomer into LL-lactide: Effects of Al, Ti, Zn and Zr compounds as catalysts.* Chemical and Pharmaceutical Bulletin, 1999. **47**(4): p. 467-471.

60. H. Nishida, T. Mori, S. Hoshihara, Y. Fan, Y. Shirai, and T. Endo, *Effect of tin on poly(l-lactic acid) pyrolysis.* Polymer Degradation and Stability, 2003. **81**(3): p. 515-523.

61. Y. Fan, H. Nishida, S. Hoshihara, Y. Shirai, Y. Tokiwa, and T. Endo, *Pyrolysis kinetics of poly(l-lactide) with carboxyl and calcium salt end structures.* Polymer Degradation and Stability, 2003. **79**(3): p. 547-562.

62. Y. Fan, H. Nishida, Y. Shirai, Y. Tokiwa, and T. Endo, *Thermal degradation behaviour of poly(lactic acid) stereocomplex.* Polymer Degradation and Stability, 2004. **86**(2): p. 197-208.

63. R. Narayan, W.M. Wu, and C.S. Criddle, *Lactide Production from Thermal Depolymerization of PLA with applications to Production of PLA or other bioproducts*. 2013, Google Patents.

64. Y. Zhang, S.K. Mallapragada, and B. Narasimhan, *Dissolution of waste plastics in biodiesel.* Polymer Engineering and Science, 2010. **50**(5): p. 863-870.

65. N. Kuzhiyil and S.C. Kong, *Energy recovery from waste plastics by using blends of biodiesel and polystyrene in diesel engines.* Energy and Fuels, 2009. **23**(6): p. 3246-3253.

66. P. Mohammadi, A.M. Nikbakht, M. Tabatabaei, K. Farhadi, A. Mohebbi, and M. Khatami far, *Experimental investigation of performance and emission characteristics of DI diesel engine fueled with polymer waste dissolved in biodiesel-blended diesel fuel.* Energy, 2012. **46**(1): p. 596-605.

67. S. Ling, Z. Qi, D.P. Knight, Y. Huang, L. Huang, H. Zhou, Z. Shao, and X. Chen, *Insight into the structure of single Antheraea pernyi silkworm fibers using synchrotron FTIR microspectroscopy.* Biomacromolecules, 2013. **14**(6): p. 1885-1892.

68. Y. Tao, W. Xu, Y. Yan, and Y. Cao, *Preparation and characterization of silk fibroin nanocrystals.* Polym. Int., 2012. **61**(5): p. 760-767.

69. B. Itim and M. Philip, *Effect of multiple extrusions and influence of PP contamination on the thermal characteristics of bottle grade recycled PET.* Polymer Degradation and Stability, 2015. **117**: p. 84-89.

70. O. Wachsen, K. Platkowski, and K.H. Reichert, *Thermal degradation of poly-l-lactide—studies on kinetics, modelling and melt stabilisation.* Polymer Degradation and Stability, 1997. **57**(1): p. 87-94.

71. H. Yu, N. Huang, C. Wang, and Z. Tang, *Modeling of poly(L-lactide) thermal degradation: Theoretical prediction of molecular weight and polydispersity index.* Journal of Applied Polymer Science, 2003. **88**(11): p. 2557-2562.

72. H.M. Khanlou, W. Hall, M.T. Heitzman, J. Summerscales, and P. Woodfield, *Technical Note: On modelling thermo-chemical degradation of poly(lactic acid).* Polymer Degradation and Stability, 2016. **134**: p. 19-21.

73. R.E. Marsh, R.B. Corey, and L. Pauling, *An investigation of the structure of silk fibroin.* Biochimica et Biophysica Acta, 1955. **16**: p. 1-34.

74. Y. Tao, W. Xu, Y. Yan, and Y. Cao, *Preparation and characterization of silk fibroin nanocrystals.* Polymer International, 2012. **61**(5): p. 760-767.

75. T. Jiang and P. Zhou, *Environment-Induced Silk Fibroin Conformation Based on the Magnetic Resonance Spectroscopy*. On Biomimetics. 2011.

76. D. Devi, N.S. Sarma, B. Talukdar, P. Chetri, K.C. Baruah, and N.N. Dass, *Study of the structure of degummed Antheraea assamensis (muga) silk fibre.* The Journal of The Textile Institute, 2011. **102**(6): p. 527-533.

77. A.F. Mohd-Adnan, H. Nishida, and Y. Shirai, *Evaluation of kinetics parameters for poly(l-lactic acid) hydrolysis under high-pressure steam.* Polymer Degradation and Stability, 2008. **93**(6): p. 1053-1058.

78. C.-S. Ha and W.-J. Cho, *Miscibility, properties, and biodegradability of microbial polyester containing blends.* Progress in Polymer Science, 2002. **27**(4): p. 759-809.

79. C. Ingrao, C. Tricase, A. Cholewa-Wójcik, A. Kawecka, R. Rana, and V. Siracusa, *Polylactic acid trays for fresh-food packaging: A Carbon Footprint assessment.* Science of The Total Environment, 2015. **537**: p. 385-398.

80. T.A. Hottle, M.M. Bilec, and A.E. Landis, *Sustainability assessments of bio-based polymers.* Polymer Degradation and Stability, 2013. **98**(9): p. 1898-1907.

81. A.E. Landis, *Cradle to Gate Environmental Footprint and Life Cycle Assessment of Poly(Lactic Acid)*, in *Poly(Lactic Acid): Synthesis, Structures, Properties, Processing, and Applications*. 2010. p. 431-441.

82. J.A. Colwill, E.I. Wright, and S. Rahimifard, *A Holistic Approach to Design Support for Bio-polymer Based Packaging.* Journal of Polymers and the Environment, 2012. **20**(4): p. 1112-1123.

83. M. Nerkar, J.A. Ramsay, B.A. Ramsay, A.A. Vasileiou, and M. Kontopoulou, *Improvements in the melt and solid-state properties of poly(lactic acid), poly-3-hydroxyoctanoate and their blends through reactive modification.* Polymer, 2015. **64**: p. 51-61.

84. R.M. Rasal, A.V. Janorkar, and D.E. Hirt, *Poly(lactic acid) modifications.* Progress in Polymer Science, 2010. **35**(3): p. 338-356.

85. T. Maharana, B. Mohanty, and Y.S. Negi, *Melt–solid polycondensation of lactic acid and its biodegradability*. Progress in Polymer Science, 2009. **34**(1): p. 99-124.

86. M.A.S. Azizi Samir, F. Alloin, and A. Dufresne, *Review of recent research into cellulosic whiskers, their properties and their application in nanocomposite field.* Biomacromolecules, 2005. **6**(2): p. 612-626.

87. D. Prodyut, D. Tarafder, A. Kumar, and V. Katiyar, *Thermally recyclable polylactic acid/cellulose nanocrystal films through reactive extrusion process.* Polymer, 2016. **87**: p. 268-282.

88. L. Petersson, I. Kvien, and K. Oksman, *Structure and thermal properties of poly(lactic acid)/cellulose whiskers nanocomposite materials.* Composites Science and Technology, 2007. **67**(11–12): p. 2535-2544.

89. A. Abdulkhani, J. Hosseinzadeh, A. Ashori, S. Dadashi, and Z. Takzare, *Preparation and characterization of modified cellulose nanofibers reinforced polylactic acid nanocomposite.* Polymer Testing, 2014. **35**: p. 73-79.

90. M. Jonoobi, J. Harun, A.P. Mathew, and K. Oksman, *Mechanical properties of cellulose nanofiber (CNF) reinforced polylactic acid (PLA) prepared by twin screw extrusion.* Composites Science and Technology, 2010. **70**(12): p. 1742-1747.

91. T.-M. Wu and C.-Y. Wu, *Biodegradable poly(lactic acid)/chitosan-modified montmorillonite nanocomposites: Preparation and characterization.* Polymer Degradation and Stability, 2006. **91**(9): p. 2198-2204.

92. D. Ju, L. Han, Z. Li, Y. Chen, Q. Wang, J. Bian, and L. Dong, *Porous poly(l-lactic acid) sheet prepared by stretching with starch particles as filler for tissue engineering.* Carbohydrate Polymers, 2016. **142**: p. 222-229.

93. J.M. Ferri, D. Garcia-Garcia, L. Sánchez-Nacher, O. Fenollar, and R. Balart, *The effect of maleinized linseed oil (MLO) on mechanical performance of poly(lactic acid)-thermoplastic starch (PLA-TPS) blends.* Carbohydrate Polymers, 2016. **147**: p. 60-68.

94. M.L. Sanyang, S.M. Sapuan, M. Jawaid, M.R. Ishak, and J. Sahari, *Development and characterization of sugar palm starch and poly(lactic acid) bilayer films.* Carbohydrate Polymers, 2016. **146**: p. 36-45.

95. S. Li, J. Xia, Y. Xu, X. Yang, W. Mao, and K. Huang, *Preparation and characterization of acorn starch/poly(lactic acid) composites modified with functionalized vegetable oil derivates.* Carbohydrate Polymers, 2016. **142**: p. 250-258.

96. S. Lv, J. Gu, J. Cao, H. Tan, and Y. Zhang, *Effect of annealing on the thermal properties of poly (lactic acid)/starch blends.* International Journal of Biological Macromolecules, 2015. **74**: p. 297-303.

97. R. Valapa, G. Pugazhenthi, and V. Katiyar, *Thermal degradation kinetics of sucrose palmitate reinforced poly(lactic acid) biocomposites.* International Journal of Biological Macromolecules, 2014. **65**: p. 275-283.

98. Y. Wang and J.F. Mano, *Influence of melting conditions on the thermal behaviour of poly(l-lactic acid).* European Polymer Journal, 2005. **41**(10): p. 2335-2342.

99. F. Signori, M.-B. Coltelli, and S. Bronco, *Thermal degradation of poly(lactic acid) (PLA) and poly(butylene adipate-co-terephthalate) (PBAT) and their blends upon melt processing.* Polymer Degradation and Stability, 2009. **94**(1): p. 74-82.

100. D. Bondeson and K. Oksman, *Dispersion and characteristics of surfactant modified cellulose whiskers nanocomposites.* Composite Interfaces, 2007. **14**(7-9): p. 617-630.

101. S. Coppola, L. Balzano, E. Gioffredi, P.L. Maffettone, and N. Grizzuti, *Effects of the degree of undercooling on flow induced crystallization in polymer melts.* Polymer, 2004. **45**(10): p. 3249-3256.

102. H. Li and M.A. Huneault, *Effect of nucleation and plasticization on the crystallization of poly(lactic acid).* Polymer, 2007. **48**(23): p. 6855-6866.

103. J. Meerveld, G.W.M. Peters, and M. Hütter, *Towards a rheological classification of flow induced crystallization experiments of polymer melts.* Rheologica Acta, 2004. **44**(2): p. 119-134.

104. N.V. Pogodina, V.P. Lavrenko, S. Srinivas, and H.H. Winter, *Rheology and structure of isotactic polypropylene near the gel point: quiescent and shear-induced crystallization.* Polymer, 2001. **42**(21): p. 9031-9043.

105. T. Ozawa, *Kinetics of non-isothermal crystallization.* Polymer, 1971. **12**(3): p. 150-158.

106. A. Jeziorny, *Parameters characterizing the kinetics of the non-isothermal crystallization of poly(ethylene terephthalate) determined by d.s.c.* Polymer, 1978. **19**(10): p. 1142-1144.

107. P. Cebe and S.-D. Hong, *Crystallization behaviour of poly(ether-ether-ketone).* Polymer, 1986. **27**(8): p. 1183-1192.

108. M. Gahleitner, *Melt rheology of polyolefins.* Progress in Polymer Science, 2001. **26**(6): p. 895-944.

109. M.R. Aghjeh, V. Asadi, P. Mehdijabbar, H.A. Khonakdar, and S.H. Jafari, *Application of linear rheology in determination of nanoclay localization in PLA/EVA/Clay nanocomposites: Correlation with microstructure and thermal properties.* Composites Part B: Engineering. **86**: p. 273-284.

110. F.M. Ghorbani, B. Kaffashi, P. Shokrollahi, S. Akhlaghi, and M.S. Hedenqvist, *Effect of hydroxyapatite nano-particles on morphology, rheology and thermal behavior of poly(caprolactone)/chitosan blends.* Materials Science and Engineering: C. **59**: p. 980-989.

111. B. Nekhamanurak, P. Patanathabutr, and N. Hongsriphan, *The Influence of Micro-/Nano-CaCO3 on Thermal Stability and Melt Rheology Behavior of Poly(Lactic Acid).* Energy Procedia. **56**: p. 118-128.

112. M.J. Solomon, A.S. Almusallam, K.F. Seefeldt, A. Somwangthanaroj, and P. Varadan, *Rheology of Polypropylene/Clay Hybrid Materials.* Macromolecules, 2001. **34**(6): p. 1864-1872.

113. L.-I. Palade, H.J. Lehermeier, and J.R. Dorgan, *Melt Rheology of High l-Content Poly(lactic acid).* Macromolecules, 2001. **34**(5): p. 1384-1390.

114. V. Verney and A. Michel, *Representation of the rheological properties of polymer melts in terms of complex fluidity.* Rheologica Acta. **28**(1): p. 54-60.

115. D. Wu, L. Wu, M. Zhang, and Y. Zhao, *Viscoelasticity and thermal stability of polylactide composites with various functionalized carbon nanotubes.* Polymer Degradation and Stability, 2008. **93**(8): p. 1577-1584.

116. M. Pluta, J.K. Jeszka, and G. Boiteux, *Polylactide/montmorillonite nanocomposites: Structure, dielectric, viscoelastic and thermal properties.* European Polymer Journal, 2007. **43**(7): p. 2819-2835.

117. S. Sinha Ray, K. Yamada, M. Okamoto, and K. Ueda, *New polylactide-layered silicate nanocomposites. 2. Concurrent improvements of material properties, biodegradability and melt rheology.* Polymer, 2003. **44**(3): p. 857-866.

118. J. Tian, W. Yu, and C. Zhou, *The preparation and rheology characterization of long chain branching polypropylene.* Polymer, 2006. **47**(23): p. 7962-7969.

119. L. Suryanegara, A.N. Nakagaito, and H. Yano, *The effect of crystallization of PLA on the thermal and mechanical properties of microfibrillated cellulose-reinforced PLA composites.* Composites Science and Technology, 2009. **69**(7–8): p. 1187-1192.

120. R. Pantani, F. De Santis, A. Sorrentino, F. De Maio, and G. Titomanlio, *Crystallization kinetics of virgin and processed poly(lactic acid).* Polymer Degradation and Stability, 2010. **95**(7): p. 1148-1159.

121. G.Z. Papageorgiou, D.S. Achilias, D.N. Bikiaris, and G.P. Karayannidis, *Crystallization kinetics and nucleation activity of filler in polypropylene/surface-treated SiO2 nanocomposites.* Thermochimica Acta, 2005. **427**(1–2): p. 117-128.

122. J.M. Raquez, Y. Murena, A.L. Goffin, Y. Habibi, B. Ruelle, F. DeBuyl, and P. Dubois, *Surface-modification of cellulose nanowhiskers and their use as nanoreinforcers into polylactide: A sustainably-integrated approach.* Composites Science and Technology, 2012. **72**(5): p. 544-549.

123. W. Yang, E. Fortunati, F. Dominici, J.M. Kenny, and D. Puglia, *Effect of processing conditions and lignin content on thermal, mechanical and degradative behavior of lignin nanoparticles/polylactic (acid) bionanocomposites prepared by melt extrusion and solvent casting.* European Polymer Journal, 2015. **71**: p. 126-139.

124. H. Tsuji, H. Takai, N. Fukuda, and H. Takikawa, *Non-isothermal crystallization behavior of poly(L-lactic acid) in the presence of various additives.* Macromolecular Materials and Engineering, 2006. **291**(4): p. 325-335.

125. M. Nofar, W. Zhu, C.B. Park, and J. Randall, *Crystallization kinetics of linear and long-chain-branched polylactide.* Industrial and Engineering Chemistry Research, 2011. **50**(24): p. 13789-13798.

126. Z. Xu, Y. Niu, Z. Wang, H. Li, L. Yang, J. Qiu, and H. Wang, *Enhanced nucleation rate of polylactide in composites assisted by surface acid oxidized carbon nanotubes of different aspect ratios.* ACS Appl Mater Interfaces, 2011. **3**(9): p. 3744-53.

127. R. Valapa, S. Hussain, P. Krishnan Iyer, G. Pugazhenthi, and V. Katiyar, *Non-isothermal crystallization kinetics of sucrose palmitate reinforced poly(lactic acid) bionanocomposites.* Polymer Bulletin, 2015. **73**(1): p. 21-38.

128. B.Y. Shin, G.S. Jo, K.S. Kang, T.J. Lee, B.S. Kim, S.I. Lee, and J.S. Song, *Morphology and rheology on the blends of PLA/CMPS.* Macromolecular Research. **15**(4): p. 291-301.

129. D. Wu, L. Wu, L. Wu, and M. Zhang, *Rheology and thermal stability of polylactide/clay nanocomposites.* Polymer Degradation and Stability, 2006. **91**(12): p. 3149-3155.

130. L. Jiang, J. Zhang, and M.P. Wolcott, *Comparison of polylactide/nano-sized calcium carbonate and polylactide/montmorillonite composites: Reinforcing effects and toughening mechanisms.* Polymer, 2007. **48**(26): p. 7632-7644.

131. Z. Zhou, Y. Zhang, Y. Zhang, and N. Yin, *Rheological behavior of polypropylene/octavinyl polyhedral oligomeric silsesquioxane composites.* Journal of Polymer Science Part B: Polymer Physics, 2008. **46**(5): p. 526-533.

132. M.J. Kashyap and A.K. Ghosh, *Processing, rheology and characterization of polypropylene nanocomposites and their blown films.* Journal of Plastic Film and Sheeting. **29**(3): p. 228-248.

133. A. Kiss, E. Fekete, and B. Pukánszky, *Aggregation of CaCO3 particles in PP composites: Effect of surface coating.* Composites Science and Technology, 2007. **67**(7–8): p. 1574-1583.

134. F. Walha, K. Lamnawar, A. Maazouz, and M. Jaziri, *Rheological, Morphological and Mechanical Studies of Sustainably Sourced Polymer Blends Based on Poly(Lactic Acid) and Polyamide 11.* Polymers 2016. **8**(61).

135. K.L. Nait-Ali, A. Bergeret, L. Ferry, and X. Colin, *Chain branching detection by Cole–Cole modeling of rheological properties changes during PET mechanical recycling.* Polymer Testing, 2012. **31**(3): p. 500-504.

136. H.M. da Costa, V.D. Ramos, and M.C.G. Rocha, *Rheological properties of polypropylene during multiple extrusion.* Polymer Testing, 2005. **24**(1): p. 86-93.

137. P.S. Garcia, C.H. Scuracchio, and S.A. Cruz, *Effect of residual contaminants and of different types of extrusion processes on the rheological properties of the post-consumer polypropylene.* Polymer Testing, 2013. **32**(7): p. 1237-1243.

138. M. Pishvaei, C. Graillat, T.F. McKenna, and P. Cassagnau, *Rheological behaviour of polystyrene latex near the maximum packing fraction of particles.* Polymer, 2005. **46**(4): p. 1235-1244.

139. D. Maier, A. Eckstein, C. Friedrich, and J. Honerkamp, *Evaluation of models combining rheological data with the molecular weight distribution.* Journal of Rheology, 1998. **42**(5): p. 1153-1173.

140. F.J. Stadler, C. Piel, J. Kaschta, S. Rulhoff, W. Kaminsky, and H. Münstedt, *Dependence of the zero shear-rate viscosity and the viscosity function of linear high-*

density polyethylenes on the mass-average molar mass and polydispersity. Rheologica Acta, 2005. **45**(5): p. 755-764.

141. M.L. Huggins, *The viscosity of dilute solutions of long-chain molecules. IV. Dependence on concentration.* Journal of the American Chemical Society, 1942. **64**(11): p. 2716-2718.

142. M. Jonoobi, J. Harun, A.P. Mathew, and K. Oksman, *Mechanical properties of cellulose nanofiber (CNF) reinforced polylactic acid (PLA) prepared by twin screw extrusion.* Composites Science and Technology. **70**(12): p. 1742-1747.

143. M. Żenkiewicz, J. Richert, P. Rytlewski, K. Moraczewski, M. Stepczyńska, and T. Karasiewicz, *Characterisation of multi-extruded poly(lactic acid).* Polym. Test., 2009. **28**(4): p. 412–418.

144. W. Defeng, L. Qiaolian, F. Saihua, C. Jianxiang, C. Yang, Q. Yaxin, and Y. Xin, *Polylactide composite foams containing carbon nanotubes and carbon black: Synergistic effect of filler on electrical conductivity.* Carbon, 2015. **95**: p. 380-387.

145. R. Jean-Marie, H. Youssef, M. Marius, and D. Philippe, *Polylactide (PLA)-based nanocomposites.* Progress in Polymer Science, 2013. **38**(10–11): p. 1504-1542.

146. K.P. Akhilesh and V. Katiyar, *Chitosan dispersed PLA films for high gas barrier applications: An industrially viable approach.* J. Mater. Sci. Eng., 2015. **04**(04).

147. A. Porras, A. Maranon, and I.A. Ashcroft, *Thermo-mechanical characterization of Manicaria Saccifera natural fabric reinforced poly-lactic acid composite lamina.* Composites, Part A, 2016. **81**: p. 105-110.

148. A. Porras, A. Maranon, and I.A. Ashcroft, *Characterization of a novel natural cellulose fabric from Manicaria saccifera palm as possible reinforcement of composite materials.* Composites, Part B, 2015. **74**: p. 66–73.

149. E. Fortunati, M. Peltzer, I. Armentano, L. Torre, A. Jiménez, and J.M. Kenny, *Effects of modified cellulose nanocrystals on the barrier and migration properties of PLA nano-biocomposites.* Carbohydr. Polym., 2012. **90**(2): p. 948–956.

150. R. Auras, B. Harte, and S. Selk, *An overview of polylactides as packaging materials.* Macromol. Biosci., 2004. **4**(9): p. 835–864.

151. M. Hiljanen-Vainio, P. Varpomaa, J. Seppälä, and P. Törmälä, *Modification of poly(L-lactides) by blending: Mechanical and hydrolytic behavior.* Macromol. Chem. Phys., 1996. **197**(4): p. 1503-1523.

152. R.M. Rasal, A.V. Janorkar, and D.E. Hirt, *Poly(lactic acid) modifications.* Prog. Polym. Sci., 2010. **35**(3): p. 338–356.

153. D.W. Grijpma, A.J. Nijenhuis, P.G.T.v. Wijk, and A.J. Pennings, *High impact strength as-polymerized PLLA.* Polym. Bull., 1992. **29**(5): p. 571–578.

154. R. Valapa, G. Pugazhenthi, and V. Katiyar, *Thermal degradation kinetics of sucrose palmitate reinforced poly(lactic acid) biocomposites.* Int. J. Biol. Macromol., 2014. **65**: p. 275-283.

155. D. Prodyut, K. Amit, and K. Vimal, *Fabrication of cellulose nanocrystal supported stable Fe(0) nanoparticles: a sustainable catalyst for dye reduction, organic conversion and chemo-magnetic propulsion.* Cellulose, 2015. **22**(6): p. 3755-3771.

156. D. Prodyut, T. Debashis, K. Amit, and K. Vimal, *Effect of cellulose nanocrystal polymorphs on mechanical, barrier and thermal properties of poly(lactic acid) based bionanocomposites.* RSC Advances, 2015. **5**(74): p. 60426-60440.

157. H.-M. Ng, L.T. Sin, T.-T. Tee, S.-T. Bee, D. Hui, C.-Y. Low, and A.R. Rahmat, *Extraction of cellulose nanocrystals from plant sources for application as reinforcing agent in polymers.* Composites Part B: Engineering, 2015. **75**: p. 176-200.

158. A. Kiziltas, B. Nazari, E. Erbas Kiziltas, D.J. Gardner, Y. Han, and T.S. Rushing, *Method to reinforce polylactic acid with cellulose nanofibers via a polyhydroxybutyrate carrier system.* Carbohydrate Polymers, 2016. **140**: p. 393-399.

159. D. Prodyut, D. Tarafder, A. Kumar, and K. Vimal, *Thermally recyclable polylactic acid/cellulose nanocrystal films through reactive extrusion process.* Polymer, 2016. **87**: p. 268–282.

160. S. Vyazovkin and C. Wight A., *Model-free and model-fitting approaches to kinetic analysis of isothermal and nonisothermal data.* Thermochim. Acta, 1999. **340–341**: p. 53–68.

161. P. Budrugeac, *The evaluation of the non-isothermal kinetic parameters of the thermal and thermo-oxidative degradation of polymers and polymeric materials: its use and abuse.* Polym. Degrad. Stab., 2000. **71**(1): p. 185–187.

162. C.-R. Li and B.T. Tong, *A new method for analysing non-isothermal thermoanalytical data from solid-state reactions.* Thermochim. Acta, 1999. **325**(1): p. 43–46.

163. P. Budrugeac, A.L. Petre, and E. Segal, *Some problems concerning the evaluation of non-isothermal kinetic parameters: Solid-gas decompositions from thermogravimetric data.* J. Therm. Anal., 1996. **47**(1): p. 123–134.

164. I. Yuzay E., R. Auras, H. Soto-Valdez, and S. Selke, *Effects of synthetic and natural zeolites on morphology and thermal degradation of poly(lactic acid) composites.* Polym. Degrad. Stab., 2010. **95**(9): p. 1769–1777.

165. S. Vyazovkin, A. Burnham K., J. Criado M., L. Pérez-Maquedm, C. Popescu, and N. Sbirrazzuoli, *ICTAC Kinetics Committee recommendations for performing kinetic computations on thermal analysis data.* Thermochim. Acta, 2011. **520**(1–2): p. 1-19.

166. M.Z. Sefain, M.H. Fadl, N.A. El-Wakil, and M.S.A. El-Salam, *Thermal behaviour of linen and chemically treated linen fibres.* Polym. Degrad. Stab., 1995. **50**(2): p. 195–198.

167. P.J.v. Ekeren, *Handbook of Thermal Analysis and Calorimetry: Applications to Polymers and Plastics* Thermochim. Acta, ed. P.K.G. Stephen Z.D. Cheng. Vol. 3. 2003. 121-123.

168. S. Vyazovkin and N. Sbirrazzuoli, *Isoconversional kinetic analysis of thermally stimulated processes in polymers*. Macromol. Rapid Commun., 2006. **27**(18): p. 1515–1532.

169. A.I. Lesnikovich and S.V. Levchik, *A method of finding invariant values of kinetic parameters.* J. Therm. Anal., 1983. **27**(1): p. 89–93.

170. P. Budrugeac, E. Segal, L.A. Pérez-Maqueda, and J.M. Criado, *The use of the IKP method for evaluating the kinetic parameters and the conversion function of the thermal dehydrochlorination of PVC from non-isothermal data.* Polym. Degrad. Stab., 2004. **84**(2): p. 311–320.

171. P. Budrugeac, J.M. Criado, F.J. Gotor, J. Malek, L.A. Pérez-Maqueda, and E. Segal, *On the evaluation of the nonisothermal kinetic parameters of (GeS2)0.3(Sb2S3)0.7 crystallization using the IKP method.* Int. J. Chem. Kinet., 2004. **36**(6): p. 309-315.

172. A.W. Coats and J.P. Redfern, *Kinetic Parameters from Thermogravimetric Data* in *Nature* 1964: pp. 68 - 69

173. Ö. Çepelioğullar, H. Haykırı-Açma, and S. Yaman, *Kinetic modelling of RDF pyrolysis: Model-fitting and model-free approaches.* Waste Management, 2016. **48**: p. 275-284.

174. F.J. Gotor, José, M. Criado, J. Malek, and N. Koga, *Kinetic analysis of solid-state reactions: The universality of master plots for analyzing isothermal and nonisothermal experiments.* Journal of Physical Chemistry A, 2000. **104**(46): p. 10777-10782.

175. D.S. Achilias, E. Panayotidou, and I. Zuburtikudis, *Thermal degradation kinetics and isoconversional analysis of biodegradable poly(3-hydroxybutyrate)/organomodified montmorillonite nanocomposites.* Thermochimica Acta, 2011. **514**(1-2): p. 58-66.

176. J.A. Nelder and R. Mead, *A simplex method for function minimization.* The Computer Journal, 1965 **7 (4)**: p. 308–313.

177. K.I.M. Mckinnon, *convergebce of the Nelder-Mead simplex method to a nonstationart point* Soc. Ind. Appl. Math., 1998. **Vol. 9, No. 1**: p. 148–158.

178. H. Zou, C. Yi, L. Wang, H. Liu, and W. Xu, *Thermal degradation of poly(lactic acid) measured by thermogravimetry coupled to Fourier transform infrared spectroscopy.* J. Therm. Anal. Calorim., 2009. **97**(3): p. 929–935.

179. Y. Aoyagi, K. Yamashita, and Y. Doi, *Thermal degradation of poly[(R)-3-hydroxybutyrate], poly[ε-caprolactone], and poly[(S)-lactide]*. Polym. Degrad. Stab., 2002. **76**(1): p. 53–59.

180. F.D. Kopinke, M. Remmler, K. Mackenzie, M. Möder, and O. Wachsen, *Thermal decomposition of biodegradable polyesters—II. Poly(lactic acid).* Polym. Degrad. Stab., 1996. **53**(3): p. 329–342.

181. H. Tsuji and I. Fukui, *Enhanced thermal stability of poly(lactide)s in the melt by enantiomeric polymer blending.* Polymer, 2003. **44**(10): p. 2891–2896.

182. T. Yang C. K., S. S. Y. Lin, and T.-H. Chuang, *Kinetic analysis of the thermal oxidation of metallocene cyclic olefin copolymer (mCOC)/TiO2 composites by FTIR microscopy and thermogravimetry (TG).* Polym. Degrad. Stab., 2002. **78**(3): p. 525–532.

183. E.-C. Chen and T.-M. Wu, *Isothermal crystallization kinetics and thermal behavior of poly(ε-caprolactone)/multi-walled carbon nanotube composites.* Polym. Degrad. Stab., 2007. **92**(6): p. 1009-1015.

184. F. Carrasco, P. Pagès, J. Gámez-Pérez, O.O. Santana, and M. L.Maspoch, *Processing of poly(lactic acid): Characterization of chemical structure, thermal stability and mechanical properties.* Polym. Degrad. Stab., 2010. **95**(2): p. 116–125.

185. A. Khawam and F. R. Douglas, *Solid-State Kinetic Models: Basics and Mathematical Fundamentals.* J. Phys. Chem. B, 2006. **110**(35): p. 17315-17328.

186. B. Saha, P.K. Reddy, and A.K. Ghoshal, *Hybrid genetic algorithm to find the best model and the globally optimized overall kinetics parameters for thermal decomposition of plastics.* Chem. Eng. J., 2008. **138**(1–3): p. 20–29.

187. C. Vogel and H. Siesler W., *Thermal Degradation of Poly(ε-caprolactone), Poly(L-lactic acid) and their Blends with Poly(3-hydroxy-butyrate) Studied by TGA/FT-IR Spectroscopy.* Macromol. Symp., 2008. **265**(1): p. 183–194.

188. M.C. Gupta and V.G. Deshmukh, *Thermal oxidative degradation of poly-lactic acid - Part I: Activation energy of thermal degradation in air.* Colloid & Polymer Science, 1982. **260**(3): p. 308-311.

189. S.H. Hyon, K. Jamshidi, and Y. Ikada, *Effects of Residual Monomer on the Degradation of DL-Lactide Polymer.* Polymer International, 1998. **46**(3): p. 196-202.

190. S. Gogolewski, M. Jovanovic, S.M. Perren, J.G. Dillon, and M.K. Hughes, *The effect of melt-processing on the degradation of selected polyhydroxyacids: polylactides, polyhydroxybutyrate, and polyhydroxybutyrate-co-valerates.* Polymer Degradation and Stability, 1993. **40**(3): p. 313-322.

191. S.H. Lee, J.I. Kim, C.S. Park, S.B. Lee, J.H. Kim, and M.S. Kim, *Preparation of intercross-linked poly(L-lactide) and epoxy resin using N-benzyl pyrazine hexafluoroantimonate.* Journal of Polymer Research, 2013. **20**(11): p. 264.

192. S. Japon, L. Boogh, Y. Leterrier, and J.A.E. Månson, *Reactive processing of poly(ethylene terephthalate) modified with multifunctional epoxy-based additives.* Polymer, 2000. **41**(15): p. 5809-5818.

193. L. Incarnato, P. Scarfato, L. Di Maio, and D. Acierno, *Structure and rheology of recycled PET modified by reactive extrusion.* Polymer, 2000. **41**(18): p. 6825-6831.

194. K. Lamnawar and A. Maazouz, *Rheological study of multilayer functionalized polymers: characterization of interdiffusion and reaction at polymer/polymer interface.* Rheologica Acta, 2006. **45**(4): p. 411-424.

195. Y.-M. Corre, J. Duchet, J. Reignier, and A. Maazouz, *Melt strengthening of poly (lactic acid) through reactive extrusion with epoxy-functionalized chains.* Rheologica Acta, 2011. **50**(7): p. 613-629.

196. Z.F. Zhou, G.Q. Huang, W.B. Xu, and F.M. Ren, *Chain extension and branching of poly(L-lactic acid) produced by reaction with a DGEBA-based epoxy resin.* Express Polymer Letters, 2007. **1**(11): p. 734-739.

197. J. Cailloux, O.O. Santana, E. Franco-Urquiza, J.J. Bou, F. Carrasco, and M.L. Maspoch, *Sheets of branched poly(lactic acid) obtained by one-step reactive extrusion–calendering process: physical aging and fracture behavior.* Journal of Materials Science, 2014. **49**(11): p. 4093-4107.

198. E.L. de Paula, F. Roig, A. Mas, J.-P. Habas, V. Mano, F.V. Pereira, and J.-J. Robin, *Effect of surface-grafted cellulose nanocrystals on the thermal and mechanical properties of PLLA based nanocomposites.* European Polymer Journal, 2016. **84**: p. 173-187.

199. Y. Bian, C. Han, L. Han, H. Lin, H. Zhang, J. Bian, and L. Dong, *Toughening mechanism behind intriguing stress-strain curves in tensile tests of highly enhanced compatibilization of biodegradable poly(lactic acid)/poly(3-hydroxybutyrate-co-4-hydroxybutyrate) blends.* RSC Advances, 2014. **4**(79): p. 41722-41733.

200. M. Tesfaye, R. Patwa, R. Kommadath, P. Kotecha, and V. Katiyar, *Silk nanocrystals stabilized melt extruded poly (lactic acid) nanocomposite films: Effect of recycling on thermal degradation kinetics and optimization studies.* Thermochimica Acta, 2016. **643**: p. 41-52.

201. M. Hiljanen-Vainio, T. Karjalainen, and J. Seppälä, *Biodegradable lactone copolymers. I. Characterization and mechanical behavior of ε-caprolactone and lactide copolymers.* Journal of Applied Polymer Science, 1996. **59**(8): p. 1281-1288.

202. M. Takamura, T. Nakamura, T. Takahashi, and K. Koyama, *Effect of type of peroxide on cross-linking of poly(l-lactide).* Polymer Degradation and Stability, 2008. **93**(10): p. 1909-1916.

203. Y. Bian, L. Han, C. Han, H. Lin, H. Zhang, J. Bian, and L. Dong, *Intriguing crystallization behavior and rheological properties of radical-based crosslinked biodegradable poly(3-hydroxybutyrate-co-4-hydroxybutyrate).* CrystEngComm, 2014. **16**(13): p. 2702-2714.

204. L.S. Nair and C.T. Laurencin, *Biodegradable polymers as biomaterials.* Prog. Polym. Sci. , 2007. **32**: p. 762–798.

205. J. Lunt, *Large-scale production, properties and commercial applications of polylactic acid polymers.* Polymer Degradation and Stability 1998. **59** p. 145-152.

206. K.M. Nampoothiri, N.R. Nair, and R.P. John, *An overview of the recent developments in polylactide (PLA) research.* Bioresource Technology, 2010. **101** p. 8493–8501.

207. E.v.d. Harst and J. Potting, *A critical comparison of ten disposable cup LCAs.* Environmental Impact Assessment Review 2013. **43** p. 86–96.

208. A. Plichta, P. Lisowska, A. Kundys, A. Zychewicz, M. De˛bowski, and Z.F. nczyk, *Chemical recycling of poly(lactic acid) via controlled degradation with protic (macro)molecules.* Polymer Degradation and Stability 2014. **108**: p. 288-296.

209. Y. Tsuneizumi, M. Kuwahara, K. Okamoto, and S. Matsumura, *Chemical recycling of poly(lactic acid)-based polymer blends using environmentally benign catalysts.* Polymer Degradation and Stability 2010 **95**: p. 1387-1393.

210. P. Mohammadi, M.T. , A.M.N. , and Z.E. , *Improvement of the cold flow characteristics of biodiesel containing dissolved polymer wastes.pdf.* Biofuel Research Journal, 2014. **1** p. 26-29.

211. M. Ozcanli, C. Gungor, and K. Aydin, *Energy Sources, Part A: Recovery, Utilization, and Environmental Effects.* Energy Sources, 2013. **35**: p. 635–647.

212. H. Tang, S.O. Salley, and K.Y.S. Ng, *Fuel properties and precipitate formation at low temperature in soy-, cottonseed-, and poultry fat-based biodiesel blends.* Fuel 2008. **87**: p. 3006–3017.

213. R.M. Joshi and M.J. Pegg, *Flow properties of biodiesel fuel blends at low temperatures.* Fuel 2007. **86** p. 143–151.

214. G. Knothe, *Dependence of biodiesel fuel properties on the structure of fatty acid alkyl esters.* Fuel Processing Technology 2005. **86**: p. 1059 – 1070.

215. Y.N. Paul C. Smith, Q. Dzuy Nguyen, Brian K. O'Neill, *Improving the low-temperature properties of biodiesel: Methods and consequences.* Renewable Energy 2010. **35**: p. 1145–1151.

216. N.K.a.S.-C. Kong, *Energy Recovery from Waste Plastics by Using Blends of Biodiesel and Polystyrene in Diesel Engines.* Energy & Fuels, 2009. **23**: p. 3246–3253.

217. H. Omidvarborna, A. Kumar, and D.-S. Kim, *Characterization of particulate matter emitted from transit buses fueled with B20 in idle modes.* Journal of Environmental Chemical Engineering 2014. **2**: p. 2335–2342.

218. S.Y. Giraldo, L.A. Rios, and N. Suárez, *Comparison of glycerol ketals, glycerol acetates and branched alcohol-derived fatty esters as cold-flow improvers for palm biodiesel.* Fuel 2013. **108**: p. 709–714.

219. S.P. Singh and D. Singh, *Biodiesel production through the use of different sources and characterization of oils and their esters as the substitute of diesel: A review*. Renewable and Sustainable Energy Reviews, 2010. **14**(1): p. 200-216.

220. J.D. Mejía, N. Salgado, and C.E. Orrego, *Effect of blends of Diesel and Palm-Castor biodiesels on viscosity, cloud point and flash point.* Industrial Crops and Products, 2013. **43**: p. 791-797.

221. Y. Wang, S. Ma, M. Zhao, L. Kuang, J. Nie, and W.W. Riley, *Improving the cold flow properties of biodiesel from waste cooking oil by surfactants and detergent fractionation.* Fuel 2011. **90**: p. 1036–1040.

222. J. Wang, L. Cao, and S. Han, *Effect of polymeric cold flow improvers on flow properties of biodiesel from waste cooking oil.* Fuel, 2014. **117**: p. 876-881.

223. Y.S.a.T.R. Sheng Han, *Impact of Alkyl Methacrylate-Maleic Anhydride Copolymers as Pour Point Depressant on Crystallization Behavior of Diesel Fuel.* Energy & Fuels, 2009. **23**: p. 2576–2580.

224. L.C. Jieni Wang , Sheng Han, *Effect of polymeric cold flow improvers on flow properties of biodiesel from waste cooking oil.* Fuel, 2014. **117**: p. 876-881.

225. C. Boshui, S. Yuqiu, F. Jianhua, W. Jiu, and W. Jiang, *Effect of cold flow improvers on flow properties of soybean biodiesel.* Biomass and Bioenergy, 2010. **34**(9): p. 1309-1313.

226. G. Dwivedi and M.P. Sharma, *Impact of cold flow properties of biodiesel on engine performance.* Renewable and Sustainable Energy Reviews, 2014. **31**: p. 650-656.

227. J.L. Espartero, I. Rashkov, S.M. Li, N. Manolova, and M. Vert, *NMR analysis of low molecular weight poly(lactic acid)s.* Macromolecules, 1996. **29**(10): p. 3535-3539.

228. C.-C. Ting and C.-C. Chen, *Viscosity and working efficiency analysis of soybean oil based bio-lubricants.* Measurement, 2011. **44**(8): p. 1337-1341.

229. L.A. Quinchia, M.A. Delgado, C. Valencia, J.M. Franco, and C. Gallegos, *Viscosity modification of different vegetable oils with EVA copolymer for lubricant applications.* Industrial Crops and Products, 2010. **32**(3): p. 607-612.

230. A.L. Lown, L. Peereboom, S.A. Mueller, J.E. Anderson, D.J. Miller, and C.T. Lira, *Cold flow properties for blends of biofuels with diesel and jet fuels.* Fuel 2014. **117**: p. 544–551.

231. L. Feng, Z. Zhang, FangWang, T. Wang, and S. Yang, *Synthesis and evaluation of alkyl acrylate-vinyl acetate-maleic anhydride terpolymers as cold flow improvers for diesel fuel.* Fuel Processing Technology, 2014. **118** p. 42–48.

Research Outcomes

List of Publications

1. **Melakuu Tesfaye** and Vimal Katiyar, "Microwave assisted synthesis of biodiesel from soybean oil: Effect of poly (lactic acid)-oligomer on cold flow properties, IC engine performance and emission characteristics." Fuel, 170,107–114 (2016)
2. **Melakuu Tesfaye,** Rahul Patwa, Remya Kommadath, Prakash Kotecha, Vimal Katiyar, Silk nanocrystals stabilized melt extruded poly (lactic acid) nanocomposite films: Effect of recycling on thermal degradation kinetics and optimization studies. Thermochimica Acta, 643, 41-52 (2016)
3. **Melakuu Tesfaye**, Rahul Patwa, Arvind Gupta, Manash Kashyap, Vimal Katiyar, Recycling of Poly (Lactic Acid)/Silk based Bionanocomposites Films and its Influence on Thermal Stability, Crystallization Kinetics, Solution and Melt Rheology. International journal of biomacromolecules (2017)
4. **Melakuu Tesfaye**, Rahul Patwa, Prodyut Dhar, Vimal katiyar, Silk nanocrystals Grafted Poly (lactic acid): the influence of Crosslinking on Rheology and Thermal Stability (under revision)
5. **Melakuu Tesfaye**, Purabi Bhagabati, Naba Kumar Kalita and Vimal Katiyar. Trends on End-of-Life Options: Recycling, Re-using and Composting of Waste Food Packages (book chapter in Press-Smithers Rapra publishing)

Papers under preparation

6. **Melakuu Tesfaye**, Rahul Patwa, Vimal katiyar, The Impact of Acid Hydrolysed Silk Fibrous on the Molar Mass Distribution and Processability Performance of PLA.
7. **Melakuu Tesfaye**, Vimal Katiyar, Alternative Recycling of Poly (lactic Acid) as Biolubricant Additive